UNIVERSITAT POLITÈCNICA DE VALÈNCIA

UNIVERSITAT
POLITÈCNICA
DE VALÈNCIA

DOCTORAL THESIS

Characterization of the Substrate Modification in Patients Undergoing Catheter Ablation of Atrial Fibrillation

Author
Aikaterini VRAKA

Supervisors
José Joaquín RIETA IBÁÑEZ
Raúl ALCARAZ MARTÍNEZ

Valencia, December 2022

BioMIT.org

DEPARTMENT OF ELECTRONIC ENGINEERING

Biosignals &
Minimally Invasive
Technologies **BioMIT**

Abstract

Atrial fibrillation (AF) continues to be the most common cardiac arrhythmia, affecting nowadays $2-4\%$ of global adult population. Considering the current trend for longevity, prognostics for AF prevalence in the forthcoming years are disheartening, while quality of life of AF individuals is often negatively affected. Despite the high popularity of catheter ablation (CA) as the major AF treatment, there is still room and need for improvement, especially in persistent AF patients. Time spent in AF has a significant impact on AF confrontation and evolution, with $1-15\%$ of paroxysmal AF patients progressing to persistent AF annually, hence facing higher complications regarding the AF therapy. Therefore, from early diagnosis to late follow-up therapy, every aspect of AF study that can contribute to the AF confrontation is of utmost importance.

CA of pulmonary veins (PVs) is based on the declaration of PVs as the primary AF foci. However, multiple atrial sites can contribute to the AF propagation, either by triggering or by sustaining the AF activity. AF or atrial substrate is the term used to describe all these sites that are involved with the AF activity due to anatomical alterations causing further electrical and functional disturbance. Precise mapping of the atrial substrate and reliable recording of the atrial substrate modification, as a positive marker after CA sessions, are critical in the combat against AF. Electrocardiograms (ECGs) and electrograms (EGMs) are vastly recruited to map the atrial substrate or evaluate the atrial substrate modification.

EGMs are mainly recruited for AF substrate mapping in order to detect any areas that provoke or perpetuate AF and indicate them as candidate CA targets after CA of PVs. This is especially important for persistent AF patients, where additional CA is often necessary in order to increase the CA efficiency. Hence, AF mapping via EGMs is an indispensable part of the CA procedure. On the other hand, with the ability to observe the atria universally, ECGs' main application is found in predicting the CA outcome by either assessing the atrial substrate modification or by analyzing electrical characteristics of the atrial component of the ECG from recordings acquired prior to CA. For recordings during AF, these are the f-waves, while for recordings in sinus rhythm (SR), these are the P-waves.

Despite the extensive analysis on either recording types, some significant gaps exist. Additional CA out of PVs increases significantly the time spent in operation room, provoking higher health risks and increasing the healthcare costs. Furthermore, whether additional CA is actually beneficial regarding the CA outcome is under dispute. Regarding the atrial substrate modification analysis, various thresholds have been adopted in order to define a prolonged P-wave, which is directly connected with the atrial substrate and poor CA prognostics. Additionally, data acquired from P-wave analysis are quite generic, refering to the entire atria, while analysis could be improved by providing more specific information.

The main objective of the present Doctoral Dissertation is to contribute to the effort of mapping the atrial substrate and atrial susbtrate modification. In order to reach that goal, the present Thesis has been developed under two main hypotheses. That the quality of information that is extracted during the atrial substrate and atrial substrate modification analysis can be improved by introducing innovative steps that achieve more exclusive and to the point information. Also, that combining ECG and EGM analysis can augment the AF mapping resolution and reveal important information regarding AF and its mechanisms.

To accomplish the main objective, the analysis is split in four parts, forming the four chapters of the Compendium of publications, based on the main hypotheses arosen. In the first part, coarse-grained correlation dimension (CGCD) has been recruited in order to contribute to more effective detection of AF drivers. CGCD was able to reliably localize the EGMs of higher complexity and the overall classification by all three AF types (I–III) yielded 84% accuracy in the worst case. In second place, an alternative P-wave analysis has been suggested, by studying separately the first and second P-wave parts, corresponding to the right (RA) and left (LA) atrium, respectively. The findings highlighted LA as the major source of atrial substrate modification after CA of PVs and underlined the importance and benefits of studying integral parts of atrial and atrioventricular (AV) components of the ECG, allowing the extraction of more relevant information. The findings of this study additionally suggest the implementation of separate first and second P-wave parts as a possible alleviation for the discrepancies in P-wave thresholds used to define a fibrotic atrial tissue.

In line with this rationale, which forms part of the main hypothesis, the different effect of left (LPVI) and right pulmonary vein isolation (RPVI) on the atrial substrate modification has been studied. This analysis aimed to increase awareness on CA mechanisms and how they interact with the underlying AF mechanisms. LPVI has been found to be the critical part of the CA procedure, being the exclusive source of P-wave shortening. The use of recordings obtained during CA has additionally allowed a more close observation of the heart rate variability (HRV) fluctuations throughout the CA procedure, revealing information regarding the effect of radiofrequency (RF) energy on the atrial tissue.

The last part of the analysis was focused on coronary sinus (CS), a fundamental atrial structure in AF mapping, in order to increase the information resolution and to take profit of already available yet unexploited resources. The most and least robust channels during sinus rhythm (SR) were defined and the utility of CS in atrial substrate modification evaluation was investigated. Although CS was not able to provide a global picture of the atrial substrate alteration, as P-waves do, it was able to record with higher sensitivity and precision the fluctuations in the atrial response during the application of the RF energy. The findings presented in this Doctoral Dissertation offer an alternative perspective on the atrial substrate modification and contribute to the overall effort on AF mapping and post-CA substrate evaluation, opening future lines of research towards a higher resolution and more efficient mapping of the AF drivers.

Resumen

La fibrilación auricular (FA) sigue siendo la arritmia cardíaca más común y afecta actualmente al $2-4\%$ de la población adulta mundial. Teniendo en cuenta la tendencia actual de la longevidad, el pronóstico de prevalencia de FA en los próximos años es desalentador, mientras que la calidad de vida de las personas con FA a menudo se ve afectada negativamente. A pesar de la gran popularidad de la ablación con catéter (AC) como el principal tratamiento de la FA, todavía hay espacio y necesidad de mejora, especialmente en pacientes con FA persistente. El tiempo del paciente en FA tiene un impacto significativo en la confrontación y evolución de la FA, con $1-15\%$ de pacientes con FA paroxística que progresan a FA persistente anualmente, por lo que enfrentan mayores complicaciones con respecto a la terapia de FA. Por lo tanto, desde el diagnóstico temprano hasta la terapia de seguimiento posterior, todos los aspectos del estudio de la FA que pueden contribuir a su confrontación son de alta importancia.

La AC de las venas pulmonares (VPs) se basa en la consideración de las VPs como focos primarios de FA. No obstante, múltiples sitios de las aurículas pueden contribuir a la propagación de la FA, ya sea desencadenando o manteniendo los focos de FA. El sustrato auricular o de FA es el término utilizado para describir todas estas regiones auriculares que están involucradas con la actividad de la FA debido a trastornos anatómicos que provocan alteraciones eléctricas o funcionales. La cartografía precisa del sustrato auricular y el registro confiable de la modificación del sustrato auricular, como marcador positivo después de las sesiones de AC, son fundamentales en la lucha contra la FA. Los electrocardiogramas (ECGs) y los electrogramas (EGMs) se emplean ampliamente para mapear el sustrato auricular o evaluar su modificación.

Los EGMs se reclutan principalmente para el mapeo del sustrato de FA con el fin de detectar áreas que provoquen o perpetúen la FA e indicarlas como objetivos de AC candidatos fuera de las VPs. Esto es especialmente importante para los pacientes con FA persistente, en los que suele ser necesaria una AC adicional para aumentar la eficacia de la primera AC. Por lo tanto, el mapeo de FA mediante EGMs es una parte indispensable del procedimiento de la AC. Por otro lado, con la capacidad de observar la actividad eléctrica auricular globalmente, la aplicación principal de los ECGs se encuentra en la predicción del resultado de la AC evaluando la modificación del sustrato auricular o analizando las características eléctricas del componente auricular en el ECG a partir de registros adquiridos antes de la AC. Para registros durante FA, estas son las ondas f, mientras que para registros durante ritmo sinusal (RS), estas son las ondas P.

A pesar del extenso análisis de cualquiera de los tipos de registro, existen algunas brechas significativas. La AC adicional fuera de las VPs aumenta significativamente el tiempo de permanencia en el quirófano, lo que provoca mayores

riesgos para la salud y aumenta los costes de atención médica. Además, se discute si la AC adicional es realmente beneficiosa con respecto al resultado de la AC de VPs exclusivamente. En cuanto al análisis de la modificación del sustrato auricular, se han adoptado varios umbrales para definir una onda P prolongada, lo que está directamente relacionado con la existencia de sustrato auricular y el mal pronóstico de la AC. Además, los datos adquiridos a partir del análisis de ondas P son bastante genéricos y se refieren a todo el tejido auricular, mientras que el análisis podría mejorarse aún más proporcionando información más específica.

El principal objetivo de la presente Tesis Doctoral es contribuir al esfuerzo de mapeo del sustrato auricular y su modificación tras la AC. Para alcanzar ese objetivo, la presente Tesis se ha desarrollado bajo dos hipótesis principales. Que la calidad de la información que se extrae durante el análisis del sustrato auricular y de su modificación puede mejorarse introduciendo innovadores pasos que logren información más exclusiva y precisa. Además, la combinación de análisis de ECG y EGM puede aumentar la resolución del mapeo de FA y revelar información importante sobre la FA y sus mecanismos.

Para cumplir con el objetivo principal, el análisis se divide en cuatro partes, conformando los cuatro capítulos del Compendio de publicaciones, a partir de las principales hipótesis planteadas. En la primera parte, se ha reclutado la dimensión de correlación de grano grueso (DCGG) para contribuir a una detección más eficaz de los factores desencadenantes de la FA. La DCGG pudo localizar de manera confiable los EGMs de mayor complejidad y la clasificación general en los tres tipos de FA arrojó una precisión de 84% en el peor de los casos. En segundo lugar, se ha sugerido un análisis alternativo de la onda P, estudiando por separado la primera y la segunda parte de la onda P, correspondientes a la aurícula derecha (AD) e izquierda (AI), respectivamente. Los hallazgos destacaron a AI como la principal fuente de alteraciones en el tejido auricular después de AC de VPs y subrayaron la importancia y los beneficios de estudiar partes integrales de los componentes auriculares y auriculoventriculares (AV) del ECG, lo que permite la extracción de información más relevante. Los hallazgos de este estudio también sugieren el estudio por separado de la primera y segunda parte de la onda P como un posible alivio de las discrepancias en los umbrales de onda P utilizados para definir un tejido auricular fibrótico.

De acuerdo con este razonamiento, que forma parte de la hipótesis principal, se ha estudiado el efecto diferente del aislamiento de las venas pulmonares izquierda (AVPIs) y derechas (AVPDs) en la modificación del sustrato auricular. Este análisis tuvo como objetivo aumentar la conciencia sobre los mecanismos de AC y cómo interactúan con los mecanismos subyacentes de la FA. Se ha encontrado que AVPI es la parte crítica del procedimiento de AC, siendo la fuente exclusiva del acortamiento de la onda P. El uso de registros obtenidos durante la AC ha permitido además una observación más cercana de las fluctuaciones de la variabilidad de la frecuencia cardíaca (VFC) a lo largo del procedimiento de AC, lo que revela información sobre el efecto de la energía de radiofrecuencia (RF) en el tejido auricular.

La última parte del análisis se ha centrado en el seno coronario (SC), una estructura auricular fundamental en el mapeo de la FA, para aumentar la resolución de la información y aprovechar los recursos ya disponibles pero no explotados. Se definieron los canales más y menos robustos durante el RS y se investigó la utilidad del SC en la evaluación de la modificación del sustrato auricular. Aunque el SC no pudo proporcionar una imagen global de la alteración del sustrato auricular, como lo hacen las ondas P, pudo registrar con mayor sensibilidad y precisión las fluctuaciones en la respuesta auricular durante la aplicación de energía de RF. Los hallazgos presentados en esta Tesis Doctoral ofrecen una perspectiva alternativa sobre la modificación del sustrato auricular y contribuyen al esfuerzo general sobre el mapeo de la FA y la evaluación del sustrato posterior a la AC, abriendo futuras líneas de investigación hacia una mejor resolución y un mapeo más eficiente de los mecanismos desencadenantes de la FA.

Resum

La fibril·lació auricular (FA) continua sent l'arítmia cardíaca més comuna i afecta actualment el $2-4\%$ de la població adulta mundial. Tenint en compte la tendència actual de la longevitat, el pronòstic de prevalença de FA en els propers anys és descoratjador, mentre que la qualitat de vida de les persones amb FA sovint es veu afectada negativament. Tot i la gran popularitat de l'ablació amb catèter (AC) com el principal tractament de la FA, encara hi ha espai i necessitat de millora, especialment en pacients amb FA persistent. El temps del pacient en FA té un impacte significatiu en la confrontació i evolució de la FA, amb $1-15\%$ de pacients amb FA paroxística que progressen a FA persistent anualment, per la qual cosa enfronten més complicacions respecte a la teràpia de FA. Per tant, des del diagnòstic primerenc fins a la teràpia de seguiment posterior, tots els aspectes de l'estudi de la FA que poden contribuir a la seva confrontació són d'alta importància.

L'AC de les venes pulmonars (VPs) es basa en la consideració de les PV com a focus primaris de FA. Això no obstant, múltiples llocs de les aurícules poden contribuir a la propagació de la FA, ja sigui desencadenant o mantenint els focus de FA. El substrat auricular o de FA és el terme utilitzat per descriure totes aquestes regions auriculars que estan involucrades amb l'activitat de la FA a causa de trastorns anatòmics que provoquen alteracions elèctriques o funcionals. La cartografia precisa del substrat auricular i el registre fiable de la modificació del substrat auricular, com a marcador positiu després de les sessions d'AC, són fonamentals en la lluita contra la FA. Els electrocardiogrames (ECGs) i els electrogrames (EGMs) s'utilitzen àmpliament per mapejar el substrat auricular o avaluar-ne la modificació.

Els EGM es recluten principalment per al mapeig del substrat de FA per tal de detectar àrees que provoquin o perpetuïn la FA i indicar-les com a objectius d'AC candidats fora de les VPs. Això és especialment important per als pacients amb FA persistent, en què sol ser necessària una AC addicional per augmentar l'eficàcia de la primera AC. Per tant, el mapeig de FA mitjançant EGM és una part indispensable del procediment de l'AC. D'altra banda, amb la capacitat d'observar globalment l'activitat elèctrica auricular, l'aplicació principal dels ECG es troba en la predicció del resultat de l'AC avaluant la modificació del substrat auricular o analitzant les característiques elèctriques del component auricular a l'ECG a partir registres adquirits abans de l'AC. Per a registres durant AF, aquestes són les ones f, mentre que per a registres durant ritme sinusal(RS), aquestes són les ones P.

Tot i l'extensa anàlisi de qualsevol dels tipus de registre, hi ha algunes bretxes significatives. L'AC addicional fora de les VP augmenta significativament el temps de permanència al quiròfan, la qual cosa provoca més riscos per a la salut

i augmenta els costos d'atenció mèdica. A més, es discuteix si lAC addicional és realment beneficiosa respecte al resultat de lAC de VPs exclusivament. Quant a l'anàlisi de la modificació del substrat auricular, s'han adoptat diversos llindars per definir una ona P perllongada, cosa que està directament relacionada amb l'existència de substrat auricular i el mal pronòstic de l'AC. A més, les dades adquirides a partir de l'anàlisi d'ones P són força genèriques i es refereixen a tot el teixit auricular, mentre que l'anàlisi es podria millorar encara més proporcionant informació més específica.

El principal objectiu de la present Tesi Doctoral és contribuir a l'esforç de mapatge del substrat auricular i la seva modificació després de l'AC. Per assolir aquest objectiu, aquesta Tesi s'ha desenvolupat sota dues hipòtesis principals. Que la qualitat de la informació que s'extreu durant l'anàlisi del substrat auricular i de la seva modificació es pot millorar introduint passos innovadors que aconsegueixin informació més exclusiva i precisa. A més, la combinació d'anàlisi d'ECG i EGM pot augmentar la resolució del mapeig d'AF i revelar informació important sobre la FA i els seus mecanismes.

Per tal de complir l'objectiu principal, l'anàlisi es divideix en quatre parts i es conforma els quatre capítols del Compendi de publicacions, a partir de les principals hipòtesis plantejades. A la primera part, s'ha reclutat la dimensió de correlació de gra gruixut (DCGG) per contribuir a una detecció més eficaç dels factors desencadenants de la FA. La DCGG va poder localitzar de manera fiable els EGM de més complexitat i la classificació general en els tres tipus d'AF va donar una precisió de 84% en el pitjor dels casos. En segon lloc, s'ha suggerit una anàlisi alternativa de l'ona P, estudiant per separat la primera i la segona part de l'ona P, corresponents a l'aurícula dreta (AD) i esquerra (AI), respectivament. Les troballes van destacar AI com la principal font d'alteracions en el teixit auricular després d'AC de VPs i van subratllar la importància i els beneficis d'estudiar parts integrals dels components auriculars i auriculoventriculars (AV) de l'ECG, cosa que permet l'extracció de informació més rellevant. Les troballes d'aquest estudi també suggereixen l'estudi per separat de la primera i la segona part de l'ona P com un possible alleugeriment de les discrepàncies en els llindars d'ona P utilitzats per definir un teixit auricular fibròtic.

D'acord amb aquest raonament, que forma part de la hipòtesi principal, s'ha estudiat l'efecte diferent de l'aïllament de les venes pulmonars esquerra (AVPI) i dretes (AVPD) en la modificació del substrat auricular. Aquesta anàlisi va tenir com a objectiu augmentar la consciència sobre els mecanismes dAC i com interactuen amb els mecanismes subjacents de la FA. S'ha trobat que AVPI és la part crítica del procediment d'AC, la font exclusiva de l'escurçament de l'ona P. L'ús de registres obtinguts durant l'AC ha permès a més una observació més propera de les fluctuacions de la variabilitat de la freqüència cardíaca (VFC) al llarg del procediment d'AC, cosa que revela informació sobre l'efecte de l'energia de radiofreqüència (RF) en el teixit auricular.

L'última part de l'anàlisi s'ha centrat en el si coronari (SC), una estructura auricular fonamental al mapeig de la FA, per augmentar la resolució de la infor-

mació i aprofitar els recursos ja disponibles però no explotats. Es van definir els canals més i menys robustos durant l'RS i es va investigar la utilitat de l'SC en l'avaluació de la modificació del substrat auricular. Tot i que l'SC no va poder proporcionar una imatge global de l'alteració del substrat auricular, com ho fan les ones P, va poder registrar amb més sensibilitat i precisió les fluctuacions a la resposta auricular durant l'aplicació d'energia de RF. Les troballes presentades en aquesta Tesi Doctoral ofereixen una perspectiva alternativa sobre la modificació del substrat auricular i contribueixen a l'esforç general sobre el mapatge de la FA i l'avaluació del substrat posterior a l'AC, obrint futures línies de recerca cap a una millor resolució i un mapatge més eficient dels mecanismes desencadenants de la FA.

Acknowledgments

This Doctoral Dissertation is a fruit of many efforts, times of distress and times of delight, bright and less bright ideas. But more than anything, this Doctoral Dissertation is a product of discussion, agreements and disagreements and continuous interchange of opinions and scientific knowledge, the very substance of investigation. I would like to express my gratitude to all those who have helped me in their way to make it until the end.

I would like to thank my supervisors, José Joaquín Rieta and Raúl Alcaraz, for giving me the opportunity to conduct this Thesis, for their continuous support and guidance, their priceless advice and inspiration, that have helped my way along this Doctoral Dissertation. Their expertise has been proved invaluable for the realization of this Thesis, which, I hope, can contribute to the improvement of the substrate modification analysis. At this point, I would also like to thank all those people whom I have shared the office with, for a shorter or longer time as well as all the members of the Cuenca group with whom I shared a really nice time during conferences.

Finally, I could not thank enough all those people that are close to me, for their immense support and love, their encouragement, their enthusiasm. Our endless conversations, both in person and by phone, your perspective on how the world should be and your kindness have a huge impact on who I am. Even the slightest bit of support and inspiration means the world to me.

Contents

Motivation, Hypothesis and Objectives

Contents

1.1 Structure of the compendium of publications

Study of the heart as a source of electricity dates back some thousands years ago and heads to the East, pointing out to chinese medicine [1]. In the later history, from the first kymograph to the first ECG depicting atrial fibrillation (AF) and from there to the discovery of pulmonary veins (PVs) as the principal source of AF, almost 200 years of scientific and medical discoveries have marked a steadily evolving trajectory that brings scientific community to today [2–4]. Entering the 21st century, an emerging number of studies have and are still investigating the mechanisms that make AF persist despite all the achievements and discoveries.

More of a philosophical than a scientific observation, the heart is a complex mechanism with no identical twin, unique for each individual, ever-changing, susceptible to each individual's natural and chemical processes. Following this rationale, personalized medicine has emerged in the field of cardiology with the objective to adapt generic observations regarding cardiac functions and AF mechanisms to each patient's needs and individual anatomy, giving birth to personalized mapping, the detection of any anatomical or electrical alterations in the atria that indicate the existence of pathologies favoring the AF. Although personalized mapping is nowadays a standard process during catheter ablation (CA) of AF and despite the attempts for extra-PV CA, AF recurrence is still a fact for many patients. As a consequence, a vast number of studies strive for providing new aspects on the AF mapping procedure. The present Doctoral Dissertation aims to contribute to this effort. Powered by the principle that evolution not only consists of searching for the new but also of questioning, reconsidering and decon-

structing what is already established, the work described in this Dissertation is a compendium of four research papers and a complementary study dealing with multiple scenarios regarding rhythm and type of AF patients entering the room for CA of PVs.

The papers included in the compendium are listed here in a chapter-wise order. An abstract of the complementary research, which is presented in Appendix A, is also provided after brief presentation of the published articles. Information on paper titles, authors, abstracts, the journals in which they were published as well as the corresponding chapter of the present Doctoral Dissertation is enclosed. In order to provide a more consistent presentation of the study conducted and to increase readability, two chapters share different adapted parts of the same research paper. In the beginning of each chapter, information on each paper's title, authors and journal of publication is provided. Appendix C includes the full version of each paper.

1.1.1   Abstracts of publications

Short-Time Estimation of Fractionation in Atrial Fibrillation with Coarse-Grained Correlation Dimension for Mapping the Atrial Substrate [5].

Aikaterini Vraka, Fernando Hornero, Vicente Bertomeu-González, Joaquín Osca, Raúl Alcaraz and José J. Rieta. *Entropy*, vol. 22, Issue 2, p. 232, 2020. Impact factor in 2020: 2.524, Q2 in " PHYSICS, MULTIDISCIPLINARY" (Journal Citation Reports - Web of Science, JCR-WOS).

Atrial fibrillation (AF) is currently the most common cardiac arrhythmia, with catheter ablation (CA) of the pulmonary veins (PV) being its first line therapy. Ablation of complex fractionated atrial electrograms (CFAEs) outside the PVs has demonstrated improved long-term results, but their identification requires a reliable electrogram (EGM) fractionation estimator. This study proposes a technique aimed to assist CA procedures under real-time settings. The method has been tested on three groups of recordings: Group 1 consisted of 24 highly representative EGMs, eight of each belonging to a different AF Type. Group 2 contained the entire dataset of 119 EGMs, whereas Group 3 contained 20 pseudo-real EGMs of the special Type IV AF. Coarse-grained correlation dimension (CGCD) was computed at epochs of 1 s duration, obtaining a classification accuracy of 100% in Group 1 and 84.0–85.7% in Group 2, using 10-fold cross-validation. The receiver operating characteristics (ROC) analysis for highly fractionated EGMs, showed 100% specificity and sensitivity in Group 1 and 87.5% specificity and 93.6% sensitivity in Group 2. In addition, 100% of the pseudo-real EGMs were correctly identified as Type IV AF. This method can consistently express the fractionation level of AF EGMs and provides better performance than previous works. Its abil-

ity to compute fractionation in short-time can agilely detect sudden changes of AF Types and could be used for mapping the atrial substrate, thus assisting CA procedures under real-time settings for atrial substrate modification.

Splitting the P-Wave: Improved Evaluation of Left Atrial Substrate Modification after Pulmonary Vein Isolation of Paroxysmal Atrial Fibrillation [6].

Aikaterini Vraka, Vicente Bertomeu-González, Fernando Hornero, Aurelio Quesada, Raúl Alcaraz and José J. Rieta. *Sensors*, vol. 22, Issue 1, p. 290, 2021. Impact factor in 2021: 3.847, Q2 in " INSTRUMENTS & INSTRUMENTATION" (Journal Citation Reports - Web of Science, JCR-WOS).

Atrial substrate modification after pulmonary vein isolation (PVI) of paroxysmal atrial fibrillation (pAF) can be assessed non-invasively by analyzing P-wave duration in the electrocardiogram (ECG). However, whether right (RA) and left atrium (LA) contribute equally to this phenomenon remains unknown.
The present study splits fundamental P-wave features to investigate the different RA and LA contributions to P-wave duration. Recordings of 29 pAF patients undergoing first-ever PVI were acquired before and after PVI. P-wave features were calculated: P-wave duration (PWD), duration of the first ($PWD_{on\text{-}peak}$) and second ($PWD_{peak\text{-}off}$) P-wave halves, estimating RA and LA conduction, respectively. P-wave onset (PW_{on}-R) or offset (PW_{off}-R) to R-peak interval, measuring combined atrial/atrioventricular and single atrioventricular conduction, respectively. Heart-rate fluctuation was corrected by scaling. Pre- and post-PVI results were compared with Mann–Whitney U-test. PWD was correlated with the remaining features. Only PWD (non-scaling: $\Delta = -9.84\%$, $p = 0.0085$, scaling: $\Delta = -17.96\%$, $p = 0.0442$) and $PWD_{peak\text{-}off}$ (non-scaling: $\Delta = -22.03\%$, $p = 0.0250$, scaling: $\Delta = -27.77\%$, $p = 0.0268$) were decreased. Correlation of all features with PWD was significant before/after PVI ($p < 0.0001$), showing the highest value between PWD and PW_{on}-R ($\rho_{max} = 0.855$). PWD correlated more with $PWD_{on\text{-}peak}$ ($\rho = 0.540$–0.805) than $PWD_{peak\text{-}off}$ ($\rho = 0.419$–0.710). PWD shortening after PVI of pAF stems mainly from the second half of the P-wave. Therefore, noninvasive estimation of LA conduction time is critical for the study of atrial substrate modification after PVI and should be addressed by splitting the P-wave in order to achieve improved estimations.

The Dissimilar Impact in Atrial Substrate Modification of Left and Right Pulmonary Veins Isolation after Catheter Ablation of Paroxysmal Atrial Fibrillation [7].

Aikaterini Vraka, Vicente Bertomeu-González, Lorenzo Fácila, José Moreno-Arribas, Raúl Alcaraz and José J. Rieta. *Journal of Personalized Medicine*, vol. 12, Issue 3, p. 462, 2022. Impact factor in 2021: 3.508, Q2

Since the discovery of pulmonary veins (PVs) as foci of atrial fibrillation (AF), the commonest cardiac arrhythmia, investigation revolves around PVs catheter ablation (CA) results. Notwithstanding, CA process itself is rather neglected. We aim to decompose crucial CA steps: coronary sinus (CS) catheterization and the impact of left and right PVs isolation (LPVI, RPVI), separately. We recruited 40 paroxysmal AF patients undergoing first-time CA and obtained five-minute lead II and bipolar CS recordings during sinus rhythm (SR) before CA (**B**), after LPVI (**L**) and after RPVI (**R**). Among others, duration, amplitude and atrial-rate variability (ARV) were calculated for P-waves and CS local activation waves (LAWs). LAWs features were compared among CS channels for reliability analysis. P-waves and LAWs features were compared after each ablation step (**B**, **L**, **R**). CS channels: amplitude and area were different between distal/medial ($p \leq 0.0014$) and distal/mid-proximal channels ($p \leq 0.0025$). Medial and distal showed the most and least coherent values, respectively. Correlation was higher in proximal ($\geq 93\%$) than distal ($\leq 91\%$) areas. P-waves: duration was significantly shortened after LPVI (after **L**: $p = 0.0012$, -13.30%). LAWs: insignificant variations. ARV modification was more prominent in LAWs (**L**: $> +73.12\%$, $p \leq 0.0480$, **R**: $< -33.94\%$, $p \leq 0.0642$). Medial/mid-proximal channels are recommended during SR. CS LAWs are not significantly affected by CA but they describe more precisely CA-induced ARV modifications.

The Relevance of Heart Rate Fluctuation When Evaluating Atrial Substrate Electrical Features in Catheter Ablation of Paroxysmal Atrial Fibrillation [8].

Aikaterini Vraka, José Moreno-Arribas, Juan M. Gracia-Baena, Fernando Hornero, Raúl Alcaraz and José J. Rieta. *Journal of Cardiovascular Development and Disease*, vol. 9, Issue 6, p. 176, 2022.

Atrial substrate modification after pulmonary vein isolation (PVI) of paroxysmal atrial fibrillation (pAF) can be assessed non-invasively by analyzing P-wave duration in the electrocardiogram (ECG). However, whether right (RA) and left atrium (LA) contribute equally to this phenomenon remains unknown. The present study splits fundamental P-wave features to investigate the different RA and LA contributions to P-wave duration. Recordings of 29 pAF patients undergoing first-ever PVI were acquired before and after PVI. P-wave features were calculated: P-wave duration (PWD), duration of the first ($PWD_{on\text{-}peak}$) and second ($PWD_{peak\text{-}off}$) P-wave halves, estimating RA and LA conduction, respectively. P-wave onset ($PW_{on}\text{-}R$) or offset ($PW_{off}\text{-}R$) to R-peak interval, measur-

ing combined atrial/atrioventricular and single atrioventricular conduction, respectively. Heart-rate fluctuation was corrected by scaling. Pre- and post-PVI results were compared with Mann–Whitney U-test. PWD was correlated with the remaining features. Only PWD (non-scaling: $\Delta = -9.84\%$, $p = 0.0085$, scaling: $\Delta = -17.96\%$, $p = 0.0442$) and $PWD_{peak\text{-}off}$ (non-scaling: $\Delta = -22.03\%$, $p = 0.0250$, scaling: $\Delta = -27.77\%$, $p = 0.0268$) were decreased. Correlation of all features with PWD was significant before/after PVI ($p < 0.0001$), showing the highest value between PWD and PW_{on}-R ($\rho_{max} = 0.855$). PWD correlated more with $PWD_{on\text{-}peak}$ ($\rho = 0.540$–0.805) than $PWD_{peak\text{-}off}$ ($\rho = 0.419$–0.710). PWD shortening after PVI of pAF stems mainly from the second half of the P-wave. Therefore, noninvasive estimation of LA conduction time is critical for the study of atrial substrate modification after PVI and should be addressed by splitting the P-wave in order to achieve improved estimations.

1.1.2   Abstract of complementary research

The adopted atrial substrate modification analysis technique after CA of AF depends on many factors such as cardiac rhythm, AF or recording type. How different information acquired via variable sources can be combined to offer a more detailed and less dependent analysis remains unknown. The aim of the present analysis step is to investigate any relationships between CA recordings acquired during different scenarios regarding CA of PVs.

Two databases were utilized. Database A: 18 persistent and paroxysmal AF patients undergoing CA of PVs. Two-minute ECG and bipolar CS recordings were extracted before (in AF) and two-minute ECG recordings were extracted after (in SR) AF at 1 kHz sampling frequency. Database B: 37 persistent and paroxysmal AF patients undergoing CA of PVs and DF sites. Ten-second ECG and bipolar CS recordings before CA (in AF) were extracted at a sampling frequency of 977 Hz and were resampled to 1 kHz. For both databases, leads V1 and II were chosen for analysis before and after CA, respectively, for ECG recordings. The highest-amplitude channel was selected for CS recordings. Recordings were denoised and, in case of lead II, ectopics cancellation was performed, if necessary. Spectral and nonlinear characteristics were calculated for V1 recordings, including dominant frequency (DF) and first harmonic (f_1) and their power spectral densities, median frequency (f_m) and sample entropy. Analysis on lead II recordings was performed recruiting P-waves features, while analysis on bipolar CS recordings was performed through CGCD analysis to calculate the organization of the AF dynamics. Correlation analysis was split in three parts, searching in the first place correlation between lead V1 and CS recordings before CA (databases A and B), then investigating the relationship between lead V1 and II recordings acquired before and after CA (database B), respectively and finishing with the investigation on correlations between CS recordings before CA and lead II recordings after CA (database B).

Results were in all cases poor to moderate. For the lead V1-CS correlation analysis (in AF) before CA, moderate results between CGCD and DF of f_1 were found (up to 48.68%, $p < 0.0340$). When separated into two categories, with low and high values, CGCD failed to predict sufficiently the class of V1 characteristics, showing classification accuracy of about $57 - 76\%$. CGCD also failed to predict the CA outcome in database B, showing classification accuracy of 59.46%, $p = 0.6839$. For the correlations between ECG recordings before (in AF) and after CA (in SR), f_m showed the highest positive and negative correlations, which were in the best case moderate (up to -66.8%, significant p: $p < 0.05$). For correlations between bipolar CS recordings before CA (in AF) and lead II recordings after CA (in SR), none of the P-wave features showed high or statistically significant correlations with CGCD values of CS recordings. The results indicate very poor relationships between surface and invasive recordings even during the same cardiac rhythm. These relationships become even weaker when the level of discrepancies augments. CGCD calculated from CS recordings failed to predict the AF outcome in CA of PVs and DF sites.

1.2   Motivation

AF is currently the most common cardiac arrhythmia in clinical practice [9, 10]. Showing a fast-growing incidence, AF prevalence is estimated at 2-4% of global adult population and is expected to increase by +60% within the next 30 years, hence considered a major health threat for the western world. Life-expectancy prolongation is an aggravating factor that is thought to directly affect the AF incidence, as increasing age is an AF predictor [10]. Strong association with heart failure, stroke, valvular heart disease and cognitive impairment as well as increased mortality contribute to the major health and quality of life impact that AF can provoke [10–15]. Regular follow-up including hospitalization and medication implies that AF requires additionally significant economical resources. Considering all the afore aspects, AF handling is an exigent multitasking process that requires efficient planning and collaboration among experts of various fields.

AF episodes self-terminating in less than 7 days are characterized as paroxysmal AF. When AF episodes are sustained for more than 7 days and up to 12 months, they are called persistent AF, while AF episodes longer than a year that can only be terminated by medical interventions are called long-lasting persistent AF. AF progress is manifested with structural, mechanical or electrical remodeling, generally described under the term atrial remodeling (AR), that sustains the AF activity and assists the AF propagation [16–18]. These mechanisms are more frequently found in persistent AF, complicating the treatment and significantly aggravating the health burden of these patients [10,15,18–20]. Early AF detection is critical in controling and inhibiting the AF activity, preventing from or mitigating significant health complications and AF progression that can also cause resistance to AF-related medication [21].

Catheter ablation (CA) of pulmonary veins (PVs) is the star AF treatment, since PVs are considered the principal foci [4, 10]. CA is especially beneficial for paroxysmal AF patients, with persistent AF patients often requiring repetitive CA sessions [10]. AF substrate, which consists of remodeled areas being more dominant in persistent AF patients, is thought to assist the AF propagation or even trigger the AF outbreak. Therefore, many studies focus on detecting the remodeled sites in order to serve as possible CA targets with the aim to increase the CA efficiency [10, 18, 20].

AF confrontation strategy should be customized upon patients' needs and relies on multiple factors. Awareness on AF-related symptoms is crucial in detecting asymptomatic AF, allowing the experts to act on time and prevent from significant worsening of the overall health condition and AF progression as well as facilitating proper classification. With that being said, characterization of the AF substrate and quantification of the burden of AF is of paramount importance and a field of continuous investigation in search of a constantly improved method that yields higher precision in detecting and evaluating fibrillatory drivers. Research has been adapted to patient-specific health conditions at the time of monitoring and various methods of AF analysis exist according to cardiac rhythm (AF or SR) or AF confrontation strategy.

AF substrate analysis can be performed either noninvasively or via intracardiac recordings mapping the atria [17, 18]. The use of electrocardiograms (ECG) is a widespread noninvasive method, allowing the assessment of the AF substrate [10]. Depending on the cardiac rhythm during the recordings, f-wave or P-wave parameters are studied in order to extract AF mechanism- or atrial remodeling-related information [22–39]. On the other hand, the high advantage of intracardiac recordings, called electrograms (EGMs), over ECGs, is the higher proximity to the atrial tissue, allowing a more detailed perspective of the studied mechanisms [17, 18]. EGM analysis is vastly used during AF mapping in order to define the candidate CA targets in the first place or to detect markers foreboding the AF recurrence [17, 40–42].

Despite the high effort on predicting or defining the optimal CA targets in order to improve the CA outcome, AF recurrence is still a fact for many patients, while low consensus exists regarding the efficiency of additional CA [10, 43, 44]. Therefore, more meticulous studies regarding the AF substrate as well as the CA procedure are needed. Combined ECG and EGM analysis, utilizing each ones advantages, could act synergistically to improve the AF substrate mapping information as well as to provide new insights in the characterization of the fibrillatory drivers sustaining AF.

1.3   Initial Hypothesis

AF ectopic activity is mainly found in PVs due to specific electrophysiological properties favoring the generation of ectopic impulses [4, 45]. Increased time

spent in AF alters the anatomy, function and electrical properties of the atria, a process called AR, leading to the triggering or preservation of the ectopic activations [16–18]. Although AR is more prominent in persistent than paroxysmal AF patients and in left (LA) than right atrium (RA), non-PV drivers can also be found in paroxysmal AF patients as well as in RA [10, 15, 16, 46]. Therefore, personalized mapping is necessary in order to detect candidate non-PV CA targets that could improve the CA outcome.

Many studies have focused on defining the optimal technique to detect non-PV targets and predict the CA outcome in order to optimize the personalized follow-up therapy. Noninvasively, atrial substrate is assessed before and after CA sessions in order to evaluate the feasibility of non-PV CA and to estimate the AF recurrence probability. For this purpose, P- and f-waves are mainly recruited to analyze recordings during SR and AF, respectively [22, 24, 25, 27–39, 47]. With the high advantage of proximity to the atrial tissue, invasive recordings are the principal source of direct AF driver mapping. EGMs recorded from zones with specific electrical characteristics indicating fibrotic tissue are recruited for this purpose, with high dominant frequency (DF), signal complexity and low voltage (LV) being preeminent indicators of fibrosis [17, 18, 40, 45, 48–55].

Despite the fact that AF susbtrate analysis has been the objective of many studies, vague definitions and threshold heterogeneity regarding the aforementioned techniques has led to contradictory results for non-PV CA [40, 43, 56]. As for the atrial substrate evaluation from ECGs, variable thresholds lead to different evaluation outcomes [30, 33, 35, 39, 57]. Considering the aforeposed issues, the initial hypothesis of the present Doctoral Thesis has been that *in detail analysis and reconsideration of elementary steps with respect to the AF confrontation and a combination of information from surface and invasive recordings may contribute to the extraction of unexploited information regarding the AF mechanisms. This information may be profitable in redesigning the AF confrontation strategy, adapted to each patient's needs and in achieving higher precision in the AF driver mapping.*

In order to extract novel information from such a well-investigated area, it is crucial to focus on the flaws of the current methods regarding AF mapping and atrial substrate evaluation and develop and suggest alternative algorithms and techniques that, if adopted, can increase significantly the amount and quality of information that can be extracted. This has been the original intention of this Doctoral Thesis.

1.4   Objectives

The main objective of ths Doctoral Thesis, as suggested by its title, is to contribute to the evaluation of the substrate modification after CA of AF. Given the amount and high quality of studies already dealing with this issue, the present Thesis is in the first place focused on the gaps that probably exist from the already developed methods aimed at the detection of candidate CA targets and at the prediction of

the CA outcome from the substrate modification analysis. After defining the main objective, the methodology has been designed consisting of smaller objectives that, cumulatively, can lead to the accomplishment of the main goal. For this purpose, five smaller-broadcast objectives have been defined. These were:

O$_1$. The development of tools able to detect with high precision fractionated EGMs, in order to define more strictly atrial zones in need of CA, mostly applied in persistent AF patients. This objective is focused on the flaws of the already existent methods for the AF mapping and attempts to contribute to the detection of active AF drivers.

O$_2$. To investigate whether RA and LA remodeling are equally affected after CA of PVs for paroxysmal AF patients. This objective attempts to provide more specific and detailed information on the substrate modification after CA of paroxysmal AF.

O$_3$. A step-by-step evaluation of CA of PVs procedure, investigating the side of PVs that is mostly affected from CA of PVs. This objective aims to study the interaction between active AF drivers and the CA procedure as well as the substrate modification progress throughout the CA procedure.

O$_4$. To investigate the capability and usefulness of critical for the CA atrial structures in the AF substrate modification evaluation. This objective aims to augment the AF substrate modification analysis resolution, by investigating the potential of invasive EGMs in the substrate modification analysis.

O$_5$. To investigate the interconnection between surface and invasive recordings, regardless of the AF type, the recordings' origin and the CA outcome. This objective attempts a less restrictive analysis of the substrate modification.

State of the art

Contents

2.1 Cardiac anatomy and blood circulation

The heart is a valvular, fibromuscular, hollow organ, the main purpose of which is to pump oxygenated blood throughout the body [58, 59]. It has the shape of an irregular cone and the size of a fist and weighs about 300 grams in adults [58, 59]. It is located in the middle mediastinum of the thorax, between right and left pleural sacs, with its anterior part being comprised at two-thirds of the right and at one-third of the left ventricle [58, 59]. The base of the heart borders with the anterior part of the oesophagus and the posterior part of the aorta. The anterior surface is located posterior to the sternum and the costal cartilages [59].

Pericardium surrounds the heart, holding and protecting it [59]. It consists of three layers, a layer of fibrous and two layers of serous pericardium [58]. Fibrous pericardium is the outermost layer. The first layer of serous pericardium is the parietal layer, which is attached to the inner surface of the fibrous pericardium. The final layer is called visceral layer or epicardium and is attached to the surface of the heart. Between parietal and visceral layers lies the pericardial cavity, which consists of a thin film of fluid and has two recesses: the transverse sinus and the oblique sinus [58, 59].

The inner wall of the heart is called endocardium. Between endocardium and epicardium lies myocardium, the thickest layer of the heart, comprised of cardiomyocytes, which are striated uninucleate muscle cells [60]. Myocardium is composed of four chambers: the right and left atria on the upper side and the right and left ventricles on the bottom side, which are in charge of pumping blood towards the body. These four chambers are attached to a figure of an eight-shaped fibrous skeleton that divides the atria and separates them electrically from the ventricles [59]. Cardiac layers are shown in Figure 2.1.
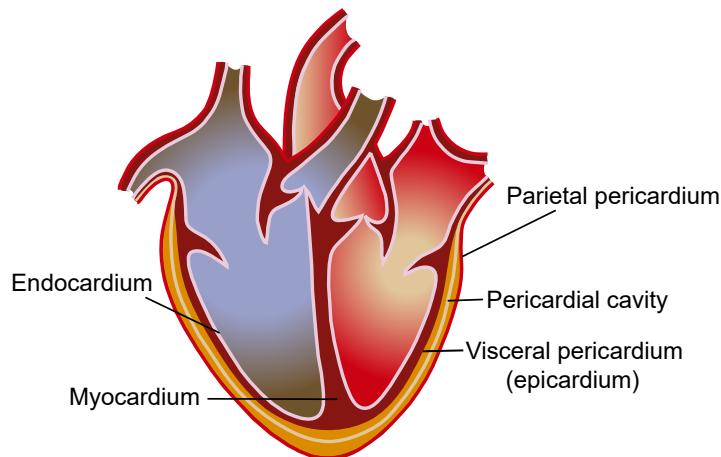
Figure 2.1: The layers of the heart [61]. Parietal pericardium is the outermost serous pericardium layer, while visceral pericardium is the innermost, attached to the surface of the heart. Pericardial cavity lies between them. Myocardium separates visceral pericardium from endocardium, which is the inner cardiac wall.

In RA are found some of the most important atrial structures. It contains crista and sulcus terminalis on the interior and the exterior side of the RA anterior wall, respectively. The posterior wall forms the interatrial septum. It is connected with the superior vena cava on the roof and the inferior vena cava and coronary sinus (CS) on the floor. To the left of CS is found tricuspid opening, which connects the RA with the right ventricle. The atrioventricular node (AV) is found above the CS opening, adjacent to the interatrial septum. The sinoatrial node (SA) is found in the junction of sulcus terminalis and superior vena cava. LA contains the PVs, which are found in the left atrial posterior wall. It is connected inferiorly with the left ventricle via the mitral opening. The right ventricle connects with the pulmonary trunk via the pulmonary valve, while the aortic valves intermediate between left ventricle and aortic root [58]. Figure 2.2 shows the cardiac chambers, while the main cardiac structures and nodes can be seen in Figure 2.3.

Veins carry deoxygenated blood from the organs to the heart and arteries carry oxygenated blood from the heart back to the organs across the body. Venous blood enters the heart through the RA, from the superior and inferior vena cava and flows towards the right ventricle through the tricuspid valve, which closes

once right ventricle fills with blood to prevent it from flowing backwards to the atria. Blood travels from the right ventricle to the pulmonary artery throught pulmonary valve and gets oxygenated in the capillaries of the right and left lungs. Oxygenated blood enters LA via PVs and flows towards left ventricle via the mitral valve. Finally, from the left ventricle, blood is pumped throughout the body via the aortic valve [62, 63]. In order to sustain the high haemodynamic pressure needed to distribute blood throughout the body, the left ventricular wall (10 mm) is two to three times as thick as the right ventricular wall ($3 - 5$ mm) [58, 59].
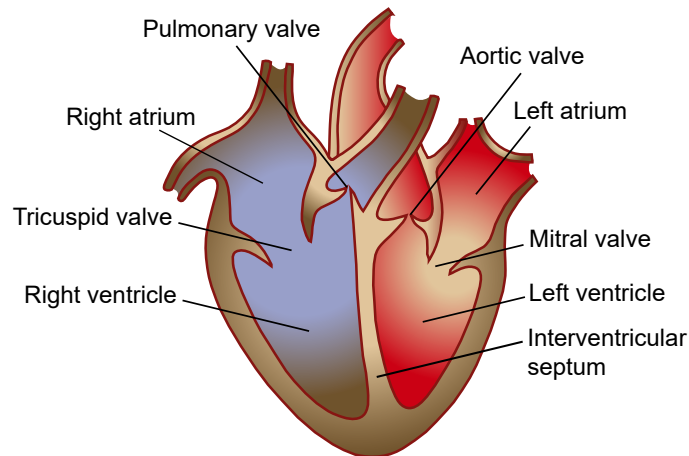
Figure 2.2: Cardiac valves and chambers [61]. RA and LA as well as right and left ventricle are the four chambers of the heart. RA connects with right ventricle via the tricuspid opening, separated by the tricuspid valve. LA, which contains the PVs, is connected with left ventricle via mitral opening, separated by the mitral valve. The aortic valve is found between the left ventricle and the aortic root.

2.2 Electrical activity of the heart

Blood circulation is achieved with the help of the cardiac contraction, allowing the pumping of the blood from the atria to the ventricles and from there, across the body. This cardiac contraction is generated by an electrical impulse which travels throughout cardiac structures, causing the activation of the heart. Cardiomyocytes are in charge of the generation of this electrical impulse. The heart is composed of two kinds of cardiomyocytes: the pacemakers and the normal cardiac cells. Pacemakers trigger the cardiac activity, while normal cardiac cells propagate it. Both kinds of cells contain electrolytes, the locomotion of which generates the electrical activity [64]. The most important electrolytes for the electrical generation are the sodium (*Na*), potassium (*K*) and calcium (*Ca*). Cell membrane contains two main gates for the movement of these electrolytes: the sodium-potassium pumps and the ion channels, as can be seen in Figure 2.4 [64].
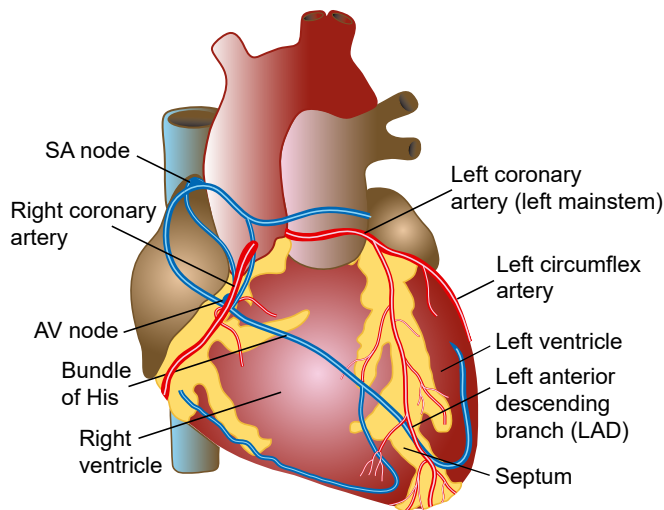
Figure 2.3: Cardiac nodes and His bundle [61]. SA node is found in RA, while AV node is attached to the interatrial septum. Main arteries can be seen in red. Arteries carry oxygenated blood from the heart to the body organs, while veins carry deoxygenated blood from the body organs to the heart. Blood oxygenation takes place in the capillaries of the right and the left lungs.

The sodium-potassium pump moves the sodium outside of the cell and the potassium inside of it. This constant advent of potassium in the cell's interior provokes a change in the intracellular potential. Ion channels allow the passage of only one electrolyte. Being voltage-gated, they control the inflow or outflow of electrolytes by the concentration gradient of the specific ion [64]. In contradistinction to sodium-potassium pumps, when potassium channels are open, potassium can leave the cell, while openning of sodium channels allow the entrance of sodium into the cell [64]. Changes in ionic concentration are responsible for the generation of the electrical impulse [64].

Propagation of the impulse is achieved by the stimulation of the normal cells as a product of a change in cell's resting potential, hence causing a temporary change in the voltage of the cell membrane, called action potential (AP) [64]. The AP is the main mechanism that yields the cardiac activation and is composed of five main phases $(0 - 4)$ and lasts for about 300 ms. Changes in ionic concentration across the cardiac activation phases can be seen in Figure 2.5. During phase 0 or *depolarization phase*, the stimulation from adjacent myocytes leads to the openning of the sodium channel, allowing the sodium to enter the cell and causing a change in the cell potential from negative (-90 mV) to positive ($+20$ mV) [64]. Afterwards, a slight potential decrease is observed due to the inflow of calcium through the openning of the calcium channels, known as phase 1. Phase 2 is also known as *plateau phase*, as potential is stabilized at about $+10$ mV and the sodium channels close. Towards the end of this phase, an incrementation on the calcium concentration inside the cell is observed, leading to mechanical contraction.
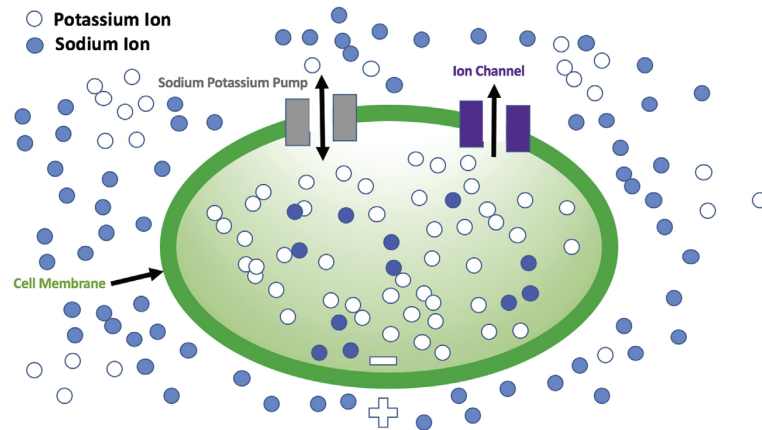
Figure 2.4: Ions in cardiac cells and main gates for ionic movement [64]. Sodium-potassium pumps allow sodium to exit the cardiac cell and potassium to enter it. Ionic channels only allow the passage of one electrolyte, complementary to the function of sodium-potassium pumps. Potassium channels only allow potassium ions to exit the cell, while sodium channels allow the sodium to enter the cell. These changes in ionic concentration provoke the electrical impulse.
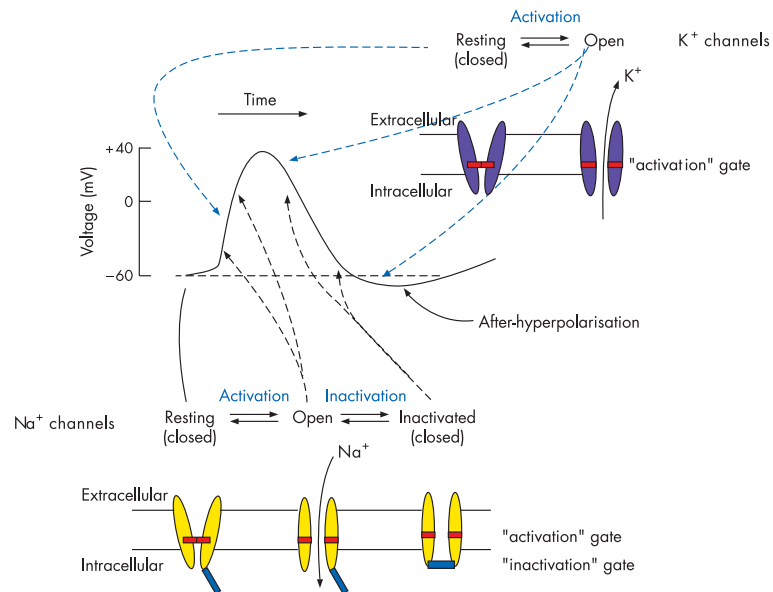
Figure 2.5: The five phases of AP [65]. Sodium channels open and sodium enters the cell, causing a change in cell potential. Then, calcium channels also open (not shown), allowing calcium to enter the cell as well. Closing of sodium channels leads to stabilization of potential, while calcium keeps entering the cell, leading to mechanical contraction. Closing of calcium channels is followed by the opening of potassium channels and the restoration of the resting potential. During the final phase, the cell's potential is stabilized. Activation and inactivation sequence of potassium (top, blue) and sodium (bottom, yellow) channels is also shown.

Plateau phase is followed by *repolarization phase* or phase 3, the main product of which is the restoration of the resting potential at -90 mV, due to the closing of the calcium and the openning of the potassium channels. Phase 4 is also called the *resting phase* and describes the maintenance of cell's potential at -90 mV [64]. After the *depolarization phase*, a cell experiences a form of necrosis for a short period of time, called refractory period, during which it cannot be stimulated again. The refractory period consists of two stages. Stage 1 is also called the *absolute refractory phase*. During this phase, it is impossible for the cell to be stimulated. Phase 2 is called *relative refractory phase* and during this period of time, the cell can be stimulated, if the electrical current is large enough to provoke a stimulation [64]. The refractory period is of paramount importance for the maintenance of the SR and the proper myocardial contraction [64].

The process of the AP cycle of a pacemaker cell is rather different than that of a normal cardiac cell. In the first place, for pacemaker cells, depolarization is self-provoked, without the need of any external stimulation. Additionally, pacemaker cells do not contract, hence phases 1 and 2 are absent. AP of a pacemaker also differs from that of a normal cell, spanning for the former from -60 to $+5$ mV [64]. Pacemaker cells are found in the SA node, the AV node and His bundle, with depolarization rate varying from one structure to another, causing distinct firing rates across the three structures [64]. Figure 2.6 shows the action potential of a normal cardiac cell and a pacemaker cell.

The heartbeat originates from the SA node and propagates throughout the atrial myocardium towards the AV node and from there to His bundle [59, 64]. The AV node is in charge of initiating the ventricular contraction, which cannot be provoked by the direct propagation of the impulse from the atria, due to the electrical isolation between atria and ventricles [64]. Apart from initating the ventricular contraction, AV node delays the electrical impulse by 0.12 s, a minimal but pivotal action to fine-tune atrial and ventricular activations [64]. The impulse then reaches His bundle, which ends to Purkinje fibers, conducting rapidly the cardiac potential throughout the ventricles [64].

Although pacemaker cells do not require external stimulation, HR is significantly affected by the autonomic nervous system (ANS) through sympathetic and parasympathetic nerve fibers spanning across the heart, regulating the heart rate (HR), the conduction velocity and the tissue contractility. Sympathetic nerves are extensively found throughout the heart, from SA and AV nodes to the atria and ventricles, while parasympathetic nerve's presence is mainly found in the SA node. The sympathetic system is connected with emotional and cognitive activity and can raise HR and contractility, while parasympathetic system affects the cardiac function in the opposite way [64].
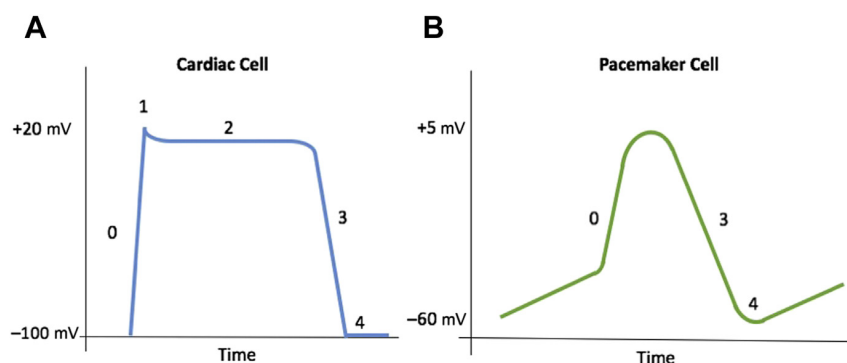
Figure 2.6: AP of a A) cardiac cell and B) pacemaker cell [64]. While AP of a normal cardiac cell passess through all five stages of activation and inactivation, pacemaker cell lacks phases one and two, due to its ability to depolarize and contract without any external stimulation. Potential in normal cardiac cells spans from about -90 to $+20$ mV, while in pacemaker cells, potential spans from -60 to $+5$ mV.

2.3 Electrocardiographic and electrographic concepts

2.3.1 The electrocardiogram

Electrical activity of the heart can be efficiently recorded from the skin via electrodes and be graphically represented by a waveform which is known as the ECG [64]. The most common ECG recording system is the 12-lead ECG system, consisting of 12 leads out of 10 electrodes placed on the chest and limbs. While electrodes record the potential from the location where they are placed, the leads measure the potential difference between two or more leads, a positive and one or more negative or reference electrodes. Depending on whether the electrodes are placed on the chest or on the limbs, the corresponding leads are called chest or limb leads. The latter are further divided into bipolar and augmented leads while the former are also known as precordial leads.

The bipolar leads are three: leads I, II and III, also called Willem Einthoven's original leads. The distribution of these leads forms a triangle, which is known as Einthoven's triangle, as can be seen from Figure 2.7 [66]. Because bipolar leads consist of electrodes from the arms or legs, they measure vectors principally in the vertical plane [67]. Lead I uses as positive electrode the electrode placed on the left arm and compares it using the electrode on the right arm as a reference, forming an angle of $0°$ in the vertical plane. Lead II uses the left leg as the positive and the right arm as the negative electrode, forming an angle of $60°$ in the vertical plane, while lead III, which forms an angle of $120°$, measures the potential difference between the left leg (positive electrode) and the left arm (reference electrode).
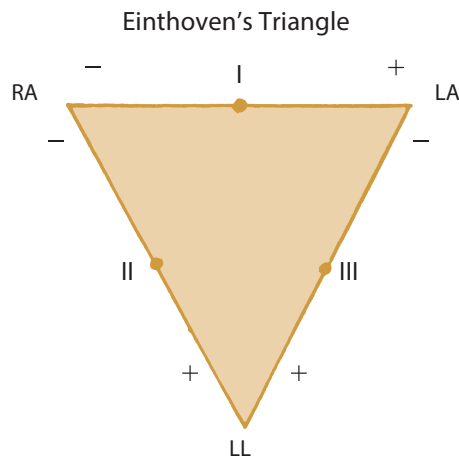
Figure 2.7: Distribution of bipolar leads I, II and III forms Einthoven's triangle. [68]. Lead I forms an angle of 0° with the vertical plane. Lead II, forms an angle of 60°, while lead III forms a triangle of 120°. For the calculation of these leads, electrodes places in the arms or legs are used.

Leads aV_R, aV_F and aV_L are called augmented or Goldberger's leads [66]. Since they use the same electrodes as bipolar leads, they also measure the cardiac electrical activity in the vertical plane. These leads are composed by one of the three limb electrodes (left or right arm and left leg), using each time one of them as the positive electrode and the average of the other two as a reference. For aV_R, right arm is the positive electrode. For aV_F, the left leg is the positive electrode, while the left arm is the positive electrode for the lead aV_L.

The chest or precordial leads compare the potential recorded from the electrodes placed on the chest with the potential from a point in the center of the thorax, called Wilson's central terminal (WCT). WCT expresses the average of the limb electrodes potentials and is found at the center of the Einthoven's triangle [66]. These leads are the fundamental leads of the 12-lead ECG system, as they contain information unable to be derived by any of the remaining leads. Chest leads can be seen in Figure 2.8. As they consist of electrodes found in the chest and the WCT point, which corresponds to the inner thorax, they observe the heart from the horizontal plane. Figure 2.9 shows the vertical and horizontal planes as well as the perspective of the leads on these two planes. In order to derive the precordial leads, placement of the corresponding electrodes is needed. For V_1, electrode is placed in the fourth intercostal space to the right of the sternum, while for V_2, to the same location to the left of the sternum. V_3 is placed diagonally between V_2 and V_4, which is placed between ribs five-six in the midclavicular line, while V_5 is placed to the same location in the anterior axillary line. Finally, V_6 is found on the same level as V_4 and V_5, in the midaxillary line [66].
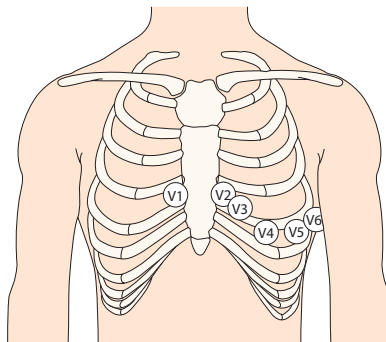
Figure 2.8: The chest leads V_1–V_6 are the fundamental leads of the 12-lead ECG system [67]. These bipolar leads compare the potential of an electrode placed on the chest, at the shown locations, with the potential of an electrode placed at the center of the thorax.
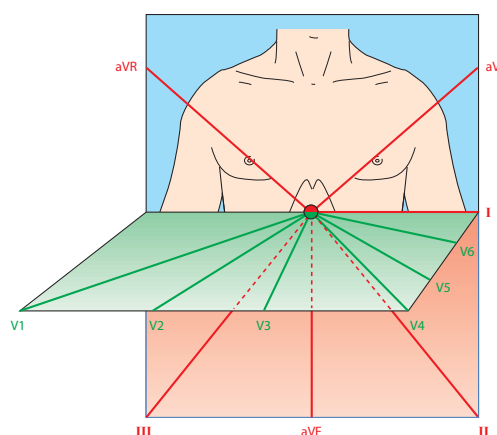
Figure 2.9: Horizontal (green) and vertical (red) planes. Bipolar and augmented leads project on the vertical and chest leads on the horizontal plane [67].

The ECG waves

A normal ECG is composed of the following waves and complexes, as can be seen in Figure 2.10: the P-wave, the QRS complex, the T-wave and the U-wave, the P-R, S-T and Q-T intervals. These waveforms illustrate the depolarization and repolarization of the cardiomyocytes of the atria and the ventricles [69]. P-wave is the first waveform to be seen from the ECG and represents the atrial depolarization. The atrial repolarization (T_a wave) is not visible from the ECG due to the larger amplitude of the QRS complex which overlaps with it.
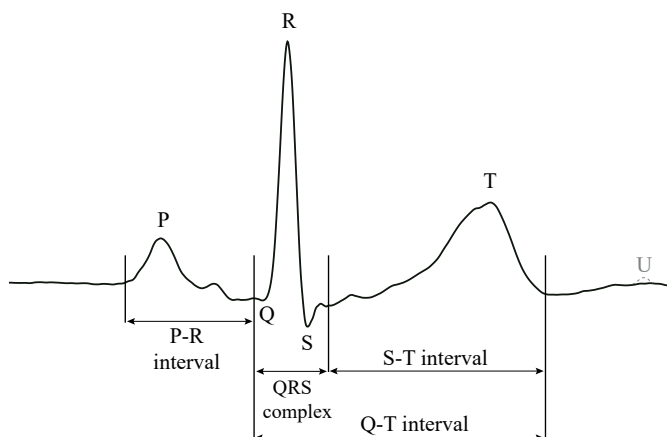
Figure 2.10: The normal ECG. P-wave represents the atrial depolarization, while QRS complex corresponds to the ventricular depolarization. T-wave represents the ventricular repolarization, while atrial repolarization overlaps with the much larger QRS complex and is hence invisible. P-R interval depicts AV conduction, while S-T interval is part of the ventricular repolarization process. U-wave, is also part of the ventricular repolarization process, but is rarely seen. Q-T interval reflects the restoration of the ventricular resting state.

QRS complex represents the ventricular depolarization. Between P-wave and QRS complex there is an isoelectric line which is called P-R interval. The cardiac activity that takes place during the P-R interval is the AV conduction and the stimulation of the cardiomyocytes on the AV node and the His bundle. Nevertheless, the electrical activity produced during the AV node and His bundle stimulation is of very low amplitude and cannot be recorded from the ECG. Ventricular repolarization is then illustrated by the S-T interval and the T-wave [69]. Although not always visible, the U-wave is a small amplitude wave following T-wave and is part of the final phase of the ventricular repolarization [69]. A more prominent U-wave may imply the existence of pathologic conditions. The Q-T interval reflects the restoration of the resting state of the ventricles. The HR is defined as the time between two successive R-waves, called R-R interval [69].

The normal duration of the ECG waveforms and intervals are:

- P-wave: less than 120 ms [70].

- QRS complex: less than 100 ms [69].

- P-R interval: 120-200 ms [69].

- Q-T interval: Depends inversely on the HR [69].

2.3.2 The electrogram

The EGM is a graphical representation of local cardiac activity obtained through electrodes from pacemakers, catheters or implantable cardioverter defibrillators [40]. Depending on the number of electrodes used to generate an EGM, they can be categorized as unipolar, bipolar and multipolar EGMs. The unipolar EGM requires a single electrode contacting the recorded tissue and a reference electrode at zero potential or WCT. A bipolar EGM is the potential difference between two adjacent electrodes. Multipolar EGMs may be Laplacian or omnipolar EGMs, which are in fact calculated by the potential difference between multiple unipolar or bipolar EGMs. Laplacian EGMs are generated by subtracting the center unipolar EGM from the unipolar EGM of a fixed electrode array surrounding it. Omnipolar EGMs are calculated by extracting the bipolar EGM with the largest amplitude within a square of four electrodes [40]. Figure 2.11 shows how each EGM type is calculated and illustrates the corresponding graphical representation of an activation.
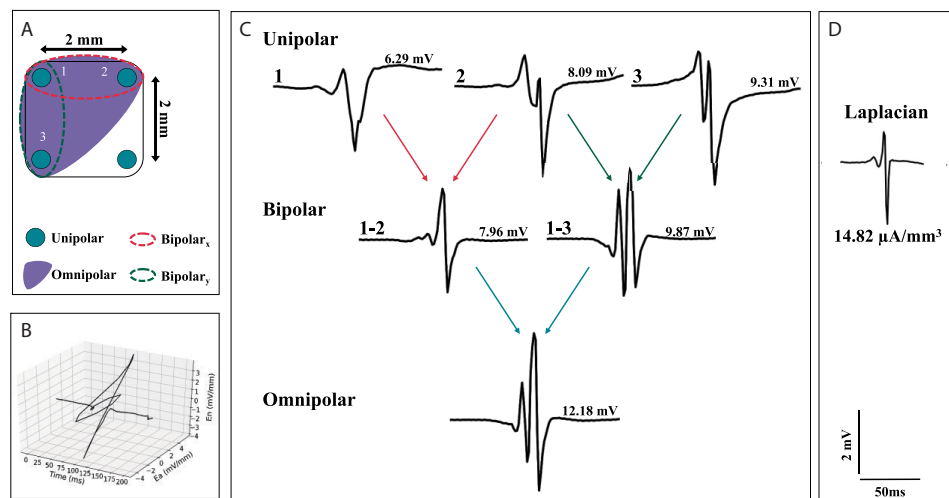
Figure 2.11: A) A square of four electrodes and how unipolar, bipolar and multipolar EGMs are calculated. B) Electrical field projections along time-axis from bipolar EGMs (1–2 and 2–3). C) Unipolar EGMs are calculated from each one of the electrodes. Bipolar EGM is calculated as the difference between adjacent electrodes 1–2 and 2–3. Two bipolar EGMs are subtracted to create an omnipolar EGM. D) The derived Laplacian EGM [40].

Unipolar and bipolar EGMs are vastly used in clinical studies during AF. The use of multipolar EGMs during AF is less extensive and mostly focused on voltage mapping in experimental environment [40]. Each EGM type has advantages and disadvantages and there are no proofs that one is superior to the others [40]. Unipolar EGMs offer an easy and reliable mapping and detection of the local activations but capture far-field potential. Bipolar EGMs are very robust regarding

far-field potential, but the amplitude and morphology strongly depends on the electrode size and specifications as well as the wavefront direction. While multipolar EGMs are insensitive both to far-field potentials and to wavefront direction, they show high computational complexity and present high interelectrode spacing requirements and loss of spatial resolution [40].

2.4 Cardiac arrhythmias

Any kind of deviation from the normal SR is called an arrhythmia. Arrhythmias can be classified according to the cardiac chamber or structure that shows the deviant from normality rhythm as [71]:

- Sinus node arrhythmias, where the SA node is the trigger point.

- Atrial arrhythmias, where the trigger is found on the atria.

- Junctional arrhythmias, where the trigger is found on the AV junction.

- Ventricular arrhythmias, where the trigger can be found on the ventricles, Purkinje fibers or His bundle branches.

- Atrioventricular blocks, where a blockage in the AV junction causes the arrhythmia.

- Bundle branch and Fascicular blocks, where the arrhythmia is caused due to the impulse blockage in the bundle branches and sub-brances.

2.5 Atrial fibrillation

2.5.1 Definition

Atrial fibrillation is an atrial tachyarrhythmia with desynchronized atrial electrical activation [10]. The AF diagnosis can be performed via ECGs by irregular R-R intervals, absence of the P-wave and the existence of irregular in time and variable in amplitude, polarity and frequency atrial activations, called f (fibrillatory) waves [10, 72]. Figure 2.12 shows a SR ECG and an AF ECG. In order for a tachyarrhythmic episode to be defined as AF, it needs to be sustained for at least 30 seconds [10]. AF symptoms include palpitations, fatigue, dyspnea, chest pain and lightheadedness. However, many AF individuals remain asymptomatic [72].

Atrial fibrillation is the most common cardiac arrhythmia, mostly affecting caucasian men of older age. The AF prevalence is 2-4% in adults [10], showing a rapid increment of about 33% in the past 20 years, while rates are expected to rise by another 66% in the forthcoming 30 years [9]. The main risk factors actively
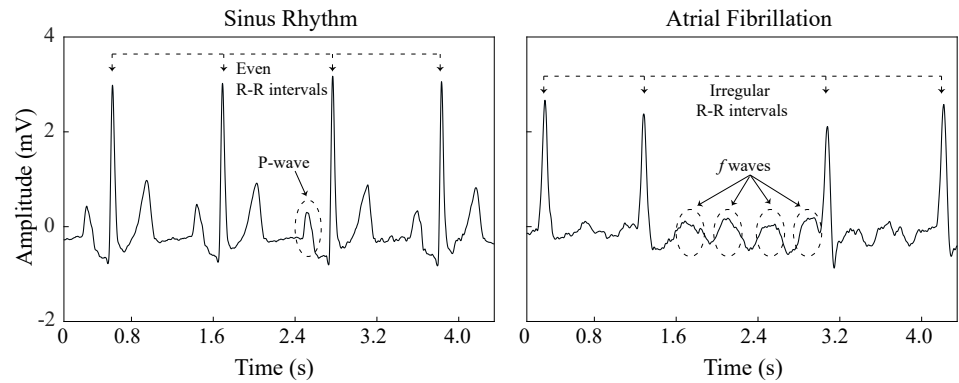
Figure 2.12: ECG examples (left) of a patient in SR and (right) of a patient in AF. In SR, P-wave is visible and R-R intervals are almost equidistant. In SR, P-wave is missing and R-R intervals are irregular. Variable *f* waves are observed.

contributing to the AF incidence are hypertension, diabetes mellitus, heart failure and obstructive sleep apnea, among others [10]. AF is a life-threatening condition, associated with higher risk of heart failure, stroke and dementia, among other pathologies [10]. Although AF is more prominent in men, women show higher mortality rates due to AF-related diseases [9, 10]. Consequences from AF episodes can be visible even within the first 3 days of the arrhythmia, contributing to thrombi formation, hence increasing the stroke risk [11, 13, 64, 72]. AF burden, time spent in AF, is a critical factor affecting the AF evolution as well as contributing to thromboembolism and ischemic brain lesions [15].

Various scoring systems have been developed to evaluate the stroke risk, each presenting different results. ATRIA and ABC show the highest performance, outperforming the remaining systems, yet showing some limitations [73]. Cardioversion to defeat AF is per se an additional aggravating factor for stroke risk, as thrombi can be caused. Hence, any cardioversion attempts should be accompanied with anticoagulants [11, 73]. Apart from stroke risk, dementia and Alzheimer can also be provoked by AF due to pathophysiological mechanisms in AF connected with the aforementioned diseases [14]. Anticoagulants could hinder the mechanisms and hence, the dementia prevalence in AF subjects [14].

2.5.2 Classification of AF

AF can be classified according to the episode's duration in one of the following categories [10]:

- Paroxysmal AF: AF terminating within 7 days of onset, either spontaneously or with intervention.

- Persistent AF: AF terminating at a time later than 7 days of onset.

- Long-standing persistent AF: AF sustained for more than 12 months.

When no longer attempts to terminate AF are performed after consensus of the patient, AF is classified as permanent. Notwithstanding, permanent AF refers to the non-active attitude of the patient and the physician towards AF confrontation and is not related to any pathophysiological condition of the patient. In case that an AF confrontation strategy is adopted, AF can be reclassified to any of the aforementioned categories [10].

The term non-paroxysmal can also be found referring to one of the AF categories other than paroxysmal AF. Non-paroxysmal AF shows distinct pathophysiological mechanisms than paroxysmal AF. Every year, 1-15% of paroxysmal AF patients progress to non-paroxysmal, whereas in a time slot of 10 years, this percentage increases up to 27-36% [10].

2.5.3 Pathophysiology of AF

AF's principal foci are PVs [4, 10], probably due to distinct electrophysiological properties of PV with respect to LA myocardiac cells [45]. PV myocardiac cells show reduced resting membrane potential, higher concentration of repolarizing outward currents and smaller plateau inward currents that may cause shorter AP duration [45]. Additionally, anatomical particularities such as the arrangement and abrupt changes of muscle fiber orientation as well as higher thickness of greater wall in interpulmonary areas may favor the AF arrhythmogenesis [45]. Nevertheless, other areas able to trigger the AF activity have been reported [45]. Alterations in atrial refractoriness or in cellular calcium homeostasis/handling, early after-depolarizations (EADs) or delayed after-depolarizations (DADs) may be the reason for the AF initiation [18, 21]. The slope acceleration in the *resting phase* of AP due to increased ion channel subunits can increase the atrial cell firing, leading to ectopic beats. Calcium overload may also cause cell firing by inducing DADs. On the other hand, EADs allow the recovery of inward calcium current, generating abnormal depolarizations [21].

AF propagation is sustained by a vulnerable substrate able to maintain the fibrillatory activity, called AF or atrial substrate [21]. The atrial substrate contains any change in atrial size or function, also known as AR [16]. Remodeling can be structural, electrical or functional. Structural remodeling refers to any changes in atrial size or volume, atrial dilation or fibrosis [16]. Inflammation and fatty infiltration can cause structural remodeling leading to conduction blocks and delays and allowing the propagation of reentrant circuits [18, 21]. During electrical remodeling, disturbance in electrical function takes place. Electrical remodeling is observed as reduced APD, shortened atrial refractoriness or fibrosis [16, 74]. Finally, decreased LA ejection fraction or contraction strain are observed during functional remodeling, caused by fibrosis [16]. Hypertension, heart failure, type II diabetes, sleep apnea, obesity and oxidative stress are some of the factors contributing to AR [18, 21, 45].

AF itself is the most critical factor leading to remodeling, hence sustaining AF [21, 45]. The cellular level mechanisms sustaining AF are complex. Rapid atrial activity can cause fibrosis through autocrine and paracrine mechanisms [45]. Heterogeneities in connexin-40, which are proteins responsible for intercellular coupling and distribution, intensified during AF, may affect anisotropic conduction [45]. During AF, inward and outward current imbalance is provoked (down-regulation of L type calcium current and incrementation of inward-rectifier potassium channels) altering APD and consequently shortening the atrial refractory period [21]. Continuous AF activity intensifies L type calcium current decrease and alters intracellular calcium handling, leading to loss of dependence on APD rate. Oxidative stress is especially contributing to L type calcium alterations [21].

Increased vagal activity may also contribute to AF sustainability by stimulating potassium channels, leading to APD abbreviation and cell membrane hyperpolarization [21]. Similar to vagal activity, electrical remodeling alters potassium channel balance and decreases outward potassium current, probably facilitating the wavefront propagation during AF [21]. Angiotensin II and transforming growth factor-β_1 (TGF-β_1) are well-known profibrotic molecules that act synergistically, provoking cardiomyocyte hypertrophy and apoptosis, therefore causing fibrosis [21]. Platelet-derived growth factor (PDGF) is an endothelial growth factor stimulating proliferation and differentiation of fibroblasts, which are connective tissue cells. PDGF provokes atrium-selective fibroblast hyperresponsiveness, a possible explanation of why AR happens to a higher extent with respect to ventricular remodeling [21].

Apart from contributing to the AF propagation, AR can have a negative effect on AF therapies. Electrical remodeling alters ion channel function, causing higher resistance to antiarrhythmic drugs [21]. The early detection and inhibition of the AF activity is therefore of vital importance, since it can reduce the remodeling effect, showing higher prognostics for SR maintenance [21]. The use of medication with antiinflammatory/antioxidant properties after CA may hinder the AF recurrence, as tissue oxidation and inflammation aggravates remodeling [21]. Moreover, drugs such as statins, AT1R (counterregulatory angiotensin II receptor) blockers, pirfenidone and heart shock protein can affect positively the AF ectopic activity and fibrosis inhibition by suppressing or preventing from angiotensin II production [21].

AR is more prominent in LA than RA. Nevertheless, not only is RA remodeling possible but also related with AF recurrence, probably because RA remodeling may be the aftermath of advanced LA remodeling [16, 46, 75]. Compared to paroxysmal AF, non-paroxysmal AF shows more extended remodeling, probably due to higher AF burden [10, 18, 20, 74]. AR is not necessarily permanent but can be reversed after CA, called in such case reverse AR [17]. Reverse structural remodeling can happen as early as 2 months after CA [16]. Although a blanking period of 2 months is also used for electrical remodeling [16], cases with early electrical remodeling observed 3 days after CA have been reported [76].

Rapid focal firing can also sustain the AF activity, apart from initiating it. This can happen even with a single circuit that is reinduced, in presence of atrial substrate sustaining the activation or by multiple reentries [21]. Two main theories regarding the AF maintenance exist. The first theory is based on chaotic wavelets surviving with the help of the atrial substrate [77–80]. More specifically, wavelets originating from the endocardium collide on the epicardial tissue in presence of structural remodeling. The second theory is based on organized focal or rotational activation. In focal activation, one central location causes tissue activation in a centrifugal way [80]. Rotational activation supports the theory of multi-phase reentries propagated around a phase singularity point, an unexcitable point that is formed by scar or fibrotic tissue [45,80].

Structural and electrical factors are pivotal in sustaining rotational activation. As mentioned afore, in rotational activity, continuous excitement of tissue surrounding an anatomic barrier takes place [45]. If propagation time is longer than cell refractory period, some cells will always be excitable, allowing the wavefronts to enter the tissue hence sustaing AF [45]. This phenomenon is more prominent when atrial dilation coexists with short refractory period, as the wavefront will follow a longer path, while cell excitability will happen sooner [45]. In case that propagation time is equal to refractory period, one leading circle is sustaining AF. This kind of activation is also known as functional reentrant circuit [45]. However, in case that propagation time is shorter than refractory period, circuit will reach to refractory tissue and will be terminated [45]. Figure 2.13 shows the different types of reentries that exist.
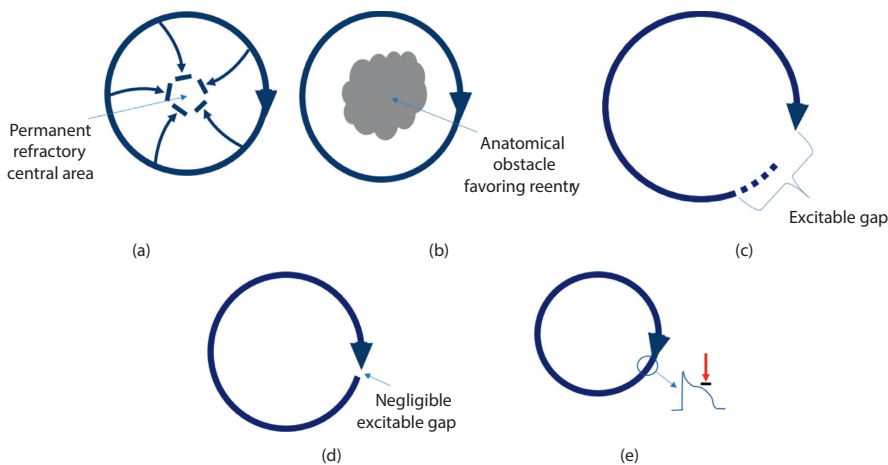
Figure 2.13: Different types of reentries. (a) One leading circle sustaining AF. (b) Continuous excitement of tissue surrounding an anatomical barrier. Reentries (c) with and (d) without excitation gap. (e) Reentry reaches refractory tissue and has to be terminated [45].

Nevertheless, reentries may not be circular but show spiral waveform and peripheral movement [45]. This happens due to extremely low but not zero depo-

larization speed of phase singularity point, allowing its movement and causing a curvature in waveform propagation pattern, the speed of which is faster in the wave tail [45]. Figure 2.14 (curvature) shows the depolarization state across cells of a spiral reentry [45].
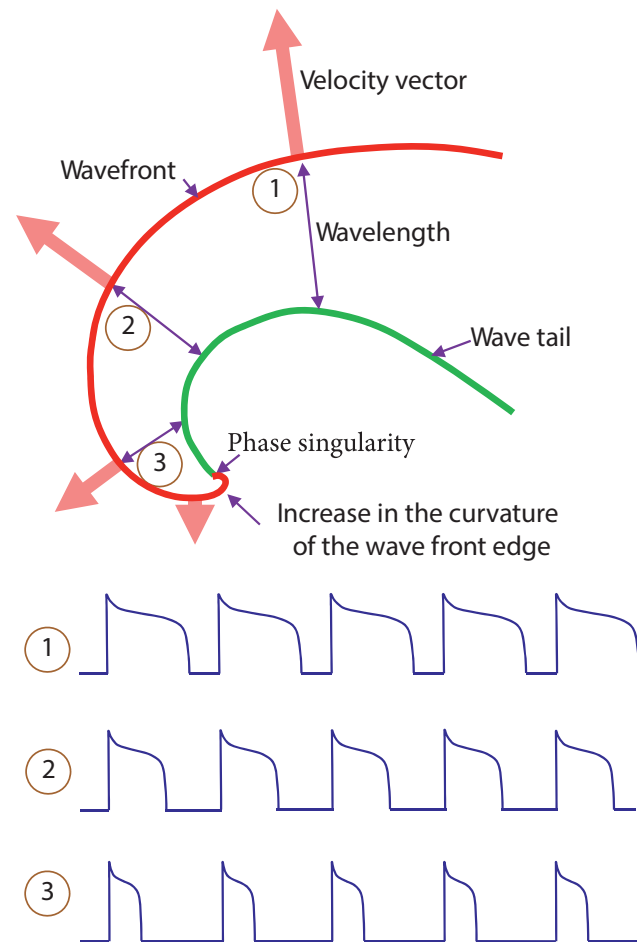
Figure 2.14: (top) Spiral reentry with peripheral movement. The red line represents the wave. The green line represents the repolarized edge (wave tail). Propagation velocity is higher in the periphery of the wave (1) than close to the phase singularity point (3), causing a continuous movement in a spiral form [45]. (bottom) Action potential at each point of the wavefront.

During AF, the atria can be contracted with a rate of 400-600 times per minute. Due to the AV node, in the absence of any AV node-related disease, only a small percentage of these activations reach the ventricles. As a consequence, although heart rhythm in AF is higher than SR, showing values of about 100 bpm in resting state, it hardly ever reaches values as high as 400 bpm [72].

2.5.4   AF treatment

Two major strategies can be adopted in order to confront AF: rate or rhythm control, with patients' needs and preferences being crucial when designing the AF management plan [10]. Rate control involves the use of drugs such as beta-blockers and amiodarone or the ablation of the atrioventricular node and the implantation of pacemaker in more demanding cases [10]. Rate control therapy is often the first choice especially in asymptomatic patients and is in many cases sufficient for the AF management [10].

Rhythm control is an alternative when outcomes of rate control are not satisfactory, while often a combination of both strategies can be proved efficient [10]. SR restoration and maintenance is the substance of rhythm control, which seems to slow down the AF progression and improve the quality of life more effectively than rate control. Pharmacological or electrical cardioversion, combined with the previous administration of antiarrhythmic drugs, are elementary rhythm control interventions [10, 17].

CA of PVs is the most popular and probably effective AF treatment, especially recommended for patients failing to sustain sinus rhythm via any of the aforementioned methods [10]. Discovery of PVs as the principal AF foci is a milestone in AF therapy, showing high success rates for paroxysmal AF patients [4, 10]. Higher complexity of AF mechanisms and atrial, structural or electrical alterations due to higher AF burden principally but not exclusively observed in persistent AF patients may intercept the favorable CA outcome, requiring repetitive procedures or CA of additional sites believed to trigger or sustain the AF activity [10, 20, 81]. Frequent sites receiving additional CA are left atrial appendage, superior vena cava, sites showing high AF complexity, low voltage areas and areas with high dominant frequency (DF) [10, 18]. Nevertheless, the effect of creating additional lesions in the atria is under dispute for some studies [10, 43, 82].

Apart from the elimination of the arrhythmogenic activity itself, CA of PVs can additionally hinder the evolution of AF-related pathologies, significantly contributing to the overall health condition of the AF individuals on a long-term basis [12]. Antiarrhythmic drugs prescription is often suggested after CA procedures, in order to mitigate CA-related side effects and formation of phenomena favoring the AF recurrence [10, 21]. Medication with antiinflammatory and antioxidant properties can prevent from tissue oxidation and inflammation, which can contribute to AF recurrence [21]. Additionally, anticoagulant therapy after CA or electrical cardioversion can prevent from thrombi formation, reducing this way the risk for stroke and dementia [11, 14, 73]. So far, anticoagulation prescription has been prioritized for non-paroxysmal AF patients. Notwithstanding, some studies highlight the need for additional prescription to paroxysmal AF patients, having them classified at risk of thromboembolism as well [15].

2.5.5   AF analysis from ECGs

ECG analysis is one of the most popular techniques for the evaluation of the AF substrate regardless of the cardiac rhythm. The advantage of ECG analysis over other noninvasive mapping techniques is the fact that atrial electrical remodeling can be exclusively assessed from ECGs. During AF, atrial activity is assessed by f-waves present in the Q-T interval [22–27]. The main idea behind this kind of analysis is to seek parameters that characterize the health of the atrial tissue or the organization of the AF dynamics in an attempt to define the probability of a successful CA outcome or AF recurrence. Various parameters can be extracted and analyzed from f-waves, with f-waves amplitude and AF cycle length (AFCL) being quite present in literature [22]. These two parameters have been directly connected with prediction of the CA outcome, where low f-wave amplitude and short AFCL are considered markers of severe fibrosis, indicating a high probability for AF recurrence [22, 25]. Additional parameters allowing the assessment of atrial substrate via f-waves analysis are the DF measuring the variability of the atrial rate, entropy or regularity analysis assessing the organization of the AF dynamics, while another interesting parameter shown to outperform established f-wave analysis techniques is the variability of the f-waves energy [22, 24, 25, 27, 28, 47].

ECG analysis is not limited to the processing of the atrial ECG components. During AF, fast-rate atrial excitations may affect the AV node properties and the regularity of the ventricular response. Hence, studying AF from the ventricular perspective can assist further the characterization of the AF dynamics and define the extent of functional impairment that AF can provoke [22]. Heart-rate variability (HRV) allows the study of cardiac rhythm regularity. As a tool, it is vasty employed during SR to assess sinus node modulation. Notwithstanding, HRV analysis can as well be applied during AF in a similar way, evaluating the response of the ventricular regularity [22]. R-R interval histograms and Lorenz plots allow the assessment of AV node refractoriness and AF activity organization [22]. Finally, nonlinear analysis allows the exploration of predictability and regularity of the ventricular response either in long- or short-term R-R series, predicting self-termination of AF [22].

Another technique aiming to characterize fibrillatory drivers from noninvasive recordings is ECG imaging (ECGI). ECGI solves the forward problem, which is the localization of the epicardial origin of the signals recorded from surface ECGs [18, 40, 83]. In order to achieve high-resolution analysis, multielectrode recordings are necessary, while the patient needs to undergo computed tomography (CT) scan. Afterwards, propagation patterns are described through maps obtained via transformation of the signals after the reconstruction of cardiac geometry, serving as detectors of foci or rotors initiating AF activity [18, 40, 83]. Body surface potential mapping (BSPM) is an ECGI technique used for this purpose [40, 45, 84–86]. Despite its ability to characterize fibrotic tissue and AF patterns without invasive recordings, BSPM has had limited clinical application due to a number of issues such as reduced reliability in cases of advanced fibrosis,

reconstruction issues due to low amplitude atrial signals and strong dependency on each patient's geometry, high sensitivity to motion artifacts and the need for a high number of electrodes which is not always available [40, 84, 85].

Noninvasive assessment of the atrial substrate during SR is vastly employed in patients before entering the surgery room for CA of AF, with the main goal of evaluating the possibility of AF recurrence. Analysis during SR recruits primarily paroxysmal AF patients, as many persistent AF patients enter the surgery room in AF. ECG recordings is the primary source of analysis, offering valuable information on atrial and atrioventricular conduction as well as sinus node regulation. P-wave analysis reveals information on the electrical remodeling. Many features can be extracted and analyzed from P-waves, such as duration, amplitude, area or dispersion [29–39]. P-wave duration is probably the most popular among them, strongly associated with fibrosis and the existence of conduction blocks or other structural remodeling phenomena [87]. As a long P-wave is associated with fibrosis, P-wave shortening is considered a favorable marker predicting the success of the CA procedure [29, 31, 32].

As with recordings during AF, ventricular excitation and its patterns can provide an interesting perspective on AF analysis during SR, showing information relevant with the tissue health. HRV analysis can offer such kind of information, as it allows the observance of R-R interval variations, which in turn reflect the ANS function [88]. In the same line as P-wave analysis, HRV studies are focused on predicting the CA outcome, with a temporal HRV reduction observed after CA predicting termination of AF [88–90].

2.5.6   AF analysis from EGMs

Despite the high importance of ECG analysis in AF substrate assessment, the distance between ECG electrodes and the atria complicates the precise detection of AF triggers during CA procedures. On the other hand, invasive mapping allows a more detailed illustration of cardiac remodeling, as EGMs are closer to the electrical source. Due to this fact, many studies have employed EGM recordings in order to localize AF triggers in search of potential non-PV ablation targets, mostly present in persistent AF patients [17, 18]. Invasive mapping includes signals obtained from mapping and ablation catheters, pacemakers or implantable cardioverter defibrillators [40]. Bibliography offers a high amount of studies analyzing signals acquired from catheters during CA, utilizing unipolar, bipolar or multipolar EGMs. These three types of EGMs have different properties and so far none is considered superior to the others, as all of them present advantages and drawbacks and the principal criteria is whether or not they fit each study's requirements [40].

EGM morphology is a sensitive issue regarding studies analyzing invasive recordings, affected by a multitude of parameters such as electrode specifications and digitization parameters. Filtering can additionally affect morphology

and waveform integrity during filtering is an object of investigation for many works [40,91]. Recording catheter plays an important role in invasive recordings analysis as well. Small catheters with a low number of electrodes require algorithm or manual annotations for further EGM analysis with a possible impact on the accuracy of the studies. On the other hand, large multielectrode catheters are more susceptible to false positives regarding activation maps due to sequential excitation of surrounding electrodes [40].

EGM recordings are specially useful in mapping during AF as they allow the detection of triggers and recordings with certain electrical characteristics implying the existence of anatomical barriers perpetuating the AF in the corresponding cardiac sites. Such an example is the focal impulse and rotor mapping (FIRM) technique, aiming to detect rotors by performing phase analysis [18, 40, 45, 92]. Despite the interesting and promising results of the original study [92], reproducibility of these results has been questioned by some studies, pointing out the risk of false detection of rotors as a result of data interpolation performed to augment the resolution [40].

Local activation time (LAT) mapping is used to identify activation patterns such as re-entries, foci or slow conduction zones by creating isochronal maps allowing the inspection of propagation evolution throughout the atria. Notwithstanding, fixed interelectrode distances and high spatial resolution are needed in order to achieve satisfactory results. Compared to bipolar signals, unipolar signals are more suitable for LAT maps, as LAT annotation in bipolar recordings assumes signal stationarity [40]. Areas with high AF frequency have also been connected with AF sustenance hence being candidate ablation targets, although with controversial results [40,93].

Measuring the atrial rate of critical sites, however, not only has an application in defining ablation targets but also in controlling the success forecast of the CA procedure, as atrial frequency reduction is thought to be a favorable marker [40]. Analysis of atrial rate during AF can be performed either in time domain, with AFCL or in frequency domain, with DF analysis [40]. Despite the inconsistency between studies regarding the outcome of CA of high frequency sites, in CS, frequency analysis has proved to be a useful criterion for additional CA applications, improving the outcome of the PVs CA procedure [55].

One of the most popular yet ambiguous techniques in detecting CA targets is the mapping of CFAEs [48]. Original CFAEs definition specifies them as low voltage atrial EGMs composed of 2 or more deflections and a highly fluctuated baseline or as EGMs with a very short CL ($\leq$ 120 ms) [48]. CFAEs are thought to be the product of endo-epicardial wavefront collision and have been connected with slow conduction areas or re-entries of fibrillatory waves [40,45,49–51]. A common problem in CFAEs detection is the inconsistency in CFAEs definition, leaving space for dissention regarding the results of additional CFAEs ablation [40,43,56]. CFAEs analysis is often combined with other trigger mapping techniques such as DF or low voltage zones in order to provide better ablation outcomes [18,40,94–

96]. Nonlinear analysis has been proved especially effective in detecting areas with CFAEs, probably due to chaotic nature of AF dynamics [5, 97, 98].

Atrial scarring plays an important role in AF perpetuation. Heterogeneous anatomy decelerates conduction of atrial activity, leading to long propagation time which allows the re-excitation of atrial cells, hence assisting the re-entry circuit creation [45]. Low-voltage EGMs are thought to correspond to zones with scarring and their ablation is another popular CA technique, which as well shows conflicting results [17, 18, 40, 52–54]. Low-voltage mapping is an EGM analysis technique that can be applied either during AF or during SR [40].

In general, complexity of AF augments with descending voltage and very low voltage zones are connected with severly remodeled tissue [40]. Nonetheless, some issues regarding low-voltage zones analysis arise. HR can affect voltage values in EGMs, which additionally depend on EGM type [40]. Moreover, the thresholds defining an atrial site as a low voltage zone vary according to studies and may furthermore depend on the recording site as well as on the electrode size and spacing [40]. Common cut-off values for low voltage zones are 0.5 mV, while areas showing EGMs with amplitude < 0.1 mV are thought to present dense scarring [18, 40]. As with CFAEs, low voltage zone mapping is often combined with additional mapping techniques in order to narrow down the zones in need of additional ablation [18, 96, 99].

During SR, extrapulmonary sites triggering or sustaining AF are identified by various techniques recruiting 12-lead ECG as well as intracardiac recordings from specific reference atrial sites [17, 42, 100, 101]. CS is one of the most common reference sites, while other auxiliar sites such as crista terminalis and superior vena cava can also be employed [42, 100]. The employment of specific reference sites during cardiac mapping allows the incrementation of mapping resolution by using only a few catheters, significantly improving the detection of AF triggers [100].

Previous works have performed an exhaustive study on techniques to map effectively non-PV triggers [42, 100]. Analysis of the earliest activation CS channel with respect to the P-wave onset as well as analysis of the activation patterns of all CS catheter channels help the clinicians define the wider area where the trigger is found in order to move the mapping catheter to the detected location and perform a detailed mapping of the area [100]. EGM characteristics such as low voltage or slow conduction velocity are also utilized during SR mapping and are thought to describe atrial scarring hence being frequent CA targets [17, 18, 41, 102, 103]. Recently, it has been also shown that a prevalence of about 31% of low-voltage tissue in AF individuals is connected with AF recurrence after CA of PVs [41]. EGM analysis can also be performed after CA in order to predict the AF recurrence probability. CS EGMs during SR or pacing can be recruited for this purpose, with EGM fractionation being a significant predictor of AF recurrence [42].

Quantification of Organization in Atrial Fibrillation Electrograms by Coarse-Grained Correlation Dimension

The content in this chapter was published in:

Contents

3.1 Introduction

CFAEs-guided ablation is often applied in addition to CA of PVs in persistent AF patients in order to reduce the AF recurrence possibilities [40, 48]. Despite the versatility of CFAEs in AF fibrosis studies, being frequently combined with other fibrotic markers [104–106] while also able to stand alone [48], the efficiency of CFAEs-guided ablation has been questioned [43, 107]. Additionally, whether

areas showing CFAEs indeed correspond to AF drivers and LV zones remains under dispute [108, 109].

CFAEs-guided ablation is based on the theory that a higher extent of fibrosis would be reflected in EGMs with high complexity, as the very definition of CFAEs indicates, due to chaotic propagation of multiple wavelets scattered through the remodeled epicardium [48, 110]. Notwithstanding, vague definition of CFAEs either as EGMs with ≥ 2 deflections and/or perturbation of the baseline or as short CL ($\leq$ 120 ms) EGMs [48] creates confusion, allowing any area presenting EGMs with the aforementioned characteristics to be considered as CFAEs. Correlation between these two definitions is additionally poor and detection of CFAEs strongly depends on the mapping system and the thresholds used [111]. The aforementioned issues highlight the need for stricter and more trustworthy criteria that can create homogeneity in CFAEs definitions, leading to higher efficiency in additional CA.

Classification of EGMs by progressing level of fractionation may contribute to detection and ablation of fibrotic areas that assist the AF perpetuation [112]. Defying the already established thresholds proposed by Nademanee et al. [48] and quantifying the chaotic nature of CFAEs using nonlinear analysis techniques can be an alternative. So far, nonlinear analysis has been principally applied via correlation dimension (CorDim) and CGCD in order to quantify the influence of anti-tachyarrhythmia pacing in model-based AF or to predict the CA outcome by RA EGMs analysis, showing in both cases satisfactory results [113, 114].

CorDim has also been used in order to quantify local nonlinear organization during AF between two atrial sites, assigning high organization results to Wells' [115] AF type I and II EGMs and poor nonlinear coupling to AF type III EGMs [116]. Finally, another study has recruited CGCD in order to classify EGMs according to AF types, showing satisfactory results especially for type I EGMs [117]. This study, however, has utilized unipolar EGMs, which may show misleading results due to difficulties in removing the ventricular activity.

Considering the relativity of CorDim and CGCD in AF organization estimation on EGMs, the scope of the present chapter is to present a technique aiming to quantify the fractionation level of bipolar EGMs of very short length. Real-time implementation of this technique on AF mapping devices could enchance the CFAEs detection and ablation results as well as capture short-duration phenomena that tend to be neglected, hence contributing to CA substrate assessment of higher resolution.

3.2 Materials

119 bipolar EGMs of 22 persistent AF patients undergoing CA for the first time were utilized. Signals were recorded during AF for 10 seconds via a Labsystem™ PRO EP recording system (Boston Scientific, Marlborough, MA, USA) with

1 kHz sampling frequency and were bandpass filtered at 0.5–500 Hz. Two experts manually classified the EGMs by AF type (I–III) according to Wells' criteria, being AF type I the least fragmented and AF type III the most fragmented cases, respectively. 11 EGMs were classified as AF type I, 36 EGMs as AF type II and 72 EGMs as AF type III.

As EGM classification by AF types led to three groups of unequal size and since there existed some type II or III EGMs not absolutely belonging to a unique AF type, a parallel analysis employing 24 EGMs, the eight most representative EGMs from each class, has been performed. Finally, since none of the EGMs was classified as AF type IV, 20 pseudo-real EGMs were created from the already existent database. AF type IV EGMs are AF type III EGMs with altering part of AF types I or II EGMs. AF types I–IV are shown in Figure 3.1. For readability reasons, the database consisting of the 24 most illustrative EGMs is called Group 1, the database consisting of all 119 EGMs is called Group 2, while the database consisting of 20 pseudo-real AF type IV EGMs is called Group 3.
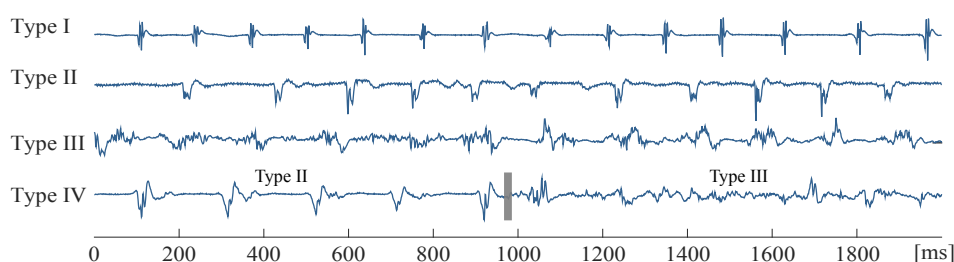
Figure 3.1: AF types I–IV. AF type IV was artificially created by concatenating an AF type II (first half) and an AF type III (second half).

Signals were firstly normalized by their root mean square (RMS), the square of the function that defined each time-series, in order to remove the bias provoked by the signal amplitude. Signals were then denoised by a 3rd order Butterworth lowpass filter with cutoff frequency set at 300 Hz and powerline interference (PLI) was removed by a wavelet-based denoising technique [91]. Signal segmentation at epochs of 1-s length was the final preprocessing step.

3.3 Methods

EGM organization was estimated by CGCD, calculating one value for each 1-s segment and then averaging across all segments of the same recording. Before the calculation of CGCD, surrogate data analysis was performed in order to check for nonlinearity in the dataset. For this purpose, 40 surrogates were created for each and every signal using the iterative amplitude adjusted Fourier transform with 95% confidence level, achieving the same amplitude distribution and power spectrum with the original time-series [118]. The amplitude of the original signals

was firstly rescaled in order to achieve Gaussian distribution, then their phases
were randomized preserving the distribution normality on average, followed by
another signal rescaling to recover the amplitude distribution of the original sig-
nal. Finally deviations in spectrum and distribution were corrected so that they
were in line with the original data. A rank-order test was used to compare the
CGCD of the original signals with the CGCD of the surrogates. As it can be seen
from Figure 3.2, CGCD values in original signals are different from the values of
the surrogates for most of the cases, therefore revealing the presence of nonlinear
dynamics and allowing the application of CGCD analysis.
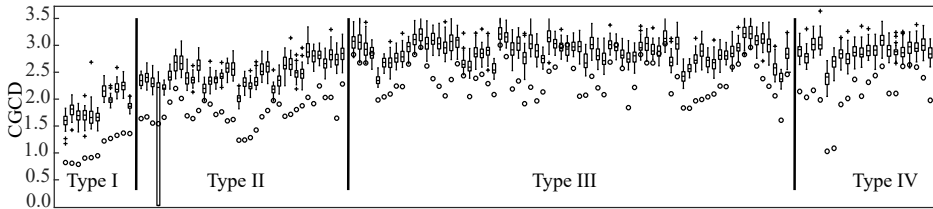
Figure 3.2: Surrogate data analysis indicating the presence of nonlinear dynamics
in the original signals. Small circle represents values of the original data, while
each boxplot represents the values of the 40 surrogates corresponding to each
time-series.

3.3.1   Coarse-grained correlation dimension

CGCD is a variation to CorDim, adjusted for signals with highly disorganized
dynamics, making a rough approach to the signal complexity and not estimat-
ing precisely the dimension [117]. Therefore, the first step for CGCD estimation
is the calculation of CorDim, which is used to assess the organization in nonlin-
ear systems [119]. CorDim is inversely proportional to the organization of the
dynamics.

Given a time-series $X = (x_1, x_2, \ldots, x_N)$ with length N, CorDim estimation
starts with its reconstruction to m dimensional phase-space with a time delay τ
between vectors of each dimension [117, 120]. For the p-th element of the time-
series, this reconstruction will then be

$$\mathbf{Y}_p^{(m)} = (x_p, x_{p+\tau}, x_{p+2\tau}, \ldots, x_{p+(m-1)\tau}), \tag{3.1}$$

with $m = 1, 2, 3 \ldots$ being the embedded dimension and $p = 1, 2, \ldots, N - (m-1)\tau$.

Afterwards, the proportion of pairs of vectors that are found closer than a
distance r, which is called the correlation integral $C^{(m)}(r)$, is estimated as

$$C^{(m)}(r) = \frac{2}{N_{ref}(N_{ref}-1)} \sum_{i=1}^{N_{ref}} \sum_{j>i}^{N_{ref}} \Theta(r - \|Y_i^{(m)} - Y_j^{(m)}\|), \qquad (3.2)$$

where Θ is the Heaviside function, and $\|Y_i^{(m)} - Y_j^{(m)}\|$ is the Euclidean distance of each pair chosen $(Y_i^{(m)}, Y_j^{(m)})$ and N_{ref} is the number of reference points, as a chosen number of the $N - (m-1)$ vectors of Equation (3.1).

When the reconstructed phase-space fully represents the data, two strongly associated points of the original signal will still be found in a close region after the phase-space reconstruction, while two highly dissociated signals will be found far apart. This is calculated in CorDim by searching for saturation areas on the double logarithmic plot of $C^{(m)}(r)$ as a function of r, plotted in sequential embedded dimensions from $m = 1, 2, \ldots, 20$ [114].

As already mentioned, CGCD does not offer precise estimations on the signal complexity or organization, but approaches them roughly by performing calculations at a fixed embedded dimension m and a finite resolution distance r_{cg}, as follows

$$CGCD^{(m)}(r_{cg}) = \frac{\mathrm{d}ln[C^{(m)}(r_{cg})]}{\mathrm{d}ln(r_{cg})}. \qquad (3.3)$$

For the calculation of the $CGCD^{(m)}(r_{cg})$, the derivative of the correlation integral curve needs to be calculated, when $r = r_{cg}$. This can be approached by the local slope of the tangent line, passing from the point $(ln(r_{cg}), ln(C^{(m)}(r_{cg}))$, calculated through two points, $(ln(r_1), ln(C^{(m)}(r_1))$ and $(ln(r_2), ln(C^{(m)}(r_2))$, surrounding the point $(ln(r_{cg}), ln(C^{(m)}(r_{cg}))$ [117]. For each epoch, CGCD was calculated and then averaged across all segments of one signal.

3.3.2 Computational parameters

Before calculating CGCD, embedded dimension m, time lag τ, distance r_{cg}, and number of reference points N_{ref} need to be specified. Parameter selection was performed according to previously established calculation methods or by multiple trials, defining the optimal solution. Choice of embedded dimension m affects the illustration of the dynamics on the reconstructed signal. A dimension smaller than the dynamics of the time-series will lead to absence of linear regions in the double logarithmic plot, due to the unsuccessful resemblance of the reconstructed signal [120]. Previous works set $m = 10$ empirically [114,117]. This study selected an embedded dimension of $m = 4$ as the optimal choice after multiple trials on CGCD calculation with $m = 1, 2, \ldots, 20$, selecting the value that yielded the highest performance without showing infinite CGCD values.

Time lag τ not only affects the adequate illustration of the dynamics on the reconstructed signal but also influences the discrimination between various AF fractionation levels, as a small value would lead to convergence of all vectors of Equation (3.1) [121]. Time lag τ is normally defined as the first time that the mutual information drops to its minimum [117], which in the present study was $\tau = 8$ ms.

When distance r_{cg} is minimized, systematic errors are also minimized, hence leading to accuracy incrementation. Nevertheless, statistical errors would increase in this case, leading to lower precision. Therefore, a trade-off between systematic and statistical errors is recommended by treating them as an entity and defining the optimal r_{cg} as the distance equal to half of the standard deviation of the time-series, normalized by its peak-to-peak amplitude [114, 117, 122].

The final parameter to be considered is the number of reference points N_{ref}. While a small N_{ref} may lead to correlation integrals of zero value for chaotic dynamics and poor statistical validity, a high number would affect the execution time of the algorithm. The lowest N_{ref} limit is normally set at 1/3 of signal length and any number higher than that can be used by balancing between the precision improvement and execution time enlargement. This study utilized $N_{ref} = 334$, which coincides with 1/3 of signal length for each epoch. In fact, the first $N_{ref} = 334$ of each epoch were used after multiple trials using $N_{ref} = 334$ randomly chosen from the set of the reconstructed vectors, leading to similar results with a significantly higher execution time.

Figure 3.3 shows how embedded dimension m and time lag τ parameters affect the signal reconstruction results for various AF type EGMs (I–III). While parameters do not affect significantly highly organized EGMs, such as type I AF EGMs, type III AF EGMs of low organization are significantly affected by the selected parameters, leading to reconstructed signals that do not resemble the original time-series in cases (iii) and (iv) of Figure 3.3.c.

3.3.3   Statistical analysis

Statistical analysis in Groups 1 and 2 was performed by classification of EGMs by AF type according to their CGCD values. This was achieved by one-vs-all receiver operating characteristics (ROC) analysis to discriminate between each one and the remaining two AF types. Afterwards, classification by AF types was performed through a decision tree with a maximum split of 2, using 10-fold cross-validation by using Matlab® Classification Learner (MathWorks, Natick, MA, USA). After testing for normality and homoscedasticity [123, 124], CGCD values were compared among the three AF types with a Kruskal-Wallis (KW) test [125] and differences between values in pairs of AF types were tested with a Mann-Whitney U-test (MWU) with Bonferroni correction [126].
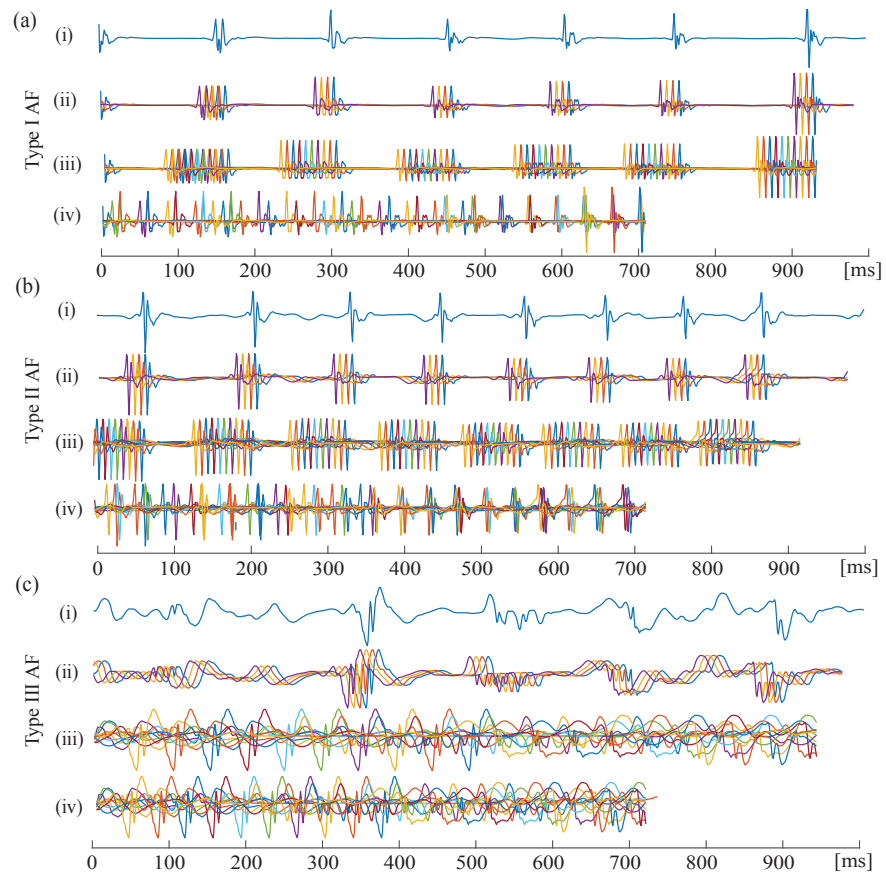
Figure 3.3: 1-s segment of (**i**) original and (**ii–iv**) reconstructed AF EGMs via CGCD. (**ii**) Reconstructed signal with time lag $\tau = 8$ ms, embedded dimension $m = 4$. (**iii**) Reconstructed signal with time lag $\tau = 8$ ms, embedded dimension $m = 10$. (iv) Reconstructed signal with time lag $\tau = 35$ ms, embedded dimension $m = 10$. (**a**) AF Type I, (**b**) AF Type II, and (**c**) AF Type III. Length p of reconstructed signal decreases as τ and m increase, as can be seen from Equation (3.1).

For Group 3, CGCD calculation and classification by AF type using the threshold obtained by the decision tree analysis on Group 2 was performed sequentially at each epoch. In case that none of the CGCD segments was classified as AF type III, the pseudo-real signal was classified to either AF type I or II according to its median CGCD value. In case that at least one of the 1-s signals was classified as AF type III, classification started over on each segment of the signal looking for epochs where it is classified as AF type I or II. In that case, pseudo-real signal was classified as AF type IV. Otherwise, it was classified as AF type III. As all of the pseudo-real EGMs were in fact AF type IV EGMs, the percentage of EGMs classified as AF type IV EGMs was calculated to evaluate the accuracy of this method. Figure 3.4 describes the steps followed for Group 3 analysis.
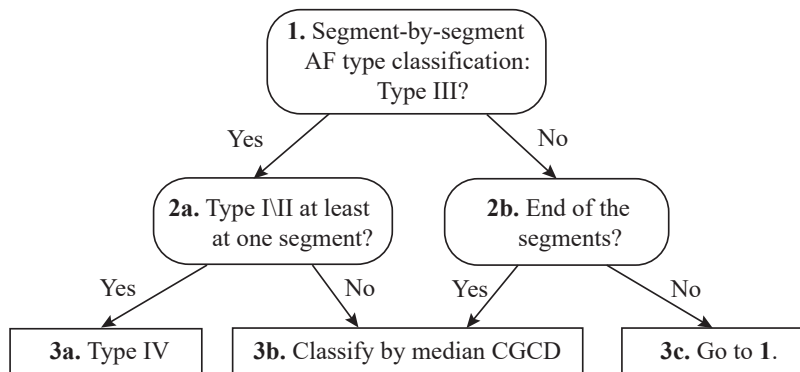
Figure 3.4: Steps and decisions taken for AF Type IV detection on the pseudo-real
recordings of Group 3 in the database.

3.4   Results

ROC analysis has shown that CGCD values at AF types I and III are absolutely
distinguishable for the remaining types both for Group 1 containing the 24 most
representative EGMs and for Group 2 containing the entire database. These re-
sults are illustrated in Figure 3.5 (a-b) for Group 1 and (c-d) for Group 2. Discrim-
ination between AF type II and the remaining AF types was not tested, since AF
type II takes values between AF types I and III.

Comparison among AF types (I–III) and between pairs of AF types has cor-
roborated the ROC results, as each AF type is distinguishable from the remaining
ones, which can be seen in Table 3.1. Figure 3.6 shows the box and whisker plots
and mean values of each AF type for Groups 1 (a) and 2 (b). It is obvious that
each AF type is distinguishable from the other ones, an observation that is more
clear for Group 1, since it contains the most representative EGMs of each AF type.
Although AF type II of Group 2 seems to take values pretty close or even over-
lapping values of AF types I or III , median values of each AF type are still clearly
distinct from the remaining types.

Table 3.1: Comparison between CGCD values to discriminate between the three
AF Types as well as for pairs of AF Types of Groups 1 and 2.

AF Types	Group 1	Group 2
AF Types I-II-III	$p = 0.00004$	$p < 0.000010$
AF Types I vs II/III	$p = 0.00010$	$p < 0.000010$
AF Types III vs I/II	$p = 0.00010$	$p < 0.000010$
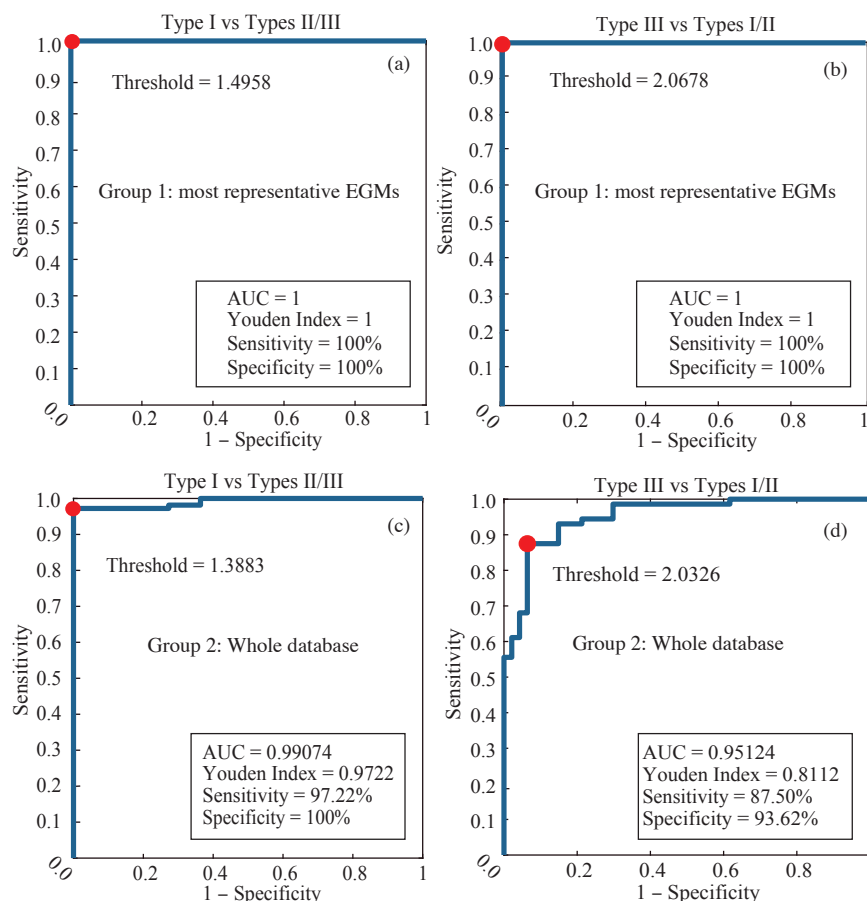
Figure 3.5: ROC curve for 1-vs-all analysis using CGCD. (**a,b**) 24 most representative EGMs in Group 1 and (**c,d**) the entire dataset analyzed in Group 2.

Classification by AF type has shown a perfect performance for Group 1, assigning correctly each AF type and achieving 100% accuracy, as can be seen from Table 3.2 and Figure 3.7.a. In Group 2, 17 out of 119 EGMs were wrongly assigned to an AF type, with maximum accuracy being 85.7% after 10-fold cross-validation. Having a look to the confusion matrix of Figure 3.7.b, 8 out of the 17 EGMs wrongly classified belonged to AF type II and were erroneously classified as AF type I (4) and AF type III (4), while the remaining 9 EGMs belonged to AF type III and were incorrectly classified as AF type II. Consequently, some overlapping may exist between AF types II and III due to the complex nature of these types and the fact that some of these EGMs did not clearly belong to an AF type, which in the first place led to the creation of Group 1. It should be noted, however, that all 17 wrongly classified EGMs of Group 2 were considered as EGMs that did not clearly belong to an AF type by the visual classification, while in any case CGCD value was consistent with their fractionation level.
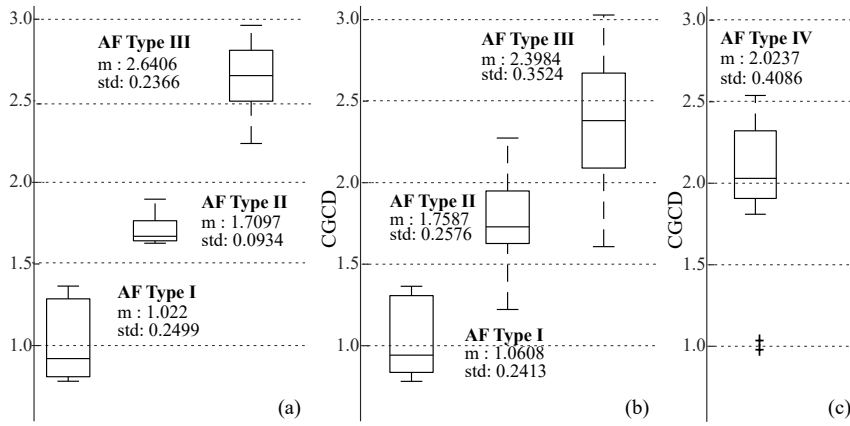
Figure 3.6: Distribution of CGCD values as a function of the AF Types, where (**a**) is for the most representative EGMs in Group 1, (**b**) for the whole database in Group 2, and (**c**) for Type IV pseudo-real EGMs in Group 3.
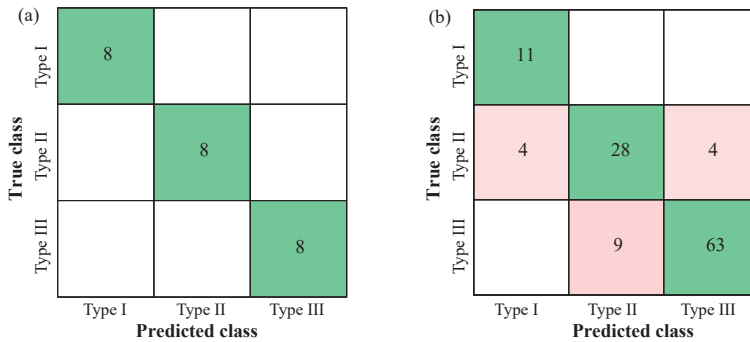
Figure 3.7: Confusion matrix for the most representative EGMs in Group 1 (a) and the whole database in Group 2 (b).

Classification thresholds for each AF type can be observed in Table 3.2 for both Groups 1 and 2. Although pretty similar, thresholds are slightly higher for each AF type in Group 1 with respect to Group 2. Scatterplots of each AF type for Groups 1 and 2 can be observed in Figure 3.8, where the clear discrimination of AF type I in both Groups and the somehow overlapped values of AF types II and III in Group 2 are highlighted. Regarding Group 3 containing the pseudo-real EGMs, the boxplots of the CGCD values for this AF type are shown in Figure 3.6.c. It is clear that median CGCD values of AF type IV EGMs are found between AF type II and III CGCD values, which is consistent to the AF type IV definition as EGMs with alternating parts of AF type III and AF types I or II EGMs. Figure 3.8 corroborates this observation, as AF type IV EGMs are scattered between AF types II and III EGMs. Therefore, a conventional CGCD analysis of these EGMs woud lead to misclassification as one of the three main

Table 3.2: Classification accuracy for Groups 1 and 2 and the corresponding thresholds for the discrimination by different AF Types. T_1, T_2, and T_3 are the thresholds for discriminating AF Types I, II, and III, respectively.

Group	Nr of EGMs	Accuracy	Wrongly classified	Threshold
1	24	100%	0	$T_1 :< 1.4958$ $T_2 :\geq 1.4958,$ < 2.0680 $T_3 :\geq 2.0677$
2	119	$84.00 - 85.70\%$	17	$T_1 :< 1.3880$ $T_2 :\geq 1.3880,$ < 2.0326 $T_3 :\geq 2.0326$

AF types. Finally, AF type IV classification has shown 100% accuracy, as 20 out of 20 pseudo-real EGMs were correctly classified as AF type IV EGMs.

Figure 3.8: Scatterplots of CGCD values for the three AF Types in the most representative EGMs of Group 1 (a), in the whole database of Group (2), and in Group 2 combined with the pseudo-real Type VI EGMs of Group 3 (c).
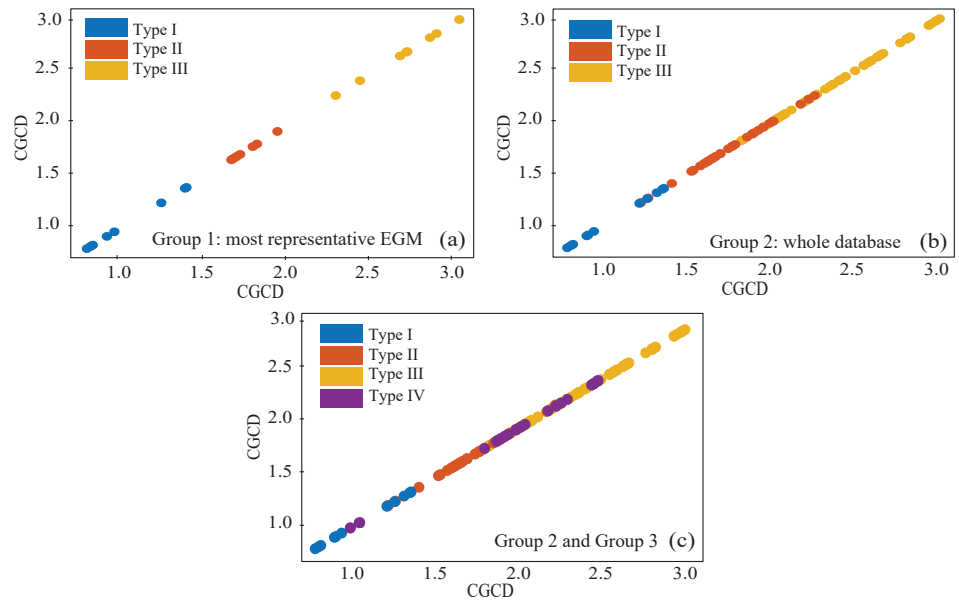
3.5   Discussion

This chapter proposes a novel technique able to quantify AF fractionation during persistent AF based on CGCD. Novelty principally springs from 1-s segment analysis, which allows the real-time mapping of the atrial susbtrate and surpasses the signal-based limitation on parameter selection, as the algorithm can be executed at any EGM length higher than one second. Additionally, analysis on 1-s segments allows the detection of short-time phenomena such as AF type IV occurrence, which would be foreseen by conventional techniques, applied in longer signals without further segmentation. As stability of the recording catheter may affect the fractionation quantification, keeping the epochs as short as one second minimizes the effects of the catheter movement, facilitating the analysis. The execution of the algorithm on segments of one second length has been decided upon trials with slightly longer (1.5 seconds) or shorter (0.5 seconds) segments. Nevertheless, results obtained did not improve the classification performance and as a result, the 1-s length segmentation has been established.

Applying chaos-based techniques on signals as short as of one second has some limitations and computational parameters should be selected with extreme caution in order to avoid infinite values. This problem arises from the fact that, in short time-series, embedded dimension m and time lag τ may be unproportionately long with respect to the data size, as already explained in Section 3.3.2. An example of a reconstructed signal with irregularly high order parameters with respect to signal length can be observed in Figure 3.3. In organized signals, such as the signal showed in Figure 3.3.a, cases (i)–(iii) seem to describe adequately the original signal. Even in high organization cases, though, highly disproportionate parameters such as in case (iv) with embedded dimension $m = 10$ and time lag $\tau = 35$ ms creates an illusion of high order chaos existence. As we move to Figure 3.3.b, which is less organized, even case (iii) seems to perform a slight overestimation of the dynamics. When dealing with chaotic signals, such as in Figure 3.3.c, dynamics in case (iii) are clearly overestimated.

The proposed technique utilized parameters of $m = 4$ for the embedded dimension, $\tau = 8$ ms for the time lag, and $N_{ref} = 334$ for the reference points, as can be seen from case (ii) of each AF type, achieving a faithful visual reconstruction of the dynamics. Even using these relatively low parameters, classification showed satisfactory results of up to 85.7% accuracy even when EGMs of conflicting experts' classification are used. As already explained, CGCD results do not express the chaos dimension of the attractors. The threshold discriminating between AF types I and II was 1.388, while a threshold of 2.033 could discriminate between AF types II and III. The signficance of these thresholds is hence limited to quantify the AF fractionation level of the EGMs and cannot be used to perform raw assessment of the dynamics found in these EGMs.

On the other hand, limiting down the embedded dimension m may lead to underestimation of the CorDim. In any case, knowing beforehand the dynamics dimension in order to decide if the signal length is sufficient is impossible. Notwith-

standing, even when underestimated through small size parameter selection, reconstructed signal will preserve up to a point the dynamics of the original signal [127, 128]. Suppression of the dynamics as an outcome of low dimensional parameter selection is mainly a problem of CorDim, which needs the dynamics to be completely unfold in order to calculate their dimension. When calculating CGCD, however, it is important to remember that not the dynamics themselves but an approach of them is being calculated. This means that, even if not completely unfold, a rough estimation of the dynamics can serve as a comparative tool among different classes, as the EGM classification by AF type. Setting the analysis in segments of one second length is therefore possible and embedded dimension and time lag dependence on segment length can be overcome. Moreover, in nonstationary dynamical systems, as in the case of AF, the use of small sized signals facilitates the observation of the changing dynamics [127].

Discrimination between AF types has been attempted in the past using various techniques such as cluster, spectral or principal component analysis [129–131]. Nonetheless, longer signal duration, low proportion of type III EGMs and lack of information regarding how implementation on AF mapping devices could be achieved do not suggest a realistic implementation of these techniques. AF fractionation has been additionally attempted to be quantified by other techniques [132, 133], with either the results being poorer than the presented technique or including a high proportion of paroxysmal AF patients in the database, which automatically leads to easier calculations due to less amount of complex EGMs. Regarding nonlinear methods, CorDim and CGCD have been previously used in order to discriminate between atrial organization levels in biophysic models or to predict the CA outcome in persistent AF patients [113, 114]. A work similar to the one presented in this chapter was developed in order to discriminate among different AF types in RA unipolar EGMs. Despite the satisfactory results, the use of unipolar EGMs in electrophysiological AF-related procedures is limited. Additionally, ventricular contamination may be present and not adequately removed due to low duration segments used in the study, a fact which would significantly alter the classification results [117, 134, 135].

3.6 Conclusions

This chapter introduced an optimized technique able to discriminate among various fractionation levels. Using 1-s epochs facilitates the calculation process by allowing the establishment of computational parameters independent from the signal length. The algorithm has shown satisfactory classification results and has been proved able to detect sudden changes in EGM fractionation, allowing the identification of AF type IV.

Separate Assessment of Left and Right Atrial Substrate Modification after Catheter Ablation of Paroxysmal Atrial Fibrillation

Contents

4.1 Introduction

So far, studies recruiting P-wave duration to conduct AF-related investigation and especially to assess the atrial substrate modification after CA, perform a uniform P-wave analysis, measuring from P-wave onset to offset [29–36,57,136–139]. When P-R interval is recruited for the same purpose, as beginning point is considered the onset of the P-wave [140–142]. Nevertheless, P-R interval is supposed to describe the AV conduction.

Despite the efficiency of P-wave duration in the CA outcome prediction either from before or after CA measurements, lack of consistency in thresholds set

in different studies [30, 33, 35, 39, 57] alerts the need to reconsider each and every parameter of the analysis. Regarding P-R interval, whether it is associated with AF-related remodeling, without considering the P-wave component, is under dispute [142]. P-wave can be further separated in two halves, corresponding the first to RA and the second to LA depolarization, following the route of the impulse throughout the atria [143, 144]. P-R interval can be partitioned in P-wave and P-R segment, the beginning point of which would be the offset of the P-wave [142].

Without implying that RA cannot be part of the atrial remodeling [42, 46, 100, 145], it is a fact that both atrial substrate [10, 18, 75] and atrial substrate modification are more prominent in LA than RA [10, 17, 61, 87, 142]. Location of PVs in LA implicate the proximity of the latter to the arrhythmogenic source as well as to the isolated tissue after CA and could be an explanation for the remodeling-prone nature of LA with respect to RA. Based on this hypotheis, this chapter performs a microscopic analysis of P-wave and P-R interval by decomposing them into integral parts each providing the highest amount of information regarding the atrial substrate alteration. Taking advantage of the ability of P-waves to illustrate the RA and LA depolarization separately, P-wave was decomposed in first (RA) and second (LA) parts and alteration in duration after CA was studied for each part. P-R interval was measured both including and excluding the P-wave component, corresponding to the atrial depolarization and atrioventricular conduction or exclusively atrioventricular conduction, respectively.

4.2   Materials

Recordings from 29 paroxysmal AF patients were employed. Patients were undergoing circumferential radiofrequency (RF) CA for the first time and were in SR throughout the procedure. CA was performed with the help of an ablation catheter isolating the left and right PVs circumferentially via RF energy. Electroanatomical mapping was guiding the procedure. After the end of PVs CA, non-inducibility was confirmed by continuous pacing. For each patient, two 5-minute 12-lead ECG recordings were acquired: before CA and right after CA was terminated. Mean time of the recordings with respect to CA initiation was 12.3 ± 3.6 minutes. Mean time of the recordings with respect to CA procedure termination was 3.9 ± 5.1 minutes. The recording system used was Labsystem™ PRO EP (Boston Scientific, Marlborough, MA, USA) and sampling frequency was set at 1 kHz.

Analysis was performed in lead II ECG recordings, since they have been found to provide high amplitude and monophasic positive morphology P-waves [146]. Software used was MATLAB© R2019b version. The first step of the preprocessing was PLI removal by a wavelet-based technique followed by muscle noise and baseline wander removal by a bidirectional lowpass filter with cut-off frequency at 70 Hz and a highpass filter with cut-off frequency at 0.8 Hz, respectively [91, 147, 148]. Ectopic beats were present in some of the recordings at a

maximum percentage of 4%. In that case, they were detected and replaced via linear interpolation [149, 150].

4.3 Methods

Detection of P-waves and R-peak was performed [151] and P-wave fiducial points were defined [152]. P-wave fiducial points included P-wave onset, peak and offset. In case of notched P-waves, P-wave peak was defined as the middle point between the two local peaks of the notched signal.

For each beat, the following features were calculated and then averaged for each signal:

1. P-wave duration (PWD): duration of the entire P-wave (onset to offset).

2. $PWD_{on\text{-}peak}$: Duration of the first part of the P-wave (onset to peak–RA depolarization).

3. $PWD_{peak\text{-}off}$: Duration of the second part of the P-wave (peak to offset– LA depolarization).

4. PW_{on}-R: P-R interval, including the P-wave (P-wave onset to R-peak–atrial and AV conduction).

5. PW_{off}-R: P-R interval, excluding the P-wave component (P-wave offset to R-peak– AV conduction).

Distance between ECG fiducial points is dependent on HR fluctuations, hence each of the aforementioned features was additionally calculated for each beat (i) after being normalized by a correction factor (CF) [153]:

$$CF_i = \frac{1000}{IBI_i},\qquad(4.1)$$

where (IBI) is the interbeat interval. Then, each normalized feature was registered as $\mathbf{A}(x)$, being x the corresponding non-normalized feature from the list provided afore. Figure 4.1 shows an example of how PWD can be modified by CF. The remaining figures are modified accordingly.

In order to compare the values measured after with respect to the values measured before CA, MWU was recruited, as data did not follow a normal distribution and were not homoscedastic. Median values were specified and each feature's modification after CA was expressed as percentage (%). Moreover, each feature was correlated with PWD by Pearson's correlation coefficient (PCC), in order to measure the dependency rate of each feature on PWD, which is the most
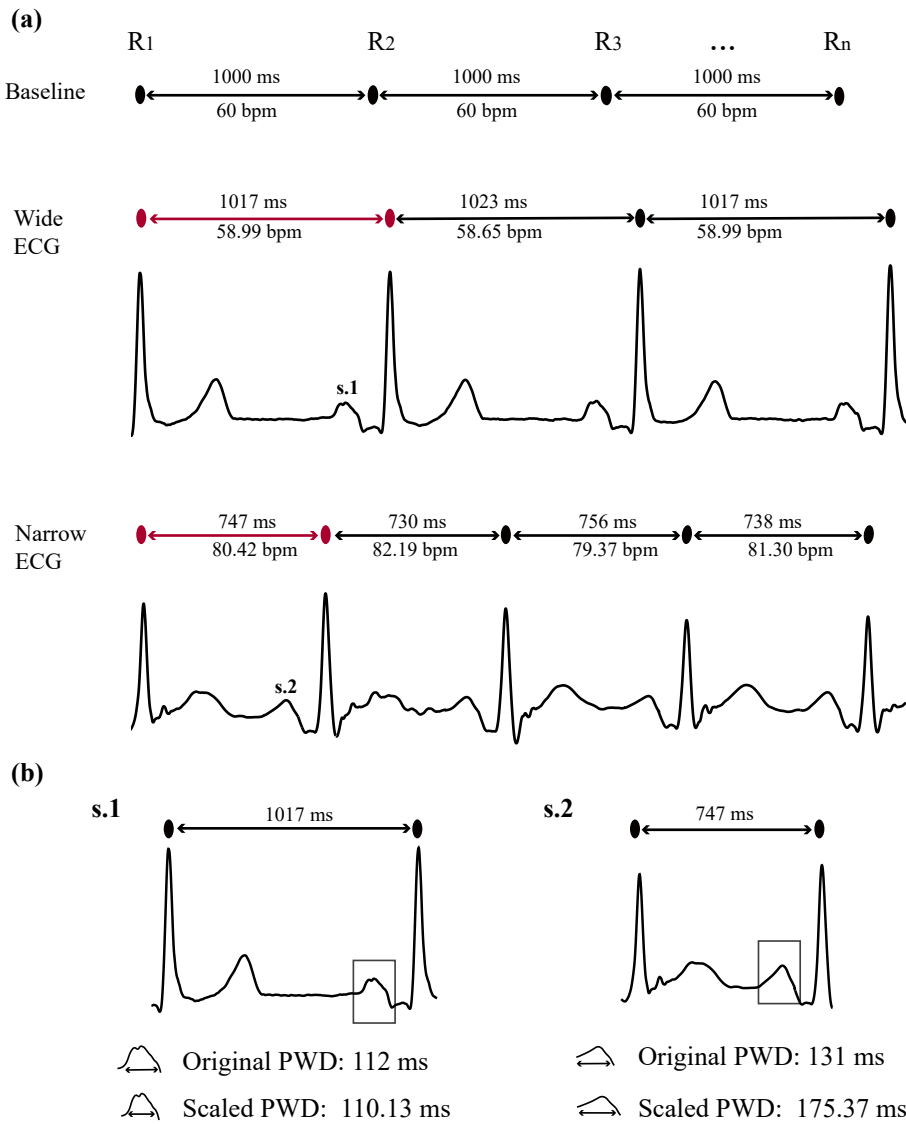
Figure 4.1: Example of P-wave scaling for interbeat intervals longer or shorter than 1000 ms. (**a**) Baseline interbeat interval at 1000 ms and interbeat intervals of a wide and a narrow ECG. Red intervals show the beats chosen to be analyzed as an example in (**b**). (**b**) *PWD* scaling for P-waves of a wide (s.1) and a narrow (s.2) signal.

relevant feature regarding the substrate modification analysis and vice versa. PCC was additionally used in order to compare the effect of CA on each feature with respect to the effect of CA on PWD. This correlation was called correlation of

variation (CoV) and was useful in defining whether any modifications observed on PWD after CA was in line with the modification on the remaining features.

4.4 Results

In cases without applying CF, when comparing the value of each feature after with respect to before CA, PWD and $PWD_{peak\text{-}off}$ (LA depolarization) got statistically shortened (-9.84%, $p = 0.0085$ and -22.03%, $p = 0.025$, respectively). After CF application, the values of the same features got statistically reduced (PWD: -17.96%, $p = 0.0442$ and $PWD_{peak\text{-}off}$: -27.77%, $p = 0.0268$). These results can be observed from Table 4.1.

Table 4.1: Statistical analysis for P-wave features before and after CA. Median values, interquartile range (IQR) and variation due to PVI. Features with statistically significant differences due to CA are shown in **bold**.

Feature	p	Median values (IQR)		Δ [%]
		Before PVI	After PVI	
PWD	**0.0085**	**122.00 (12.00)**	**110.00 (11.00)**	**-9.84**
$PWD_{on\text{-}peak}$	0.5289	67.00 (14.00)	61.00 (11.00)	-8.96
PWD$_{peak\text{-}off}$	**0.0250**	**59.00 (8.00)**	**46.00 (7.00)**	**-22.03**
$PW_{on} - R$	0.5585	246.00 (10.00)	244.00 (11.00)	-0.81
$PW_{off} - R$	0.3519	127.00 (8.00)	140.00 (7.00)	$+10.24$
A(PWD)	**0.0442**	**123.63 (15.08)**	**101.42 (12.15)**	**-17.96**
A($PWD_{on\text{-}peak}$)	0.3651	64.59 (13.00)	60.19 (10.97)	-6.81
A(PW$_{peak\text{-}off}$)	**0.0268**	**59.89 (8.55)**	**43.26 (7.55)**	**-27.77**
A($PW_{on} - R$)	0.3924	264.96 (14.11)	262.19 (12.73)	-1.04
A($PW_{off} - R$)	0.6507	130.47 (9.00)	139.11 (9.62)	$+6.62$

Despite the fact that it was the P-wave part that corresponds to LA depolarization that was significantly and principally modified after CA, correlation between PWD and $PWD_{peak\text{-}off}$ was moderate regardless of the recording (before or after CA) and the application of CF, as can be observed from Figure 4.2. On the other hand, correlation between PWD and $PWD_{on\text{-}peak}$ (RA depolarization) was notably higher ($0.7458 - 0.8051$). PWD showed the highest correlation with $PW_{on} - R$ and the lowest correlation with PW_{off}-R. These results are of no surprise, considering that $PW_{on} - R$ incorporates the entire P-wave, hence being closely related to it, while PW_{off}-R is calculated completely apart from the P-wave, hence being independent from it.

Although the CF has potentiated the correlations between PWD and each and every feature, the effect is more prominent when CoV is assessed. Before CF application, it seems that the effect of CA on PWD is different than the effect
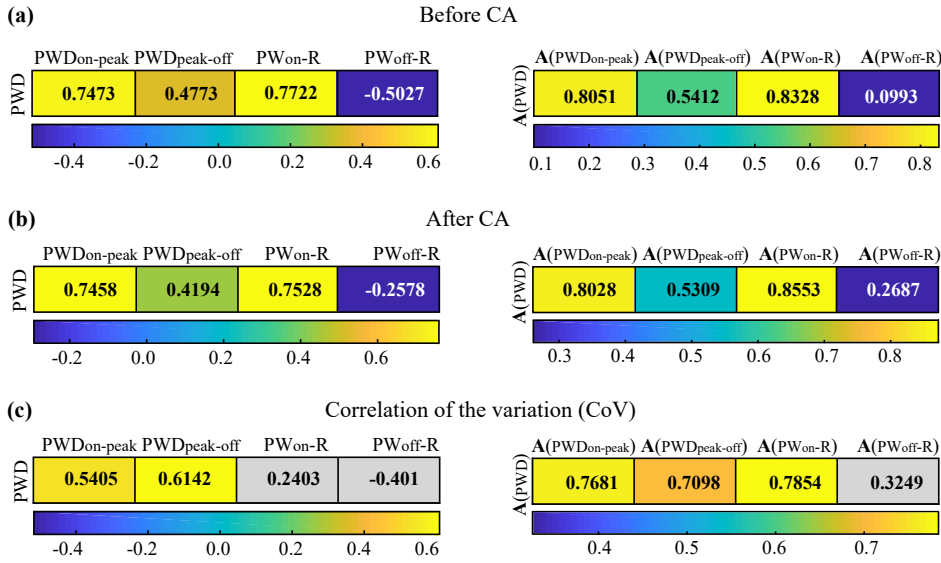
Figure 4.2: Correlation matrices for the relationship between *PWD* and the remaining features. Values without scaling are on the left column and with scaling on the right. (**a**) Results before CA. (**b**) Results after CA. (**c**) Results for the correlation of the variation. Gray cells show statistically insignificant relationships.

of CA on PW_{on}-R (CoV: 0.2403, $p > 0.05$). Notwithstanding, after CF application, a rather similar effect of CA in PWD and PW_{on}-R is observed (CoV: 0.7854, $p < 0.05$). Regarding the first and second P-wave parts, before CF, CoV between PWD and $PWD_{on-peak}$ was slightly lower than $PWD_{peak-off}$ (0.5405 versus 0.6142, $p < 0.05$ for both). Nevertheless, after CF application, CoV between PWD and the former became higher than CoV between PWD and the latter (0.7681 versus 0.7098, $p < 0.05$ for both).

4.5   Discussion

This work has focused on analyzing separately atrial and atrioventricular components from the ECG, vastly used to evaluate the atrial substrate and predict the AF outcome [29–36, 57, 137, 138, 140, 140–142]. Apart from the main analysis, a secondary analysis considering the effect of HR-fluctuations, which seem to intensify due to RF CA [154], has been performed. The degree of dependence between the entire P-wave and each P-wave part has been investigated by PCC. P-wave was found to be more related to the first P-wave part, corresponding to RA depolarization with respect to the second P-wave part. As shown in Table 4.1, RA depolarization lasts longer than LA depolarization. Additionally, RA is the first part to be depolarized, with the normal SR being regulated by sinus node,

which is found in RA [143, 144]. Hence, higher correlation between atrial depolarization, including both atria and RA depolarization time, is of no surprise.

The effect of CA on the entire PWD has also been found to be more consistent with the effect of CA on the first part of the P-wave. Considering all the afore results, PWD shortening would be expected to stem from the modification of the RA due to CA. Nevertheless, Table 4.1 reveals a preeminent shortening on the duration of the second P-wave part, corresponding to shortening of the LA depolarization time, an effect that additionally remains almost intact, although slightly potentiated, after the application of CF. Interestingly enough, shortening of the first P-wave part was observed to a lesser extent, while lacking statistical significance. Considering all the afore, it can be concluded that PWD alteration is provoked due to alteration of the second P-wave part after CA, while the stronger correlation between the first P-wave part and the entire PWD affects the overall PWD analysis, leading to underestimation of the atrial substrate modification. This observation could be an explanation for the various thresholds oscillating between 120 ms and 140 ms in order to define a prolonged P-wave connected with the existence of the atrial substrate [30, 33, 136, 138].

P-R interval is another metric employed to predict the AF outcome [140–142]. However, as it is normally measured from P-wave onset, any modifications observed on this metric may be directly affected by the atrial remodeling. Indeed, P-R interval, measured from the P-wave onset, showed the highest correlation with PWD. Decomposing P-R interval, it can be observed that it consists of three parts that could be analyzed individually: LA depolarization, RA depolarization and AV conduction. As already mentioned, LA depolarization is critical in substrate alteration after CA, with RA depolarization playing a less important role.

P-R interval both including and excluding the P-wave has not been statistically altered by CA. Nevertheless, P-R interval without the P-wave component, describing the AV conduction, seems to be prolonged after CA, although not statistically. In fact, a short PW_{off}-R may be the byproduct of P-wave lengthening, hence being related with AF incidence [140, 142]. Therefore, PW_{off}-R lengthening could be linked with the restoration of the AV conduction time as an outcome of the substrate alteration in the atria after CA. If this is the case, when P-wave is included in the P-R interval calculation, this phenomenon will be as well masked, misleading the results. This observation highlights once more the necessity to study integral and further indivisible parts of the ECG in order to obtain a more precise and reliable perspective of the AF and its mechanisms on the heart.

4.6   Conclusions

Decomposing and separately studying P-wave and P-R interval components is crucial in properly evaluating the atrial substrate and its alteration after CA. PWD may mask the degree of modification of the LA substrate, the study of which is pivotal in atrial remodeling. AV conduction may be useful in AF-related studies.

Nevertheless, its calculation starting from the onset of the P-wave may lead to underestimation of the AF mechanisms in the AV conduction function. When atrial and AV components are studied separately, analysis becomes more robust to HR fluctuations.

Substrate Modification Evaluation after Catheter Ablation of Left and Right Pulmonary Veins

Contents

5.1 Introduction

As already mentioned in the previous chapter, P-wave analysis is vastly recruited to assess the outcome after CA of PVs [29–31, 33, 35, 37, 87, 137, 138]. Besides P-waves, HRV plays an important role in AF recurrence prediction, due to the high relevance between ANS regulation and AF occurence [88, 89, 155]. Despite the efficiency of the aforementioned studies, the CA outcome prediction process could be optimized by analyzing independently the impact of LPVI and RPVI on the atrial substrate modification.

The effectuation of this method requires no additional CA steps or resources, as electrophysiology laboratories normally acquire ECG signals throughout the CA procedure. Therefore, the recording during the transition from LPVI to RPVI

or viceversa is already available and same methods as in traditional P-waves or HRV analysis can be applied. The study to be introduced in this chapter performed P-wave and HRV analysis in recordings acquired before, during and after CA. Recordings during CA correspond to LPVI, while recordings after CA correspond to RPVI. Results indicate that LPVI is in the foreground regarding atrial substrate alteration for paroxysmal AF CA.

5.2 Materials

12-lead ECG recordings from 40 paroxysmal AF patients undergoing RFCA for the first time were utilized for the study. Preprocessing methods performed in this chapter were similar to that from chapter 4, described in Materials section 4.2. PVI order was the following for all 40 patients: first LPVI was accomplished by a crown surrounding both LPVs, followed by RPVI by a crown surrounding both RPVs. Apart from the recordings before and after CA, a 5-minute 12-lead ECG recording during CA was acquired and the same preprocessing methods were performed. As with recordings before and after CA, the selected channel for the recording during CA was lead II. Recording during CA was acquired right after LPVI termination and before RPVI initiation. For readability issues, the three recording points have been matched with three steps (**B**, **L** and **R**). Step **B** corresponds to recordings acquired before CA, step **L** corresponds to recordings acquired during CA (after LPVI), while step **R** corresponds to recordings acquired after the end of CA (after RPVI).

Figure 5.1 illustrates the evolution of each CA step and the conditions that need to be fulfilled in order for the CA of each PV side (LPVI or RPVI) to be considered as critical for the atrial substrate modification. From Figure 5.1.a can be observed that step **B** corresponds to the initiation of the procedure (neither LPVI nor RPVI have been performed), step **L** corresponds to the termination of LPVI, meaning that 100% of LPVI has been accomplished and we are in the middle of the procedure. Finally, step **R** corresponds to the termination of RPVI and at the same time, to the termination of the CA procedure. Figure 5.1.b indicates the conditions under which each side of PVI is considered key for the atrial substrate alteration. If a statistically significant change is observed between the **B–L** steps, it stems from the LPVI, which is therefore considered critical. If a change is observed between the **L–R** steps, RPVI is considered the key. Changes provoked by RPVI can also be observed if a statistically significant change between steps **B–R** is reported. In that case, however, statistically significant changes between the **B–L** steps need to be excluded priorly.
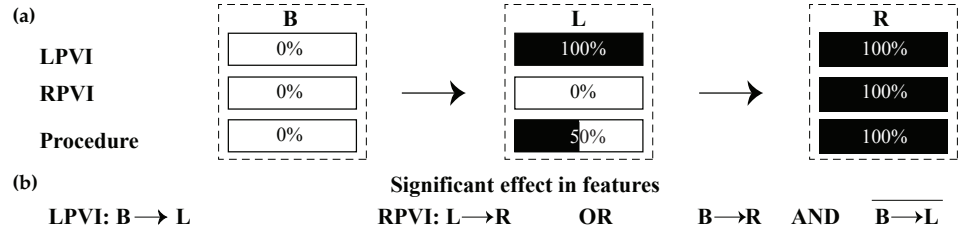
Figure 5.1: (**a**) Steps of CA procedure for which recordings were extracted and analyzed. In step **B**, no ablation has been performed yet (0%). In step **L**, LPVI has been completed (100%) and hence, we are in the middle of the procedure (50%). Step **R** corresponds to RPVI and to the end of the procedure. Therefore, each step is completed (100%). (**b**) Conditions in order for LPVI or RPVI to have a significant effect on the features under analysis.

5.3 Methods

As in chapter 4, detection and delineation of P-waves and QRS complexes was performed, visually inspected by an expert [151, 152]. Once preprocessing and delineation was finished, features were calculated for each and every P-wave and were averaged across each recording. These were: *P-wave duration (PWD)*, *amplitude*, *RMS* value, area (*PosAr*) and *slope rate* [5].

Briefly explained, *PWD* was the interval between the onset and offset of each P-wave. Amplitude includes both the positive amplitude (*PosAmp*) and the peak-to-peak amplitude (*PPAmp*). As lead II shows monophasic, positive morphology signals, these two features tend to converge. Nevertheless, both were calculated in case that significant differences existed. *RMS* value is the quadratic mean of the function that defines the signal. The *PosAr* was calculated as the cumulative positive areas, by integrating the positive signal over time. *Slope rate* was the rhythm of increasing slope at i% of the activation, where $i = 5$, 10, 20. *Slope rate* was caculated according to the following equation:

$$S_i = \frac{Amp(t_i) - Amp(t_{onset})}{t_i - t_{onset}}, \tag{5.1}$$

where $Amp(t_i)$ is the amplitude at the i% of the activation duration, $Amp(t_{onset})$ is the amplitude at the onset of the activation, t_i is the sample point at the i% of the activation duration and t_{onset} is the sample point corresponding to the onset of the activation.

Apart from the aforementioned activation-wise features, additional features were calculated at each recording, meaning that only one value per recording was provided and no signal averaging was necessary. Morphology variability (*MV*) and *dispersion* were calculated involving P-waves. For *MV*, an adaptive

signed correlation index (ASCI) was utilized to correlate a reference signal made by the 20 most similar P-waves with each P-wave activation. Unlike other studies, *dispersion* was computed by recruiting only lead II, as the difference between the 25th and 75th percentiles of the PWD of each recording.

Moreover, time-domain HRV features were calculated. Normally, HRV features describe the AV node and ventricular response, measured by variation in R-R interval series. In this chapter, however, features were measured in a way that they described the atrial response, utilizing P-wave to P-wave series, instead. Due to this reason, they will be referred as atrial-rate variability (ARV) features. These features, were the standard deviation of normal-to-normal beat interval (*SDNN*), variance of normal to normal beat interval (*VARNN*) and RMS of successive interbeat differences (*RMSSD*), where in this case each beat was defined by the P-wave instead of the R peak.

As in chapter 4, HR fluctuations were compensated by a CF, as described in 4.1. Normality and homoscedasticity were tested as in chapters 3 and 4 and non-parametric tests were employed. Each feature is compared among the three steps (**B**, **L** and **R**) with KW and comparison between each pair of steps has been performed with MWU with Bonferroni correction. Moreover, median and interquartile range values were calculated and the quantitative difference between each two steps in terms of percentage was called percentage of variation (POV) and calculated by the following formula:

$$POV(r_i) = (\frac{V_2}{V_1} - 1) \times 100 \ [\%], \tag{5.2}$$

where r_i is the recording of the ith patient, V_2 is the value of each feature at the posterior step and V_1 is the value of the same feature at the prior step. MWU was utilized to test how POV was modified between ablation steps **B–L** and **L–R**. The HR at each ablation step was finally calculated and compared among all steps with KWU.

5.4 Results

Table 5.1 shows the HR values at each of the three steps. A slight, though not statistically significant, reduction in HR after LPVI (step **B**) can be observed. KW results indicated that the HR values were comparable among the three steps. The results of the multistep comparison as well as the comparison in pairs of channels are shown in Table 5.2 for all the features. It can be observed that *PWD* varied statistically among the three steps. Having a look to the paired comparisons, variation was seen in the **B–L** and **B–R** comparisons, while the **L–R** comparison was not statistically significant. Considering Figure 5.1.b, this implies that the statistically significant results obtained from the **B–R** comparisons probably stem from the **B–L**, which in that case is critical in *PWD* modification. None of the

remaining features varied significantly after any of the steps. Notwithstanding, a trend was observed for amplitude features as well as for *RMSSD* after **L**.

Table 5.1: Heart-rate at each ablation step and comparison between three steps (KW). As result indicated a non-significant comparison, no MWU has been performed. KW: Kruskal-Wallis; MWU: Mann-Whitney U-test; B: before CA; L: after LPVI; R: after RPVI.

	B	**L**	**R**
Median (iqr)	57.2 (17.0)	55.0 (12.0)	58.6 (13.4)
KW		0.7713	

Table 5.2: Results for KW and MWU tests. Statistically significant results are marked with (∗). Due to Bonferroni correction, threshold for MWU (last three columns) is $\alpha = 0.0167$.

	KW	**MWU**		
Features		**B-L**	**B-R**	**L-R**
PWD [ms]	0.003∗	0.001∗	0.009∗	0.558
$PosAmp$ [mV]	0.084	0.055	0.097	0.319
$PPAmp$ [mV]	0.084	0.056	0.097	0.319
RMS [mV]	0.144	0.103	0.150	0.275
$PosAr$ [$mV \times ms$]	0.141	0.103	0.103	0.438
S_5 [mV/ms]	0.162	0.110	0.235	0.211
S_{10} [mV/ms]	0.178	0.117	0.420	0.150
S_{20} [mV/ms	0.336	0.384	0.693	0.133
S_{max}[mV/ms]	0.823	0.987	0.602	0.602
A(PWD)	0.159	0.141	0.079	0.740
A($PosAr$)	0.144	0.085	0.110	0.716
A(S_5)	0.367	0.261	0.235	0.537
A(S_{10})	0.441	0.248	0.402	0.558
A(S_{20})	0.801	0.693	0.837	0.517
A(S_{max})	0.994	0.962	1.000	0.912
MV	0.476	0.189	0.624	0.646
$Dispersion$ [ms]	0.310	0.208	0.176	0.949
$SDNN$	0.136	0.133	0.862	0.060
$VARNN$	0.136	0.133	0.862	0.060
$RMSSD$	0.136	0.052	0.962	0.069

Median values are shown in Table 5.3. POV, describing the modification of each feature after each step, is described in Table 5.4, which additionally shows the result of the comparison between the direct effect of steps **L** and **R**, measured by the **B–L** and **L–R** comparison. After LPVI (step **L**), *PWD* fell from 120 to 104 ms, registering a shortening of −13.30%. Not only did RPVI not achieve any additional *PWD* shortening, but also a slight increment has been recorded, with *PWD* reaching up to 106.5 ms. MWU for the variation observed between these two steps indicates a different effect of LPVI than RPVI (see last column of Table 5.4). Although not statistically important, similar trends were observed from the amplitude features. Finally, the opposite phenomenon has been observed regarding *RMSSD*, where LPVI caused an ARV increment, partially restored after RPVI.

Table 5.3: Median (interquartile) values for each feature.

Features	Median B	L	R
PWD [*ms*]	120.0 (12.00)	104.0 (13.00)	106.5 (21.00)
PosAmp [*mV*]	0.428 (0.303)	0.354 (0.290)	0.374 (0.232)
PPAmp [*mV*]	0.431 (0.303)	0.356 (0.290)	0.374 (0.232)
RMS [*mV*]	0.263 (0.179)	0.214 (0.179)	0.230 (0.232)
PosAr [*mV* × *ms*]	24.63 (12.94)	16.57 (14.62)	20.39 (9.98)
S_5 [*mV/ms*]	0.005 (0.002)	0.007 (0.004)	0.006 (0.002)
S_{10} [*mV/ms*]	0.007 (0.002)	0.008 (0.004)	0.007 (0.003)
S_{20} [*mV/ms*]	0.010 (0.005)	0.011 (0.003)	0.009 (0.005)
S_{max} [*mV/ms*]	0.010 (0.004)	0.009 (0.004)	0.008 (0.004)
A(*PWD*)	119.5 (57.39)	106.9 (26.04)	101.0 (36.91)
A(*PosAr*)	26.10 (16.94)	19.40 (14.16)	22.12 (14.01)
A(S_5)	0.004 (0.004)	0.006 (0.006)	0.006 (0.003)
A(S_{10})	0.006 (0.003)	0.007 (0.007)	0.007 (0.004)
A(S_{20})	0.010 (0.005)	0.010 (0.008)	0.009 (0.006)
A(S_{max})	0.009 (0.007)	0.008 (0.006)	0.008 (0.006)
MV	0.605 (0.329)	0.753 (0.335)	0.675 (0.467)
Dispersion [*ms*]	12.00 (4.000)	11.00 (7.000)	10.00 (4.000)
SDNN	94.25 (55.32)	99.91 (71.96)	84.28 (62.10)
VARNN	8.8×10^3 (1.07×10^4)	9.9×10^3 (1.77×10^4)	7.1×10^3 (1.21×10^4)
RMSSD	95.44 (59.68)	126.79 (95.29)	92.51 (61.73)

Results after application of CF were not in line with the aforementioned results regarding duration, where no statistically significant difference was observed, although again LPVI achieved major reductions in *PWD* (**B-L** on Table 5.4).

Table 5.4: POV for between every two ablation steps and comparison between POV of successive step transitions **B-L** and **L-R**. Statistically significant results are shown in (∗). POV: percentage of variation.

Features	B-L [%]	L-R [%]	B-R [%]	MWU (BL-LR)
PWD	−13.30	0.00	−11.01	$< 0.0001*$
PosAmp	−16.65	3.86	−11.25	0.0556
PPAmp	−16.04	3.80	−11.52	0.0556
RMS	−18.51	7.51	−12.39	0.1032
PosAr	−25.68	6.50	−20.72	0.1032
S_5	30.95	−13.75	12.95	0.1101
S_{10}	15.75	−11.23	−0.73	0.1173
S_{20}	12.84	−18.35	−7.87	0.3843
S_{max}	−5.40	−6.96	−11.99	0.9874
$\mathbf{A}(PWD)$	−13.73	1.60	−14.49	0.1412
$\mathbf{A}(PosAr)$	−24.54	6.60	−19.65	0.0847
$\mathbf{A}(S_5)$	58.69	−9.34	43.87	0.2614
$\mathbf{A}(S_{10})$	13.41	−4.38	8.45	0.2482
$\mathbf{A}(S_{20})$	3.35	−6.44	−3.30	0.6925
$\mathbf{A}(S_{max})$	−6.60	−1.21	−7.74	0.9621
MV	15.00	−6.11	−0.42	0.1892
Dispersion	−22.42	22.22	−9.55	0.2084
SDNN	28.39	−24.27	0.28	0.1249
VARNN	64.86	−42.64	0.57	0.1249
RMSSD	45.15	−28.30	0.26	$0.0445*$

A trend in that case is observed in the **B–R** comparison, probably due to a cumulative CA effect in the AF substrate. Otherwise, POV after step **R** on Table 5.4 would have indicated a *PWD* reduction, which would be further confirmed by a significant **L–R** variation from Table 5.2. CF application additionally indicated a reductive trend for *PosAr* after LPVI, which was not observed from the original features. Some of the most interesting POV observed are shown for the respective features in Figure 5.2, allowing a better illustration of *PWD* and $\mathbf{A}(PWD)$ variations after each step. As ARV features showed the opposite trend, with increasing values after LPVI and decreasing after RPVI, they are also included in the figure.

5.5 Discussion

The study described in this chapter has focused on understanding the role of each PV side ablation to the modification of P-wave and ARV features, vastly
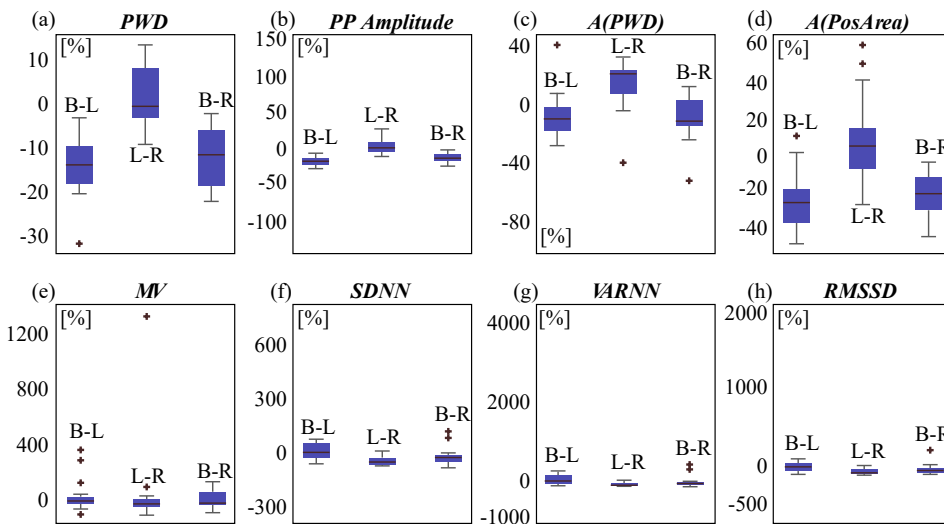
Figure 5.2: Representation of significant alterations illustrated as boxplots of POV between the defined ablation steps for selected features. (a) Variations in PWD; (b) variations in PP amplitude; (c) variations in PWD after CF application; (d) variations in area after CF application; (e) variations in MV; (f)–(h) variations in time domain ARV features (SDNN, VARNN and RMSSD, respectively). Notice that the y-axis is in different scale for each feature. B-L: variation after LPVI; L-R: variation after LPVI; B-R: variation between the beginning and end of CA.

recruited to analyze the AF substrate alteration. To accomplish this, additional recordings obtained during CA procedures, corresponding to LPVI termination, were analyzed. When a conventional analysis was performed, a signficant P-wave shortening has been observed (results in **B–R** comparison), implying the significant role of PVs CA for AF substrate modification, as already demonstrated by a plethora of studies [29–31, 33, 35, 37, 87, 137, 138]. When a separate LPVI and RPVI analysis was performed, the shortening has been found to stem from LPVI, as the significant **B–L** comparison indicated. In fact, LPVI yielded a 13.30% decrease of *PWD* from 120 to 104 ms. This decrease was actually the 100% of the observed decrease throughout the procedure, as RPVI has caused a slight *PWD* increase. A possible deviation of $1 - 2$ ms in P-wave delineation precision may be the reason for the increased values after RPVI. However, considering the duration values, this possible imprecision is $< +2.00\%$ of the values range, hence considered acceptable. Although CF did not reveal any hidden relationships and did not maintain the statistical value of the original analysis, the role of LPVI as the principal *PWD* reductor was preserved.

ARV analysis showed a non-significant reduction after RPVI, which corresponded to the CA procedure termination. This result is in line with previous HRV analysis studies [88, 89, 155]. Interestingly enough, ARV was increased after LPVI, a detail normally missed in a typical before-after analysis. This trend can

be explained by the RF energy effect, directly applied to the atrial tissue during step **L**, which has been found to cause HRV increase and HR decrease [154, 156]. In line with the aforementioned studies, HR was indeed slightly yet not statistically significantly decreased in step **L**. RF energy exposure may have additionally affected up to a point amplitude values, which showed a trend for reduction after LPVI and the overall procedure, as also shown in previous studies [31] yet registering a slight increase after RPVI.

5.6 Conclusions

P-wave shortening, extensively reported in previous studies, stems from LPVI, which is the critical part of CA of PVs for paroxysmal AF patients. RF exposure causes temporary ARV incrementation, which is immediately reversed after the CA procedure termination. Without employing recordings during CA, the observation of this phenomenon would probably have been lost.

Evaluation of Substrate Modification after Catheter Ablation of Atrial Fibrillation from Coronary Sinus Electrograms

Contents

6.1 Introduction

AF mapping is a fundamental step of CA in order to detect AF triggers and areas favoring the AF perpetuation. CS is vastly used as a reference during AF mapping, allowing the localization of AF drivers. CS location between RA and LA is the strong advantage of CS as a CA reference, forming an interatrial bridge and facilitating the AF perpetuation [54, 157–160]. Due to its strategical position, CS catheterization allows the mapping of the entire atria, depending on the channel which pacing is applied to [161–163].

Although P-waves analysis is considered a reliable method for the AF substrate modification evaluation, proximity of intracardiac recordings to the atria makes them a more reliable and desirable source of observation with respect to the AF substrate and the AF substrate modification [40]. Nevertheless, mapping catheters are constantly in a state of motion, not allowing the acquirement of stationary recordings for a time longer than a few seconds or minutes. Due to its utilization as a CA reference, CS recordings are available for analysis throughout and after the procedure, hence being a candidate source of AF substrate modification evaluation.

CS catheterization is performed with the most proximal pair of electrodes (9–10) placed close to RA and the most distal pair of electrodes (1–2) placed close to LA [42, 100]. A number of issues affects the catheterization procedure as well as the quality of CS recordings. Variable CS anatomy and shape, vivid cardiac contraction and atrial fibrosis as well as anatomical alterations of adjacent to CS structures across cardiac cycle affect the recording quality, especially from the extreme electrode pairs [164–169].

The present chapter analyzes in detail the possibility of assessing the AF substrate modification from CS recordings. The first step is the quality assessment of CS channels in order to define the most and least recommendable channels for analysis during SR. Afterwards, using the established P-waves and HRV analysis presented in chapter 4, correlations between P-waves and time-domain ARV features are calculated. Finally, AF substrate modification is assessed from CS recordings and a rough comparison between AF substrate modification from CS recordings with respect to P-waves and ARV analysis results from chapter 5 is performed in Section 6.5.

6.2 Materials

The study described in this chapter shares the database, ECG preprocessing and delineation methods with chapter 5, being lead II the channel under analysis for this chapter as well. As in chapter 5, three recording points were used, being these **B**–before CA, **L**–during CA (after LPVI) and **R**–after CA. Bipolar recordings from a decapolar CS catheter with 1 kHz sampling frequency were addition-

ally obtained and denoised, removing the PLI, the baseline fluctuation and the ventricular activity, whenever it was observed [91, 170]. Local activation waves (LAWs) were afterwards detected and delineated, using a five-point moving average filter to smooth each LAW [5, 171]. Channels of bipolar CS catheter were: distal (D), mid-distal (MD), medial (M), mid-proximal (MP) and proximal (P).

6.3 Methods

6.3.1 P-wave and CS LAWs features calculation

P-wave and time-domain ARV features as described in chapter 5 were calculated. CS LAWs features were calculated in the same way as P-wave and ARV features, using LAWs instead of P-waves for analysis and ARV calculation. An additional feature was calculated for LAWs, called number of deflections and inflections (*NODI*). Deflections and inflections of each LAW were calculated using two auxiliary baselines at $\pm 25\%$ of LAWs amplitude. Increasing NODI is proportional to increasing signal complexity and, hence, AF severity. As in chapters 4 and 5, CF was used to mitigate the effect of HR fluctuations.

6.3.2 Statistical analysis

As in the previous chapters, non-parametric tests were performed due to non-normal and non-homoscedastic results. CS channels analysis was performed using *Duration*, *Amplitude*, *Area* and *NODI* features. Values of these features among all channels were compared with a KW test in order to define whether the value of a feature was different from channel to channel. Deeper analysis, comparing the values for each pair of two channels with a MWU test with Bonferroni correction with threshold $\alpha_1 = 0.005$, was then performed. Median values and one-vs-all analysis for CS channels was calculated with a MWU test with Bonferroni correction, in order to specify not only which channel deviated from the remaining ones, but also whether this deviation was connected with a better or worse signal quality. Threshold in that case was $\alpha_2 = 0.01$. Finally, how the reference morphology of each channel correlated with the reference morphologies of the remaining channels was calculated using an ASCI with 12% tolerance.

For the remaining analysis of correlations between CS LAWs and P-waves as well as for the AF substrate evaluation from CS recordings, analysis on CS recordings was performed utilizing a unique CS channel. This channel varied from patient to patient but was the same for one patient, across the three recording points. Channel selection was performed between the most robust channels, as defined from the first part of the analysis presented in this chapter, using high amplitude and low baseline fluctuation as criteria. For the correlation analysis,

all CS LAWs features, except for *NODI* were used and compared with P-wave
features results from chapter 5.

Correlations were investigated both between CS LAWs and P-waves of one
recording point (Figure 6.1.a), performing a LAW-to-P-wave comparison and for
the effect of each CA step on CS recordings, cross-correlated with the effect of
each CA step on lead II recordings (Figure 6.1.b). For comparison between each
LAW and P-wave, Pearson's correlation and linear regression [172] with 10-fold
cross-validation tested linear correlations. Afterwards, cross-quadratic sample
entropy (CQSE) with $m = 1$ and $r = 0.35$ was used to test non-linear correlations
[173, 174]. For the effect of each CA step on bipolar CS recordings, POV was first
calculated as in chapter 5.3. Then, correlation between variation (CV) of P-waves
and CS LAWs was calculated with Pearson's correlation.
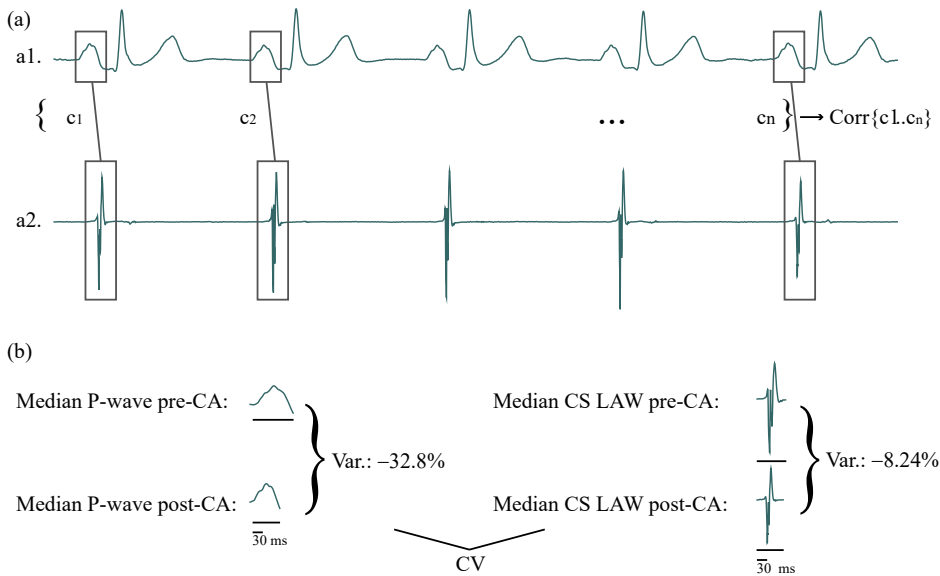
Figure 6.1: (a) Calculation of LAW-to-P-wave correlations and (b) correlations be-
tween the effect of CA on lead II and CS recordings. LAW-to-P-wave correlations
are calculated by an activation-to-activation comparison. On the other hand, the
correlations between the effect of CA on lead II and CS recordings (CV) is cal-
culated by comparing the variation of P-wave features with the variation of the
corresponding LAW features after CA.

Finally, substrate modification was evaluated from CS recordings. For this
purpose, all calculated features were recruited. Statistical analysis in this case is
the same as described in chapter 5, comparing between CA steps with KW and
MWU test with Bonferroni corrections, additionally calculating median values at
each recording point and POV between two recording points.

6.4 Results

6.4.1 Reliability analysis of CS channels

How features varied among channels as well as in pairs of channels can be seen from Table 6.1, where only pairs of channels that showed statistically significant differences can be seen. Amplitude and area values were different between D and M or MP channels, showing additionally either some trends or statistically significant results when MP channel is compared with MD channel. Due to Bonferroni correction, threshold is $\alpha_1 = 0.005$. Furthermore, channels D and M showed a trend for *Duration*. One-vs-all analysis as well as median values are then shown in Figure 6.2. Channels D, M and MP varied significantly with respect to the remaining channels. As it can be observed, D channel showed the lowest values for amplitude- and area-related features, while M and MP channels showed the highest values for the same features. Regarding *Duration*, although results did not reach statistical significance, D channel showed the highest value, followed by MD channel, while MP and P channels showed the first and second lowest values, respectively.

Figure 6.3 shows how reference morphology of each channel correlated with the remaining channels. Although, as expected, all channels showed strongly related morphologies between them, these were higher in the proximal area (including mainly MP and P channels) and lower in the distal area (consisting of MD and D channels).
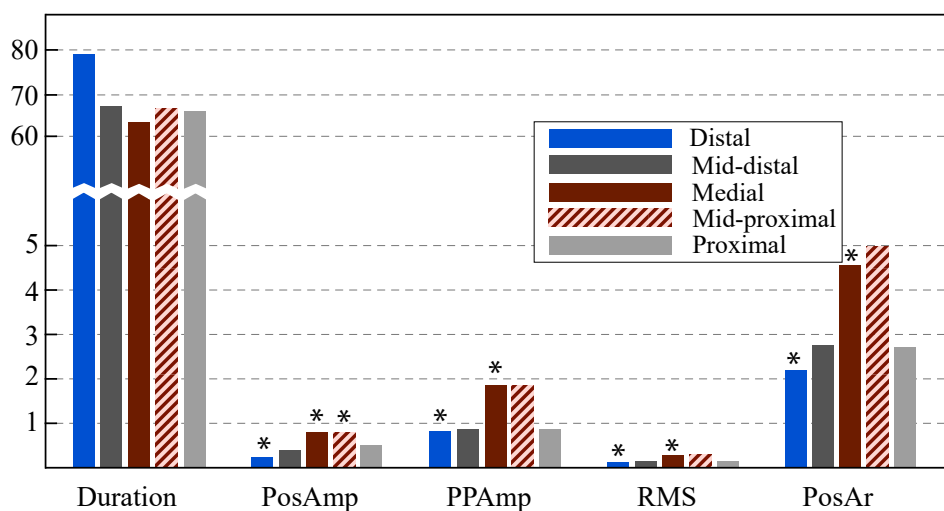

Figure 6.2: Bar graph for the median values of the analyzed features at each one of the CS channels. Note the break in the vertical scale for the feature *Duration*. Asterisk (*) indicates channels that showed a different than the rest value in the respective features, according to 1-vs-all analysis.

Table 6.1: Comparison among (KW) and between (MWU) channels. Asterisk (*) indicates statistically significant results. Only the most significant channel pairs are shown. Threshold α_1 is used for MWU analysis.

	KW	MWU				
		D-M	D-MP	MD-M	MD-MP	MP-P
Duration	0.2136	0.0188	0.0893	0.3502	0.8927	0.7001
PosAmp	< 0.0001 *	< 0.0001 *	< 0.0001 *	0.0053	0.0038 *	0.0502
PPAmp	0.0001 *	< 0.0001 *	0.0002 *	0.0087	0.0182	0.0491
RMS	0.0003 *	0.0001 *	0.0007 *	0.0053	0.0409	0.0950
PosAr	0.0008 *	0.0003 *	0.0020 *	0.0080	0.0491	0.0950
Deflections	0.7925	0.6217	0.2458	0.9749	0.5681	0.7430
Inflections	0.8045	0.6324	0.7477	0.9840	0.4349	0.2354
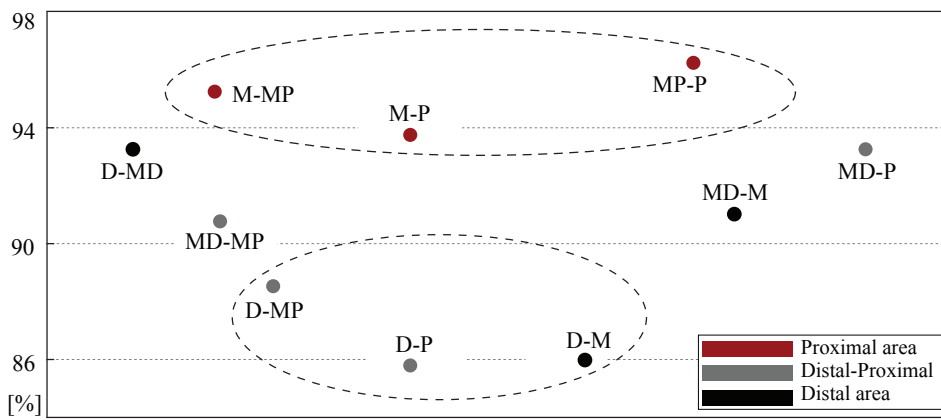
Figure 6.3: Correlations between LAWs morphology of all channel pairs. The upper and bottom ellipse areas show the channel pairs that correlated the most and least, respectively. Red pairs correspond to proximal area (medial-to proximal), black to distal area (medial to distal) and gray the distal-proximal area.

6.4.2   Correlations between lead II and CS recordings

Figure 6.4 consists of an illustrative example of how CF application alters the pattern of CS LAWs and P-waves *Duration*, leading to higher similarity, as can be observed in Figure 6.4.a and hence higher correlation, as can be observed from Figure 6.4.b. Pearson's correlations between each CS LAW and P-wave, averaged for each signal, is shown in Figure 6.5. Before CF, significant correlations were found for amplitude and area features as well as for S_{max}, but were weak for all recording points.
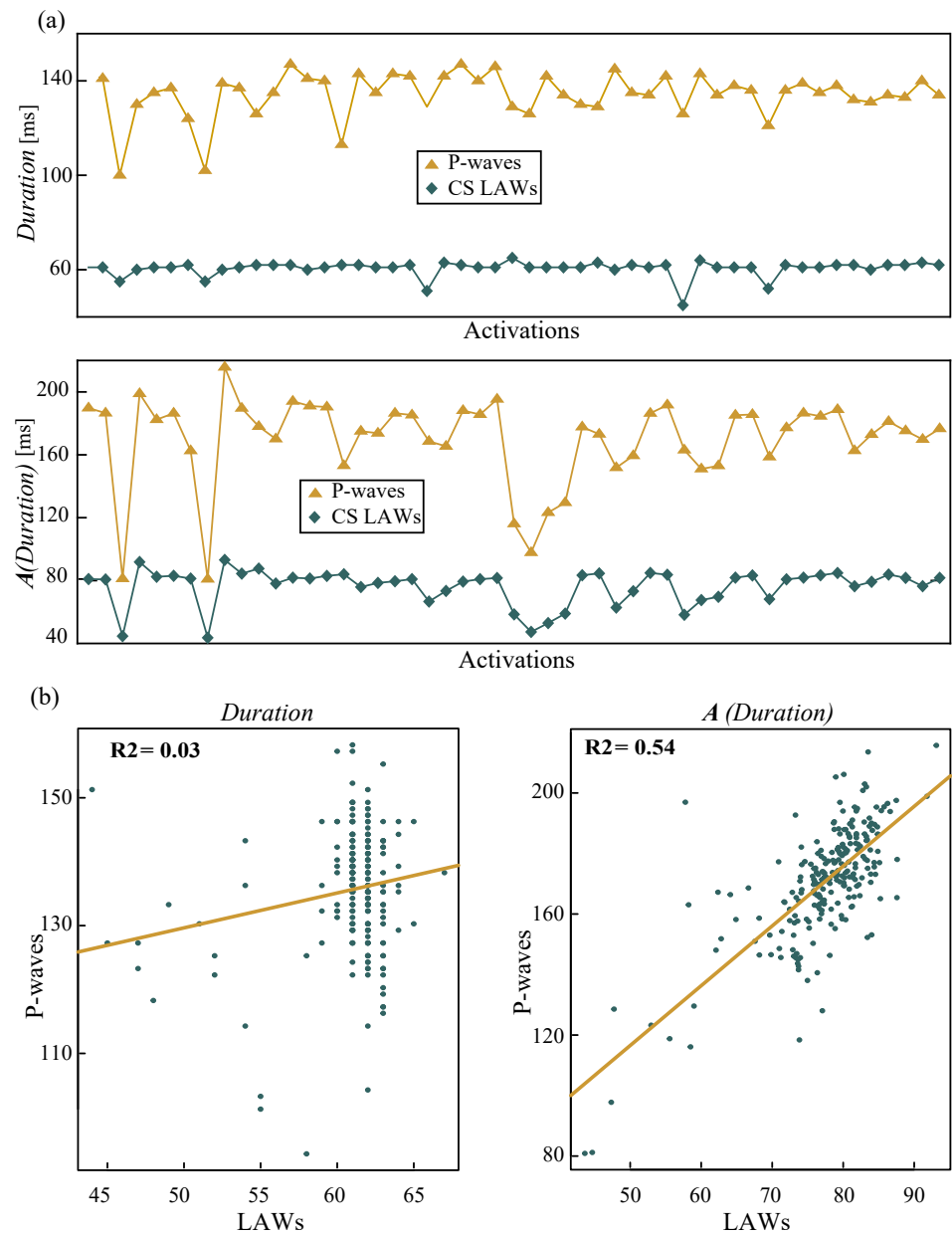
Figure 6.4: Example showing how CF affects the correlation of the computed features. (a) Time instance of 50 activations for correlation of *Duration*, unprocessed (top) and after CF (bottom). (b) Linear regression of the same recording before (left) and after (right) CF . Linear correlation has increased from $R^2 = 0.03$ to $R^2 = 0.54$.
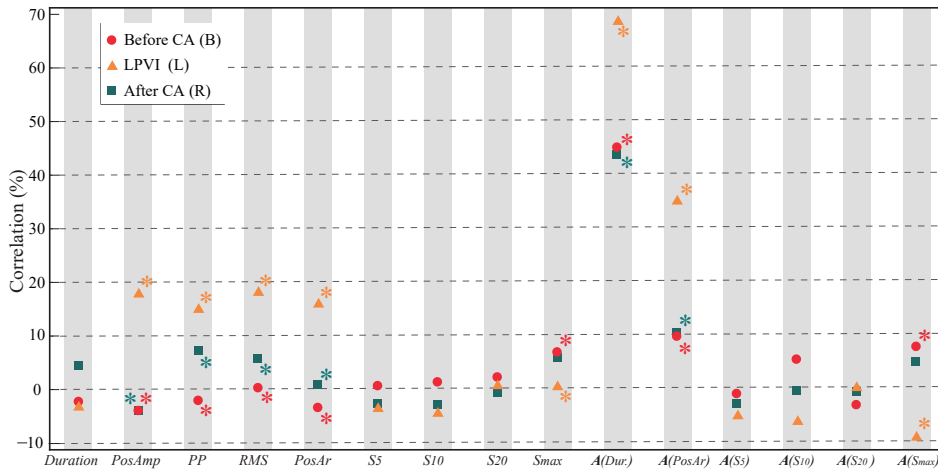
Figure 6.5: Pearson correlation between surface and invasive features of each activation, measured before CA (red), after LPVI (green) and after the end of the CA procedure (blue). Statistically significant results are marked with asterisk (∗).

CF achieves a notable incrementation of $\mathbf{A}(Duration)$ (+43.82% to +69.91%, $p < 0.0001$) and a relatively lower, but still high enough, increase in $\mathbf{A}(PosAr)$. Results for LR showed similar trends with Pearson's correlation and are not illustrated. As mentioned afore, CF has significantly increased correlation of *Duration*.

Regarding non-linear analysis, median CQSE values can be seen in Figure 6.6. These span from 0.6 to 1.2, indicating insignificant non-linear relationships. It is intresting to observe that CF application did not affect CQSE analysis. Whether CA steps have affected in a similar way the lead II and bipolar CS recordings can be observed from the CV results of Table 6.2. Before CF, only *RMS* in the final part of the CA (**L–R**) and S_{10} in the first part of the CA (**B–L**), showed small to moderate statistically significant correlations. CF has managed to enhance signficantly the correlations for $\mathbf{A}(Duration)$ and $\mathbf{A}(S_{10})$. Finally, time-domain ARV features have shown quite similar trends for P-waves and LAWs, especially after the end of CA, while weak to moderate correlations have been observed after LPVI.

6.4.3   AF substrate assessment from CS recordings

Tables 6.3 and 6.4 show the median values of all features at each recording point and the statistical results of the comparison between values from different recording points, respectively. Due to Bonferroni correction, threshold α_2 is 0.0167. As it can be observed, for LAWs-related features, no statistically significant changes have been recorded. Notwithstanding, a trend for *MV* between **B** and **L** can be observed. Variations are more prominent in ARV features, showing mostly a trend especially when modifications between **B** and **L** and **L** and **R** are observed.
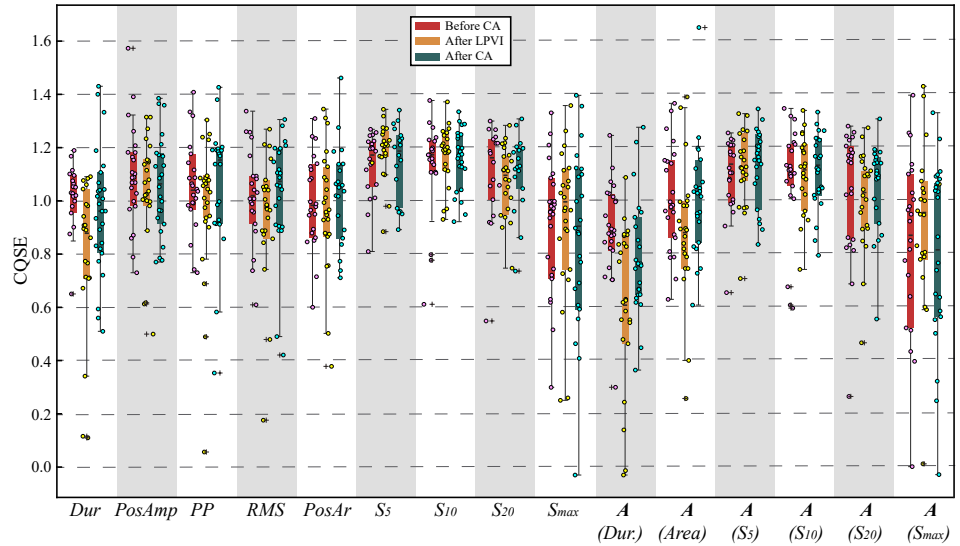
Figure 6.6: Combined boxplot with scatterplot for CQSE between surface and invasive features before (left), after LPVI (center) and after full CA (right).

Table 6.2: Pearson's correlations (ρ%) and p values between LAWs and P-waves for CV every two ablation steps. Statistically significant results are shown in **bold**.

Feature	CV_{B-L}		CV_{B-R}		CV_{L-R}	
	ρ [%]	p value	ρ [%]	p value	ρ [%]	p value
Duration	34.82	0.1567	13.31	0.5984	−17.58	0.4854
PosAmp	6.16	0.8081	11.40	0.6253	38.24	0.1173
PP	8.67	0.7326	3.56	0.8885	39.20	0.1077
RMS	1.41	0.9556	18.28	0.4679	**54.07**	**0.0205**
PosAr	−43.37	0.0722	−20.56	0.4131	36.60	0.1352
S_{10}	**26.29**	**0.0009**	22.54	0.3684	10.44	0.6803
S_{20}	26.29	0.2919	−26.10	0.2955	7.77	0.7593
S_{max}	−14.36	0.5690	−14.37	0.5695	31.11	0.2089
A(*Duration*)	**85.72**	**< 0.0001**	**78.89**	**< 0.0001**	**53.90**	**0.0210**
A(*PosAr*)	2.76	0.9135	9.01	0.7220	42.64	0.0776
A(S_{10})	**73.23**	**0.0055**	18.91	0.4523	15.06	0.5508
A(S_{20})	28.33	0.2546	−28.46	0.2523	5.88	0.8167
A(S_{max})	−3.91	0.8776	−39.45	0.1052	28.70	0.2482
SDNN	**48.33**	**0.0422**	**92.75**	**< 0.0001**	**89.15**	**< 0.0001**
VARNN	17.44	0.4883	**92.23**	**< 0.0001**	**86.63**	**< 0.0001**
RMSSD	42.12	0.0817	**51.23**	**0.0297**	**94.20**	**< 0.0001**

Table 6.3: Median (interquartile) values for each feature of the CS LAWs. As highest peak is often found in negative amplitude in LAWs, slope rate in $\mathbf{A}(S_{max})$ is negative.

	Median		
Features	**B**	**L**	**R**
Duration [ms]	100.5 (14.00)	97.50 (18.00)	90.00 (23.00)
PosAmp [mV]	0.492 (0.987)	0.509 (0.893)	0.641 (0.775)
PPAmp [mV]	1.361 (2.624)	1.382 (1.495)	1.570 (1.462)
RMS [mV]	0.150 (0.345)	0.151 (0.195)	0.181 (0.218)
PosAr [mV×ms]	4.407 (5.175)	3.718 (5.160)	3.985 (4.836)
Deflections	3.000 (1.000)	3.000 (1.000)	3.000 (1.000)
Inflections	3.000 (1.000)	3.000 (1.000)	2.500 (1.000)
S_5 [mV/ms]	3.2×10^{-4} (2.1×10^{-4})	3.9×10^{-4} (3.4×10^{-4})	3.8×10^{-4} (5.0×10^{-4})
S_{10} [mV/ms]	$4.3 \times 10^{-4})$ (6.0×10^{-4})	$4.4 \times 10^{-4})$ (5.2×10^{-4})	4.9×10^{-4} (4.8×10^{-4})
S_{20} [mV/ms]	3.8×10^{-4} (0.003)	4.7×10^{-4} (0.001)	5.3×10^{-4} (0.001)
S_{max} [mV/ms]	−0.018 (0.058)	−0.019 (0.027)	−0.021 (0.044)
$\mathbf{A}(Duration)$	104.8 (32.83)	102.1 (23.50)	91.25 (33.19)
$\mathbf{A}(PosAr)$	4.446 (6.861)	3.503 (4.345)	3.832 (4.737)
$\mathbf{A}(S_5)$	3.6×10^{-4} (1.9×10^{-4})	4.1×10^{-4} (3.9×10^{-4})	3.4×10^{-4} (4.1×10^{-4})
$\mathbf{A}(S_{10})$	4.4×10^{-4} (0.001)	4.2×10^{-4} (3.6×10^{-4})	4.7×10^{-4} (0.001)
$\mathbf{A}(S_{20})$	4.1×10^{-4} (0.003)	3.9×10^{-4} (0.001)	5.1×10^{-4} (0.001)
$\mathbf{A}(S_{max})$	−0.015 (0.049)	−0.016 (0.030)	−0.019 (0.047)
MV	0.028 (0.048)	0.100 (0.103)	0.067 (0.351)
Dispersion [ms]	2.500 (3.000)	2.000 (4.000)	2.000 (6.000)
SDNN	74.18 (57.56)	96.51 (94.74)	61.75 (73.48)
VARNN	5.5×10^3 (7.9×10^3)	9.4×10^3 (2.0×10^4)	3.4×10^3 (1.1×10^4)
RMSSD	98.87 (86.99)	127.4 (119.8)	90.40 (74.41)

This observation is further corroborated from Table 6.5, which shows the POV after each CA step as well as the comparison between two consecutive steps (**B–L** and **L–R**). After LPVI, a significant increase of *MV* is observed. ARV features

grow impressively after LPVI, with *VARNN* increasing by 225.9%, later showing a decrease.

Table 6.4: Results for KW and MWU tests for CS LAWs. Statistically significant results are shown in (∗). Due to Bonferroni correction, threshold for MWU (last three columns) is $\alpha_2 = 0.0167$.

Features	KW	MWU		
		B-L	B-R	L-R
Duration [*ms*]	0.108	0.241	0.055	0.217
PosAmp [*mV*]	0.835	0.646	0.887	0.602
PPAmp [*mV*]	0.942	0.740	0.937	0.837
RMS [*mV*]	0.847	0.740	0.912	0.558
PosAr [*mV* × *ms*]	0.896	0.670	0.837	0.788
Deflections	0.916	0.682	0.889	0.828
Inflections	0.915	0.878	0.810	0.695
S_5 [*mV/ms*]	0.732	0.624	0.837	0.438
S_{10} [*mV/ms*]	0.767	0.764	0.558	0.558
S_{20} [*mV/ms*]	0.932	0.887	0.962	0.669
S_{max}[*mV/ms*]	0.996	0.937	0.987	0.987
A(*Duration*)	0.159	0.669	0.060	0.200
A(*PosAr*)	0.882	0.669	0.693	0.937
A(S_5)	0.753	0.558	0.837	0.517
A(S_{10})	0.771	0.912	0.558	0.537
A(S_{20})	0.836	0.710	0.812	0.580
A(S_{max})	0.967	0.887	0.788	0.912
MV	0.056	0.018	0.113	0.692
Dispersion [*ms*]	0.676	0.461	0.923	0.451
SDNN	0.056	0.048	0.912	0.041
VARNN	0.056	0.048	0.912	0.041
RMSSD	0.049∗	0.026	0.764	0.064

6.5   Discussion

Vivid cardiac contraction and variable CS anatomy can have a significant effect on the signal quality of the CS channels, even during SR. Channels from the distal area show longer CS LAWs and lower amplitude signals. Additional relatively lower correlation between their morphologies indicate a tendency to record higher amount of noise and discourage their recruitment. On the contrary, channels from the medial to mid-proximal area (M, MP) have shown the shortest

Table 6.5: POV for between every two ablation steps for P-waves and LAWs and comparison between POV of successive step transitions **B-L** and **L-R**. Statistically significant results are shown in **(∗)**. POV: percentage of variation.

Features	B-L [%]	L-R [%]	B-R [%]	MWU (BL-LR)
Duration	−5.49	−1.93	−7.46	0.6576
PosAmp	−3.58	0.52	−6.51	0.6464
PPAmp	−7.79	−2.15	−5.09	0.7397
RMS	0.82	19.91	20.89	0.7397
PosAr	−5.23	−1.74	−4.06	0.6693
S_5	22.47	−1.82	20.24	0.6239
S_{10}	1.34	11.74	13.24	0.7637
S_{20}	25.89	12.20	41.24	0.8868
S_{max}	4.37	7.75	12.46	0.9370
A(*Duration*)	−3.89	−4.46	−9.84	0.6693
A(*PosAr*)	−2.90	−3.86	−19.94	0.6693
A(S_5)	14.18	−16.49	−4.65	0.5583
A(S_{10})	−4.10	11.80	7.21	0.9118
A(S_{20})	−5.64	32.58	25.10	0.7160
A(S_{max})	4.11	17.70	22.53	0.8868
MV	144.9	−5.93	172.1	0.0176∗
Dispersion	0.00	80.00	0.00	0.4613
SDNN	79.80	−33.94	0.92	0.0480∗
VARNN	225.9	−55.91	1.93	0.0480∗
RMSSD	73.12	−36.30	5.43	0.0257∗

CS LAWs and signals of higher amplitude with rather correlated morphologies. Hence, M and MP channels are strongly recommended, as more robust channels able to record better quality signals. Previous studies analyzing CS EGM fractionation report clinically useful information extracted from P and M channels or lack of clinically useful information from D channel, corroborating the findings presented in this chapter [42, 93, 162].

The second step of the analysis presented in this chapter has been the investigation of any kind of correlations between CS LAWs and P-waves, either directly from recordings acquired from the same recording points or by investigating if the effect of CA can be similarly observed from P-waves or CS LAWs. Despite the fact that this study did not lead to the revelation of any important correlations, it foregrounded the CF as an essential step before the comparison between surface and invasive recordings, being clearly illustrated in Figure 6.4.

CF application significantly improved the correlation between *Duration* of CS LAWs and P-waves, whether it was applied at an activation-to-activation basis or for the comparison between CA steps, possibly due to the effect of RF energy, which is probably more intense in the CS recordings due to proximity with the atrial tissue. This may explain the reason why incrementation in correlation was more intense in **B** (during LPVI), which RF energy is directly applied at the time of the recording.

ARV features showed weaker correlations during LPVI, further validating the usefulness of CF, implying variations of CS LAWs on a different degree than P-waves. After CA, ARV features showed high correlations, possibly due to ANS withdrawal after RFCA, as suggested by previous studies [88, 89]. Previous studies have investigated any possible correlations between surface and invasive recordings, mostly in order to confirm the utility of non-invasive methods to map the AF substrate [175]. In this context, some of them report significant correlations between atrial features and RA recordings, both during AF and during SR [176–178]. Nevertheless different invasive recordings and patient cohort with respect to the study presented in this chapter does not allow a direct comparison.

After correlating electrical features from the CS and lead II recordings, we have focused on the atrial substrate modification observation exclusively from the CS recordings. The rationale behind this step is to investigate whether CS can be a reliable structure to observe the AF substrate alteration and if its recruitment for this purpose can offer additional information to the analysis. Regarding the first part, CS LAWs modifications observed from CS recordings are not indicative of the AF substrate modification, lacking significant alterations, a result further affirmed by the previous step of low CS-lead II features' correlations. However, ARV and *MV* modifications were prominent in CS, allowing a very precise picture of how RF affects the atrial structure. Comparing with the respective lead II ARV results, presented in chapter 5, CS allows a more detailed observation of the ARV fluctuations, which is reasonable considering the advantage of invasive recordings being closer to the atria. Therefore, CS recordings can be useful in order to potentiate the information extracted from the AF substrate modification analysis with respect to the effect of RF on the atrial tissue.

6.6   Conclusions

Channels from the medial area (M, MP) are highly encouraged for a more reliable CS recordings analysis. Electrical features from the CS recordings do not correlate well with the respective ECG features, implying the non-suitability of CS recordings to observe the universal AF substrate modification. In any case, when surface and invasive recordings are correlated, the former application of a CF in order to mitigate the HR fluctuations is highly recommended. CS recordings can be useful in observing the fluctuations in ARV due to RF energy and

their analysis along with ECG recordings may provide useful information to the AF substrate alteration studies.

Discussion

Contents

Although the main findings from the studies described in the published articles have already been discussed in the corresponding chapters 3–6, this brief but condensed chapter accentuates the most important parts of each work and brings them together along with the findings of the complementary research that will be presented in the next chapter, offering a wider and simultaneously more accurate picture of the entire research work conducted in this Doctoral Thesis.

7.1   Discussion

AF substrate analysis is of paramount importance in order to increase the efficiency of CA and improve the quality of life of AF patients [10]. ECGs and EGMs are critical for this purpose, each contributing in a different way to the AF substrate characterization [18, 40]. While ECGs offer a generalized and universal perspective regarding the existence of remodeling, EGMs allow the precise localization of AF drivers from the study of various EGMs characteristics, such as low voltage and CFAEs that indicate the existence of fibrotic tissue [17, 18, 22, 40]. Among the recruited EGM features, CFAEs have received increasing attention [18, 40, 179], as fractionation is thought to stem from the collision of multiple chaotic wavelets, hence being an indicator of fibrosis [110]. In fact, increased fractionation is connected with increased fibrosis, with CFAEs representing the existence of remodeling and being candidate CA targets [40].

One of the most common issues regarding CFAEs analysis is the confusion generated from their definition, which allows diverse interpretation, leading to overdetection and, therefore, to poor CA results and increased health risk for the individuals [40, 43, 48, 56, 108, 179]. This observation led to the conduction of the first work described in this Doctoral Thesis, in chapter 3. The main objective of the described study, linked with the first objective of chapter 1.4, was the development of an algorithm able to discriminate between low and high fractionated EGMs, which represent passive and active phenomena, respectively [108]. Efficiently discriminating highly fractionated EGMs from less chaotic signals allows the detection of CFAEs with higher precision, improving the AF substrate estimation process.

Previous attempts to quantify the AF fractionation were neglectful of discriminating between AF types II and III EGMs, which is actually the most challenging and critical part for an efficient CFAEs detection, while other works did not include a sufficient amount of type III AF EGMs [129–131]. Moreover, most of the studies were performed over recordings of 4 s or even longer, being unable to provide real-time results, as dynamics during AF might change quickly. One of these works [129] defined the best set of nonlinear and frequency-domain parameters via cluster analysis in order to discriminate between AF types in 6-s long AF EGMs. Apart from the fact that a low number of type III EGMs was included ($<$ 29% of total EGMs, while 44% of the EGMs belonged to AF type I) leading to an easier classification, discrimination via *t*-test was confirmed, but some overlaps between successive AF types were found. Therefore, the method was suggested in order to discriminate between AF type I and III EGMs, a rather easy and straightforward task.

The next study including a relatively low proportion of AF type III EGMs (35% of total recordings) specified a feature set of time-, frequency-domain and morphological parameters for the classification among AF types [130]. Despite the impressive classification accuracy of 97.7% using 7 features, lowered to 88.3% using 5 features, results need to be verified on a higher proportion of AF type III EGMs. Additionally, although 4 s is a satisfactory segment length, very quick phenomena such as AF type IV EGMs need higher time resolution in order to be reliably detected. Another study [131] dealing with the same issue discriminated between AF types I and a grouped AF II/III type, a fact that significantly simplifies the procedure and yields accuracy as high as 93% but fails to define the active AF drivers, which is the original objective of the study presented in this Doctoral Thesis. Moreover, the study is performed on 90 s signals, which does not allow the tracking of changing dynamics, which is dominant in AF recordings.

The final work to include a low proportion of highly fractionated EGMs utilized wavelet transform and a classification by four increasing fractionation degrees on 1.5-s long EGMs [132]. This study, as already mentioned afore, only included 9.7% of the most fractionated EGMs, corresponding to AF type III EGMs, while the ROC results were lower with respect to the results mentioned in chapter 3 of the present Doctoral Thesis, showing 81.8% of sensitivity and 90.2% of specificity.

Haley et al. [133] developed an algorithm to quantify EGM fractionation, which, similar to the work in chapter 3, can be used to detect active AF drivers as EGMs with a high fractionation level. Nevertheless, this study, tested on 80 4-s EGMs, showed moderate results of 78% correlation between the method and the experts' classification and ROC values of $77 - 81\%$ for sensitivity and 81% AUC. Besides the moderate results, this study included 66% of paroxysmal AF EGMs, which generally show lower complexity and therefore better results.

The study presented in chapter 3 recruited CGCD in order to quantify the EGM fractionation and use the results in order to discriminate among and between AF types, with the aim to define active AF targets as AF type III EGMs

with CGCD values. The application of CGCD or CorDim in AF organization studies, however, has been previously introduced. CorDim was recruited in order to distinguish among different levels of atrial organization during pacing in biophysical models [113], while CGCD from right atrial EGMs before CA of AF drivers found in LA was able to predict the AF termination during the CA procedure [114]. Finally, another study, which is directly related to the study presented in chapter 3, employed CGCD in order to discriminate between different AF types on 4-s right atrial unipolar EGMs. Despite the success in classification by AF type, the use of unipolar EGMs has little relevance nowadays, as most of the recording softwares extract channels of bipolar EGMs. Additionally, despite the fact that ventricular activity removal was performed, ventricular residuals, which are pretty common after ventricular cancellation of short unipolar segments, might affect the CGCD results, significantly altering the findings of the study.

In contrast to the aforementioned studies, the developed algorithm presented in chapter 3 operates over 1-s segments, facilitating the setting of length independent parameters according to the optimal results. Apart from parameter selection, analysis over 1-s segments allowed the detection of sudden changes in AF fractionation, leading to 100% detection accuracy for AF type IV EGMs and up to 85.7% classification accuracy among AF types I–III EGMs, setting a threshold of 1.388 for the discrimination between AF types I and II EGMs and a threshold of 2.033 for the discrimination between AF types II and III EGMs. These results offer a more realistic approach to the CFAEs detection problem, as the parameter independence and the constant updating of the CGCD value allow the improved detection of active AF drivers. It should be additionally highlighted the excellent (100%) classification performance when EGMs that were clearly belonging to a specific AF type were exclusively used, foregrounding the robust structure of the suggested technique.

A common point often discussed when using correlation dimension is the data length and the corresponding dimension of the attractor, which may be underestimated due to limitations on the embedded dimension. The use of CGCD can be a solution to this issue, as CGCD does not offer a strict estimation on the chaos level present in EGMs, but makes a rough approximation instead, which serves the efficient detection of CFAEs and is able to be applied over 1-s segments at the same time. The study described in chapter 3 takes advantage of this CGCD attribute and builds up a method oriented to the CFAEs definition problem. Therefore, it can be implemented on real-time AF mapping devices or serve as a baseline for future studies with variable data length that are interested in the CGCD method.

While chapter 3 was focused on a technique aiming to assist cardiac mapping during AF, the studies described in chapters 4–6 deal with cardiac mapping during SR via ECG analysis. The P-wave of an ECG reflects the atrial depolarization and its duration is indicative of the existence or absence of conduction delay and, therefore, fibrosis [87]. Due to this fact, P-wave analysis is considered one of the most popular features for the evaluation of the AF substrate during SR and the

prediction of the CA outcome [29–35]. Towards the same direction, P-R interval reflects the AV conduction and is considered a reliable predictor regarding the CA outcome [57, 140, 142].

Despite the high popularity of the aforementioned features, studies tend to analyze the entire P-wave assuming an equal contribution of RA and LA to the substrate alteration. Similarly, the P-R interval is analyzed including the P-wave component, consequently being highly dependent on the P-wave modification and not offering a realistic estimation of the AV conduction alteration as a function of CA. The study presented in chapter 4 aimed to define, if any, the atrium (RA or LA) which was mostly affected by CA of PVs and highlight the necessity of analyzing integral parts of the ECG components, which would allow a more detailed evaluation of the AF substrate, as already explained in the second objective of chapter 1.4.

The main findings of this study give prominence to the second P-wave part, corresponding to LA depolarization. Considering PVs location and the prevalence of atrial remodeling in LA, these results come of no surprise, even if paroxysmal AF patients with no prominent remodeling have been recruited [16]. Higher correlation between the first P-wave part (RA depolarization) and entire P-wave imply the underestimation of substrate modification after CA in case of analyzing the entire P-wave uniformly, since RA depolarization time is not significantly affected from CA. RA effect may be an important factor when it comes to thresholding, as entire P-wave shortening may not correspond to reverse electrical remodeling.

In the same context, P-R analysis, which is also considered relevant to AF substrate modification and AF recurrence [140–142], is significantly affected by the P-wave component. P-R segment, measured without considering the P-wave component, reflects the AV node function, one of the most critical parts for the cardiac function and blood circulation. This segment can be modified as an outcome of P-wave alteration in an inversely proportional way [140, 142]. This modification may also be masked when P-R interval includes the atrial component, deducting relevant information from the AF substrate analysis. The study described in chapter 4 brought the aforementioned issues to the fore, highlighting the need for reappraisal of the way atrial components of ECG recordings are being analyzed.

The analysis included normalization due to the effect of HR fluctuation as a result of RF application during CA [154, 156]. This step was found critical in the assessment of the correlation between the effect of CA on the entire P-wave duration and the effect of CA on the P-R interval, when the P-wave was included in the measurements, a result which would otherwise have been missed. The results of this study contribute to the localization of the most critical atrial side, which is key in the further investigation of the AF mechanisms during and after CA of PVs as well as in designing a more efficient CA strategy and procedure.

Chapter 5 unfolds towards the same direction, exploring and analyzing separately the LPVI from the RPVI effect to the AF substrate modification, in line with

the next objective of chapter 1.4. As in chapter 4, the analysis described in chapter 5 aims to optimize the substrate modification analysis. The proposed method is quite simple and requires no additional resources. In order to be achieved, P-waves are analyzed at three time instances, describing atrial activity before CA, right after LPVI and right after RPVI. The results of this study suggested LPVI as the principal factor causing P-wave shortening. Thereby, AF substrate modification could be accredited in the first place to LPVI. The study described in this as well as in the previous chapter offer a more detailed perspective on the atrial alterations provoked by CA, the cornerstone of AF and can serve as a reference for future studies or CA sessions, with the objective of a higher resolution AF substrate modification analysis.

This chapter also included the analysis of ARV (atrial rate variability-atrial response), the equivalent of which (HRV-ventricular response) is considered a powerful CA outcome predictor [17, 89]. Although results regarding the ARV attenuation after CA were in line with previous studies [17, 89], the analysis of recordings during CA allowed the observation of an extraordinary ARV increment. This phenomenon might be the outcome of RF exposure, which was found to increase HRV and decrease HR, both observations being in line with the findings of the study presented in Chapter 5. This information is relatively unknown, although totally reasonable and can be further utilized to study the atrial response to RF energy and the possible connection that this might have with the AF substrate alteration.

Moving from surface ECG to invasive EGM recordings, chapter 6 presents a detailed study on CS recordings and their potential utilization for a more precise AF substrate analysis. The triggering point for this work has been the ability of intracardiac recordings of critical CA structures to offer more realistic information with respect to the AF substrate, in line with the fourth objective of chapter 1.4. The principal reason why studies mainly recruit surface recordings to assess AF substrate and predict the CA outcome from CA recordings is the constant movement of the mapping catheters. As CS catheterizaton is a fundamental step of CA, stability of CS recordings suggest their use for the aforementioned purpose. The analysis described in chapter 6 investigated this assumption, performing a thorough analysis on CS recordings and their utility in assessing the AF substrate.

The first part of the study analyzed the most recommended channels to be extracted, with robustness to cardiac contractions and noise as well as morphology homogeneity as principal criteria. Extreme channels and especially distal channel have been found susceptible to noise, a conclusion in line with previous studies [93]. On the other hand, medial and mid-proximal channels seem to be the most reliable and their extraction is recommended. The second part of this study consisted of a correlation analysis between P-waves and CS LAWs. The rationale behind this step has been to investigate whether AF substrate and AF substrate modification assessed from CS recordings are in line with the findings from the P-waves analysis, corroborating in such case the importance of the latter and suggesting the alternative implementation of the former in future studies.

The results suggested weak correlations between CS and ECG recordings. Nevertheless, the need of normalizing according to HR fluctuations has arisen as an essential part before any comparison between surface and invasive recordings. During RF CA, HR and ARV fluctuations are registered to a different extent from surface and invasive sources, with the latter being considered a more precise reference point due to proximity to the tissue receiving RF. This different degree of fluctuations may mask any correlations, as has been clearly demonstrated by the study presented in chapter 6.

The final part of the analysis consisted of a raw analysis of the AF substrate modification from the CS recordings. As this analysis did not show any significant results, in contrast with the respective P-wave analysis presented in chapter 5, the conclusion that AF substrate modification cannot be reliably evaluated from CS recordings has been derived. The reason for this observation may be the different perspective of P-waves with respect to CS LAWs, with the first being able to observe the entire atria and register cumulative differences, while the second providing local information regarding CS function. Findings from chapter 4 corroborate this assumption, as LA has been found to be the principal and foremost source of AF substrate alteration, implying a non-uniform effect of CA on the atria. Despite the inability of CS recordings to assess the AF substrate modification, CS recordings are useful in observing ARV fluctuations, recording a significantly higher extent of ARV alterations throughout the CA procedure. This phenomenon has been present in all recordings but more prominent in recordings after LPVI, when RF energy was being directly applied. Therefore, CS recordings may consist of a more trustworthy measurement of HR and ARV alterations and their complementary analysis is highly recommended.

The works described in chapters 3–6 contribute to the improvement of the quality of information extracted during AF substrate analysis, using both EGMs, in order to target areas of active AF drivers and ECGs, in order to observe more in detail the substrate modification taking place during SR and after CA. The main point of all the aforementioned works is to optimize the AF substrate analysis procedure. Nevertheless, AF substrate evaluation is strongly dependent on the AF type (paroxysmal or persistent) and the cardiac rhythm (AF or SR) during the recordings acquisition. Appendix A, which will be presented subsequently, attempts a combined study of paroxysmal and persistent AF patients entering the operational room in AF and leaving in SR. For this purpose, ECG and EGM recordings in AF before CA have been analyzed, including f-wave analysis for lead V_1 of ECGs and CGCD analysis, as described in chapter 3 for the analysis of CS during AF, utilizing the information acquired from chapter 6 [22–27]. Additional lead II ECG recordings in SR have been recruited after CA and P-wave analysis, as described in chapters 4 and 5, has been performed. Due to catheter disconnection right after CA, analysis of CS recordings after CA (in SR) was not possible.

In the first place, correlations between f-wave features from ECG recordings and CGCD from CS EGM recordings were tested in two databases, performing

PV-only CA in the first case and additional DF site ablation in the latter. The second database included only pre-CA recordings in AF [180], while the first database included both pre- and post-CA recordings. The results did not show significant correlations between any of the investigated features. The reason for this finding might be the different source of recordings (surface vs invasive) or the fact that f-waves represent the activations of the entire atria, while CGCD of CS recordings only assesses the organization of the CS structure, in coherence with chapter 6 regarding the poor correlation between P-wave and CS recordings during SR. As follow up information of the second database was available, the predictive power of CGCD regarding the CA outcome was also investigated. Nevertheless, CGCD did not show any predictive ability regarding the CA outcome.

The next step included correlations between f-wave features from V_1 recordings before CA and P-wave features from lead II recordings after CA. The lack of follow-up information, which would allow the further correlation between the results and the CA outcome, as well as the use of a different lead, probably imply that the results would be biased and cannot be superpositioned on general conclusions regarding the analysis of recordings from V_1 and lead II before and after CA. Correlations were in this step as well insignificant, with f_m, the median frequency or the frequency that includes the half of the 3-9 Hz power spectral density (PSD) [180], being the feature showing the highest absolute correlation with the P-wave features, a reasonable observation as f_m is proportional to DF, which has been found to be higher for the patients without AF recurrence [180].

The final step consisted of the calculation of correlations between CGCD features from CS EGM recordings before CA and lead II P-wave features after CA. Similar to the previous cases, this step contains a higher amount of bias due to the lack of follow-up information and a totally different source of recordings (invasive vs surface, CS-focused vs including the entire atria). As expected, no significant correlations have been found in that case either. The classification between high-value and low-value P-wave features has also disproved CGCD as a reliable classifier regarding P-wave features. As already explained, there are many factors that may have influenced these results, such as the lack of follow-up information or the different origin of the recordings. Correction of HR-fluctuations has been applied in this case without achieving an improvement of the results.

Following the last objective set in chapter 1.4, the analysis performed in appendix A included various scenarios of substrate analysis and investigated any correlations between them, without finding any significant relationships. Notwithstanding, significant limitations regarding the conduction of this analysis exist. In the first place, the lack of follow-up information did not allow the further separation of lead II ECG recordings regarding the CA outcome, which would lead to a more efficient analysis and more trustworthy results. Additionally, the attempt to search for any correlations between invasive recordings, with more accurate but very limited information and surface recordings, with more generic yet global information is risky, as it has already been proved in chapter 6. In any case, the

findings of appendix A are coherent with the findings of chapter 6, with CS being in both scenarios (AF or SR) unable to be in line with the corresponding information from the ECG recordings. Due to the aforementioned limitations, though, the possibility that CS or other atrial sites can be predictive of the CA outcome or the P-wave modification should not be completely discarded.

Contributions, Conclusions and Future Lines of Research

Contents

This chapter goes through the original contributions of the research articles that formed the core of the present Doctoral Thesis and highlights the main conclusions that can be derived. Although each of the chapters of the compendium of publications include the corresponding conclusions, the present chapter provides a spherical perspective on the most important achievements and suggests research lines that could be introduced in the future in order to complete and improve the research work.

8.1   Contributions

The main contributions (Cb) of each published article that forms part of the compendium of publications are listed here:

Cb$_1$. Discrimination among different AF type EGMs using CGCD can assist the AF drivers detection by offering a more accurate CFAEs mapping. Although CGCD has been used in the past to discriminate among various AF types [117], the work described in [181] was the first to apply CGCD in bipolar EGMs. Additionally, this study introduced the signal segmentation to 1 s epochs, which removed any signal length dependencies and led to the establishment of fixed parameters according to the best classification accuracy as well as to successful detection of AF type IV EGMs. The resutls highlighted the success of CGCD as a reliable EGM fractionation estimator.

Cb$_2$. Separate assessment of RA and LA reverse remodeling after CA of paroxysmal AF. Separate study of first and second P-wave parts were proposed

and applied for the first time in [6]. The study indicated the LA as the major source of P-wave shortening and accentuated the importance of studying integral and indivisible components of the ECG recordings in order to evaluate with higher precision the AF substrate modification. This study has also corroborated previous findings suggesting the high influence of the atrial depolarization in AV node regulation.

Cb₃. Separate assessment of LPVI and RPVI effect on AF substrate modification on paroxysmal AF patients [7]. The pivotal role of LPVI, provoking the principal AF substrate modification after CA of paroxysmal AF, has been revealed for the first time. This study stressed the importance of analyzing the recordings acquired during CA of AF and assisted in the further understanding of the AF mechanisms during CA via RF energy.

Cb₄. Recruiting CS recordings for a higher resolution analysis of the AF mechanisms during CA of PVs in paroxysmal AF patients. In [7], the most and least reliable CS catheter channels in faithfully illustrating the AF dynamics during SR have been defined. By a thorough analysis, this study suggested the medial and mid-proximal channels as the ones able to record reliably and with the least amount of noise the AF dynamics during SR. In [8], analysis of any possible correlations between electrical features acquired from CS recordings or atrial components of ECG recordings posed the very important issue of normalizing data in order to mitigate the HR effect before any parallel analysis of surface-invasive recordings, especially when RF energy is mediating. Along with the conclusion that CS recordings are more efficient in recording any HR-related change in the atrial regulation due to proximity with the tissue under ablation [7], the aforementioned studies suggested the complementary use of CS recordings in order to augment the mapping resolution of the AF dynamics during CA of paroxysmal AF.

8.2　Conclusions

Each and every published article presented in this Doctoral Thesis contains some conclusions (Cc). Sometimes impressive and prominent, while other times to a lesser extent, each of the drawn inferences has contributed its piece to the characterization of the substrate modification of the AF patients and to the further understanding of the AF mechanisms during CA of PVs. The main conclusions that can be derived from the compendium of articles are listed below:

Cc₁. Although AF drivers in persistent AF patients span throughout the atria, additional CA of fibrotic areas after CA of PVs shows controversial results. While CFAEs mapping and ablation is a promising technique to improve CA outcome on persistent AF patients, CFAEs definition allows the interpretation of many sites as candidate CA targets, leading to conflicting CA results and unnecessary risks for the AF patients. CFAEs mapping using CGCD method allows the successful detection of the most fractionated

EGMs, which are possible AF drivers. Applying 1 s segmentation on EGM recordings allows the analysis of any data length and removes common problems arising during CGCD implementation. Moreover, analysis on segments as short as 1 s allows the mapping process to capture any short-time changes in the EGM morphology.

Cc2. Despite the high popularity on P-waves analysis to assess the AF substrate modification after CA of paroxysmal AF and hence to predict the AF outcome, apparent inconsistencies on thresholds regarding the detection of remodeled tissue highlight the need for reconsideration on this technique. Studying integral parts of P-waves and P-R intervals allows the researchers to go deeper into the AF mechanisms and observe with higher efficiency the AF substrate modification. LA reverse remodeling is the principal source of P-wave shortening in paroxysmal AF patients. Nevertheless, the high correlation between RA and entire atrial depolarization time leads to underestimation of the AF substrate modification. Additionally, including the P-wave to the P-R interval analysis is a common technique. In this case, however, the results are significantly affected by the P-wave component and any changes in AV node regulation, that can be used to asisst further the AF substrate modification observation, are enshrouded. Disagreements in thresholds may stem from the trend of uniform P-wave and P-R interval analysis and results could be significantly improved from separate analysis of integral atrial and AV parts of the ECG.

Cc3. Despite the importance of PVs on the AF triggering and perpetuation, AF substrate modification is traditionally analyzed by comparing recordings acquired before and after CA. Recordings during CA of PVs are widely available and can be recruited in order to obtain a more detailed picture on the AF mechanisms during CA. P-wave shortening is at almost 100% provoked after LPVI in paroxysmal AF patients. Electrophysiologists should pay more attention to the proper isolation of left PVs, while future studies are suggested to analyze recordings during CA sessions.

Cc4. CS is a critical structure in AF perpetuation as well as in AF mapping and could be recruited to add up to the AF substrate evaluation analysis, as CS recordings with a stationary catheter are being recorded during CA. Notwithstanding, CS channels are susceptible to noise and CS catheterization may be a complex procedure, significantly affecting the quality of the recordings. After a deep analysis on the channels able to capture more faithfully the AF dynamics, medial and mid-proximal channels are considered the most robust and are hence recommended for analysis in recordings acquired during SR. On the contrary, extreme channels and especially distal channel, are exposed to higher amount of noise.

Cc5. When the search of any relationships between surface and invasive recordings during RF CA is attempted, normalization of the electrical features that depend on HR is highly recommended, as invasive recordings are able to capture with higher sensitivity any RF-induced changes, masking the real

surface-invasive connections. Due to higher proximity with the atrial tissue, CS recordings were also found more accurate in registering ARV and morphology related changes and their analysis along with ECG recordings may increase the mapping resolution of the AF substrate.

8.3   Future Lines of Research

Research is a never-ending process. One of the main attributes of investigation is the generation of further questions and research possibilities every time that an answer is attempted to be given. This emerges as an outcome of the widening of horizons and the broadening of perspectives that each answer offers as a part of the very nature of research. The present Doctoral Thesis is part of this process. Thus, new research lines have arisen from the findings of the work presented in the compendium of publications of this Doctoral Thesis.

The recruitment of fixed-length CGCD as a fractionation estimator of bipolar EGM recordings has opened up the possibility of utilizing this metric during AF mapping in order to detect candidate CA targets. Therefore the clinical applicability of this method remains to be validated. A future line of this work could hence be the application of CGCD analysis in a large database of AF patients undergoing additional CFAEs ablation, in order to relate the active AF drivers found through CGCD analysis with the CA outcome. In this case, the first step of this study would be the creation of an extended database with AF patients undergoing CA of CFAEs after CA of PVs and with follow-up information. The CGCD study presented in this Doctoral Thesis lacks comparison with other nonlinear indices recruited to assess the AF organization in EGM recordings. Besides coming up with optimal methods for AF mapping, this comparison could suggest the combinational use of CGCD and other techniques in order to improve the CA outcome.

Chapters 4 and 5 suggested the reconsideration of established techniques and AF substrate modification analysis methods by adopting simple and feasible additional steps that can increase significantly the understanding of the AF mechanisms and the prediction of the CA outcome or the design of the follow-up therapy. Through the work described in these chapters, the LA depolarization time shortening and the LPVI procedure have been demonstrated as keys for the AF substrate modification. Despite the importance of the aforementioned findings, the lack of follow-up information of the AF patients is a significant limitation. Consequently, a possible extension of these studies could include follow-up information in order to investigate whether P-wave shortening stemming from LA depolarization time abbreviation and LPVI realization is directly connected with successful CA outcome or is a temporal side-effect of RF application.

Furthermore, the analysis has been conducted using paroxysmal AF patients, where atrial remodeling is not prominent. The results of this study could therefore be further validated in persistent AF patients showing exclusively LA or LA

and RA remodeling. Separate first and second P-wave part evolution could also be investigated in re-do procedures and LPVs reconnection could be assessed and related with P-wave shortening results after LPVI. Finally, the sources of P-wave shortening have been studied in CA of PVs applications. In case of extrapulmonary AF drivers, however, the critical LA and LPVI assumptions remain to be validated.

A multi-approach study of the role of CS in AF substrate modification observation has been performed and described in chapter 6. Channels from the two extremes of the CS catheter have been found to be less reliable, while median and mid-proximal channels, found in the middle and middle-to-RA part of the atria, were the most recommended. Nevertheless, this analysis has been performed in SR, where cardiac anatomy vary in a different way across the cardiac cycle than in AF. Thereby, the conclusions derived from this study only apply in AF dynamics during SR. As CS EGMs are vastly analyzed during AF, the same analysis in recordings obtained during AF would be interesting albeit quite complicated due to multiple activations and high fractionation. The application of CF in order to mitigate any HR-related effects on the surface and invasive recordings has been found critical in order to unmask any correlations, while ARV analysis has been considered more efficient in CS recordings due to proximity with atrial tissue. A future research line would therefore be to connect these ARV fluctuations, more prominent during LPVI due to RF, with the CA outcome. For the actualization of this study as well, follow up information is considered necessary.

Appendices

Appendix **A**

Study of Similarities Between Organization and Electrical Features of the Atria Before and After Catheter Ablation of Atrial Fibrillation

Contents

Given the analysis developed and performed in the previous chapters 3–6, the next reasonable step would lead us towards the mitigation of the highest possible number of dependencies regarding the analysis of the fibrillatory drivers in patients undergoing CA of AF. Two of the most common factors affecting the analysis is the AF type (paroxysmal or persistent) and the cardiac rhythm (AF or SR) during recordings, both associated with different AF dynamics on the AF substrate. Moreover, analysis is highly dependent on the recording type (ECGs or EGMs), clearly marking the direction of the study and affecting the interpretation of the results. The current section describes the attempt to define any relationships between ECG and EGM recordings, acquired before and after CA of both paroxysmal and persistent AF patients. Although the work presented in this section does not belong to the compendium of articles, nor has it been submitted for publication, the structure of the chapter is preserved, including Introduction, Materials, Methods, Results, Discussion and Conclusions.

A.1 Introduction

Chapter 3 presented a method able to quantify EGM fractionation, useful in AF mapping during CA procedures. Although the method has been tested on persistent AF patients, the AF category that principally needs non-PV CA [10], the AF substrate is not a persistent AF exclusivity. Chapters 4 and 5 then assessed the usefulness of analyzing integral parts of the P-waves, leading to separate RA and LA substrate alteration evaluation as well as the different contribution of LPVI and RPVI to AF substrate alteration, recruiting in both cases P-waves and atrial HRV (called ARV) analysis. These chapters analyzed recordings from paroxysmal AF patients in SR both before and after CA. As for chapter 6, an atrial structure critical for the AF mapping and CA procedure realization, the CS, has been thoroughly analyzed, although without showing important contribution to the AF substrate modification assessment. This study utilized recordings from paroxysmal AF patients, being in SR before and after CA, as well.

Considering the aforementioned chapters, one can see that the AF substrate modification has been principally evaluated on patients entering the operational room in SR. Nevertheless, in many cases, AF patients enter the room in AF and either unsuccesful attempts of SR restoration or other reasons lead to CA realization during AF. Many studies have been dedicated to AF mechanisms analysis during AF. Many of them have been already summarized in chapter 2.5.5 and chapter 2.5.6. AF dynamics can be assessed noninvasively from the f-waves. Information relative to AF organization able to predict AF termination or recurrence or to discriminate between AF types can be extracted [22–26, 28, 47, 180, 182–184]. Spatiotemporal characteristics or nonlinear analysis have been shown to be especially effective for these purposes.

For EGMs, many techniques already described in chapter 2.5.6 exist with the aim to detect remodeled areas that could serve as candidate non-PV CA targets in the first place. LAT mapping, CFAEs and LV zones detection are some of them [18, 40, 48]. In chapter 3, CGCD has been presented as an efficient method to discern among the three main AF types (I–III) and detect short-time phenomena. Nevertheless, the principal function of CGCD is the EGM fractionation quantification, which in fact leads to the discrimination between AF types. As EGM fractionation is actually indicative of the AF organization [40], CGCD might be useful to extract information similar to noninvasive organization analysis during AF. Although this is a perilous speculation, organization assessed from EGMs might be up to a point related with AF substrate features acquired from ECG analysis after CA of PVs, establishing a form of relationship that might serve as a complementary index to forecast the possible reverse electrical remodeling.

Considering all the afore, substrate analysis technique strongly depends on the cardiac rhythm when the procedure starts (SR or AF), on the type of recordings available for analysis (surface ECG or invasive EGMs) and on whether the individual is a paroxysmal or persistent AF patient. The aim of the present chapter is to investigate any possible relationships between recordings of different

origin and/or type in order to serve as a first step for less dependent analyses. ECG and CS bipolar recordings during AF obtained before CA of persistent and paroxysmal AF are analyzed. ECG recordings during SR after CA of the same patients are also analyzed. Any correlations between surface and invasive pre-CA recordings, between surface pre- and post-CA recordings as well as between invasive pre-CA and surface post-CA recordings are investigated.

A.2   Materials

Two different databases were utilized for this study. Database A consisted of 18 patients undergoing circumferential RF CA for the first time. Out of the 18 total patients, 15 were persistent AF patients (83.33%) and 3 were paroxysmal AF patients (16.66%). Patients entered the room in AF. Two-minute 12-lead ECG and bipolar CS recordings before CA (in AF) were extracted. Two-minute 12-lead ECG recordings after CA (in SR) were also extracted. CS recordings after CA were not available as intracardiac catheters were disconnected right after the CA termination. Sampling frequency was set at 1 kHz.

Database B utilized 37 out of 49 patients undergoing circumferential RF CA for the first time, followed by CA of DF sites, as described elsewhere [180]. The reason why the remaining 11 patients were discarded were low quality CS recordings. Patients entered the room in AF. Twenty-one patients (56.76%) were paroxysmal AF patients and the remaining 16 patients (43.24%) were persistent AF patients. Ten-second 12-lead ECG and bipolar CS recordings before CA (in AF) were extracted at 977 Hz sampling frequency and were upsampled to 1 kHz.

For both databases, lead V1 has been selected for surface ECG analysis for recordings in AF and lead II for recordings during SR. For bipolar CS recordings, the channel with the highest amplitude has been selected. Preprocessing of leads V1 and II from both databases followed the steps and utilized the software described in chapter 4.2. For lead V1 recordings in AF, no ectopic beat cancellation was performed, as this step is pointless for AF recordings. Instead, adaptive QRST cancellation was applied, leading to a signal reflecting exclusively the atrial activity [170]. This method detects and extracts each QRST segment by an adaptive QRST template that is updated after each beat [170]. Preprocessing of CS recordings followed the steps described in chapter 6, apart from ventricular activity cancellation, which was not visible due to constant activations of the CS recordings in AF. Nonetheless, visual inspection of CS recordings using R peaks of ECG recordings as a reference was performed and no distinguishable ventricular activity has been observed.

A.3 Methods

For lead V1 recordings of both databases, spectral and nonlinear analysis has been performed. The selected features have been previously proved to be able to characterize AF organization, hence being candidate metrics in order both to extract AF related information and to relate with EGM organization indices described in chapter 3 [47, 180, 184]. These features were the following:

1. DF within the 3-9 Hz range (DF_{3-9}) [180]: The highest amplitude peak in the 3-9 Hz range.

2. First harmonic (f_1) [180]: The first harmonic of the signal, as the highest peak in a 2 Hz window around $2 \times DF_{3-9}$.

3. Normalized PSD DF (NP(DF)) [180]: PSD was obtained from the Welch periodogram, using a Hamming window of 4096 points, 2048 points of overlapping (50%) and a 10240-points Fast Fourier Transform (FFT). The NP(DF) is the PSD of DF normalized by the total power found within the 3-9 Hz range, as follows

$$NP(DF) = \frac{PSD(DF_{3-9})}{\Sigma_{f=3Hz}^{f=9Hz}PSD(f)}. \tag{A.1}$$

4. Normalized PSD of f_1 (NP(f_1)) [180]: NP(f_1) was calculated by replacing PSD(DF_{3-9}) in the numerator of equation A.1 with f_1.

5. 3 dB bandwidth (b_0) [180]: Feature b_0 was calculated from the following equation

$$b_0 = f_h - f_l, \tag{A.2}$$

where f_h and f_l where the closest to the DF frequencies for which the normalized PSD was equal to half of the NP(DF).

6. Normalized PSD of b_0 (NP(b_0)) [180]: This feature can be calculated by (DF_{3-9}) in the numerator of equation A.1 with b_0.

7. Ratio between DF and f_1 (γ) [180]: This feature is calculated by the following equation

$$\gamma = ln(\frac{NP(DF)}{NF(f_1)}). \tag{A.3}$$

8. Median frequency (f_m) [180]: Median frequency f_m is the frequency up to which the 50% of the entire 3-9 Hz range PSD is included. In order to define f_m, the cumulative sum of the PSD starting from 3 Hz is calculated, until it reaches the 50% of the 3-9 Hz PSD

$$\Sigma_{f=3Hz}^{f=f_m} PSD(f) = 0.5 \times \Sigma_{f=3Hz}^{f=9Hz} PSD(f). \tag{A.4}$$

9. Average power of the atrial activity (RMS_f): This feature is calculated from the RMS value of the atrial activity signal.

10. The f-wave amplitude (FWA): The median amplitude of the atrial activity signal.

11. Spectral flatness measure (SFM) [184]: SFM is a measure of spectral content distribution of a signal. It is calculated as

$$SFM = \frac{10^{\frac{1}{n} \times \Sigma_{f=3Hz}^{f=9Hz} log_{10} PSD(f)}}{\overline{PSD}}, \tag{A.5}$$

where n is the number of iterations between $f = 3$ Hz and $f = 9$ Hz and $\overline{PSD}$ is the mean of PSD of the atrial activity signal in the 3-9 Hz range.

12. Sample entropy (SE) [47]: For SE calculation, various parameters were used in search of the optimal results. Nevertheless, two different combinations (S_1 and S_2) have shown similar results and were hence utilized. S_1 was calculated using $m = 2$ and a matching tolerance equal to $r_1 = 0.4 \times sd$, while S_2 was calculated using $m = 3$ and a matching tolerance equal to $r_2 = 0.24 \times sd$, where sd is the standard deviation of the signal. Before SE calculation, main atrial wave (MAW) was calculated. MAW is the principal waveform that best describes the atrial organization signal. After QRST cancellation, the first step of MAW analysis was the PSD calculation as described in NP(DF) calculation, using a 8192-pointts FFT. DF was also calculated from PSD in the 3-9 Hz range. MAW was then calculated from selective filtering using a 3 dB bandwidth and 256 filter coefficients. Figure A.1 shows the conversion from a V1 ECG into a MAW signal.

For lead II recordings, P-wave analysis features presented in chapters 4 and 5 were calculated. For CS recordings, CGCD as presented in chapter 3 was calculated for each patient.

A.3.1 Statistical analysis

Various groups, depending on the recordings for which a relationship was investigated, were utilized.

A. Correlations between surface and invasive recordings before CA

For the correlations between surface and invasive pre-CA recordings, three groups of analysis were formed. The first group (G1) contained the 21 paroxysmal AF patients of Database B. The second group (G2) contained all 37 patients of Database
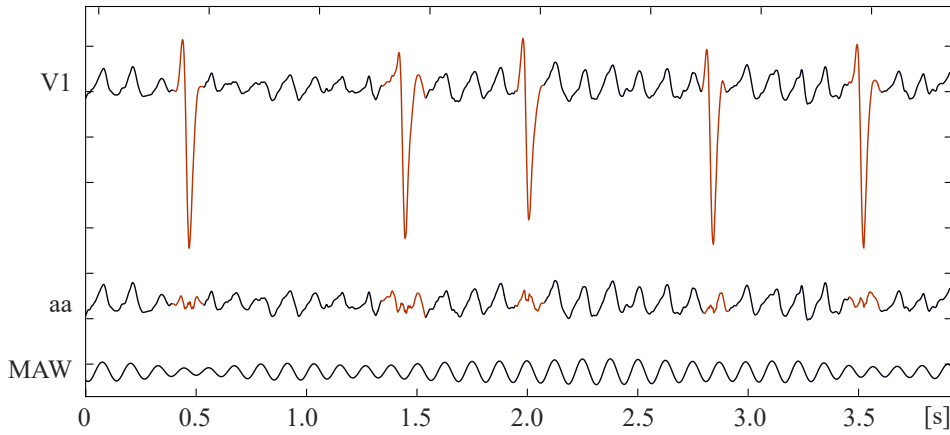
Figure A.1: Four seconds of a lead V1 ECG signal (top) converted to an atrial activity (aa) signal (middle), which was then converted to a MAW (bottom). QRS complex and the corresponding signal substituting the ventricular activity are shown in orange.

B. The third group (G3) contained all patients of both databases A and B (55 paroxysmal and persistent AF patients). Analysis has also been performed utilizing exclusively Database A as well as only persistent patients of databases A and B, without showing improved results. Hence, this analysis is not shown.

In the first place, Pearson's correlation between CGCD of CS recordings and features calculated for lead V1 recordings, described in Section A.3, was calculated. This analysis was performed in all three groups (G1, G2, G3). Additionally, two extra groups were created out of Database B, being the first the AF recurrence (G_{yes}) and the second the no-recurrence (G_{no}) groups. Out of 37 patients of Database B, 14 experienced AF recurrence in follow up (6 paroxysmal, 8 persistent) and 23 patients preserved SR (15 paroxysmal, 8 persistent). After Pearson correlation analysis being applied to all of the aforementioned groups, classification of CGCD values of CS recordings according to V1 features has been attempted. The idea behind this attempt was to define whether V1 feature values, which have previously been connected with AF recurrence, can be qualitatively estimated from CS recordings in an attempt to establish an indirect connection between CS recordings and CA outcome.

For the classification calculation, firstly the optimal value to discriminate above high and low values of each feature was defined by a ROC curve using the V1 features to classify between two groups of CGCD values (opposite classification). Thresholds for CGCD groups were obtained by coarse tree analysis results of chapter 3 on AF type II and III EGMs, as none of the CS recordings presented type I AF EGMs. Classification of CGCD values by V1 features was then performed, applying leave-one-out cross-validation. All linear and non-linear binary classificators from Matlab® Classification Learner (MathWorks, Natick, MA, USA)

were tested and the one showing the optimal classification accuracy in most of the cases has then been selected, including Naive Bayes, classification trees and support vector machine (SVM). The classifier showing the optimal results was logistic regression. ROC analysis has also been calculated. Finally, CGCD as predictor of AF recurrence has been investigated. For this purpose, G_{yes} and G_{no} groups were recruited and classification and ROC analysis of CGCD values by CA outcome (yes/no AF recurrence) was performed. Apart from CGCD calculation from the median value of all 1-s segments, as explained in chapter 3, the maximum and minimum CGCD values were recruited for this purpose.

B. Correlations between surface pre-CA and post-CA recordings

For correlations between lead V1 pre-CA and lead II post-CA recordings, only Database A was utilized, as Database B did not include lead II recordings in SR after CA. Pearson correlation was calculated between V1 features and P-wave features of lead II. Afterwards, binary classification of V1 features according to low and high P-wave feature values has been calculated. For the classification analysis, only PWD, $PWD_{on-peak}$, $PWD_{off-peak}$, $PW_{on} - R$ and $PW_{off} - R$, both normal and after CF application, were used. Dispersion was also used. The rationale behind this classification analysis was the search for V1 features that could be related with AF substrate alteration after CA, according to P-wave analysis. Nevertheless, this step is rather controversial, since follow-up information was not available for Database A and mechanisms acting during CA may affect significantly the pre-CA V1 and post-CA P-wave relationships. Hence, it should be previously clarified that any relationships found from this step are not straightforward and cannot be superimposed to any pre-post CA analysis.

Thresholds for P-wave features have been defined according to previous publications, relating P-wave feature values with AF substrate and substrate alterations. Whenever slightly moving threshold led to marginal values ($\pm 1 - 5$ ms) classification improvement, threshold was changed accordingly. The following thresholds have then been applied:

- PWD: Class 1 consisted of values $\leq$ 95 ms and $\geq$ 120 ms, while class 2 contained the remaining values [138].

- $PWD_{on-peak}$: Class 1 consisted of values $\leq$ 55 ms and class 2 contained values $>$ 55 ms. As no previous data about optimal threshold for this feature are offered, original threshold was set according to a normal P-wave definition ($85 - 120$ ms), considering that RA depolarization is longer than LA depolarization. Hence, $PWD_{on-peak}$ threshold should be between $50 - 70$ ms. After trying many thresholds, optimal value was found at 55 ms.

- $PWD_{off-peak}$: In the same way as $PWD_{on-peak}$, threshold of $PWD_{off-peak}$ was defined after multiple trials within $35 - 50$ ms range. Optimal threshold was found at 49 ms.

- $PW_{on} - R$: Considering previous studies, a normal PR interval would not exceed 200 ms. Nevertheless, PR interval is traditionally calculated up to Q point, while this study extended its measurement until R peak. Hence, threshold was prolonged to 240 ms.

- $PW_{off} - R$: Accordingly, threshold for $PW_{off} - R$ class 1 was set between 115 and 160 ms, considering both prolonged and very short P-wave cases.

- *Dispersion*: As dispersion, explained in chapter 5, is calculated in a different way than normally, threshold used was set upon multiple trials defining the best classification accuracy. This indicated a threshold of 10 ms for this value.

Values after CF application have utilized the same thresholds as normal values, considering a slight threshold change ($\pm 1 - 5$ ms) as explained previously.

C. Correlations between invasive pre-CA and surface post-CA recordings

Database A was the only one to be used for this case as well. PCC has been calculated between CGCD and P-wave features and classification of CS recordings (CGCD values) according to P-wave features has been performed, using the aforementioned thresholds. The idea behind this analysis was to investigate whether CGCD from preablative CS recordings can be related in any way with the P-wave features after CA. As in case B, this analysis contains a sort of bias and since no follow-up is available, the translative power of any possible relationships will be reduced.

A.4   Results

A. Correlations between surface and invasive recordings before CA

Table A.1 shows the correlation results for groups G1–G3. Correlations are moderate to low for all groups, with the only statistically significant values being recorded for DF_{3-9} and f_1 and f_m for G1 (only paroxysmal AF patients) and G3 (all patients). None of the features in G2 correlated significantly with CGCD. Correlations between CGCD and f_m, NP(f_1), SFM, S_1 or S_2 have shown a trend. Correlations between CGCD and V1 characteristics are as well shown in Table A.2, separated between groups with and without AF recurrence.

Table A.1: PCC and p values between CGCD and V1 spectral and nonlinear parameters for groups G1–G3. Statistically significant results are shown in **bold**.

CGCD	G1		G2		G3	
	PCC [%]	p	PCC [%]	p	PCC [%]	p
DF_{3-9}	**48.68**	**0.0246**	25.88	0.1220	**28.65**	**0.0340**
f_1	**45.96**	**0.0361**	26.95	0.1067	**27.81**	**0.0398**
NP(DF)	−26.94	0.2476	−29.33	0.9921	−18.34	0.1802
NP(f_1)	−36.40	0.1047	−24.45	0.1285	−24.05	0.0769
b_0	−3.34	0.8858	17.01	0.3142	5.99	0.6641
NP(b_0)	−31.4	0.1656	−24.08	0.1511	−14.15	0.3028
f_m	42.99	0.0518	30.29	0.0684	**31.84**	**0.0178**
γ	14.61	0.5275	5.02	0.7678	11.46	0.4049
RMS_f	−4.58	0.8438	26.32	0.1150	−19.82	0.1468
FWA	2.94	0.8994	11.81	0.4864	−17.25	0.2078
SFM	26.6	0.2445	−31.06	0.0613	−21.72	0.1112
S_1	36.55	0.1032	23.08	0.1694	26.37	0.0517
S_2	37.29	0.0959	23.01	0.1690	**26.63**	**0.0494**

Table A.2: Pearson's correlations and p values between CGCD and V1 spectral and nonlinear parameters for patients with (G_{yes}) and without (G_{no}) AF recurrence.

CGCD	G_{yes}		G_{no}	
	Pearson [%]	p	Pearson [%]	p
DF_{3-9}	**49.19**	**0.0172**	−6.67	0.8208
f_1	**46.16**	**0.0266**	−2.12	0.9425
NP(DF)	−18.44	0.3995	−42.30	0.1318
NP(f_1)	**−43.82**	**0.0390**	18.53	0.5260
b_0	−15.17	0.4744	**53.80**	**0.0472**
NP(b_0)	−26.31	0.2551	−19.42	0.5059
f_m	**44.79**	**0.0321**	11.80	0.7036
γ	28.42	0.1888	−27.35	0.3440
RMS_f	−10.04	0.6485	**53.85**	**0.0470**
FWA	−8.87	0.6873	45.04	0.1060
SFM	−19.04	0.3843	−43.29	0.1221
S_1	38.97	0.0660	5.76	0.8448
S_2	39.16	0.0646	5.51	0.8517

Again, some moderate to low correlations are observed. Interestingly, these are mostly registered in the AF recurrence group, including dominant frequency and first harmonic related features, as well as f_m. SE in this group showed a trend. On the other hand, only b_0 and RMS_f show a moderate, statistically significant correlation with CGCD.

The classification accuracy of CGCD values by f-waves charasteristics (low or high values) in groups G1–G3 is then illustrated in Figure A.2. These results do not indicate a high predictive value of CGCD regarding any of the V1 characteristics, with accuracy ranging between $57 - 76\%$. SE is the only feature that shows a relatively strong connection with CGCD in all groups, being this additionally confirmed by statistically significant accuracy values, while DF_{3-9}, NP(f_1), f_m and RMS_f showed moderate and statistically significant classification accuracy in some cases. Finally, how accurately CGCD can predict the CA outcome is estimated in Table A.3, where classification accuracy as well as the CGCD threshold and the median values of patients with and without AF recurrence are shown. CGCD is clearly a poor predictor, showing moderate classification accuracy (59.46–62.16%) and comparable median values between patients with and without AF recurrence.
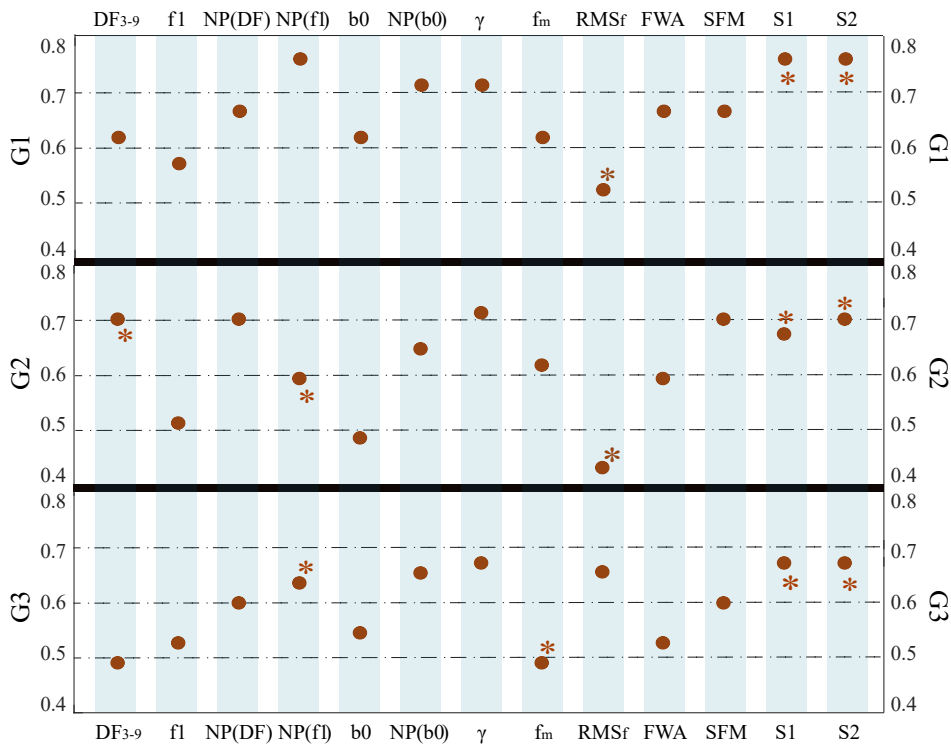
Figure A.2: Classification accuracy $(0 - 1)$ of CGCD value by V1 characteristics for groups G1–G3. Statistically significant results are indicated by an asterisk $(*)$.

Table A.3: Classification and ROC analysis results for CGCD by CA result: AF recurrence (YES) or no recurrence (NO). The last two columns show the median values of each group.

CGCD	Acc [%]	p	Sens [%]	Spec [%]	AUC	Thresh.	YES	NO
Median	59.46	0.6839	78.57	34.78	0.5404	1.9715	2.1150	2.1165
Max	59.46	0.4337	64.29	52.17	0.5776	2.6662	2.8177	2.6516
Min	62.16	0.9501	57.14	47.33	0.5062	1.6727	1.6897	1.7216

B. Correlations between surface recordings acquired before and after CA

Correlations between V1 features and P-waves measured before and after CA, respectively, are shown in Table A.4 for the features showing the strongest relationships. As before, correlations are in the best case moderate, with f_m feature actually showing the highest and most significant inverse correlations with many PWD related features. Correlations are not significantly altered after CF application. Classification accuracy of lead V1 characteristics by binary P-wave characteristics classes (low and high values) is shown in Figure A.3. Accuracy results are insignificant and moderate to low, indicating weak connection between characteristics measured from lead V1 before CA and P-waves analysis performed after CA. Once more, f_m shows the best accuracy results in most of the cases.

Table A.4: Correlations and p values between V1 and P-waves features. Only features with statistically significant results/trends are shown. Features S_1 and S_2 showed similar results, with S_2 showing slightly better values. Hence, due to lack of space, only S_2 is shown. Statistically significant results are indicated in **bold**.

|	f_1		f_m		RMS_f		S_2	
	Corr [%]	p	Corr [%]	p	Corr [%]	p	Corr [%]	p
PWD	−19.4	0.441	−41.0	0.091	−9.3	0.713	−38.7	0.112
Dispersion	46.3	0.053	**47.0**	**0.049**	−6.9	0.787	45.1	0.060
$PWD_{on\text{-}peak}$	−4.5	0.859	**−53.6**	**0.022**	30.3	0.222	−15.7	0.535
$PWD_{peak\text{-}off}$	−19.5	0.439	0.5	0.986	**−48.4**	**0.042**	−35.6	0.416
$PW_{on} - R$	−13.2	0.602	−41.3	0.089	−21.2	0.399	−22.0	0.380
A(*PWD*)	−11.7	0.644	**−59.6**	**0.009**	14.0	0.580	−35.6	0.417
A(*PosAr*)	−22.0	0.380	**−57.3**	**0.013**	38.4	0.116	−39.9	0.101
A($PWD_{on\text{-}peak}$)	−6.2	0.808	**−66.8**	**0.002**	36.1	0.141	−23.2	0.355
A($PW_{on} - R$)	−7.9	0.756	**−58.3**	**0.111**	9.4	0.712	−24.1	0.336
A($PW_{off} - R$)	−2.6	0.911	−45.4	0.058	2.9	0.910	−10.2	0.686
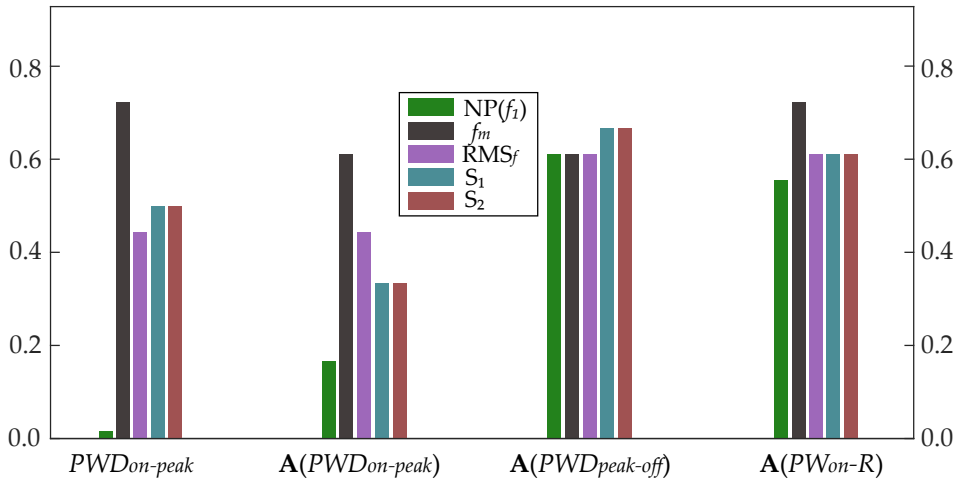
Figure A.3: Classification accuracy $(0 - 1)$ of V1 characteristics by P-wave characteristics. Only features with the highest accuracy are shown. None of the results was statistically signficant.

C. Correlations between invasive pre-CA and surface post-CA recordings

Figure A.4 shows the correlations between CGCD values measured at CS recordings before CA and P-wave features calculated from lead II recordings after CA. As expected from the previous analysis, CGCD values are poorly correlated with P-waves, with amplitude and area values showing the highest and the only significant inverse correlations. As in the previous case, CF application does not seem to affect the correlations. Additionally, classification of CGCD values by P-waves characteristics indicate CGCD as an unsuitable predictor of P-wave values (accuracy 44.44–72.22%), revealing once more the weak relationship between CGCD values and P-waves, as shown in Table A.5.
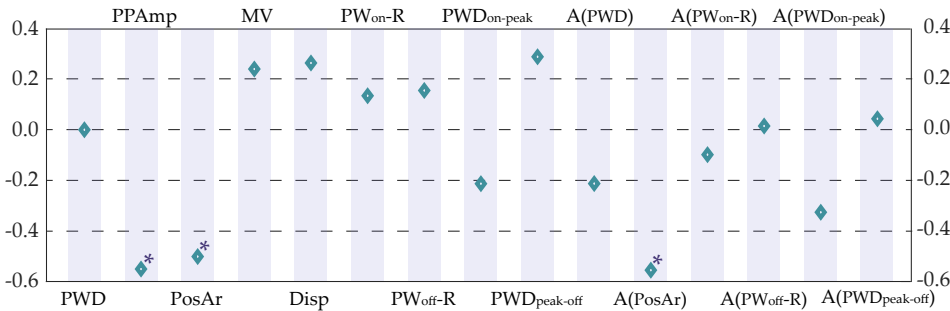
Figure A.4: Pearson's correlation $(-1$ to $+1)$ of CGCD values with P-wave characteristics. Some results have been omitted due to lack of space. Statistically significant results are marked with an asterisk $(*)$.

Table A.5: Classification and ROC analysis results for CGCD by P-wave characteristics.

Feature	Acc [%]	p	Sens [%]	Spec [%]	AUC
PWD	66.67	0.2570	60.00	92.31	0.6769
$Dispersion$	44.44	0.3896	71.43	54.55	0.6234
$PWD_{on\text{-}peak}$	55.56	0.3538	88.89	55.56	0.6296
$PWD_{peak\text{-}off}$	55.56	0.8209	42.86	72.73	0.5325
$PW_{on} - R$	72.22	0.1674	64.29	75.00	0.7321
$PW_{off} - R$	61.11	0.1309	70.00	62.50	0.7125
$\mathbf{A}(PWD)$	55.56	0.1898	83.33	66.67	0.6944
$\mathbf{A}(PWD_{on\text{-}peak})$	55.56	0.3538	88.89	55.564	0.6296
$\mathbf{A}(PWD_{peak\text{-}off})$	61.11	0.0744	72.73	71.43	0.7532
$\mathbf{A}(PW_{on} - R)$	66.67	0.8514	58.33	50.00	0.5278
$\mathbf{A}(PW_{off} - R)$	66.67	0.9254	58.33	50.00	0.5139

A.5   Discussion

The present chapter describes the analysis of pre- and post-CA recordings from paroxysmal and persistent AF patients, entering the operational room in AF. This includes the analysis of lead V1 ECG and bipolar CS EGM recordings obtained before CA in AF as well as the analysis of lead II ECG recordings obtained after CA in SR. The main objective is to define any possible relationships between measurements of different origin that could serve as additional analysis or could even replace the traditional ECG analysis techniques.

Lead V1 for ECG recordings in AF has been chosen to comply with previous studies, since it shows high amplitude f-waves [22, 180, 185], while for ECG recordings in SR, lead II has been selected as it shows the highest amplitude P-waves, respectively [67]. Recordings from CS catheter has been selected due to the wide availability throughout the CA procedure and the fact that it provides recordings always acquired from the same tissue point, as described in chapter 6. The main idea was to relate CGCD analysis with spatial or nonlinear analysis in AF or with P-waves analysis in SR, techniques previously proved to have clinical signficance with respect to CA outcome and AF substrate modification analysis.

The first step of this analysis consisted of correlations between features acquired from lead V1 ECGs and features acquired from bipolar CS recordings. Two databases were used for this purpose, including PVI-only in one case (Database A) and additional CA of DF sites in the second (Database B). Three analysis groups have been formed including paroxysmal AF patients (G1), patients with additional CA (paroxysmal and persistent AF-G2) as well as the entire database, including both paroxysmal and persistent AF patients as well as PVI only and

additional CA applications (G3). The reason why analysis on database A (PVI only) and on persistent AF patients is not presented were the small data size and the lack of improved results in the former and latter cases, respectively. In general, poor correlations have been observed at any of the three groups, with paroxysmal AF group (G1) showing the best results, yet not satisfactory, for DF and first harmonic and a strong trend for median frequency. Regarding G2 and G3, results were similar, with G3 showing some values indicating statistical significance which can be attributed to the larger data size with respect to G2.

Given that the database utilized in this study shares the most part with the database employed in the study from Alcaraz et al. [180], an inverse correlation between CGCD and DF and first harmonic would be expected, as CGCD augments with higher AF complexity, while low DF and first harmonic as well as median frequency were, although not statistically, connected with AF recurrence. On the other hand, the first harmonic (f_1) and median frequency (f_m) formed the best predictive model for persistent AF patients, which explains the significant yet moderate correlation between CGCD and median frequency, in this study, especially in G3.

Regarding SE, statistically significant and low correlations have been observed. However, due to its similar nature with CGCD, quantifying regularity, higher correlations were expected [186]. Nevertheless, apart from the different origin of the two recordings (ECGs in case of SE, EGMs in case of CGCD), the fact that CGCD was measured exclusively from CS recordings and not from multiple atrial locations, may explain this outcome. As already shown in chapter 6, ECG characteristics measured from lead II and EGM characteristics measured from CS are weakly related in SR, with ECG recordings being able to capture the alterations on a global atrial level and CS providing local information. On the other hand, as CS is a critical structure in AF perpetuation [54,157–160] and given the importance of DF analysis in CS recordings [55], high CGCD and SE correlations from CS and lead V1 would not be completely unexpected. Similar to correlations between CGCD and spectral and nonlinear features from lead V1 recordings, classification of CGCD values by two categories of each V1 feature (high and low values) showed moderate classification accuracy, with the highest values being attributed to the same V1 features as in correlation analysis.

Two different groups, consisting of the patients showing AF recurrence (G_{yes}) and no-AF recurrence (G_{no}), were then formed. Different correlations have been observed in each of the two groups, with results in AF recurrence group being similar to that from G1–G3 analysis, while the group without AF recurrence showed a higher correlation with b_0 and the average f-waves power (RMS_f). The fact that the same groups use paroxysmal and persistent AF patients may affect some of the results, as most of the features have shown different trends in paroxysmal than persistent AF patients, leading to unexpected results and hence to obscure conclusions about the CGCD connection with the AF substrate [180].

The ability of CGCD to predict the CA outcome has then been investigated, suggesting CGCD as a poor predictor unable to precisely estimate the CA out-

come. In fact, when median CGCD is utilized, as has the analysis been developed so far, AF patients with and without AF recurrence show almost identical CGCD values, with patients with AF recurrence showing slightly lower CGCD values. This observation could partially explain the weird correlations with spectral characteristics presented in the afore paragraph.

Once the relationships between CGCD and spectral and nonlinear characteristics have been defined, the analysis proceeded with the investigation of any connection between characteristics measured from lead V1 during AF before CA and P-waves characteristics measured right after CA. As it has already been disclaimed in Section A.3.1, lack of follow-up information and the use of different ECG leads probably include a sort of bias in this analysis step. Consequently, no significant correlations are expected. Indeed, correlations were mostly weak or moderate, with the higest positive and negative correlations found between f_m and P-wave features.

Interestingly enough, f_m has been the feature always showing one of the highest and most signfiicant correlations with CGCD in the previous analysis as well. A low f_m value would suggest that higher spectral concentration is observed in lower frequencies and vice versa. As DF and first harmonic have been shown to be higher for no AF recurrence patients, hence connected with better prognostics and probably to a less present AF substrate, their inverse correlation with P-wave indices is expected. Indeed, Table A.4 shows negative moderate correlations with PWD related features. As expected, classification accuracy of spectral characteristics by P-wave features has failed to show any connection between lead V1 features calculated before CA and lead II features calculated after CA. In any case, f_m showed once more the highest accuracy for most of the features.

The analysis has been finalized with the search of any connection between the pre-CA CS recordings and post-CA lead II recordings. This analysis contains a higher amount of bias, as besides the fact that no follow-up information is available, the origin of the two recordings is different, with CS recording measuring local information on the CS and lead II measuring global information concerning the entire atria, assessed noninvasively. Correlations seem to be statistically insignificant and weak, spanning from -0.6 to $+0.4$. The highest correlations have been observed (inversely) with the amplitude and area features. Although a P-wave amplitude or area attenuation is considered positive regarding the AF substrate modification, measuring raw values of just one recording and not the variation trend of a pre-post CA comparison of the same feature does not allow any conclusions, as amplitude depends on multiple factors, including recording quality. Regarding CGCD, however, it should be noted that any amplitude bias is removed prior to analysis, as explained in chapter 3.

Finally, when classification of CGCD values by P-wave features is attempted, it seems that CGCD is unable to predict a high or low P-wave feature value, as indicated from the moderate classification accuracies. In all analysis cases, CF application does not seem to improve or alter significantly the correlation or classification outcome.

A.6   Conclusions

CGCD analysis from CS recordings is not strongly related to spectral and nonlinear analysis from lead V1 recordings before CA. CGCD analysis is not a good predictor regarding the CA outcome in procedures applying PVI and additional DF CA. Spectral and nonlinear characteristics from lead V1 recordings during AF before CA have also been proved unrelated to P-waves characteristics from lead II recordings during SR after CA. CGCD before CA is not related with P-waves analysis after CA either. It should be noted that no follow-up information is available and hence any mechanisms acting during CA cannot be recognized, severely affecting the before-after CA analysis results.

Scientific achievements

Contents

B.1 Publications

B.1.1 JCR indexed articles

1. **A. Vraka**, F. Hornero, V. Bertomeu-González, J. Osca, R. Alcaraz J.J, Rieta. Short-Time Estimation of Fractionation in Atrial Fibrillation with Coarse-Grained Correlation Dimension for Mapping the Atrial Substrate.
   Entropy 2020, vol. 22, Issue 2, p. 232, doi: `https://doi.org/10.3390/e22020232`.

2. **A. Vraka** , V. Bertomeu-González, F. Hornero, A. Quesada, R. Alcaraz, J.J. Rieta. Splitting the P-Wave: Improved Evaluation of Left Atrial Substrate Modification after Pulmonary Vein Isolation of Paroxysmal Atrial Fibrillation. Sensors 2022, vol.1, Issue 22, p. 290, doi: `https://doi.org/10.3390/s22010290`.

3. **A. Vraka** , V. Bertomeu-González, L. Fácila, J. Moreno-Arribas, R. Alcaraz, J.J. Rieta. The Dissimilar Impact in Atrial Substrate Modificationof Left and Right Pulmonary Veins Isolation after Catheter Ablation of Paroxysmal Atrial Fibrillation. Journal of Personalized Medicine 2022, vol.3, Issue 12, p. 462, doi: `https://doi.org/10.3390/jpm12030462`.

4. **A. Vraka**, J. Moreno-Arribas, J.M. Gracia-Baena, F. Hornero, R. Alcaraz, J.J. Rieta. The Relevance of Heart Rate Fluctuation when Evaluating Atrial Substrate Electrical Features in Catheter Ablation of Paroxysmal Atrial Fibrillation. Journal of Cardiovascular Development and Disease, vol.9, Issue 6, p.176, doi: `https://doi.org/10.3390/jcdd9060176`.

5. D. Osorio, **A.Vraka**, A. Quesada, F. Hornero, R. Alcaraz, J.J. Rieta. An Efficient Hybrid Methodology for Local Activation Waves Detection under Complex Fractionated Atrial Electrograms of Atrial Fibrillation. Sensors 2022, vol. 22, Issue 14, p.5345, doi: `https://doi.org/10.3390/s22145345`.

6. D. Osorio, **A. Vraka**, J. Moreno-Arribas, V. Bertomeu-González, R. Alcaraz, J.J. Rieta. Comparative Study of Methods for Cycle Length Estimation in Fractionated Electrograms of Atrial Fibrillation. Journal of Personalized Medicine 2022, vol. 12, Issue 10, p. 1712, doi: `https://doi.org/10.3390/jpm12101712`.

B.1.2 International conferences

1. **A. Vraka**, J. Osca, V. Bertomeu-González, M.A. Arias, F. Hornero, R. Alcaraz, J.J. Rieta. Automatic Quantificaton of Fractionation in Atrial Fibrillation Electrograms for Substrate Mapping. Atrial Signals Conference, October 14 – 15, 2019, Bordeaux, France. Poster presentation.

2. **A. Vraka**, D. Osorio, L. Faes, A. Quesada, O. Cano, R. Alcaraz, J.J. Rieta. A Multichannel Local Activation Wave Detector for Improved Localization of Dominant Reentries in Electrograms of Atrial Fibrillation. Atrial Signals Conference, October 14 – 15, 2019, Bordeaux, France. Poster presentation.

3. **A. Vraka**, F. Hornero, J. Osca, L. Faes, R. Alcaraz and J.J. Rieta. Assisting Electrophysiological Substrate Quantification in Atrial Fibrillation Ablation. 2019 E-Health and Bioengineering Conference (EHB), Iasi, Romania, November 21 – 23, 2019, pp. 1-4, doi: `https://doi.org/10.1109/EHB47216.2019.8969928`.

4. **A. Vraka**, D. Osorio, V. Bertomeu-González, F. Ravelli, R. Alcaraz and J.J. Rieta. Detection of Dominant Reentries in Multichannel Electrograms of Atrial Fibrillation. 2019 E-Health and Bioengineering Conference (EHB), Iasi, Romania, November 21 – 23, 2019, pp. 1-4, doi: `https://doi.org/10.1109/EHB47216.2019.8969992`.

5. **A. Vraka**, F. Hornero, A. Quesada, L. Faes, R. Alcaraz and J.J. Rieta. Reliability of Local Activation Waves Features to Characterize Paroxysmal Atrial Fibrillation Substrate During Sinus Rhythm. 2020 Computing in Cardiology Conference, (online) Rimini, Italy, September 13 – 16, 2020, url: `https://ieeexplore.ieee.org/document/9344134`.

6. **A. Vraka**, V. Bertomeu-González, J. Osca, F. Ravelli, R. Alcaraz and J.J. Rieta. Study on How Catheter Ablation Affects Atrial Structures in Patients with Paroxysmal Atrial Fibrillation: The Case of the Coronary Sinus. 2020 E-Health and Bioengineering Conference (EHB), (online) Iasi, Romania, October 29 – 30, 2020, doi: `https://doi.org/10.1109/EHB50910.2020.9280243`.

7. **A. Vraka**, F. Hornero, A. Quesada, L. Faes, R. Alcaraz and J.J. Rieta. Reliable Paroxysmal Atrial Fibrillation Substrate Assessment During Sinus Rhythm Through Optimal Estimation of Local Activation Waves Dynamics. 2020 E-Health and Bioengineering Conference (EHB), (online) Iasi, Romania, October 29 – 30, 2020, doi: `https://doi.org/10.1109/EHB50910.2020.9280159`.

8. **A. Vraka**, V. Bertomeu-González, F. Hornero, L. Faes,, R. Alcaraz and J.J. Rieta. Linear and Nonlinear Correlations Between Surface and Invasive Atrial Activation Features in Catheter Ablation of Paroxysmal Atrial Fibrillation. 2021 Computing in Cardiology Conference, (online) Brno, Czech Republic, September 12 – 15, 2021, doi: `https://ieeexplore.ieee.org/document/9662868`.

9. **A. Vraka**, V. Bertomeu-González, F. Hornero, L. Sörnmo, R. Alcaraz and J.J. Rieta. Alternative Time-Domain P-wave Analysis for Precise Information on Substrate Alteration After Pulmonary Vein Isolation for Atrial Fibrillation. 2021 E-Health and Bioengineering Conference (EHB), (online) Iasi, Romania, November 18 – 19, 2021, doi: `https://doi.org/10.1109/EHB52898.2021.9657541`.

10. **A. Vraka**, F. Hornero, A. Quesada, F. Ravelli, R. Alcaraz and J.J. Rieta. Parallel Study on Surface and Invasive Recordings Across Catheter Ablation Steps of Paroxysmal Atrial Fibrillation. 2021 E-Health and Bioengineering Conference (EHB), (online) Iasi, Romania, November 18 – 19, 2021, doi: `https://doi.org/10.1109/EHB52898.2021.9657695`.

11. **A. Vraka**, V. Bertomeu-González, F. Hornero, P. Langley, R. Alcaraz and J.J. Rieta. Are Coronary Sinus Features Reflecting the Effect of Catheter Ablation of Atrial Fibrillation as P-waves Do? 2021 E-Health and Bioengineering Conference (EHB), (online) Iasi, Romania, November 18 – 19, 2021, doi: `https://doi.org/10.1109/EHB52898.2021.9657639`.

12. **A. Vraka**, V. Bertomeu-González, L. Sörnmo, R. Zangróniz, R. Alcaraz and J.J. Rieta. The P-wave Time-domain Significant Features to Evaluate Substrate Modification After Catheter Ablation of Paroxysmal Atrial Fibrillation, 2022 Computing in Cardiology Conference, Tampere, Finland, September 4 – 7, 2022, doi: `https://cinc.org/2022/Program/accepted/11_Preprint.pdf`.

13. **A. Vraka**, J. Moreno-Arribas, J.M. Gracia-Baena, F. Ravelli, R. Alcaraz and J.J. Rieta. Left Pulmonary Veins Isolation: The Cornerstone in Noninvasive Evaluation of Substrate Modification After Catheter Ablation of Paroxysmal Atrial Fibrillation, 2022 Computing in Cardiology Conference, Tampere, Finland, September 4 – 7, 2022, doi: `https://cinc.org/2022/Program/accepted/12_Preprint.pdf`.

14. **A. Vraka**, A. Quesada, F. Hornero, A. Martínez-Rodrigo, R. Alcaraz and J.J. Rieta. A Novel Strategy for Signal Reconstruction of Noisy Segments

in Photoplethysmographic Recordings, 2022 E-Health and Bioengineering Conference (EHB), (hybrid) Iasi, Romania, November 17 – 19, 2022, AC-CEPTED FOR PUBLICATION.

B.1.3 National conferences

1. **A. Vraka**., F. Hornero, J. Oscai, O. Cano, R. Alcaraz and J.J. Rieta. Evaluacion Automática de la Fragmentación en Electrogramas de Fibrilación Auricular para Evaluación del Sustrato Auricula. Actas del XXXVII Congreso Anual de la Sociedad Española de Ingeniería Biomédica, pages 45-48, Santander, España, November 27 – 29, 2019, ISBN 978-84-09-16707-4.

2. **A. Vraka**, D. Osorio, V. Bertomeu-González, A. Ibáñez Criado, R. Alcaraz and J.J Rieta. Localización Mejorada de Activaciones Dominantes en Fibrilación Auricular Mediante Detección Multicanal. Actas del XXXVII Congreso Anual de la Sociedad Española de Ingeniería Biomédica, pages 195-198, Santander, España, November 27 – 29, 2019, ISBN 978-84-09-16707-4.

3. **A. Vraka**, V. Bertomeu-González, F. Hornero, A. Quesada, R. Alcaraz and J.J Rieta. Efecto de la Ablación por Catéter Sobre Ciertas Estructuras Auriculares de Pacientes con Fibrilación Auricular Paroxística: El Caso del Seno Coronario. Actas del XXXVIII Congreso Anual de la Sociedad Española de Ingeniería Biomédica, pages 105-108, online, November 27 – 29, 2020, ISBN 978-84-09-25491-0.

4. **A. Vraka**, F. Hornero, V. Bertomeu-González, J. Osca, R. Alcaraz and J.J Rieta. Confiabilidad de Ondas de Activación Local para Evaluar el Sustrato Auricular de Pacientes con Fibrilación Auricular Paroxística. Actas del XXXVIII Congreso Anual de la Sociedad Española de Ingeniería Biomédica, pages 430-433, online, November 27 – 29, 2020, ISBN 978-84-09-25491-0.

5. **A. Vraka**, F. Hornero, V. Bertomeu-González, A. Quesada, R. Alcaraz and J.J Rieta. Análisis Paso a Paso de Registros de Ablación por Catéter en Fibrilación Auricular Paroxística. XXXIX Congreso Anual de la Sociedad Española de Ingeniería Biomédica, pages 147-159, online, November 25 – 26, 2021, ISBN 978-84-09-36054-3.

6. **A. Vraka**, V. Bertomeu-González, F. Hornero, A. Quesada, R. Alcaraz and J.J Rieta. Diferencias Entre Patrones de Ondas P y Ondas de Activación Local del Seno Coronario Durante Ablación por Catéter de Fibrilación Auricular Paroxística. XXXIX Congreso Anual de la Sociedad Española de Ingeniería Biomédica, pages 155-158, online, November 25 – 26, 2021, ISBN 978-84-09-36054-3.

7. **A. Vraka**, A. Quesada, F. Hornero, V. Bertomeu Gonzalez, R. Alcaraz and J.J Rieta. La Importancia de la Aurícula Izquierda en la Alteración del Sustrato Auricular tras Ablación por Catéter de Fibrilación Auricular Paroxística .

XXXIX Congreso Anual de la Sociedad Española de Ingeniería Biomédica, pages 83-86, online, November 25 – 26, 2021, ISBN 978-84-09-36054-3.

B.2   Awards

1. **IEEE International, E-Health and Bioengineering Conference 2019 (EHB 2019), Young researcher first prize** for the study entitled " Assisting Electrophysiological Substrate Quantification in Atrial Fibrillation Ablation" by **A. Vraka**, F. Hornero, J. Osca, L. Faes, R. Alcaraz and J.J. Rieta.

2. **Computing in Cardiology 2021 Conference, winner of the Bill and Gary Sanders Poster Award** for the study entitled "Linear and Nonlinear Correlations Between Surface and Invasive Atrial Activation Features in Catheter Ablation of Paroxysmal Atrial Fibrillation" by **A. Vraka**, V. Bertomeu-González, F. Hornero, L. Faes, R. Alcaraz and J.J. Rieta.

3. **XXXIX Congreso Anual de la Sociedad Española de Ingeniería Biomédica 2021 (CASEIB 2021), runner up of the José María Ferrero Corral award** for the study entitled "XXXIX Congreso Anual de la Sociedad Española de Ingeniería Biomédica" by **A. Vraka**, A. Quesada, F. Hornero, V. Bertomeu-González, R. Alcaraz and J.J Rieta.

Compendium of publications: published papers

Contents

Article

Short-Time Estimation of Fractionation in Atrial Fibrillation with Coarse-Grained Correlation Dimension for Mapping the Atrial Substrate

Aikaterini Vraka [1], Fernando Hornero [2], Vicente Bertomeu-González [3], Joaquín Osca [4], Raúl Alcaraz [5] and José J. Rieta [1,*]

[1] BioMIT.org, Electronic Engineering Department, Universitat Politecnica de Valencia, 46022 Valencia, Spain; aivra@upv.es

[2] Cardiac Surgery Department, Hospital Universitari i Politecnic La Fe, 46026 Valencia, Spain; hornero_fer@gva.es

[3] Cardiology Department, Hospital Universitario de San Juan de Alicante, 03550 Alicante, Spain; vbertog@gmail.com

[4] Electrophysiology Section, Hospital Universitari i Politecnic La Fe, 46026 Valencia, Spain; joaquinosca@gmail.com

[5] Research Group in Electronic, Biomedical and Telecommunication Engineering, University of Castilla-La Mancha, 16071 Cuenca, Spain; raul.alcaraz@uclm.es

* Correspondence: jjrieta@upv.es

Abstract: Atrial fibrillation (AF) is currently the most common cardiac arrhythmia, with catheter ablation (CA) of the pulmonary veins (PV) being its first line therapy. Ablation of complex fractionated atrial electrograms (CFAEs) outside the PVs has demonstrated improved long-term results, but their identification requires a reliable electrogram (EGM) fractionation estimator. This study proposes a technique aimed to assist CA procedures under real-time settings. The method has been tested on three groups of recordings: Group 1 consisted of 24 highly representative EGMs, eight of each belonging to a different AF Type. Group 2 contained the entire dataset of 119 EGMs, whereas Group 3 contained 20 pseudo-real EGMs of the special Type IV AF. Coarse-grained correlation dimension (CGCD) was computed at epochs of 1 s duration, obtaining a classification accuracy of 100% in Group 1 and 84.0–85.7% in Group 2, using 10-fold cross-validation. The receiver operating characteristics (ROC) analysis for highly fractionated EGMs, showed 100% specificity and sensitivity in Group 1 and 87.5% specificity and 93.6% sensitivity in Group 2. In addition, 100% of the pseudo-real EGMs were correctly identified as Type IV AF. This method can consistently express the fractionation level of AF EGMs and provides better performance than previous works. Its ability to compute fractionation in short-time can agilely detect sudden changes of AF Types and could be used for mapping the atrial substrate, thus assisting CA procedures under real-time settings for atrial substrate modification.

Keywords: atrial fibrillation; catheter ablation; signal processing; chaos theory; coarse-grained correlation dimension; complex fractionated atrial electrograms; nonlinear analysis

---

1. Introduction

Atrial fibrillation (AF) is the most common cardiac arrhythmia in the developed countries [1], with its rates expected to increase by 2.5 times until year 2050 [2]. Being associated with high mortality risks, the scientific and medical interest of AF is focused both on the understanding of its mechanisms and on candidate treatments [1]. For the latter case, the AF clinical stage, which can be distinguished in paroxysmal, persistent, long-standing persistent, and permanent AF is of high importance. Paroxysmal

AF is self-terminating usually within the first 48 hours but can last up to 7 days. Persistent AF (peAF) is characterized by episodes with a duration longer than 7 days, while long-standing peAF lasts at least for a year. Permanent AF exists when its termination is impossible or not recommended and the presence of arrhythmia is accepted by both the clinician and the patient [3].

Common AF treatments include electrical [4] and pharmacological [5] cardioversion and catheter [6] or surgical ablation [7]. After the first reference on the arrhythmogenic role of pulmonary veins (PVs) [8] more than twenty years ago, catheter ablation (CA) targeting PVs foci, a procedure called pulmonary vein isolation (PVI), became the most popular of these treatments. Despite the well-established dominion of this technique up to present, the AF recurrence rate in patients with peAF remains higher than 50% in many cases [9,10].

A possible explanation for the lack of satisfactory results is that foci are triggered in PVs, but re-entrant mechanisms utilize other sites of the atrium and the coronary sinus (CS) musculature for the perpetuation of AF [11]. A vast amount of literature contributes to the effort in understanding these mechanisms [12–14]. The most prevalent views attribute the AF either to relatively stable and re-entrant electrical rotors [15] or to epicardial breakthroughs springing from deeper layers of the atrial wall and causing multiple wavefronts due to conduction blocks [16]. The latter perspective is connected to a well-known assumption that peAF is more complicated than paroxysmal due to the structural remodeling of the atria. This remodeling includes, among others, dilatation, scarring, and fibrosis, mostly located on the left side of the atria and remodeled areas are thought to form the pathophysiologic substrate of AF [17].

Fibrosis, in particular, is considered the key change that favors the propagation of irregular and ectopic activations, as it weakens the intercellular connectivity and provokes endo-epicardial electrical dissociation [18–20]. Whether fibrosis is the main cause of peAF or the long-term fibrillation provokes it remains unclear [14], whereas it is clear the need for the elimination of the AF substrate. For this purpose, additional ablation based on specific electrogram (EGM) characteristics that possibly indicate the fibrotic tissue, known as substrate modification, is performed. Low-voltage (LV) areas are a candidate target, as reduced signal amplitude is connected to scarring [21]. Relevant studies have shown that additional ablation of LV zones effectively reduces the percentage of AF recurrence [22,23], but the rates of recurrence-free cases depend on the extent up to which LV areas span through the left atrium (LA), which in turn varies among patients [22–24].

Highly repetitive re-entrant wavefronts are found in LA sites with high dominant frequency (DF), which have also been investigated as possible remodeled areas [25,26]. However, little or no connection between DF sites in LA and AF elimination was found [27,28]. By contrast, DF in CS has been proven to be able to indicate the patients who need additional ablation [11].

Another one and possibly the most popular indicator of atrial tissue fibrosis is EGM fractionation, which can be considered as a projection of the multiple wavelets scattered through the epicardium and passing simultaneously by the measured point. Highly fractionated EGMs, commonly known as complex fractionated atrial electrograms (CFAEs), are linked to higher incidence rates of re-entrant mechanisms and thus to higher severity of fibrosis [18]. The first successful attempt to distinguish CFAEs that can be targets for substrate modification and effectively eliminate them, reported very high AF recurrence-free rates of 91%, even after one year of follow-up [29].

A high number of studies since then have added precious information in the mapping of AF substrate. Combining CFAEs analysis with LV zones or DF sites has been a subject under investigation as well, with quite controversial results. One study localized CFAEs within CS before and after antral PVI and found DF and EGM complexity to decrease in consistency with ablation efficacy in peAF, implicating the need for simultaneous CS analysis [11]. On the other hand, other studies disprove DF as an independent predictor of ablation guided by highly fragmented EGMs [27,30] or find a spatial proximity of DF sites to areas with CFAEs [30]. Detection of CFAEs in frequency domain highly depends on the technique used. Although Fourier Transform (FT) is the standard method for DF calculation, some alternative techniques have reported improved results. A transform based on

the averaging of the various ensembles of a signal has demonstrated reduced measurement error in CFAEs identification [31]. A following study based on this technique [32] showed improved time and frequency resolution in comparison with discrete FT and found the dominant spectral parameters to be higher in peAF than paroxysmal AF, suggesting that AF activation patterns are more regular and stable in peAF patients. Although there are indications that LV zones in sinus rhythm (SR) can adequately predict AF sustaining CFAEs [33], another study has found that there is no necessary correlation between them and LV sites [34].

The comparison between CFAE-based ablation and other AF mapping and ablation methods [35,36] as well as the poor correlation between CFAEs areas and AF drivers [37] has led many studies to consider the ablation of CFAEs to be of little success. These studies, however, do not deny CFAEs as ablation targets. They simply highlight the need for a stricter definition to avoid unnecessary lesions. CFAEs are defined either as EGMs composed by two or more deflections and/or perturbation of the baseline with continuous deflection or as EGMs with a very short cycle length (CL) (≤ 120 ms) [29]. Correlation between these two definitions is poor, whereas CFAEs locations vary upon the patient and the definition used [30,38].

The demanding need for an accurate and reliable definition of CFAEs is therefore clear, so that their contribution to the AF substrate is loyally depicted. One quite straightforward indicator is the estimation of fractionation level of the EGMs [39]. As it was previously mentioned, low-fractionated EGMs may reflect passive phenomena, but as the fractionation level augments, it is more possible to depict regions of fibrotic tissue. As fractionated EGMs express the superposition of more than one wavelets simultaneously propagating through different directions in the atria, a nonlinear metric may be able to better quantify their fractionation level, and therefore the number and the organization level of the activations that they depict.

This behavior of EGMs as nonlinear dynamical systems has been investigated by several studies [40–44], using a chaos-theory based technique known as correlation dimension (CorDim). CorDim quantifies the level of randomness of a strange attractor and has been used to assess the organization and complexity of EGMs. Hoekstra et al. [40] used coarse-grained CorDim (CGCD) and correlation entropy to classify unipolar epicardial EGMs recorded at the free wall of right atrium by AF Types, as described by Wells et al. [45]. Although this work came out with some very interesting results, the use of unipolar instead of bipolar EGMs narrows down the robustness of the findings. Censi et al. used CGCD and surrogate data in order to assess the nonlinear coupling of cardiac time-series and assumed that the indices used for this purpose may serve for the classification of EGMs by AF Types [41]. In 2014, Luca et al. used CorDim for the quantification of the influence of anti-tachyarrhythmia pacing in model-based AF and suggested it as a discrimination metric of atrial activity organization [43]. Later in 2016, another relevant study used CGCD in right atrial (RA) EGMs before and during catheter ablation for the assessment of peAF complexity [44]. Results revealed a predictive value of this index for the ablation outcome.

Taking advantage of the theoretical and experimental background of all these works, we recruited CGCD as a fractionation index of the atrial EGMs. This work is based on the hypothesis that CGCD is linked to the fragmentation level of EGMs in a pro rata basis and its use can effectively estimate the AF type of patients even in recordings as short as one second in length. The aim of this study is to present a method with real-time implementation capabilities on the mapping devices that can precisely detect areas of high fractionation EGMs as well as short-duration phenomena, so that the AF substrate can be efficiently removed.

The manuscript is organized as follows. Section 2 presents the study population and data acquisition and introduces the theoretical background of the concepts used in the study. It also provides information on the computational parameters and the methods used for the CGCD estimation as well as the statistical analysis, the outcomes of which are presented in Section 3. Next, Section 4 discusses about the main findings and some important issues to be taken into account regarding the study, whereas Section 5 explains the main limitations of the study as well as the context within which

some choices have been made. Finally, Section 6 highlights the most relevant aspects of the study introducing the concluding remarks.

2. Methods

2.1. Study Population and Data Acquisition

The database employed in this study consisted of 119, 10 s duration bipolar EGMs of 22 peAF patients undergoing CA for the first time, after their signed informed consent. Data were obtained using a Labsystem™PRO EP recording system (Boston Scientific, Marlborough, MA, USA) with a sampling frequency set at 1 kHz and a bandpass filter at 0.5–500 Hz. EGMs were visually inspected and classified according to their AF type following Wells' criteria [45]. There are three main AF Types: AF Type I is characterized by discrete activations with a stable isoelectric line, whereas AF Type II is also characterized by discrete activations, with the baseline presenting perturbations of varying degrees. AF Type III lacks either discrete complexes or isoelectric intervals. There is also AF Type IV, which is consistent with AF Type III, with altering parts of AF Types I or II. Figure 1 shows an example of different AF Types.
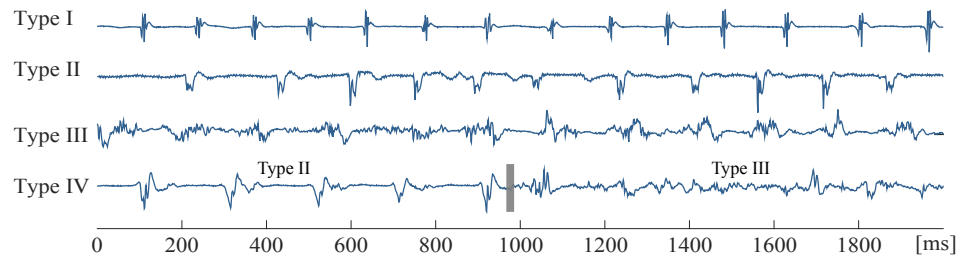
Figure 1. Example of bipolar atrial fibrillation (AF) electrograms (EGMs) of different Types. AF Type IV consists of alternating Type I/II and Type III segments.

In total, 11 EGMs were classified by two expert physicians as Type I, 36 as Type II, and 72 as Type III. Visual classification by AF type can be confusing in cases that an EGM does not clearly belong to an AF type. To make a fair assessment of CGCD as a fractionation index, eight EGMs from each category were selected as the most representative of their type. Additionally, 20 pseudo-real EGMs were created by the concatenation of parts of real EGMs to create some Type IV electrograms.

Data analysis has been performed on three groups. Group 1 consisted of the 24 most representative EGMs, eight of each type, selected by the two experts, as the EGMs that undoubtedly belonged to the assigned type. These EGMs represented the common choice of the experts, with each one of them being blinded to the selection of the other one. Group 2 consisted of all the electrograms of the database, whereas Group 3 contained the 20 pseudo-real Type IV electrograms.

2.2. Coarse-Grained Correlation Dimension

Randomness of the dynamics characterizing AF can be assessed by CorDim, a well-known measure of the organization of nonlinear dynamical systems [46]. The main idea of this method claims that by reconstructing the observed time-series in phase space, one can assess its stochastic nature by calculating the distance between elements of the time-series and comparing it with a resolution distance r. In other words, a set of nondeterministic (chaotic) points will occupy more space than a set of deterministic ones. The dimensionality of this space is expressed as CorDim.

The first step for the calculation of CorDim is the phase-space reconstruction of the given time-series, with the reconstructed system preserving the dynamical characteristics of the original dataset [47]. More specifically, given a N-points long time series $X = (x_1, x_2, \ldots, x_N)$, one can

reconstruct it to the m dimensional phase-space using a time delay τ between vectors [40,48]. Phase-space reconstruction of the p-th element of X will then be

$$\mathbf{Y}_p^{(m)} = (x_p, x_{p+\tau}, x_{p+2\tau}, \dots, x_{p+(m-1)\tau}), \tag{1}$$

where $m = 1, 2, 3 \dots$ is the embedded dimension and $p = 1, 2, \dots, N - (m-1)\tau$.

The second step after phase-space reconstruction is completed is the estimation of the correlation integral [46], which calculates the proportion of pairs of vectors that are closer to each other than a distance r,

$$C^{(m)}(r) = \frac{2}{N_{ref}(N_{ref}-1)} \sum_{i=1}^{N_{ref}} \sum_{j>i}^{N_{ref}} \Theta(r - \|Y_i^{(m)} - Y_j^{(m)}\|), \tag{2}$$

where Θ is the Heaviside function, and $\|\cdot\|$ is the Euclidean distance of each pair chosen and N_{ref} is the number of reference points, as a chosen number of the $N - (m-1)$ vectors of Equation (1).

For the computation of CorDim, we search for saturation areas (linear regions) on the double logarithmic plot of $C^{(m)}(r)$ as a function of r, plotted in sequential embedded dimensions from $m = 1, 2, \dots, 20$ [44]. By taking a look at the correlation integral, one can see that CorDim is inversely proportional to the organization of the underlying dynamics. This can be explained by the fact that two strongly associated points will not be very far away from each other, when the reconstructed phase-space faithfully represents the original data. On the other hand, highly irrelevant or weakly associated points will be found in random positions that, when averaged through the whole dataset, will be significantly far away from each other.

In cardiac signals, specially in significantly fragmented EGMs dominated by highly disorganized dynamics, the lack of regions of saturation and, as a result, the incapacity of a reliable description of the reconstructed dynamics by the correlation integral, is always a possibility to be considered [40,44]. A slight variation of the correlation integral, known as CGCD can nevertheless still be used to measure the organization of the dynamics of invasive cardiac recordings [40]. More of a comparative measure between the complexity of the signals than a precise dimension estimator [44], CGCD makes a rough estimation of this complexity at a fixed embedded dimension m and a finite resolution distance r_{cg}, thus

$$CGCD^{(m)}(r_{cg}) = \frac{dln[C^{(m)}(r_{cg})]}{dln(r_{cg})}, \tag{3}$$

being the selected nonlinear index applied in the present work to atrial EGMs of AF with the aim to estimate their fractionation. For the calculation of the $CGCD^{(m)}(r_{cg})$ from the double logarithmic plot of $C^{(m)}(r)$ as a function of the distance r, we need to calculate the derivative of the correlation integral curve, when $r = r_{cg}$. This can be approached by the local slope of the tangent line, passing from the point $(ln(r_{cg}), ln(C^{(m)}(r_{cg}))$, calculated through two points, $(ln(r_1), ln(C^{(m)}(r_1))$ and $(ln(r_2), ln(C^{(m)}(r_2))$, surrounding the point $(ln(r_{cg}), ln(C^{(m)}(r_{cg}))$ [40].

2.3. Selection of Computational Parameters

As mentioned in Section 2.2, for the computation of CGCD, it is necessary to set the following parameters; the embedded dimension m, the time lag τ, the distance r_{cg}, and the number of reference points N_{ref}. The choice of these parameters is very important for both the optimal operation and the discriminative power of CGCD between AF fractionation levels and is hereby discussed in detail.

2.3.1. Embedded Dimension

Correct embedded dimension m is important for the loyal resemblance of the reconstructed signal. According to Hoekstra et al. [40], m needs to be sufficiently large so that dynamics are faithfully described by the reconstructed signal. In case that m is smaller than the dimension of the dynamics

under analysis, double logarithmic plot will present no linear regions [48]. Optimal m can vary from signal to signal, it is necessary though to set a global m value and analyze the dynamics over it. The choice of m in previous works was empirical and chosen to $m = 10$ [40,44].

2.3.2. Time Lag

The other factor influencing both resemblance precision of the reconstructed signal and discrimination power through AF fractionation levels is time lag τ. When choosing a small time lag, all points in Equation (1) will tend to become indistinguishable [49]. A common choice for τ is to be equal to the first minimum of the mutual information [40].

2.3.3. Distance in Phase Space

Selection of distance r_{cg} affects both accuracy and precision of the method. By scaling it down, a better control of systematic errors and thus an increase in accuracy is achieved. At the same time, however, statistical errors are augmented and consequently precision drops down. It is important, therefore, to choose r_{cg} as a trade-off between these two parameters. Theiler [50] suggested that systematic and statistical errors are treated as an entity and tried to find the optimal r_{cg} for its reduction. A distance r_{cg} equal to half of the standard deviation of the time-series, normalized by its peak-to-peak amplitude is commonly used [40].

2.3.4. Reference Points

Wise choice of reference points N_{ref} is important for the statistical precision of the dimension analysis. A choice of a small N_{ref} would lead to poor statistical validity [50] and the risk of calculating a correlation integral of zero value would be present for dynamics of high-dimensional chaos. Regarding the lowest limit, N_{ref} equal to 1/3 of total points of the time-series was found to be acceptable [50]. Speaking of the upper limit, the choice must be made taking into consideration the execution time of the algorithm, which significantly increases when the time series is quite long and the percentage of precision improvement that is succeeded.

2.4. Data Preprocessing and Analysis

To minimize the influence of signal amplitude on CGCD, each signal was firstly normalized by its root mean square (RMS) value. RMS value is the square of the function that defines the time-series. As signal amplitude varies from recording to recording, normalizing by a standard value would be of no meaning. Using RMS value hence, the time-series is normalized while the information is kept intact.

After that, signal preprocessing continued by using a 3rd-order Butterworth lowpass filter with cut-off frequency at 300 Hz and a wavelet-based denoising technique which reduces effectively high frequency noise [51]. Finally, EGMs were segmented to 1 s intervals. Segmentation of signals in short-time intervals is a choice that will be later discussed.

CGCD was computed for each time-series at the segmented 1 s intervals and then the final CGCD value was obtained by the median index of all the intervals. Parameter selection of CGCD was made so that the comparative analysis of fractionation of each EGM is optimal. First, the time when mutual information dropped to its first minimum was calculated. Analysis indicated that for our dataset, this value was for $\tau = 8$ ms. N_{ref} was firstly set equal to 1/3 of signal length, that is, in our case, 334 points. After multiple trials choosing the 334 embedded vectors randomly from the set of the reconstructed vectors, we concluded to the use of the first 334 vectors of each segment, as this choice provided similar results to the random choice case and a highly improved execution time. Distance r_{cg} was computed for each signal equal to half of its standard deviation, normalized by its peak-to-peak amplitude [44]. Finally, CGCD was computed for different embedded dimensions from $m = 1, 2, \ldots, 20$ and the dimension providing the most discriminative power and avoiding infinite CGCD values was selected. As an illustration of the process, Figure 2 shows the reconstructed signals of different AF Types for various parameters. Selection of embedded dimension m is a procedure that needs extreme

care and its choice will be further discussed in Section 4. In this study, dimension $m = 4$ was the optimal choice.
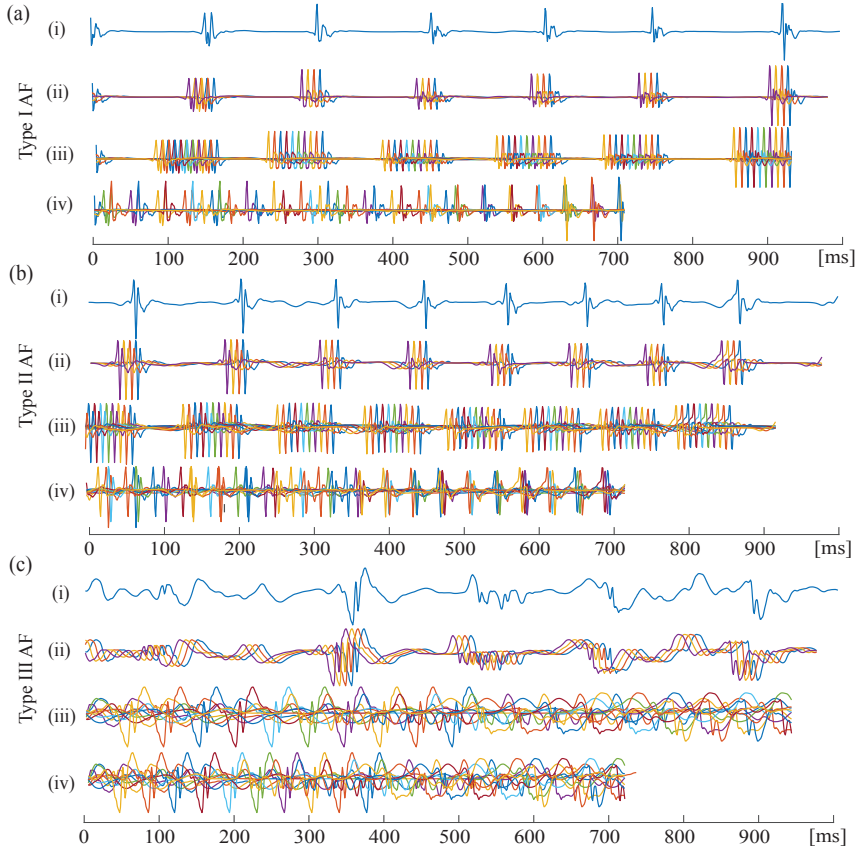
Figure 2. Example of one second segment of (**i**) original and (**ii–iv**) reconstructed AF electrograms via CGCD. (**ii**) Reconstructed signal with time lag $\tau = 8$ ms, embedded dimension $m = 4$. (**iii**) Reconstructed signal with time lag $\tau = 8$ ms, embedded dimension $m = 10$. (**iv**) Reconstructed signal with time lag $\tau = 35$ ms, embedded dimension $m = 10$. (**a**) AF Type I, (**b**) AF Type II, and (**c**) AF Type III. Length p of reconstructed signal decreases as τ and m increase, as can be seen from Equation (1).

With the aim to specify the optimal parameters, the method was tested using different number of reference points N_{ref}. However, these trials did not improve the classification accuracy, while they increased significantly the execution time. The number of reference points was therefore kept to $N_{ref} = 334$.

2.5. Surrogate Data Analysis

Before applying nonlinear techniques for data analysis, one should look for any indicators of nonlinearity in the dataset. This can be achieved by the method of the surrogate data, where for each time series, a specific number of surrogate signals is created so that they share given linear properties with the original one. Then, one or more nonlinear indices are computed for both the original and the reconstructed series and the statistical differences between them are investigated. Nonlinearity

is present in the original dataset if the index differs significantly from the index of the surrogates in most of the time series [52]. Surrogate data analysis is hardly used for the rejection of the existence of chaotic behavior in the time series. On the contrary, the presence of nonlinearity revealed by the surrogate analysis is a strong indicator of chaotic behavior [53].

For each signal, 40 surrogates were created using the iterative amplitude adjusted Fourier transform (iaaFT) [54], corresponding to 95% confidence level. The iaaFT is an alternative of the amplitude adjusted Fourier transform (AAFT) technique [52] with corrected deviations in spectrum and distribution [54] in line with the original data. First of all, the amplitude of the original time series is rescaled in order to have a Gaussian distribution. Afterwards the phases of the reconstructed signals are randomized in a way that conserves the normality of the distribution on average and then the reconstructed signals are rescaled to fit with the amplitude distribution of the original signal. The iaaFT method finishes with the iterative correction described earlier in this paragraph. The produced surrogate signals have the same amplitude distribution and power spectrum with the original signal. The CGCD of the original signals was compared with the CGCD values of the surrogates using a rank-order test. In case of statistically different CGCD values, the null hypothesis of linearity is rejected and the original data are considered nonlinear.

2.6. Statistical Analysis

For Groups 1 and 2, CGCD values were used to classify EGMs by AF type. Firstly, one-vs-all receiver operating characteristics (ROC) analysis was used to assess the discrimination by CGCD. Afterwards, a decision tree was used in order to evaluate statistically the discriminative power of CGCD. For this purpose, Matlab® Classification Learner (MathWorks, Natick, MA, USA) performed a coarse-tree analysis with a maximum split of 2, using 10-fold cross-validation. Normality and homoscedasticity of the median values for the three AF Types were tested with Shapiro–Wilk [55] and Levene tests [56], respectively. According to the results of the above tests, statistical differences between the median values of the three AF Types of each group were verified with the Kruskal–Wallis test [57], whereas statistical differences between the median values in pairs of AF Types were also tested, using a Mann–Whitney U test [58] with Bonferroni correction.

For Group 3 of pseudo-real EGMs, an algorithm assigning the EGMs under analysis to one of the AF Types (I, II, III, and IV) was developed. The algorithm was firstly performing CGCD analysis as described in Section 2.4. Then, using the thresholds obtained by the decision tree analysis on Group 2, CGCD value was assessed at each 1-s segment. If an EGM was classified as Type III by at least one of its segments, segment-by-segment classification by AF type started over on this specific EGM. If at least one of its segments is classified as Type I or II, the EGM is finally assigned to AF Type IV. Figure 3 shows the steps followed for the Group 3 analysis. Evaluation on this group was based on the percentage of pseudo-real EGMs correctly classified as Type IV.
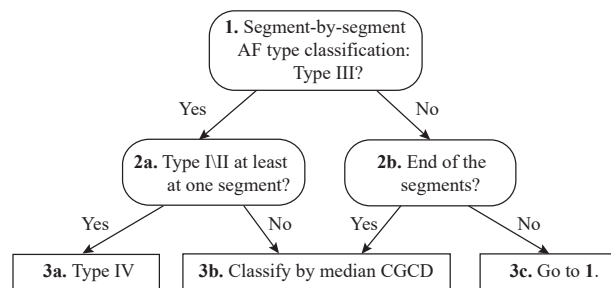
Figure 3. Illustration of algorithm steps and decisions taken for AF Type IV detection on the pseudo-real recordings of Group 3 in the database.

3. Results

3.1. Surrogate Data Analysis

CGCD values of most of the time series differed significantly from their surrogates. Thus, the application of nonlinear techniques is justified from the presence of nonlinear dynamics, confirmed by the surrogate data analysis. Figure 4 shows the CGCD values for all the AF Types for original and surrogate data, where the index values of the surrogate data are higher than the index values of the original ones.
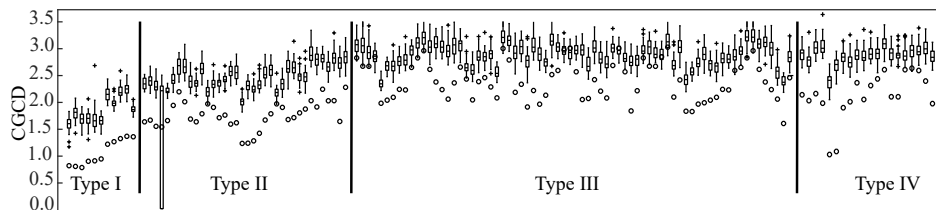
Figure 4. Surrogate data analysis indicating coarse-grained CorDim (CGCD) values for the entire database. Values of original data are presented with a small circle, whereas surrogate values are depicted as boxplots, generated from the 40 surrogates corresponding to each time series.

3.2. Statistical Analysis

The box plots and ROC curves from the three defined Groups can be seen in Figures 5 and 6, respectively. CGCD showed a very strong discriminative power for the 24 most representative EGMs in Group 1, where all EGMs were classified by AF type in consistency with the visual classification. The area under the ROC curve (AUC) and the Youden index in this group were 1, when the discriminative power of CGCD as a fractionation index between AF Type I and AF Types II and III was tested. The same values were obtained when efficient discrimination between AF Type III and AF Types I and II was tested. Applying ROC curve for discrimination of AF Type II from AF Types I and III was of no meaning, as AF Type II takes values that lie in between AF Types I and III.
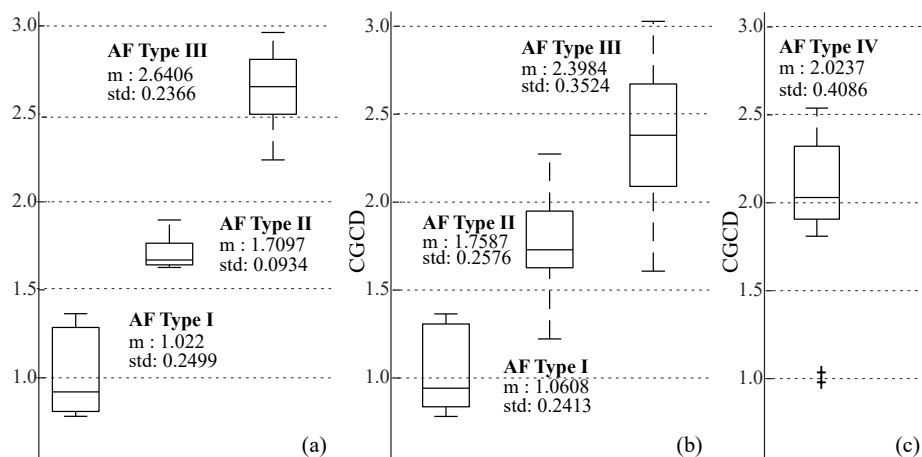
Figure 5. Box plots illustrating the distribution CGCD values as a function of the AF Types, where (**a**) is for the most representative EGMs in Group 1, (**b**) for the whole database in Group 2, and (**c**) for Type IV pseudo-real EGMs in Group 3.
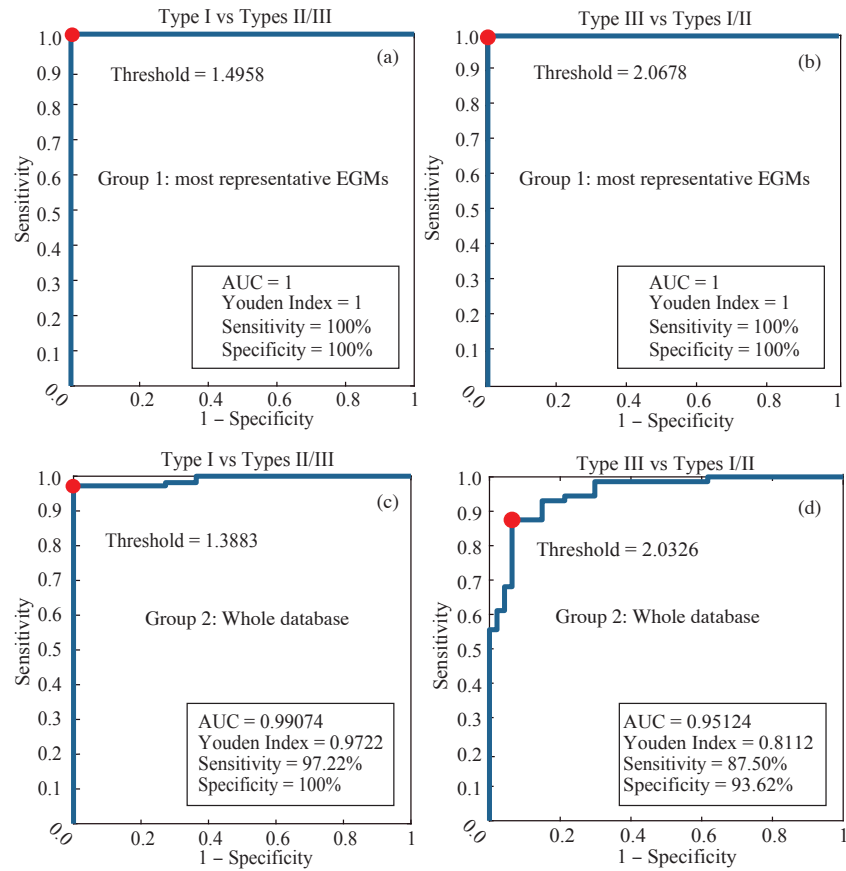
Figure 6. Receiver operating characteristics (ROC) curve analysis of discrimination between AF Types
by using CGCD as a fractionation index. (**a**,**b**) Curves for the 24 most representative EGMs in Group 1
and (**c**,**d**) curves for the whole dataset analyzed in Group 2. AUC: area under the ROC curve.

For the whole database in Group 2, Figure 5b shows that AF Type II takes some values that may
overlap with values of AF Types I and III, as expected. Still, mean values are well discriminated at
each AF type. Figure 6c,d show a quite high discriminative power, although the AUC was a little bit
lower than Group 1. AF Type I in this group was well discriminated from the other two AF Types,
while AF Type III was slightly less well defined, due to the ambiguity of this AF type in some cases.
Yet, the AUC was 0.95 and the Youden Index 0.81, which are still quite high.

Finally, as Group 3 contains AF Type IV EGMs, their mean values are mainly in between AF Types
II and III, as Figure 5c shows. This suggests that in a CGCD analysis without 1 s segmentation, these
EGMs would be classified either as AF Type II or as AF Type III. In the end, AF Types I, II and III of
Groups 1 and 2 can be well discriminated according to their box plots shown in Figure 5, whereas AF
Type IV CGCD values coincide with the corresponding AF Types II and III.

Statistical differences between AF Types for Groups 1 and 2 as well as between pairs of AF Types,
are shown in Table 1. Median CGCD values were statistically different for the AF Types of both groups,
both when they were tested separately and in pairs.

Table 1. Statistical differences between the median CGCD values to discriminate between the three AF Types as well as for pairs of AF Types of Groups 1 and 2.

AF Types	Group 1	Group 2
AF Types I-II-III	$p = 0.00004$	$p < 0.000010$
AF Types I vs. II/III	$p = 0.00010$	$p < 0.000010$
AF Types III vs. I/II	$p = 0.00010$	$p < 0.000010$

In Group 2, 104 (87.39%) EGMs were correctly classified by their AF type, according to the ROC analysis thresholds. Of the 15 wrongly classified EGMs, six belonged to AF Type II (83.33% classified correctly) and nine belonged to AF Type III (87.5% classified correctly). Regarding Group 3, 20 out of 20 pseudo-real EGMs (100%) were correctly classified by AF Type IV, according to the segment-by-segment analysis presented in Figure 3.

Classification tree analysis using 10-fold cross-validation showed 100% accuracy for Group 1 and 84.0–85.70% accuracy for Group 2, with 17 EGMs wrongly classified by their AF Type. These results are summarized on Table 2 and Figure 7. Mean CGCD values and standard deviation of AF Types of these two groups can be seen on Table 3, while the classification trees are shown on Figure 8. Note that wrongly classified EGMs of Group 2 were the most controversial regarding to their AF type classification. Still, in that case, CGCD was in consistency with their fractionation level.
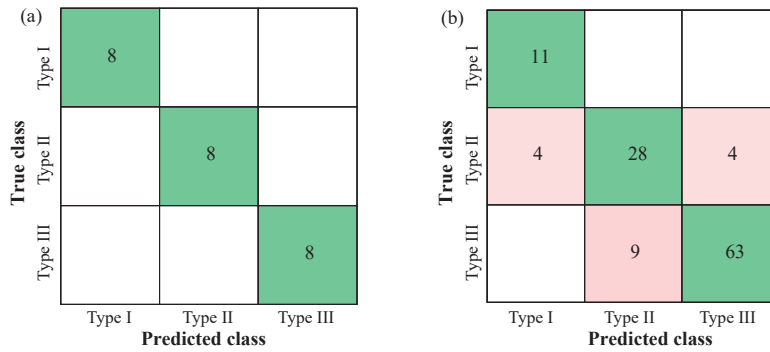
Figure 7. Confusion matrices for the most representative EGMs in Group 1 (**a**) and the whole database in Group 2 (**b**). All EGMs in Group 1 were correctly classified by their AF type, whereas 17 EGMs of Group 2 were wrongly classified.
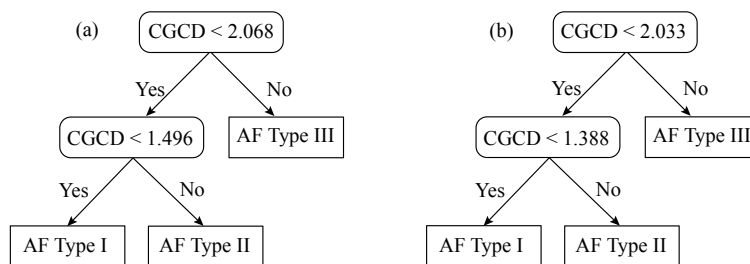
Figure 8. Decision tree together with thresholds obtained to classify EGMs by their AF Type through the application of CGCD. Scheme for the most representative EGMs in Group 1 (**a**) and for the whole database in Group 2 (**b**).

Table 2. Classification accuracy by coarse decision tree for Groups 1 and 2 and the corresponding thresholds for the discrimination by different AF Types. T_1, T_2, and T_3 are the thresholds for discriminating AF Types I, II, and III, respectively.

Group	Nr of EGMs	Accuracy	Wrongly Classified	Threshold
1	24	100%	0	$T_1 :< 1.4958$ $T_2 :\geq 1.4958, < 2.0680$ $T_3 :\geq 2.0677$
2	119	84.00–85.70%	17	$T_1 :< 1.3880$ $T_2 :\geq 1.3880, < 2.0326$ $T_3 :\geq 2.0326$

Table 3. Mean and standard deviation of CGCD values of Groups 1 and 2 for AF Types I, II, and III. Results are presented as mean $\pm$ standard deviation.

AF Type	Group 1	Group 2
Type I	1.0220 ± 0.2499	1.0608 ± 0.2413
Type II	1.7097 ± 0.0934	1.7587 ± 0.2576
Type III	2.6406 ± 0.2366	2.3884 ± 0.3524

Finally, the scatterplots of Groups 1, 2, and combined Groups 2 and 3 can be seen on Figure 9. Values of the three AF Types are clearly distinguished in Group 1 by CGCD. Furthermore, although in Group 2 there are some misplaced AF Types II and III values, there is a clear pattern discriminating among the three AF Types as well. As expected, median CGCD values of AF Type IV in Figure 9c do not occupy a specific area, but span through the AF Types I–III values.
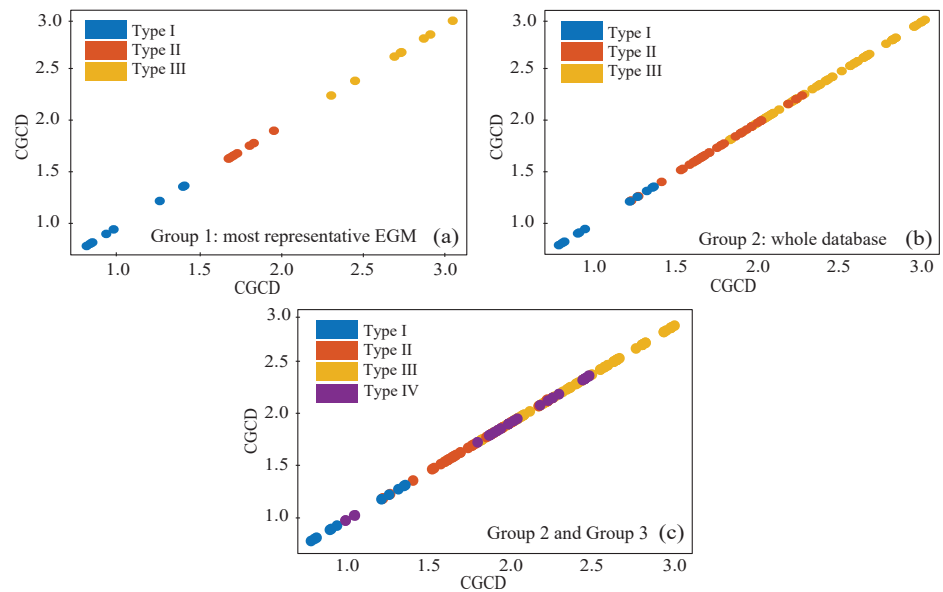
Figure 9. Scatterplots of CGCD values for the three AF Types in the most representative EGMs of Group 1 (**a**), in the whole database of Group 2 (**b**), and in Group 2 combined with the pseudo-real Type VI EGMs of Group 3 (**c**).

4. Discussion

This study showed that CGCD can estimate reliably the different fractionation levels that are present in AF EGMs. The idea of a metric that can faithfully quantify AF fractionation, and therefore organization of AF dynamics has been investigated in the past [59,60]. However, there is still need for a robust fractionation index that can operate optimally in short execution time and independently of parameters setting, so that it can be efficiently used for mapping the atrial substrate in AF.

One of the first works addressing a method to discriminate between different AF Types applied cluster and spectral analysis to 6 s duration EGMs and defined the best set of four parameters, presenting statistically significant differences between the main three AF Types [61]. The study recruited, nevertheless, a low proportion of AF Type III EGMs. As AF Type III is the most complex case of EGM fractionation and could indicate candidate ablation targets, this class should be emphasized in these kind of studies. Similarly, a newer study applied a set of various parameters, including time and spectral domain and morphological analysis in 4 s length signals [62]. Although it presented notably high classification accuracy with an optimal subset of seven parameters, the proportion of AF Type III EGMs was 35% of the overall dataset. As discrimination gets more complicated as the signal fractionation increases, a higher number of AF Type III EGMs would be necessary to verify the excellence of the classification accuracy presented in the aforementioned study.

In the same context, Kirchner et al. [63] applied principal component analysis (PCA) and cluster analysis for the discrimination between regular and irregular AF types of 90 s duration EGMs. With regular types being AF Type I EGMs and irregular types being AF Types II and III EGMs, the classification accuracy as high as 93% presented in this study misses the most significant and complicated part, the discrimination between AF Types II and III EGMs. Additionally, although these studies report results of high interest, no information on how the presented methods could be implemented on mapping devices is provided. With the shortest signal duration being 4 seconds, real-time mapping of AF using these methods is difficult to be accomplished.

Another work attempting to estimate the degree of AF fractionation involved atrial EGMs of 1.5 s duration that were recorded before the CA procedure [59]. The algorithm was based on the wavelet transform and the second differentiation of segments with continuous electrical activity, to find inflection points and compute the fractionation index (FI). Correlation between manual classification and the FI on highly fractionated EGMs yielded 81.8% sensitivity and 90.2% specificity, being these values poorer than the 87.5% sensitivity and 93.62% specificity that the present work achieved for the whole dataset of highly fractionated EGMs of Type III AF.

Haley et al. [60] developed an automated algorithm for the quantification of the percentage of AF fractionation in both paroxysmal and persistent AF EGMs of 4 s duration. The assessment of the algorithm was based on the correlation between the experts' and the algorithm's estimation of fractionation and achieved 77% sensitivity and 80% specificity. However, this study included paroxysmal AF patients (66.6% of the study population), which tend to have less complex AF EGMs and thus, automatic classification becomes significantly easier.

Nonlinear methods have been used by different studies for the assessment of AF organization, in terms of mean entropy [64] and correlation entropy [40], CorDim [43], and CGCD [40,44]. CorDim was found to discriminate between different levels of atrial organization in an AF-induced biophysical model [43]. CGCD in right atrial EGMs of persistent AF patients was analyzed before and after CA, and a relationship between the AF organization expressed as CGCD before the CA and the termination of AF after the CA was revealed [44].

The most interesting previous work to our study was performed by Hoekstra et al. [40], which applied CGCD analysis on right atrial unipolar EGMS of four seconds. They found that CGCD was able to distinguish among different AF Types. In spite of the fact that a promising application of CGCD to AF EGMs was revealed, this work contained only unipolar EGMs, which are quite unusual in daily electrophysiological procedures of AF ablation. In addition, the risk of significant ventricular contamination under unipolar recordings is high [65], and despite the QRS subtraction that was

performed, four seconds is not an adequate interval for an effective ventricular removal [40,66]. As ventricular deflections can be even larger than atrial in unipolar EGMs, the corresponding CGCD values may very likely appear altered.

Bearing in mind all the aforementioned considerations, this is the first complete study to involve atrial bipolar EGMs and to perform analysis on 1 s segments with CGCD, establishing the optimal parameters that can be chosen for the highest performance. Being able to operate in small time segments is a very important parameter, as analysis intervals affect both the functionality and the performance of the algorithm, when it has to be applied in real-time. For this purpose, analysis on segments of 1.5 s and 0.5 s duration has also been applied. Classification accuracy was 76.5% using coarse-tree analysis and 10-fold cross-validation for the case of 1.5 s segmentation and 80.7% for the 0.5 s segmentation case. AF Type III was discriminated from the other two AF types using a one-vs-all ROC analysis with Sensitivity and Specificity of 86.11% and 89.30%, respectively, in the 1.5 s segmentation analysis, whereas Sensitivity and Specificity values for the equivalent 0.5 s case were 91.67% and 85.11%, respectively. Sensitivity and Specificity for the discrimination of AF Type I from the other two types were 96.3% and 100% respectively in both cases. As the aforementioned values did not overpass the analysis using 1 s window length, the latter segment was chosen for the analysis presented in this study. Moreover, in fractionation analysis, the stability of the recording catheter is an important issue [59] and analyzing in 1 s segments eliminates this barrier, facilitating the recording and shortening the whole procedure duration.

Selection of computational parameters is another issue that should be taken into consideration when the CGCD is estimated. So far, none of the previous works have agreed to the parameters being used, whereas time-series of different size were analyzed. Using 1 s fixed segments removes this ambiguity, as the parameters with the highest discriminative power can be chosen and incorporated as global computational parameters. To this respect, the short-time analysis introduced in the present work allows the method to catch sudden changes in AF fractionation. As it has been shown in Section 3, AF Type IV can be easily detected by second-to-second analysis. Furthermore, when the median CGCD value over segments longer than 1 s of AF Type IV EGMs is used, there is no discrimination of AF Type IV from the other three AF Types and it can be misclassified either as AF Type II or AF Type III. This means that in other methods involving larger analysis times, AF Type IV would be very likely ignored.

Apart from the aforesaid advantages of opting for 1 s analysis, this decision may involve the hazard of obtaining infinite CGCD values, in case that computational parameters are not carefully chosen. More detailed explanations about how CorDim and CGCD can be used in small data segments is included in the Appendix A. After multiple trials with different parameters, this work found the optimal computational parameters for the 1 s analysis to be $m = 4$ for the embedded dimension, $\tau = 8$ ms for the time lag, and $N_{ref} = 334$ for the reference points. Even with a relatively low embedded dimension, the algorithm could discern different fractionation levels, expressing a trustworthy comparison between them. It is necessary, however, to adjust the threshold values of different AF levels and to be able to understand what do these thresholds mean. This study found a threshold of 1.388 to discriminate between AF Type I and AF Type II and a threshold of 2.033 for the discrimination of AF Types II and III, for the case where the whole dataset is used. This does not mean that dynamics in AF Type III are 2-dimensional. Thresholds are only used in order to distinguish the degree of fractionation and are strongly linked to computational parameters, which in turn are a trade-off between optimal performance and functionality.

5. Limitations

The uneven choice of data size among the three AF Types may arise some oppositions to the robustness of this work. For this reason, it is necessary to explain the motivations of this choice. As mentioned in Section 2.1, AF type I is characterized by organized signals, with a clear, almost isoelectric line in between the atrial activations. Given the carefully chosen computational parameters, reconstruction of AF type I signals is not complex and the corresponding CGCD values are located in a

well-defined region. In fact, AF Type I EGMs could be missed from the analysis without any change at all in the CGCD performance, since all EGMs of this category were correctly classified using 10-fold cross-validation. It was therefore decided to keep the proportion of AF Type I EGMs at almost 10% with respect to the whole dataset. Regarding the AF type II EGMs, as they almost span both AF Type I and AF Type III, involving a relatively low but significant percentage of 30% of the overall data size would add up the fidelity of the fractionation index, without distracting from the real challenge, which is to discriminate in high-fractionation environments.

Pre-selection of the most indicative EGMs (Group 1) as the first step of the analysis may be also criticized. Creation of this group allowed us to observe the performance in a completely controlled environment and ensure that the algorithm works in perfect consistency with the fractionation degree of the AF EGMs selected and annotated by expert physicians. In the next step, analysis included the whole dataset, which contains highly ambiguous EGMs and it was still operating optimally. In addition, thresholds for the AF Type IV EGMs detection were extracted from the whole dataset analysis (Group 2), as it is a more representative ensemble.

This work reported previous studies applying CGCD techniques in AF EGMs, providing a brief description of their aim. However, the dataset and CGCD methodology used in this work are different from these studies and therefore, a straightforward comparison between the presented study and these ones is not possible.

6. Conclusions

The present work has introduced, for the first time, the validity of CGCD as a reliable index to automatically estimate fractionation of bipolar AF EGMs. The use of epochs of 1 s length has facilitated the optimal setting of the CGCD computational parameters. The method has provided a higher classification ability than previous works dealing with the same challenging problem. Furthermore, calculation over 1 s segments provides short-time information and can agilely detect sudden changes in fractionation level of AF EGMs, leading to AF Type IV identification. Finally, given its short-time operation capabilities, this methodology could be used for mapping the atrial substrate, thus assisting ablation procedures under real-time settings for atrial substrate modification.

Appendix A. Phase-Space Reconstruction and Correlation Dimension Using Small Data Size

Let $X = (x_1, x_2, \ldots, x_N)$ be a time-series of length N, as described in Section 2.2. Its signal reconstruction in the m-th phase-space will contain $N - (m - 1) \cdot \tau$ vectors. The i-th vector of the signal can be seen in Equation (1). In this study, N was equal to 1000 sample points, dimension m was equal to 4, and τ to 8 sample points. As sampling frequency was 1 kHz, each sample equals to 1 ms. Therefore, the first vector element in the signal will have coordinates $\mathbf{Y}_1^4 = (x_1, x_9, x_{17}, x_{25})$ [67]. The reconstructed signal, will then look like the (ii) case of Figure 2.

As length of the reconstructed signal gets shorter in higher embedded dimensions and time lags, selection of these parameters should be done in consistency with the data size. This is a major problem for the most studies, as data of different sizes require different parameter values. The choice should be a trade off between preserving as many sample points and therefore as much information as possible and choosing a dimension into which dynamics of the attractor can be unfold.

The problem when using a small data size is that the range of embedded dimensions that can be used is limited and, as a result, the CorDim of the attractor can be significantly underestimated, as there is no sufficient space to span. A trustworthy calculation for the CorDim is that it lies well below $2 \cdot log_{10} N$. As a result, for a data size of $N = 1000$ samples, a CorDim of 6 is the maximum that can be safely calculated [68]. It is, however, impossible to know a priori the dimension of the dynamics of the attractor, and consequently impossible to know if the length of the given time-series will be sufficient. Although a small embedded dimension may suppress the dynamics so that they look smaller than they really are, the signal reconstruction is still not free of the effect of the attractor [69]. This means that when the signal is reconstructed, even when using small parameters, the dynamics are preserved yet not fully expressed. This can be easily visualized from the resemblance of the reconstructed signal to the original one, even in the complicated AF Type III cases, as seen in Figure 2 case (*ii*) [67].

Of course this is a problem when we want to measure the CorDim, as there is a high risk of mistaken estimations. As described in Section 2.2, the estimation of this parameter is done by looking for linear regions in the plot of $ln(C^{(m)}(r))$ as a function of $ln(r)$ for different values of m. The value of each one of that curves at a distance r results from the average of the N_{ref*} points, which are the vectors from N_{ref} (where $N_{ref*} \leq N_{ref}$) for which $\Theta = 1$ for that specific r. In other words, only a specific number (N_{ref*}) of the N_{ref} vectors that are closer to each other than a distance r will participate in the plot. When the dimension of the dynamics is bigger than the embedded dimension, the number of points will scale for different values of r. When the embedded dimension is big enough and the dynamics are completely expressed, the number of points does not vary significantly and the curve becomes smoother. This is where the CorDim is computed at. As data size becomes smaller, N_{ref} and N_{ref*} become smaller as well. This leads to shorter scaling regions and the CorDim is wrongly computed to a smaller value [69].

This problem can be overcome with the use of CGCD, instead of CorDim. When CGCD is calculated, values obtained do not represent the real dimension of the underlying dynamics. Instead, it serves as a comparative measure between dynamics of different classes. This way, the dependence on the data size is completely avoided. On the contrary, the use of small datasets is even preferred in nonstationary dynamical systems, as they can follow the changing dynamics of the time-series [69]. It is therefore highly recommended the use of analysis segments as short as 1 s to catch short-life patterns and emancipate from the problem of varying computational parameters.

References

1. Kirchhof, P.; Benussi, S.; Kotecha, D.; Ahlsson, A.; Atar, D.; Casadei, B.; Castella, M.; Diener, H.G.; Heidbuchel, H.; Hendriks, J.; et al. 2016 ESC Guidelines for the management of atrial fibrillation developed in collaboration with EACTS. The Task Force for the management of atrial fibrillation of the European Society of Cardiology (ESC). Developed with the special contribution of the European Heart Rhythm Association (EHRA) of the ESC. *Eur. J. Cardio-Thorac. Surg.* **2016**, *18*, 1609–1678.
2. Go, A.S.; Hylek, E.M.; Phillips, K.A.; Chang, Y.C.; Henault, L.E.; Selby, J.V.; Singer, D.E. Prevalence of diagnosed atrial fibrillation in adults: National implications for rhythm management and stroke prevention: The anticoagulation and risk factors in atrial fibrillation (ATRIA) study. *JAMA* **2001**, *285*, 2370–2375. [CrossRef] [PubMed]
3. Camm, A.J.; Kirchhof, P.; Lip, G.Y.H.; Schotten, U.; Savelieva, I.; Ernst, S.; Gelder, I.C.V.; Al-Attar, N.; Hindricks, G.; Prendergast, B.; et al. Guidelines for the management of atrial fibrillation: The Task Force for the Management of Atrial Fibrillation of the European Society of Cardiology (ESC). *Eur. Heart J.* **2010**, *31*, 2369–2429. [CrossRef] [PubMed]
4. Goette, A.; Honeycutt, C.; Langberg, J.J. Electrical remodeling in atrial fibrillation: Time course and mechanisms. *Circulation* **1996**, *94*, 2968–2974. [CrossRef] [PubMed]
5. Chugh, S.S.; Roth, G.A.; Gillum, R.F.; Mensah, G.A. Global burden of atrial fibrillation in developed and developing nations. *Glob. Heart* **2014**, *9*, 113–119. [CrossRef] [PubMed]

6. Cappato, R.; Calkins, H.; Chen, S.A.; Davies, W.; Iesaka, Y.; Kalman, J.; Kim, Y.H.; Klein, G.; Natale, A.; Packer, D.; et al. Updated worldwide survey on the methods, efficacy, and safety of catheter ablation for human atrial fibrillation. *Circ. Arrhythmia Electrophysiol.* **2010**, *3*, 32–38. [CrossRef] [PubMed]

7. Cox, J.L.; Canavan, T.E.; Schuessler, R.B.; Cain, M.E.; Lindsay, B.D.; Stone, C.; Smith, P.K.; Corr, P.B.; Boineau, J.P. The surgical treatment of atrial fibrillation. II. Intraoperative electrophysiologic mapping and description of the electrophysiologic basis of atrial flutter and atrial fibrillation. *J. Thorac. Cardiovasc. Surg.* **1991**, *101*, 406–426. [CrossRef]

8. Haïssaguerre, M.; Jaïs, P.; Shah, D.C.; Takahashi, A.; Hocini, M.; Quiniou, G.; Garrigue, S.; Le Mouroux, A.; Le Métayer, P.; Clémenty, J. Spontaneous Initiation of Atrial Fibrillation by Ectopic Beats Originating in the Pulmonary Veins. *N. Engl. J. Med.* **1998**, *339*, 659–666. [CrossRef]

9. Brooks, A.G.; Stiles, M.K.; Laborderie, J.; Lau, D.H.; Kuklik, P.; Shipp, N.J.; Hsu, L.F.; Sanders, P. Outcomes of long-standing persistent atrial fibrillation ablation: A systematic review. *Heart Rhythm* **2010**, *7*, 835–846. [CrossRef]

10. Kornej, J.; Schumacher, K.; Zeynalova, S.; Sommer, P.; Arya, A.; Weiß, M.; Piorkowski, C.; Husser, D.; Bollmann, A.; Lip, G.Y.H.; et al. Time-dependent prediction of arrhythmia recurrences during long-term follow-up in patients undergoing catheter ablation of atrial fibrillation: The Leipzig Heart Center AF Ablation Registry. *Sci. Rep.* **2019**, *9*, 1–7. [CrossRef]

11. Yoshida, K.; Ulfarsson, M.; Tada, H.; Chugh, A.; Good, E.; Kuhne, M.; Crawford, T.; Sarrazin, J.F.; Chalfoun, N.; Wells, D.; et al. Complex electrograms within the coronary sinus: Time- and frequency-domain characteristics, effects of antral pulmonary vein isolation, and relationship to clinical outcome in patients with paroxysmal and persistent atrial fibrillation. *J. Cardiovasc. Electrophysiol.* **2008**, *19*, 1017–1023. [CrossRef] [PubMed]

12. Lau, D.H.; Schotten, U.; Mahajan, R.; Antic, N.A.; Hatem, S.N.; Pathak, R.K.; Hendriks, J.M.L.; Kalman, J.M.; Sanders, P. Novel mechanisms in the pathogenesis of atrial fibrillation: practical applications. *Eur. Heart J.* **2016**, *37*, 1573–1581. [CrossRef] [PubMed]

13. Lau, D.H.; Linz, D.; Schotten, U.; Mahajan, R.; Sanders, P.; Kalman, J.M. Pathophysiology of Paroxysmal and Persistent Atrial Fibrillation: Rotors, Foci and Fibrosis. *Heart Lung Circ.* **2017**, *26*, 887–893. [CrossRef] [PubMed]

14. Schotten, U.; Dobrev, D.; Platonov, P.G.; Kottkamp, H.; Hindricks, G. Current controversies in determining the main mechanisms of atrial fibrillation. *J. Intern. Med.* **2016**, *279*, 428–438. [CrossRef]

15. Narayan, S.M.; Krummen, D.E.; Rappel, W.J. Clinical mapping approach to diagnose electrical rotors and focal impulse sources for human atrial fibrillation. *J. Cardiovasc. Electrophysiol.* **2012**, *23*, 447–454. [CrossRef]

16. Allessie, M.A.; De Groot, N.M.S.; Houben, R.P.M.; Schotten, U.; Boersma, E.; Smeets, J.L.; Crijns, H.J. Electropathological substrate of long-standing persistent atrial fibrillation in patients with structural heart disease longitudinal dissociation. *Circ. Arrhythmia Electrophysiol.* **2010**, *3*, 606–615. [CrossRef]

17. Verma, A.; Wazni, O.M.; Marrouche, N.F.; Martin, D.O.; Kilicaslan, F.; Minor, S.; Schweikert, R.A.; Saliba, W.; Cummings, J.; Burkhardt, J.D.; et al. Pre-existent left atrial scarring in patients undergoing pulmonary vein antrum isolation: An independent predictor of procedural failure. *J. Am. Coll. Cardiol.* **2005**, *45*, 285–292. [CrossRef]

18. Konings, K.T.; Kirchhof, C.J.; Smeets, J.R.; Wellens, H.J.; Penn, O.C.; Allessie, M.A. High-density mapping of electrically induced atrial fibrillation in humans. *Circulation* **1994**, *89*, 1665–1680. [CrossRef]

19. Eckstein, J.; Zeemering, S.; Linz, D.; Maesen, B.; Verheule, S.; Van Hunnik, A.; Crijns, H.; Allessie, M.A.; Schotten, U. Transmural conduction is the predominant mechanism of breakthrough during atrial fibrillation: Evidence from simultaneous endo-epicardial high-density activation mapping. *Circ. Arrhythmia Electrophysiol.* **2013**, *6*, 334–341. [CrossRef]

20. Verheule, S.; Tuyls, E.; Gharaviri, A.; Hulsmans, S.; Van Hunnik, A.; Kuiper, M.; Serroyen, J.; Zeemering, S.; Kuijpers, N.H.L.; Schotten, U. Loss of continuity in the thin epicardial layer because of endomysial fibrosis increases the complexity of atrial fibrillatory conduction. *Circ. Arrhythmia Electrophysiol.* **2013**, *6*, 202–211. [CrossRef]

21. Chang, S.L.; Tai, C.T.; Lin, Y.J.; Wongcharoen, W.; Lo, L.W.; Tuan, T.C.; Udyavar, A.R.; Chang, S.H.; Tsao, H.M.; Hsieh, M.H.; et al. Biatrial substrate properties in patients with atrial fibrillation. *J. Cardiovasc. Electrophysiol.* **2007**, *18*, 1134–1139. [CrossRef] [PubMed]

22. Rolf, S.; Kircher, S.; Arya, A.; Eitel, C.; Sommer, P.; Sergio, R.; Gaspar, T.; Bollmann, A.; Altmann, D.; Piedra, C.; et al. Tailored atrial substrate modification based on low-voltage areas in catheter ablation of atrial fibrillation. *Circ. Arrhythmia Electrophysiol.* **2014**, *7*, 825–833. [CrossRef] [PubMed]

23. Jadidi, A.S.; Lehrmann, H.; Keyl, C.; Sorrel, J.; Markstein, V.; Minners, J.; Park, C.I.; Denis, A.; Jaïs, P.; Hocini, M.; et al. Ablation of Persistent Atrial Fibrillation Targeting Low-Voltage Areas with Selective Activation Characteristics. *Circ. Arrhythmia Electrophysiol.* **2016**, *9*, e002962. [CrossRef] [PubMed]

24. Yamaguchi, T.; Tsuchiya, T.; Fukui, A.; Kawano, Y.; Otsubo, T.; Takahashi, Y.; Hirota, K.; Murotani, K.; Eshima, K.; Takahashi, N. Impact of the extent of low-voltage zone on outcomes after voltage-based catheter ablation for persistent atrial fibrillation. *J. Cardiol.* **2018**, *72*, 427–433. [CrossRef] [PubMed]

25. Mansour, M.; Mandapati, R.; Berenfeld, O.; Chen, J.; Samie, F.H.; Jalife, J. Left-to-right gradient of atrial frequencies during acute atrial fibrillation in the isolated sheep heart. *Circulation* **2001**, *103*, 2631–2636. [CrossRef]

26. Mandapati, R.; Skanes, A.; Chen, J.; Berenfeld, O.; Jalife, J. Stable microreentrant sources as a mechanism of atrial fibrillation in the isolated sheep heart. *Circulation* **2000**, *101*, 194–199. [CrossRef]

27. Takahashi, Y.; O'Neill, M.D.; Hocini, M.; Dubois, R.; Matsuo, S.; Knecht, S.; Mahapatra, S.; Lim, K.T.; Jaïs, P.; Jonsson, A.; et al. Characterization of Electrograms Associated With Termination of Chronic Atrial Fibrillation by Catheter Ablation. *J. Am. Coll. Cardiol.* **2008**, *51*, 1003–1010. [CrossRef]

28. Atienza, F.; Almendral, J.; Jalife, J.; Zlochiver, S.; Ploutz-Snyder, R.; Torrecilla, E.G.; Arenal, Á.; Kalifa, J.; Fernández-Avilés, F.; Berenfeld, O. Real-time dominant frequency mapping and ablation of dominant frequency sites in atrial fibrillation with left-to-right frequency gradients predicts long-term maintenance of sinus rhythm. *Heart Rhythm* **2009**, *6*, 33–40. [CrossRef]

29. Sunsaneewitayakul, B.; Schwab, M.; Khunnawat, C.; Vasavakul, T.; McKenzie, J.; Ngarmukos, T.; Kosar, E.; Nademanee, K. A new approach for catheter ablation of atrial fibrillation: mapping of the electrophysiologic substrate. *J. Am. Coll. Cardiol.* **2004**, *43*, 2044–2053. [CrossRef]

30. Lee, G.; Roberts-Thomson, K.; Madry, A.; Spence, S.; Teh, A.; Heck, P.M.; Kumar, S.; Kistler, P.M.; Morton, J.B.; Sanders, P.; et al. Relationship among complex signals, short cycle length activity, and dominant frequency in patients with long-lasting persistent AF: A high-density epicardial mapping study in humans. *Heart Rhythm* **2011**, *8*, 1714–1719. [CrossRef]

31. Ciaccio, E.; Biviano, A.; Whang, W.; Coromilas, J.; Garan, H. A new transform for the analysis of complex fractionated atrial electrograms. *Biomed. Eng. Online* **2011**, *10*. [CrossRef] [PubMed]

32. Ciaccio, E.J.; Biviano, A.B.; Garan, H. Computational method for high resolution spectral analysis of fractionated atrial electrograms. *Comput. Biol. Med.* **2013**, *43*, 1573–1582. [CrossRef] [PubMed]

33. Tsai, W.C.; Lin, Y.J.; Tsao, H.M.; Chang, S.L.; Lo, L.W.; Hu, Y.F.; Chang, C.J.; Tang, W.H.; Tuan, T.C.; Udyavar, A.R.; et al. The optimal automatic algorithm for the mapping of complex fractionated atrial electrograms in patients with atrial fibrillation. *J. Cardiovasc. Electrophysiol.* **2010**, *21*, 21–26. [CrossRef] [PubMed]

34. Teh, A.W.; Kistler, P.M.; Lee, G.; Medi, C.; Heck, P.M.; Spence, S.J.; Sparks, P.B.; Morton, J.B.; Sanders, P.; Kalman, J.M. The relationship between complex fractionated electrograms and atrial low-voltage zones during atrial fibrillation and paced rhythm. *Europace* **2011**, *13*, 1709–1716. [CrossRef] [PubMed]

35. Lin, Y.J.; Lo, M.T.; Chang, S.L.; Lo, L.W.; Hu, Y.F.; Chao, T.F.; Chung, F.P.; Liao, J.N.; Lin, C.Y.; Kuo, H.Y.; et al. Benefits of Atrial Substrate Modification Guided by Electrogram Similarity and Phase Mapping Techniques to Eliminate Rotors and Focal Sources Versus Conventional Defragmentation in Persistent Atrial Fibrillation. *JACC Clin. Electrophysiol.* **2016**, *2*, 667–678. [CrossRef] [PubMed]

36. Verma, A.; Jiang, C.y.; Betts, T.R.; Chen, J.; Deisenhofer, I.; Mantovan, R.; Macle, L.; Morillo, C.a.; Haverkamp, W.; Weerasooriya, R.; et al. Approaches to Catheter Ablation for Persistent Atrial Fibrillation (STAR AF II). *N. Engl. J. Med.* **2015**, *372*, 1812–1822. [CrossRef] [PubMed]

37. Ammar-Busch, S.; Reents, T.; Knecht, S.; Rostock, T.; Arentz, T.; Duytschaever, M.; Neumann, T.; Cauchemez, B.; Albenque, J.P.; Hessling, G.; et al. Correlation between atrial fibrillation driver locations and complex fractionated atrial electrograms in patients with persistent atrial fibrillation. *Pacing Clin. Electrophysiol.* **2018**, *41*, 1279–1285. [CrossRef] [PubMed]

38. Almeida, T.P.; Chu, G.S.; Salinet, J.L.; Vanheusden, F.J.; Li, X.; Tuan, J.H.; Stafford, P.J.; Ng, G.A.; Schlindwein, F.S. Minimizing discordances in automated classification of fractionated electrograms in human persistent atrial fibrillation. *Med. Biol. Eng. Comput.* **2016**, *54*, 1695–1706. [CrossRef]

39. De Bakker, J.M.T.; Wittkampf, F.H.M. The Pathophysiologic Basis of Fractionated and Complex Electrograms and the Impact of Recording Techniques on Their Detection and Interpretation. *Circ. Arrhythmia Electrophysiol.* **2010**, *3*, 204–213. [CrossRef]

40. Hoekstra, B.P.; Diks, C.G.; Allessie, M.A.; De Goedb, J. Nonlinear Analysis of Epicardial Atrial Electrograms of Electrically Induced Atrial Fibrillation in Man. *J. Cardiovasc. Electrophysiol.* **1995**, *6*, 419–440. [CrossRef]

41. Censi, F.; Barbaro, V.; Bartolini, P.; Calcagnini, G.; Michelucci, A.; Cerutti, S. Non-linear coupling of atrial activation processes during atrial fibrillation in humans. *Biol. Cybern.* **2001**, *85*, 195–201. [CrossRef] [PubMed]

42. Alcaraz, R.; Rieta, J.J. Review: Application of non-linear methods in the study of atrial fibrillation organization. *Med. Biol. Eng. Comput.* **2013**, *33*, 239–252. [CrossRef]

43. Luca, A.; Vesin, J.M. Correlation Dimension as a Measure of the Atrial Fibrillation Capture during Atrial Septal Pacing. *Comput. Cardiol.* **2014**, *41*, 545–548.

44. Luca, A.; Buttu, A.; Pruvot, E.; Pascale, P.; Bisch, L.; Vesin, J.M. Nonlinear analysis of right atrial electrograms predicts termination of persistent atrial fibrillation within the left atrium by catheter ablation. *Physiol. Meas.* **2016**, *37*, 347–359. [CrossRef]

45. Wells, J.L.; Karp, R.B.; Kouchoukos, N.T.; Maclean, W.A.; James, T.N.; Waldo, A.L. Characterization of Atrial Fibrillation in Man: Studies Following Open Heart Surgery. *Pacing Clin. Electrophysiol.* **1978**, *60*, 426–438. [CrossRef]

46. Grassberger, P.; Procaccia, I. Measuring the strangeness of strange attractors. *Physica D* **1983**, *9*, 189–208. [CrossRef]

47. Takens, F. Detecting strange attractors in turbulence. In *Dynamical Systems and Turbulence*; Springer: Berlin, Germany, 1981; pp. 366–381. [CrossRef]

48. Corana, A.; Casaleggio, A.; Rolando, C.; Ridella, S. Efficient computation of the correlation dimension from a time series on a LIW computer. *Parallel Comput.* **1991**, *17*, 809–820. [CrossRef]

49. Fraser, A.M.; Swinney, H.L. Independent coordinates for strange attractors from mutual information. *Phys. Rev. A* **1986**, *33*, 1134–1140. [CrossRef]

50. Theiler, J. Statistical precision of dimension estimators. *Phys. Rev. A* **1990**, *41*, 3038–3051. [CrossRef]

51. Martínez-Iniesta, M.; Ródenas, J.; Alcaraz, R.; Rieta, J.J. Waveform Integrity in Atrial Fibrillation: The Forgotten Issue of Cardiac Electrophysiology. *Ann. Biomed. Eng.* **2017**, *45*, 1890–1907. [CrossRef]

52. Theiler, J.; Eubank, S.; Longtin, A.; Galdrikian, B.; Doyne Farmer, J. Testing for nonlinearity in time series: The method of surrogate data. *Physica D* **1992**, *58*, 77–94. [CrossRef]

53. Nakamura, T.; Small, M.; Hirata, Y. Testing for nonlinearity in irregular fluctuations with long-term trends. *Phys. Rev. E* **2006**, *74*, 026205-1–026205-8. [CrossRef] [PubMed]

54. Schreiber, T.; Schmitz, A. Surrogate time series. *Physica D* **2000,** *142*, 346–382. [CrossRef]

55. Shapiro, S.S.; Wilk, M.B. An analysis of variance test for normality (complete samples). *Biometrika* **1965**, *52*, 591–611. [CrossRef]

56. Mandelbrot, B. Contributions to Probability and Statistics: Essays in Honor of Harold Hotelling (Ingram Olkin, Sudhist G. Ghurye, Wassily Hoeffding, William G. Madow, and Henry B. Mann, eds.). *SIAM Rev.* **1961**, *3*, 80. [CrossRef]

57. Kruskal, W.H.; Wallis, W.A. Use of Ranks in One-Criterion Variance Analysis. *J. Am. Stat. Assoc.* **1952**, *47*, 583–621. [CrossRef]

58. Mann, H.B.; Whitney, D.R. On a Test of Whether one of Two Random Variables is Stochastically Larger than the Other. *Ann. Math. Stat.* **1947**, *18*, 50–60. [CrossRef]

59. Křemen, V.; Lhotská, L.; MacAš, M.; Čihák, R.; Vančura, V.; Kautzner, J.; Wichterle, D. A new approach to automated assessment of fractionation of endocardial electrograms during atrial fibrillation. *Physiol. Meas.* **2008**, *29*, 1371–1381. [CrossRef]

60. Haley, C.L.; Gula, L.J.; Miranda, R.; Michael, K.A.; Baranchuk, A.M.; Simpson, C.S.; Abdollah, H.; West, A.J.; Akl, S.G.; Redfearn, D.P. Validation of a novel algorithm for quantification of the percentage of signal fractionation in atrial fibrillation. *Europace* **2013**, *15*, 447–452. [CrossRef]

61. Barbaro, V.; Bartolini, P.; Calcagnini, G.; Martelli, F.; Morelli, S. A comparison of methods for the classification of atrial fibrillation from intra-atrial electrograms. In Proceedings of the 20th Annual International Conference of the IEEE Engineering in Medicine and Biology Society, Hong Kong, China, 29 October–1 November 1998; pp. 94–97. [CrossRef]

62. Nollo, G.; Marconcini, M.; Faes, L.; Bovolo, F.; Ravelli, F.; Bruzzone, L. An automatic system for the analysis and classification of human atrial fibrillation patterns from intracardiac electrograms. *IEEE Trans. Biomed. Eng.* **2008**, *55*, 2275–2285. [CrossRef]

63. Kirchner, M.; Faes, L.; Olivetti, E.; Riccardi, R.; Scaglione, M.; Gaita, F.; Antolini, R. Local electrical characterisation of human atrial fibrillation. *Comput. Cardiol.* **2000**, *27*, 499–502. [CrossRef]

64. Cirugeda-Roldán, E.; Novak, D.; Kremen, V.; Cuesta-Frau, D.; Keller, M.; Luik, A.; Srutova, M. Characterization of complex fractionated atrial electrograms by sample entropy: An international multi-center study. *Entropy* **2015**, *17*, 7493–7509. [CrossRef]

65. Corino, V.D.A.; Rivolta, M.W.; Sassi, R.; Lombardi, F.; Mainardi, L.T. Ventricular activity cancellation in electrograms during atrial fibrillation with constraints on residuals' power. *Med. Eng. Phys.* **2013**, *35*, 1770–1777. [CrossRef] [PubMed]

66. Rieta, J.J.; Hornero, F.; Alcaraz, R.; Moratal, D. Ventricular artifacts cancellation from atrial epicardial recordings in atrial tachyarrhythmias. In Proceedings of the 29th Annual International Conference of the IEEE Engineering in Medicine and Biology Society, Lyon, France, 23–26 August 2007. [CrossRef]

67. Huffaker, R.G. Phase Space Reconstruction from Time Series Data: Where History Meets Theory. In Proceedings of the 2010 International European Forum, Innsbruck-Igls, Austria, 8–12 February 2010.

68. Williams, G. *Chaos Theory Tamed*, 1st ed.; CRC Press: Boca Raton, FL, USA, 1997. [CrossRef]

69. Havstad, J.W.; Ehlers, C.L. Attractor dimension of nonstationary dynamical systems from small data sets. *Phy. Rev. A* **1989**, *39*, 845–853. [CrossRef] [PubMed]

Article

Splitting the P-wave: Improved Evaluation of Left Atrial Substrate Modification after Pulmonary Vein Isolation of Paroxysmal Atrial Fibrillation

Aikaterini Vraka[1] , Vicente Bertomeu-González[2] , Fernando Hornero[3] ,
Aurelio Quesada[4] , Raúl Alcaraz[5] and José J. Rieta[1,*]

[1] BioMIT.org, Electronic Engineering Department, Universitat Politecnica de Valencia, 46022 Valencia, Spain;{aivra, jjrieta}@upv.es
[2] Clinical Medicine Department, Miguel Hernández University, 03202 Elche, Spain; vbertomeu@umh.es
[3] Cardiovascular Surgery Department, Hospital Clínico Universitario de Valencia, 46010 Valencia, Spain; hornero_fer@gva.es
[4] Arrhythmia Unit, Cardiology Department, General University Hospital Consortium of Valencia, 46014 Valencia, Spain; quesada_aur@gva.es
[5] Research Group in Electronic, Biomedical and Telecommunication Engineering, University of Castilla-La Mancha, 16071 Cuenca, Spain; raul.alcaraz@uclm.es
* Correspondence: jjrieta@upv.es

Abstract: Atrial substrate modification after pulmonary vein isolation (PVI) of paroxysmal atrial fibrillation (pAF) can be assessed non-invasively by analyzing P-wave duration in the electrocardiogram (ECG). However, whether right (RA) and left atrium (LA) contribute equally to this phenomenon remains unknown. The present study splits fundamental P-wave features to investigate the different RA and LA contributions to P-wave duration. Recordings of 29 pAF patients undergoing first-ever PVI were acquired before and after PVI. P-wave features were calculated: P-wave duration (PWD), duration of the first ($PWD_{on\text{-}peak}$) and second ($PWD_{peak\text{-}off}$) P-wave halves, estimating RA and LA conduction, respectively. P-wave onset (PW_{on}-R) or offset (PW_{off}-R) to R-peak interval, measuring combined atrial/atrioventricular and single atrioventricular conduction, respectively. Heart-rate fluctuation was corrected by scaling. Pre- and post-PVI results were compared with Mann–Whitney U-test. PWD was correlated with the remaining features. Only PWD (non-scaling: $\Delta = -9.84\%$, p = 0.0085, scaling: $\Delta = -17.96\%$, p = 0.0442) and $PWD_{peak\text{-}off}$ (non-scaling: $\Delta = -22.03\%$, p = 0.0250, scaling: $\Delta = -27.77\%$, p = 0.0268) were decreased. Correlation of all features with PWD was significant before/after PVI ($p < 0.0001$), showing the highest value between PWD and PW_{on}-R ($\varrho_{max} = 0.855$). PWD correlated more with $PWD_{on\text{-}peak}$ ($\varrho = 0.540$–0.805) than $PWD_{peak\text{-}off}$ ($\varrho = 0.419$–0.710). PWD shortening after PVI of pAF stems mainly from the second half of the P-wave. Therefore, noninvasive estimation of LA conduction time is critical for the study of atrial substrate modification after PVI and should be addressed by splitting the P-wave in order to achieve improved estimations.

Keywords: atrial fibrillation; pulmonary vein isolation; atrial substrate modification; P-wave; left atrium

1. Introduction

With a fast-growing incidence and prevalence around the world, atrial fibrillation (AF) is currently the most common cardiac arrhythmia [1]. It is additionally connected with a plenty of other comorbidities, which can augment the hospitalization duration and frequency and affect significantly the patients' quality of life [1]. AF is considered a supraventricular tachyarrhythmia, with desynchronized atrial electrical activations triggered principally in the pulmonary veins (PVs) and being propagated all over the atria. As a consequence, AF is characterized in the electrocardiogram (ECG) by the absence of

discrete P-waves which are replaced by low-amplitude and irregular fibrillatory waves, causing a faster and irregular heart rate [1,2].

As AF initiation is mainly attributed to the pulmonary veins (PVs), PV isolation (PVI) is considered the star AF treatment [1,3]. Paroxysmal AF patients, suffering from short AF episodes that cardiovert spontaneously in less than 7 days, benefit especially from PVI, probably because arrhythmogenic activity is often limited to PVs [1,4]. Nevertheless, persistent AF patients, showing longer AF episodes that may significantly affect the atrial structure and function, may not respond positively to the PVI procedure in the long term, requiring repeated PVI sessions in some cases [1,4,5]. Apart from PVs, various right (RA) and left atrial (LA) sites additionally contribute to the AF perpetuation due to fibrosis, forming the so-called atrial substrate [6–11]. Frequent non-PV triggers are crista terminalis, interatrial septum, LA posterior wall, LA appendage, coronary sinus and ligament of Marshall. These triggers can be detected by studying the activation patterns with the help of multipolar mapping and recording catheters placed in coronary sinus and PVs [6]. When non-PV triggers are detected, focal ablation of the sites provoking the AF activation in combination with PVI is suggested in order to obtain improved results [6].

While PVI and focal ablation can eliminate AF triggers, AF propagation can be further sustained due to changes in the atrial substrate, known as atrial remodeling [1,12]. Remodeling can take place at the structural, functional or electrical level, either showing different mechanisms that contribute to the AF perpetuation. Atrial fibrosis is the common denominator of these changes [12,13]. In this respect, additional ablation based on specific electrogram characteristics that possibly indicate the fibrotic tissue is performed sometimes [14] with the assistance of automatic AF fractionation estimators [15] or by the localization of low-voltage areas, which indicate the presence of atrial scar [16,17]. Notwithstanding, extensive ablation can have adverse effects in individuals and should be sparse and in any case performed with caution [18]. Hence, meticulous atrial mapping is a necessary step during each ablation procedure whether or not non-PV ablation takes place. With that being said, the AF confrontation is not limited to PVI but requires a detailed and in depth analysis of the substrate modification provoked by PVI, in order to plan efficiently the personalized follow-up strategy and reduce the possibility of AF recurrence [19].

PVI procedure is performed by electrically isolating the PVs, in order to impede the transmission of ectopic and chaotic electrical activities towards the atria. The effect of PVI in the atrial anatomy is mainly observed in the LA, where recovery of normative atrial function, known as reverse remodeling, takes place, indicating a favorable PVI outcome [1,3,12,20,21]. Timely detection of any changes implying the presence or absence of reverse remodeling is critical in decision-making regarding the next step after PVI, as additional ablation or other strategies should be adopted in order to avoid early AF recurrence, an ominous marker of a non-successful procedure [1].

Changes in the atrial substrate can be assessed noninvasively by the analysis of the P-waves, which are the atrial component of the surface ECG. In fact, a vast amount of studies focus on analyzing the P-wave duration, which describes the atrial conduction time throughout the atria [20]. Long or very short P-waves and long P-R interval are connected with conduction slowing due to fibrosis or shortening of atrial refractoriness and are predictors of AF recurrence [12,22–30]. Therefore, the hypothesis that P-wave shortening indicates a less heterogeneous tissue and a favorable PVI outcome has been supported by many studies [20,26,27,31,32]. P-wave duration is also useful in predicting the AF onset, with higher variability and longer P-waves alerting the possibility of a forthcoming AF episode [33]. A significant advantage of the P-waves analysis is that it allows atrial substrate modification assessment as early as the moment after the end of the PVI session, in contrast with other techniques that require some blanking period [21].

Despite the usefulness of P-wave analysis in atrial substrate alteration assessment, there is still room for improvement. Difference in thresholds defining a prolonged P-wave can induce confusion and significantly affect the decision for the follow-up treatment to be adopted [22,23,29,34]. While agreement of a universal threshold would be the optimal

solution, differences in study population as well as P-wave delineation sensitivity complicate significantly this task. With the P-wave analysis gaining more and more popularity, attention to detail may enhance the noninvasive evaluation of substrate modification after PVI. P-wave consists of two parts. The first part, from the onset to the peak of the P-wave, corresponds to the depolarization of the RA. Activation is propagated from the RA to the LA through Bachmann bundle or the area proximal to coronary sinus, thus yielding the second part of the P-wave [35,36].

Although remodeling can be present in both atria [10], it is LA which is principally affected from substrate modification after PVI. Notwithstanding, studies so far analyze the P-wave duration from the onset to the offset of the P-waves, thus including both atria indivisibly. By contrast, splitting the P-wave and studying its second half involves focusing on the atrium with the highest impact on the atrial substrate alteration, the LA. This would lead to a more precise noninvasive estimation of the atrial substrate modification after PVI and a deeper understanding of the AF mechanisms, facts that could contribute to the decision-making, leading to the planning of a more efficient follow-up strategy.

The aim of the present study is to demonstrate the relevance of the second P-wave half analysis in investigating the atrial substrate modification provoked by PVI in order to improve the personalized therapy. For this purpose, the alterations of the P-wave temporal characteristics after PVI are assessed, with a special focus on the separate analysis of RA and LA modification, as manifested by the first and second halves of the P-wave, respectively.

2. Materials and Methods

2.1. Materials

A database of 29 paroxysmal AF patients undergoing circumferential radiofrequency (RF) PVI was employed. Patients had not undergone any PVI procedure in the past and 5-min continuous standard 12-lead ECG recordings at a sampling frequency of 1 kHz were acquired before and after PVI for each patient by a Labsystem™ PRO EP recording system (Boston Scientific, Marlborough, MA, USA). Patients were in sinus rhythm (SR) during the procedure. Recordings before PVI were acquired 7–23 min before the initiation of the PVI procedure (mean time of the initiation of the pre-PVI recording: 12.3 ± 3.6 min before PVI). Recordings after PVI were acquired 1–12 min after PVI (mean time of the initiation of the post-PVI recording: 3.9 ± 5.1 min after confirmation of successful PVI). Isolation was guided by electroanatomical mapping and performed with an ablation catheter encircling the left and right PVs, emitting RF energy to achieve complete electric insulation. The PVI endpoint was AF non-inducibility, confirmed by continuous pacing after the isolation of each PV. In order to facilitate the analysis, lead II was chosen and extracted for processing, since this channel provides P-waves of high amplitude and monophasic positive morphology [37].

2.2. Signal Preprocessing

Preprocessing and analysis were performed with MATLAB© R2019b version. Signal was denoised by a wavelet-based denoising method to remove the powerline interference, followed by a bidirectional low-pass filtering with cut-off frequency at 70 Hz for the muscle noise removal and the removal of baseline wander with a high-pass filter with cut-off frequency at 0.8 Hz [38,39]. Ectopic beats were detected and cancelled in order to be replaced by linearly interpolated beats [40,41]. Although not all recordings contained ectopic beats, in case of presence, they did not exceed the 4% of total beats. Finally, for each recording, P-waves were detected and R-peaks and P-wave fiducial points were defined [42,43], as can be observed in Figure 1a. In normal P-waves, peak (b) was defined as the maximum point of the signal between (a) and (c) of Figure 1a. In case of notched P-waves, the peak was defined as the middle point between the two local peaks.
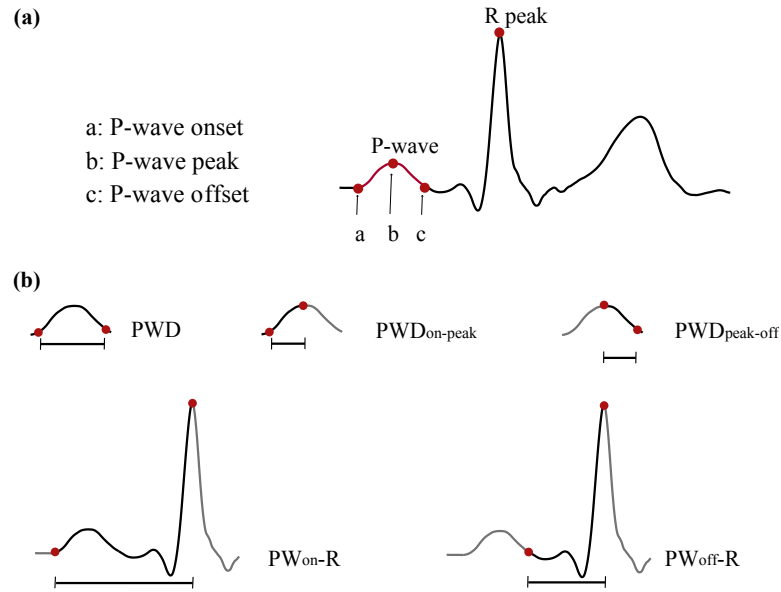
Figure 1. (**a**) Fiducial points of P-waves and R peaks. (**b**) Calculated temporal characteristics.

2.3. P-wave Temporal Characteristics

After the detection of fiducial points for each P-wave, the following P-wave temporal characteristics were defined (see Figure 1b):

- P-wave duration (*PWD*): distance from the P-wave onset to the P-wave offset. Measures the atrial depolarization duration from the beginning of the RA until the end of the LA activation.
- $PWD_{on\text{-}peak}$: distance from the P-wave onset to the P-wave peak. Measures the RA depolarization duration.
- $PWD_{peak\text{-}off}$: distance from the P-wave peak to the P-wave offset. Measures the LA depolarization duration.
- $PW_{on}\text{-}R$: distance from the P-wave onset to the R peak. Measures the atrial depolarization and the atrioventricular conduction durations.
- $PW_{off}\text{-}R$: distance from the P-wave offset to the R peak. Measures the atrioventricular conduction duration independently from the atrial depolarization.

As all of the abovementioned features are affected by heart rate (HR) fluctuations, a correction factor (*CF*) is recommended to compensate for the bias inserted [44]. In this study, the *CF* is based on a 60 bpm HR, which corresponds to an interbeat interval (*IBI*) of 1000 ms (one beat per second). Hence, the *CF* is calculated for the *i*-th P-wave falling within the *i*-th *IBI* as

$$CF_i = \frac{1000}{IBI_i}. \tag{1}$$

Figure 2 shows an example of how P-waves belonging to *IBI*s longer or shorter than 1000 ms are scaled according to *CF*. It can be observed that *CF* scales linearly the employed features with respect to HR. Given the direct exposure of atrial tissue to RF energy, it was assumed that atrial components of the ECG are directly affected from the RF applications, as RF energy has a significant effect on HR [45]. Features scaled with the *CF* will be represented in the remaining manuscript as $\mathbf{A}(x)$, where *x* is the name of the various features described previously.
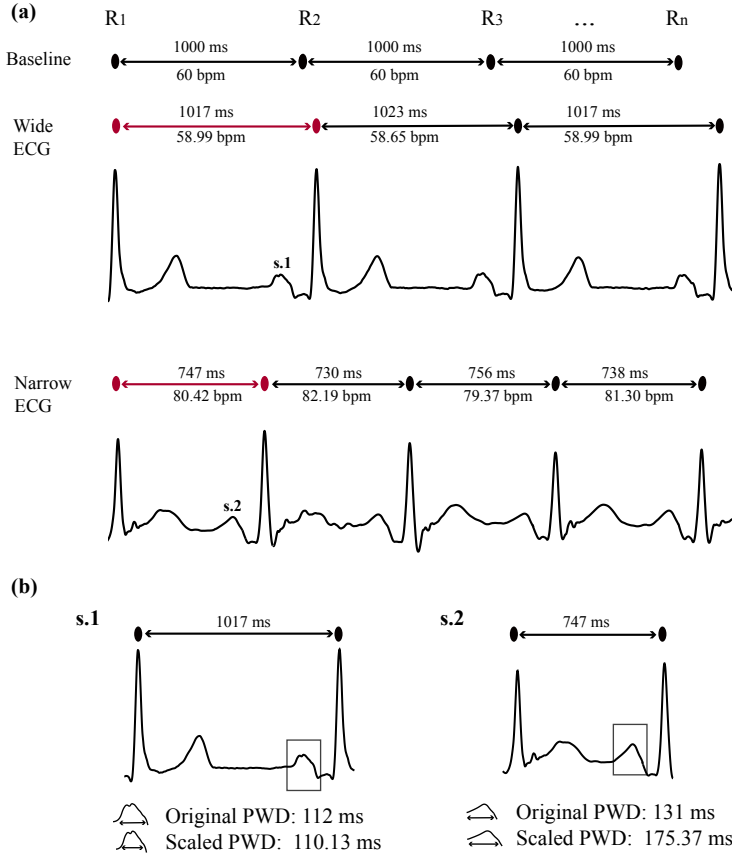
Figure 2. Example of P-wave scaling for interbeat intervals longer or shorter than 1000 ms. (**a**) Baseline interbeat interval at 1000 ms and interbeat intervals of a wide and a narrow ECG. Red intervals show the beats chosen to be analyzed as an example in (**b**). (**b**) *PWD* scaling for P-waves of a wide (s.1) and a narrow (s.2) signal. Wide signal: P-wave is shrunk after scaling. Narrow signal: P-wave is lengthened after scaling. The remaining features are scaled accordingly.

2.4. Correlation between PWD and the Remaining Temporal Characteristics

Being *PWD* one of the most employed features in studies evaluating the atrial substrate alteration, it is used as the baseline of the present study. Correlations between *PWD* and the remaining features were calculated. For each recording before and after *PVI*, correlations were computed for every single beat with Pearson's correlation coefficient (PCC) and then averaged across the entire signal. Moreover, correlation of the variation (CoV) caused in features by *PVI* was calculated between *PWD* and the rest of the characteristics. CoV between *PWD* and each of the remaining features was calculated by PCC at a recording basis, performing a single calculation for each patient. Given feature x, variation due to *PVI* was calculated as follows

$$\Delta(x) = \frac{x_{after\ PVI}}{x_{before\ PVI}} - 1. \tag{2}$$

2.5. Statistical Analysis

Data normality and homoscedasticity were tested with Saphiro–Wilk and Levene tests, respectively [46,47]. Results indicated the employment of a Mann–Whitney U-test to compare values before and after PVI. Additionally, median values and variation due to PVI in form of percentage have been calculated by multiplying Equation (2) by 100%.

3. Results

Statistical results can be seen in Table 1, where median values and interquartile ranges before and after PVI as well as the variation due to PVI can be observed. These results are further illustrated in Figure 3, where the box and whisker plots of each feature before and after PVI are presented.

PWD decreased significantly due to PVI ($\Delta = -9.84\%$, $p = 0.0085$). The same tendency was observed when PWD was scaled by the CF, where the statistical power was weaker, albeit still significant ($\Delta = -17.96\%$, $p = 0.0442$). Distance from P-wave peak to P-wave offset was also statistically reduced after the PVI procedure and to a higher degree than PWD ($\Delta = -22.03\%$, $p = 0.0250$). Unlike PWD, the statistical power of $PWD_{peak\text{-}off}$ was not affected by scaling while the decreasing tendency remained ($\Delta = -27.77\%$, $p = 0.0268$). $PWD_{on\text{-}peak}$ did not shorten significantly regardless of the application of CF (up to -8.96%, $p > 0.3651$). None of the P-R features showed statistically significant variations ($p > 0.05$) either.

Table 1. Statistical analysis for P-wave features before and after PVI. Median values, interquartile range (IQR) and variation due to PVI. Features with statistically significant differences due to PVI are shown in **bold**.

Feature	p	Median Values (IQR)		Δ [%]
		Before PVI	After PVI	
PWD	**0.0085**	**122.00 (12.00)**	**110.00 (11.00)**	**−9.84**
$PWD_{on\text{-}peak}$	0.5289	67.00 (14.00)	61.00 (11.00)	−8.96
PWD$_{\text{peak-off}}$	**0.0250**	**59.00 (8.00)**	**46.00 (7.00)**	**−22.03**
$PW_{on}\text{-}R$	0.5585	246.00 (10.00)	244.00 (11.00)	−0.81
$PW_{off}\text{-}R$	0.3519	127.00 (8.00)	140.00 (7.00)	+10.24
A(PWD)	**0.0442**	**123.63 (15.08)**	**101.42 (12.15)**	**−17.96**
A($PWD_{on\text{-}peak}$)	0.3651	64.59 (13.00)	60.19 (10.97)	−6.81
A(PW$_{\text{peak-off}}$)	**0.0268**	**59.89 (8.55)**	**43.26 (7.55)**	**−27.77**
A($PW_{on}\text{-}R$)	0.3924	264.96 (14.11)	262.19 (12.73)	−1.04
A($PW_{off}\text{-}R$)	0.6507	130.47 (9.00)	139.11 (9.62)	+6.62

Correlations investigated in recordings before and after PVI showed strong and statistically significant relationships between PWD and the first part of the P-wave ($PWD_{on\text{-}peak}$, before PVI: PCC= 0.747, $p < 0.0001$, after PVI: PCC = 0.746, $p < 0.0001$) and between PWD and the interval from the onset of the P-wave to the R-peak ($PW_{on}\text{-}R$, before PVI: PCC = 0.772, $p < 0.0001$, after PVI: PCC = 0.753, $p < 0.0001$). These relationships were further corroborated after scaling by the CF, as can be observed in Figure 4.

Correlation between PWD and $PWD_{peak\text{-}off}$ was found to be moderate (before PVI: PCC = 0.477, $p < 0.0001$, after PVI: PCC = 0.419, $p < 0.0001$), with CF slightly potentiating this effect, still to a moderate level (before PVI: PCC = 0.541, $p < 0.0001$, after PVI: PCC = 0.531, $p < 0.0001$).

A weaker correlation between PWD and all features was found regarding the effect of PVI. For P-wave components, correlation with $PWD_{on\text{-}peak}$ was slightly lower than correlation with $PWD_{peak\text{-}off}$, as can be seen from Figure 4. Nevertheless, application of CF reverted this observation, with $PWD_{on\text{-}peak}$ being again slightly more correlated with PWD than $PWD_{peak\text{-}off}$. While in pre- and post-PVI cases $PW_{on}\text{-}R$ showed notably higher correlation with PWD than the rest of the features, CoV of $PW_{on}\text{-}R$ was remarkably low and insignificant. Notwithstanding, CF application not only boosted this relationship but also led to the highest concordance between the variations observed in $PW_{on}\text{-}R$ and PWD. On the other hand, correlation with $PW_{off}\text{-}R$ was negative before normalization and positive but low after normalization, with both results not being statistically significant.
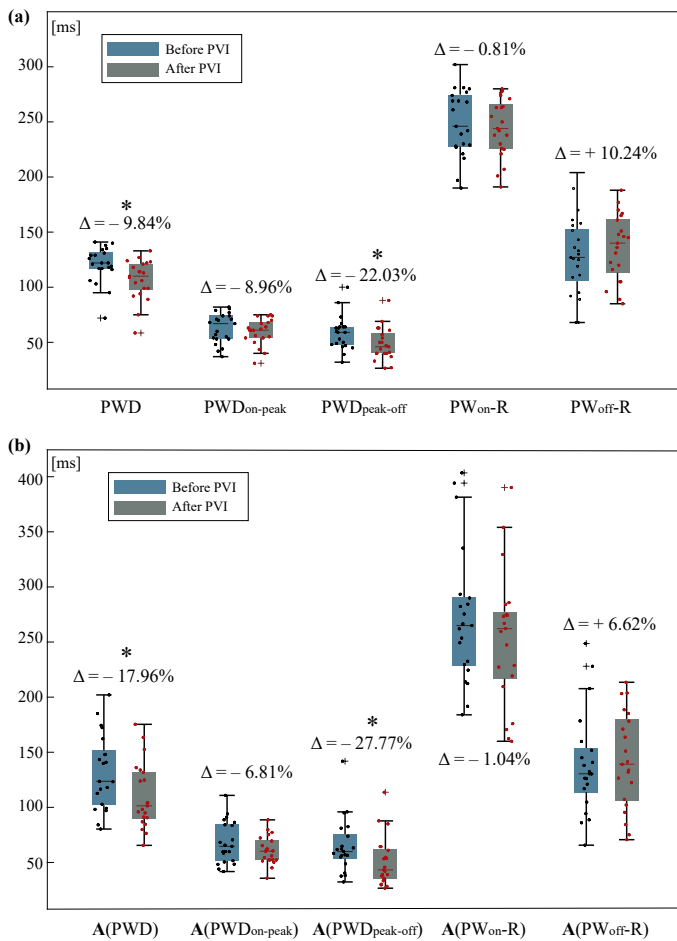
Figure 3. Boxplot with scatterplots for the analyzed features before and after PVI. (**a**) Boxplots for raw features. (**b**) Boxplots for scaled features according to the correction factor. The symbol (•) stands for normal values whereas (+) stands for outliers. Variation due to PVI (Δ) is additionally shown. Significant variations are shown in (∗).

4. Discussion

P-wave duration is a popular tool in studying various cardiac pathologies [48]. In AF, P-wave duration is an evaluator of the conduction delay provoked by fibrotic areas [23,28,29,34]. These areas might be found either in RA or LA or both atria [10]. Nevertheless, RA and LA are not equally affected by PVI, which has a major effect in LA function [21].

Despite the disproportionate effect of PVI on RA and LA, studies insist on evaluating the substrate alterations as a homogeneous phenomenon, complicating the planning of an efficient follow-up treatment for AF individuals. Several works have defined thresholds for prolonged PWD varying from 120 ms to 140 ms, a difference which is not negligent when considering a tissue to be remodelled [23,28,29,34]. Deviations in the cut-off points may stem from different pathologies or AF types present in the database. P-wave delineation may additionally affect the calculated PWD, with a small deviation either in P-wave onset or offset showing significant differences in the results.

Given that LA alteration is the major phenomenon after PVI procedures and the fact that P-wave from lead II can be split in two parts corresponding to the depolarization of each of the atria, a separate analysis of the two P-wave parts would be more meaningful when precision in calculations is an important issue. The present study attempted a

(a)   Before PVI

	$PWD_{on\text{-}peak}$	$PWD_{peak\text{-}off}$	$PW_{on\text{-}R}$	$PW_{off\text{-}R}$
PWD	0.7473	0.4773	0.7722	-0.5027

-0.4   -0.2   0.0   0.2   0.4   0.6

	$A(PWD_{on\text{-}peak})$	$A(PWD_{peak\text{-}off})$	$A(PW_{on\text{-}R})$	$A(PW_{off\text{-}R})$
A(PWD)	0.8051	0.5412	0.8328	0.0993

0.1   0.2   0.3   0.4   0.5   0.6   0.7   0.8

(b)   After PVI

	$PWD_{on\text{-}peak}$	$PWD_{peak\text{-}off}$	$PW_{on\text{-}R}$	$PW_{off\text{-}R}$
PWD	0.7458	0.4194	0.7528	-0.2578

-0.2   0.0   0.2   0.4   0.6

	$A(PWD_{on\text{-}peak})$	$A(PWD_{peak\text{-}off})$	$A(PW_{on\text{-}R})$	$A(PW_{off\text{-}R})$
A(PWD)	0.8028	0.5309	0.8553	0.2687

0.3   0.4   0.5   0.6   0.7   0.8

(c)   Correlation of the variation (CoV)

	$PWD_{on\text{-}peak}$	$PWD_{peak\text{-}off}$	$PW_{on\text{-}R}$	$PW_{off\text{-}R}$
PWD	0.5405	0.6142	0.2403	-0.4010

-0.4   -0.2   0.0   0.2   0.4   0.6

	$A(PWD_{on\text{-}peak})$	$A(PWD_{peak\text{-}off})$	$A(PW_{on\text{-}R})$	$A(PW_{off\text{-}R})$
A(PWD)	0.7681	0.7098	0.7854	0.3249

0.4   0.5   0.6   0.7

Figure 4. Correlation matrices for the relationship between *PWD* and the remaining features. Values without scaling are on the left column and with scaling on the right. (**a**) Results before PVI. (**b**) Results after PVI. (**c**) Results for the correlation of the variation. Gray cells show statistically insignificant relationships.

separate P-wave first and second part analysis in order to investigate in detail the RA and LA modifications provoked by PVI. Additionally, P-R interval was also decomposed in parts describing separate atrial and atrioventricular conduction. The findings of this novel approach are quite interesting.

Duration of the entire P-wave was significantly shortened after PVI. This observation is in line with a plethora of previous studies [23,24,28,29,31,32]. When analyzing the first and second P-wave parts separately, a significant shortening was only observed in the second part of the P-wave, describing the reduction in LA depolarization time. Not only was the duration of the second P-wave part shortened due to PVI, but also the statistical power of this alteration remained unaffected from scaling by the CF. By contrast, statistical power of the entire P-wave was moderated after scaling. Among many formulas offered in the literature, a linear model was chosen for the normalization, as linear scaling shows less correlation with HR, hence being less HR-dependent [49–51]. Nevertheless, the choice of other formulas can be adopted without altering the main findings of the analysis. At the same time, the first part of the P-wave remained almost intact regardless of the CF, implying a much lower impact of PVI on RA function. It should also be highlighted that the degree of shortening of the second part of the P-waves was the highest among all employed characteristics. This stresses the importance on focusing on the second P-wave part, which is in fact the principal source of the P-wave shortening that is reported by many studies.

The significance of the second P-wave part in clinical environment was recently appreciated in a study that investigated the correlation of P-wave parameters with inter- and intra-atrial conduction times measured via invasive analysis, finding a relatively high correlation between the second P-wave part and LA conduction times [52]. The study additionally used surface and invasive parameters to discern between AF occurrence and non-AF occurrence during electrophysiological studies of a randomly chosen set of patients. The authors found the second part of the P-wave to be a good independent predictor for AF occurrence. These results corroborate the findings of the present study, implying a direct relationship between the second P-wave part and pathophysiologic phenomena observed during AF, thus highlighting the importance of studying the P-wave separately.

Despite the fact that the second but not the first part of the P-waves got significantly shortened after PVI, it was the first part that correlated in a stronger way with the entire P-wave duration. Normal sinus rhythm heartbeat starts in sinus node, which is the first site to be depolarized and then is propagated through other right atrial sites towards the LA [35,36]. Sinus node plays a significant role in P-wave morphology. Additionally, it takes more time for the right than the left atrial depolarization, as described in Section 3. These facts may lead to a higher overall correlation between the duration of the first P-wave part and the duration of the entire P-wave. Therefore, when the alteration of the entire P-wave duration is assessed, RA depolarization may affect the result, masking the degree of modification of the LA function, which should be the primal focus point. This observation explains the lower shortening rate of the entire P-wave duration with respect to the shortening of the second half of the P-wave and the fluctuations in statistical power when CF has been applied for PWD.

P-wave duration showed the highest correlation with the P-R interval, when measured from the initiation of the RA depolarization until the R-peak. At the same time, P-R part measured from the end of the LA depolarization until the R-peak not only showed the lowest correlations but also marked insignificant results, when the PVI effect was assessed. This implies the fact that P-R interval is highly dependent on the atrial activity and does not exclusively express the atrioventricular conduction. In fact, although PW_{on}-R has shown a negligible and nonsignificant reduction after PVI, PW_{off}-R seems to have been increased. Therefore, P-R prolongation reported in previous studies may actually be caused by prolongation of the atrial depolarization time and its interpretation may be misleading. These results are in line with previous studies dealing with this issue, where additionally a correlation between short PW_{off}-R and AF incidence has been found in long PW_{on}-R, as prolongation is provoked by PWD lengthening in this case [12,25]. These findings highlight the necessity of partial analysis of the atrial and atrioventricular ECG components rather than studying the P-wave and P-R interval indivisibly.

The hypothesis that the P-R interval, thought to assess the atrioventricular conduction, is highly dependent on the atrial depolarization has led a previous work to the study of the separate atrial and atrioventricular components of the P-R interval, which coincide with the features of the present study [12]. Interestingly enough, a prolongation of the first P-wave part, corresponding to the RA depolarization, has been found to be associated with AF in a stronger way than the prolongation of the LA P-wave component. It should be highlighted, however, that substantial differences exist between the aforementioned and the present study.

In the first place, the utilized database also included patients with pathologies other than AF, while AF patients would mostly fall into the persistent AF category. Different pathologies or different AF types may also be manifested by RA conduction slowing. As mentioned afore, P-wave duration prolongation is not an exclusive paroxysmal AF phenomenon [48] and hence, connection between prolongation of the first half of the P-wave and AF incidents can be observed. Additionally, recordings were not obtained during PVI procedure. The main scope of the current study is a high-definition analysis on how PVI alters the atrial substrate, by looking deeper into the exact effect on each atrium separately. Consequently, the main finding of the present study is the shortening and significant alteration of LA and the significance of the study of $PWD_{peak-off}$ in atrial substrate modification evaluation after PVI. Finally, while P-wave duration and duration of the first P-wave part were calculated in the same way as in the present study, a different, indirect strategy was recruited to compute the second part of the P-wave. Since a straightforward calculation of the second part of the P-wave is missed, a deviation between the real and estimated LA depolarization time may exist.

In radiofrequency sessions, heart rate fluctuations are observed as an outcome of the autonomous nervous system stimulation [45]. These alterations may in turn affect the temporal P-wave and P-R features [44]. In a previous study, P-R prolongation was connected with lower heart rate [25]. Therefore, when dealing with temporal features, a scaling is

suggested in order to unmask any potential changes that are distorted by the variable heart rate. This aspect was taken into consideration in the current analysis, by adding an extra step of scaling each feature with respect to a 60 bpm heart rate. Although it did not affect significantly the statistical results of the pre-post analysis, it did play a significant role in the assessment of the correlations between *PWD* and the remaining features, potentiating each and every relationship, especially when the PVI-induced variation was examined. This way it was possible to identify the high correlation between the PVI effect on P-wave duration and on P-R interval, which would otherwise be ignored, thus showing a misleading lack of connection between the P-R interval and the atrial depolarization modification due to PVI.

The aforementioned aspects highlight the importance of reconsidering the way that the atrial substrate alterations after PVI are being evaluated in paroxysmal AF patients from surface ECG recordings. The present study has provided an in-detail perspective of how atrial depolarization time is shortened after PVI, with LA conduction time being the center of this modification. It is demonstrated that studying the second half of the P-wave can lead to a more accurate evaluation of the atrial substrate alteration, one of the most controversial and delicate issues in planning personalized AF follow-up strategies. Moreover, studying exclusively the second P-wave part facilitates the delineation process. As one of the two fiducial points that need to be specified, the P-wave peak, can be reliably and easily detected, the ambiguity regarding the partial P-wave delineation is significantly lower with respect to the entire P-wave delineation. Therefore, adopting the aforementioned strategy can facilitate the procedure and enhance the precision and robustness of the substrate alteration estimation.

5. Conclusions

The second part of P-waves is the most relevant in evaluating the atrial substrate modification from surface recordings after PVI, outperforming the entire P-wave analysis. Hence, splitting the P-wave in two parts and focusing on the second P-wave part is highly recommended. For the assessment of the atrioventricular conduction alterations, the atrial component should be subtracted. Scaling is a necessary step for studies investigating the correlation between depolarization time of various atrial and atrioventricular components and should also be considered by future studies.

References

1. Hindricks, G.; Potpara, T.; Dagres, N.; Arbelo, E.; Bax, J.J.; Blomström-Lundqvist, C.; Boriani, G.; Castella, M.; Dan, G.A.; Dilaveris, P.E.; et al. 2020 ESC Guidelines for the diagnosis and management of atrial fibrillation developed in collaboration with the European Association of Cardio-Thoracic Surgery (EACTS). *Eur. Heart J.* **2020**, *42*, 374–498. https://doi.org/10.1093/eurheartj/ehaa612.

2. Haissaguerre, M.; Jaïs, P.; Shah, D.C.; Takahashi, A.; Hocini, M.; Quiniou, G.; Garrigue, S.; Le Mouroux, A.; Le Métayer, P.; Clémenty, J. Spontaneous initiation of atrial fibrillation by ectopic beats originating in the pulmonary veins. *N. Engl. J. Med.* **1998**, *339*, 659–666. https://doi.org/10.1056/NEJM199809033391003.

3. Shah, D. Electrophysiological evaluation of pulmonary vein isolation. *Eur. Eur. Pacing Arrhythmias Card. Electrophysiol. J. Work. Groups Card. Pacing Arrhythmias Card. Cell. Electrophysiol. Eur. Soc. Cardiol.* **2009**, *11*, 1423–1433. https://doi.org/10.1093/europace/eup289.

4. Oral, H.; Knight, B.P.; Tada, H.; Özaydın, M.; Chugh, A.; Hassan, S.; Scharf, C.; Lai, S.W.; Greenstein, R.; Pelosi, F., Jr.; et al. Pulmonary vein isolation for paroxysmal and persistent atrial fibrillation. *Circulation* **2002**, *105*, 1077–1081. https://doi.org/10.1161/hc0902.104712.

5. Clarnette, J.A.; Brooks, A.G.; Mahajan, R.; Elliott, A.D.; Twomey, D.J.; Pathak, R.K.; Kumar, S.; Munawar, D.A.; Young, G.D.; Kalman, J.M.; et al. Outcomes of persistent and long-standing persistent atrial fibrillation ablation: a systematic review and meta-analysis. *EP Europace* **2018**, *20*, f366–f376. https://doi.org/10.1093/europace/eux297.

6. Santangeli, P.; Marchlinski, F.E. Techniques for the provocation, localization, and ablation of non-pulmonary vein triggers for atrial fibrillation. *Heart Rhythm* **2017**, *14*, 1087–1096. https://doi.org/10.1016/j.hrthm.2017.02.030.

7. Boles, U.; Gul, E.E.; Enriquez, A.; Starr, N.; Haseeb, S.; Abdollah, H.; Simpson, C.; Baranchuk, A.; Redfearn, D.; Michael, K.; Hopman, W.; Glover, B. Coronary Sinus Electrograms May Predict New-onset Atrial Fibrillation After Typical Atrial Flutter Radiofrequency Ablation (CSE-AF). *J. Atr. Fibrillation* **2018**, *11*, 1809. https://doi.org/10.4022/jafib.1809.

8. de Groot, N.M.; Allessie, M.A. Pathophysiology of atrial fibrillation: focal patterns of activation. *Pacing Clin. Electrophysiol.* **2019**, *42*, 1312–1319. https://doi.org/10.1111/pace.13777.

9. Jadidi, A.; Nothstein, M.; Chen, J.; Lehrmann, H.; Dössel, O.; Allgeier, J.; Trenk, D.; Neumann, F.J.; Loewe, A.; Müller-Edenborn, B.; Arentz, T. Specific Electrogram Characteristics Identify the Extra-Pulmonary Vein Arrhythmogenic Sources of Persistent Atrial Fibrillation - Characterization of the Arrhythmogenic Electrogram Patterns During Atrial Fibrillation and Sinus Rhythm. *Sci. Rep.* **2020**, *10*, 9147. https://doi.org/10.1038/s41598-020-65564-2.

10. Kharb, R.K.; Knops, P.; van der Does, L.J.; Kik, C.; Taverne, Y.J.; Roos-Serote, M.C.; Heida, A.; Oei, F.B.; Bogers, A.J.; de Groot, N.M. Simultaneous Endo-Epicardial Mapping of the Human Right Atrium: Unraveling Atrial Excitation. *J. Am. Heart Assoc.* **2020**, *9*, e017069. https://doi.org/10.1161/JAHA.120.017069.

11. Li, C.Y.; Zhang, J.R.; Hu, W.N.; Li, S.N. Atrial fibrosis underlying atrial fibrillation. *Int. J. Mol. Med.* **2021**, *47*, 1–1. https://doi.org/10.3892/ijmm.2020.4842.

12. Smith, J.W.; O'Neal, W.T.; Shoemaker, M.B.; Chen, L.Y.; Alonso, A.; Whalen, S.P.; Soliman, E.Z. PR-Interval Components and Atrial Fibrillation Risk (from the Atherosclerosis Risk in Communities Study). *Am. J. Cardiol.* **2017**, *119*, 466–472. https://doi.org/10.1016/j.amjcard.2016.10.016.

13. Nattel, S.; Burstein, B.; Dobrev, D. Atrial remodeling and atrial fibrillation: mechanisms and implications. *Circ. Arrhythmia Electrophysiol.* **2008**, *1*, 62–73. https://doi.org/https://doi.org/10.1161/CIRCEP.107.754564.

14. Verma, A.; Jiang, C.Y.; Betts, T.R.; Chen, J.; Deisenhofer, I.; Mantovan, R.; Macle, L.; Morillo, C.A.; Haverkamp, W.; Weerasooriya, R.; et al. Approaches to Catheter Ablation for Persistent Atrial Fibrillation (STAR AF II). *N. Engl. J. Med.* **2015**, *372*, 1812–1822. https://doi.org/10.1056/NEJMoa1408288.

15. Vraka, A.; Hornero, F.; Bertomeu-González, V.; Osca, J.; Alcaraz, R.; Rieta, J.J. Short-Time Estimation of Fractionation in Atrial Fibrillation with Coarse-Grained Correlation Dimension for Mapping the Atrial Substrate. *Entropy* **2020**, *22*, 232. https://doi.org/10.3390/e22020232.

16. Kircher, S.; Arya, A.; Altmann, D.; Rolf, S.; Bollmann, A.; Sommer, P.; Dagres, N.; Richter, S.; Breithardt, O.A.; Dinov, B.; et al. Individually tailored vs. standardized substrate modification during radiofrequency catheter ablation for atrial fibrillation: a randomized study. *Eur. Eur. Pacing Arrhythmias Card. Electrophysiol. J. Work. Groups Card. Pacing Arrhythmias Card. Cell. Electrophysiol. Eur. Soc. Cardiol.* **2018**, *20*, 1766–1775. https://doi.org/10.1093/europace/eux310.

17. Dhakal, B.P.; Hutchinson, M.D. Left Atrial Electroanatomical Voltage Mapping to Characterize Substrate and Guide Ablation. *Curr. Treat. Options Cardiovasc. Med.* **2020**, *22*, 1–23. https://doi.org/10.1007/s11936-020-00833-x.

18. Kumar, P.; Mounsey, J.P. Atrial Substrate Modification for Atrial Fibrillation: Striving to Get Smarter. *Circ. Arrhythmia Electrophysiol.* **2017**, *10*, e005840. https://doi.org/10.1161/CIRCEP.117.005840.

19. Xie, X.; Yang, G.; Li, X.; Yu, J.; Zhang, F.; Ju, W.; Chen, H.; Li, M.; Gu, K.; Cheng, D.; et al. Prevalence and Predictors of Additional Ablation Beyond Pulmonary Vein Isolation in Patients With Paroxysmal Atrial Fibrillation. *Front. Cardiovasc. Med.* **2021**, *8*, 690297. https://doi.org/10.3389/fcvm.2021.690297.

20. Simpson, R.J.; Foster, J.R.; Gettes, L.S. Atrial excitability and conduction in patients with interatrial conduction defects. *Am. J. Cardiol.* **1982**, *50*, 1331–1337. https://doi.org/10.1016/0002-9149(82)90471-4.

21. Maille, B.; Das, M.; Hussein, A.; Shaw, M.; Chaturvedi, V.; Williams, E.; Morgan, M.; Ronayne, C.; Snowdon, R.L.; Gupta, D. Reverse electrical and structural remodeling of the left atrium occurs early after pulmonary vein isolation for persistent atrial fibrillation. *J. Interv. Card. Electrophysiol. Int. J. Arrhythm. Pacing* **2020**, *58*, 9–19. https://doi.org/10.1007/s10840-019-00576-1.
22. Cheng, S.; Keyes, M.J.; Larson, M.G.; McCabe, E.L.; Newton-Cheh, C.; Levy, D.; Benjamin, E.J.; Vasan, R.S.; Wang, T.J. Long-term outcomes in individuals with prolonged PR interval or first-degree atrioventricular block. *JAMA* **2009**, *301*, 2571–2577. https://doi.org/10.1001/jama.2009.888.
23. Blanche, C.; Tran, N.; Rigamonti, F.; Burri, H.; Zimmermann, M. Value of P-wave signal averaging to predict atrial fibrillation recurrences after pulmonary vein isolation. *Eur. Eur. Pacing Arrhythmias Card. Electrophysiol. J. Work. Groups Card. Pacing Arrhythmias Card. Cell. Electrophysiol. Eur. Soc. Cardiol.* **2013**, *15*, 198–204. https://doi.org/10.1093/europace/eus251.
24. Wu, J.T.; Dong, J.Z.; Sang, C.H.; Tang, R.B.; Ma, C.S. Prolonged PR interval and risk of recurrence of atrial fibrillation after catheter ablation. *Int. Heart J.* **2014**, *55*, 126–130. https://doi.org/10.1536/ihj.13-231.
25. Park, J.; Kim, T.H.; Lee, J.S.; Park, J.K.; Uhm, J.S.; Joung, B.; Lee, M.H.; Pak, H.N. Prolonged PR interval predicts clinical recurrence of atrial fibrillation after catheter ablation. *J. Am. Heart Assoc.* **2014**, *3*, e001277. https://doi.org/10.1161/JAHA.114.001277.
26. Kizilirmak, F.; Demir, G.G.; Gokdeniz, T.; Gunes, H.M.; Cakal, B.; Guler, E.; Karaca, İO.; Omaygenç, M.O.; Yılmaz, F.; Olgun, F.E.; Kilicaslan, F. Changes in Electrocardiographic P Wave Parameters after Cryoballoon Ablation and Their Association with Atrial Fibrillation Recurrence. *Ann. Noninvasive Electrocardiol. Off. J. Int. Soc. Holter Noninvasive Electrocardiol.* **2016**, *21*, 580–587. https://doi.org/10.1111/anec.12364.
27. Hu, X.; Jiang, J.; Ma, Y.; Tang, A. Novel P-Wave Indices to Predict Atrial Fibrillation Recurrence After Radiofrequency Ablation for Paroxysmal Atrial Fibrillation. *Med Sci. Monit. Int. Med J. Exp. Clin. Res.* **2016**, *22*, 2616–2623. https://doi.org/10.12659/msm.896675.
28. Chen, Q.; Mohanty, S.; Trivedi, C.; Gianni, C.; Della Rocca, D.G.; Canpolat, U.; Burkhardt, J.D.; Sanchez, J.E.; Hranitzky, P.; Gallinghouse, G.J.; et al. Association between prolonged P-wave duration and left atrial scarring in patients with paroxysmal atrial fibrillation. *J. Cardiovasc. Electrophysiol.* **2019**, *30*, 1811–1818. https://doi.org/10.1111/jce.14070.
29. Pranata, R.; Yonas, E.; Vania, R. Prolonged P-wave duration in sinus rhythm pre-ablation is associated with atrial fibrillation recurrence after pulmonary vein isolation-A systematic review and meta-analysis. *Ann. Noninvasive Electrocardiol. Off. J. Int. Soc. Holter Noninvasive Electrocardiol.* **2019**, *24*, e12653. https://doi.org/10.1111/anec.12653.
30. Auricchio, A.; Özkartal, T.; Salghetti, F.; Neumann, L.; Pezzuto, S.; Gharaviri, A.; Demarchi, A.; Caputo, M.L.; Regoli, F.; De Asmundis, C.; et al. Short P-Wave Duration is a Marker of Higher Rate of Atrial Fibrillation Recurrences after Pulmonary Vein Isolation: New Insights into the Pathophysiological Mechanisms Through Computer Simulations. *J. Am. Heart Assoc.* **2021**, *10*, e018572. https://doi.org/10.1161/JAHA.120.018572.
31. Van Beeumen, K.; Houben, R.; Tavernier, R.; Ketels, S.; Duytschaever, M. Changes in P-wave area and P-wave duration after circumferential pulmonary vein isolation. *Eur. Eur. Pacing Arrhythmias Card. Electrophysiol. J. Work. Groups Card. Pacing Arrhythmias Card. Cell. Electrophysiol. Eur. Soc. Cardiol.* **2010**, *12*, 798–804. https://doi.org/10.1093/europace/eup410.
32. Maan, A.; Mansour, M.; Ruskin, J.N.; Heist, E.K. Impact of catheter ablation on P-wave parameters on 12-lead electrocardiogram in patients with atrial fibrillation. *J. Electrocardiol.* **2014**, *47*, 725–733. https://doi.org/10.1016/j.jelectrocard.2014.04.010.
33. Alcaraz, R.; Martínez, A.; Rieta, J.J. Role of the P-wave high frequency energy and duration as noninvasive cardiovascular predictors of paroxysmal atrial fibrillation. *Comput. Methods Programs Biomed.* **2015**, *119*, 110–119. https://doi.org/10.1016/j.cmpb.2015.01.006.
34. Salah, A.; Zhou, S.; Liu, Q.; Yan, H. P wave indices to predict atrial fibrillation recurrences post pulmonary vein isolation. *Arq. Bras. Cardiol.* **2013**, *101*, 519–527. https://doi.org/10.5935/abc.20130214.
35. Baranchuk, A.; de Luna, A.B. The P-wave morphology: what does it tell us? *Herzschrittmachertherapie+ Elektrophysiologie* **2015**, *26*, 192–199. https://doi.org/10.1007/s00399-015-0385-3.
36. Van Steenkiste, G.; Vera, L.; Decloedt, A.; Schauvliege, S.; Boussy, T.; van Loon, G. Endocardial electro-anatomic mapping in healthy horses: Normal sinus impulse propagation in the left and right atrium and the ventricles. *Vet. J. (Lond. Engl. 1997)* **2020**, *258*, 105452. https://doi.org/10.1016/j.tvjl.2020.105452.
37. De Bacquer, D.; Willekens, J.; De Backer, G. Long-term prognostic value of P-wave characteristics for the development of atrial fibrillation in subjects aged 55 to 74 years at baseline. *Am. J. Cardiol.* **2007**, *100*, 850–854. https://doi.org/10.1016/j.amjcard.2007.04.017.
38. Sörnmo, L.; Laguna, P. Electrocardiogram (ECG) Signal Processing. In *Wiley Encyclopedia of Biomedical Engineering*; John Wiley and Sons: Hoboken, NJ, USA, 2006; Volume 2, pp. 1298–1313. https://doi.org/10.1002/9780471740360.ebs1482.
39. García, M.; Martínez-Iniesta, M.; Ródenas, J.; Rieta, J.J.; Alcaraz, R. A novel wavelet-based filtering strategy to remove powerline interference from electrocardiograms with atrial fibrillation. *Physiol. Meas.* **2018**, *39*, 115006. https://doi.org/10.1088/1361-6579/aae8b1.
40. Martínez, A.; Alcaraz, R.; Rieta, J.J. Ventricular activity morphological characterization: ectopic beats removal in long term atrial fibrillation recordings. *Comput. Methods Programs Biomed.* **2013**, *109*, 283–92. https://doi.org/10.1016/j.cmpb.2012.10.011.
41. Choi, A.; Shin, H. Quantitative Analysis of the Effect of an Ectopic Beat on the Heart Rate Variability in the Resting Condition. *Front. Physiol.* **2018**, *9*, 922. https://doi.org/10.3389/fphys.2018.00922.
42. Martínez, A.; Alcaraz, R.; Rieta, J.J. Application of the phasor transform for automatic delineation of single-lead ECG fiducial points. *Physiol. Meas.* **2010**, *31*, 1467–85. https://doi.org/10.1088/0967-3334/31/11/005.

43. González, F.; Alcaraz, R.; Rieta, J.J. Electrocardiographic P-wave Delineation Based on Adaptive Slope Gaussian Detection. In Proceedings of the Computing in Cardiology, CinC 2007, Rennes, France, 24–27 September 2017. Available online: www.cinc.org (accessed on: 10 March 2020). https://doi.org/10.22489/CinC.2017.236-033.

44. Toman, O.; Hnatkova, K.; Smetana, P.; Huster, K.M.; Šišáková, M.; Barthel, P.; Novotný, T.; Schmidt, G.; Malik, M. Physiologic heart rate dependency of the PQ interval and its sex differences. *Sci. Rep.* **2020**, *10*, 2551. https://doi.org/10.1038/s41598-020-59480-8.

45. Misek, J.; Belyaev, I.; Jakusova, V.; Tonhajzerova, I.; Barabas, J.; Jakus, J. Heart rate variability affected by radiofrequency electromagnetic field in adolescent students. *Bioelectromagnetics* **2018**, *39*, 277–288. https://doi.org/10.1002/bem.22115.

46. Levene, H. Robust Tests for Equality of Variances. In *Contributions to Probability and Statistics: Essays in Honor of Harold Hotelling*; Olkin, I., Ed.; Stanford University Press: Palo Alto, CA, USA, 1960; pp. 278–292.

47. Shapiro, S.S.; Wilk, M.B. An analysis of variance test for normality (complete samples). *Biometrika* **1965**, *52*, 591–611. https://doi.org/10.1093/biomet/52.3-4.591.

48. Yokota, A.; Kabutoya, T.; Hoshide, S.; Kario, K. Automatically assessed P-wave predicts cardiac events independently of left atrial enlargement in patients with cardiovascular risks: The Japan Morning Surge-Home Blood Pressure Study. *J. Clin. Hypertens. (Greenwich Conn.)* **2021**, *23*, 301–308. https://doi.org/10.1111/jch.14136.

49. Karjalainen, J.; Viitasalo, M.; Mänttäri, M.; Manninen, V. Relation between QT intervals and heart rates from 40 to 120 beats/min in rest electrocardiograms of men and a simple method to adjust QT interval values. *J. Am. Coll. Cardiol.* **1994**, *23*, 1547–1553. https://doi.org/https://doi.org/10.1016/0735-1097(94)90654-8.

50. Rautaharju, P.M.; Zhang, Z.M. Linearly scaled, rate-invariant normal limits for QT interval: eight decades of incorrect application of power functions. *J. Cardiovasc. Electrophysiol.* **2002**, *13*, 1211–1218. https://doi.org/10.1046/j.1540-8167.2002.01211.x.

51. Luo, S.; Michler, K.; Johnston, P.; Macfarlane, P.W. A comparison of commonly used QT correction formulae: the effect of heart rate on the QTc of normal ECGs. *J. Electrocardiol.* **2004**, *37*, 81–90. https://doi.org/10.1016/j.jelectrocard.2004.08.030.

52. Carmona Puerta, R.; Lorenzo Martínez, E.; Rabassa López-Calleja, M.A.; Padrón Peña, G.; Castro Torres, Y.; Cruz Elizundia, J.M.; Rodríguez González, F.; García Vázquez, L.Á.; Chávez González, E. New Parameter of the Second Half of the P-Wave, P-Wave Duration, and Atrial Conduction Times Predict Atrial Fibrillation during Electrophysiological Studies. *Med Princ. Pract. Int. J. Kuwait Univ. Health Sci. Cent.* **2021**, *30*, 462–469. https://doi.org/10.1159/000518262.

Section C.3. The Dissimilar Impact in Atrial Substrate Modification of Left and 151
Right Pulmonary Veins Isolation after Catheter Ablation of Paroxysmal Atrial
Fibrillation

Article

The Dissimilar Impact in Atrial Substrate Modification of Left and Right Pulmonary Veins Isolation after Catheter Ablation of Paroxysmal Atrial Fibrillation

Aikaterini Vraka [1] [iD]**, Vicente Bertomeu-González** [2] [iD]**, Lorenzo Fácila** [3] [iD]**,
José Moreno-Arribas** [2] [iD]**, Raúl Alcaraz** [4] [iD] **and José J. Rieta** [1,*] [iD]

[1] BioMIT.org, Electronic Engineering Department, Universitat Politecnica de Valencia, 46022 Valencia, Spain;
     aivra@upv.es; jjrieta@upv.es
[2] Cardiology Department, Saint John's University Hospital, 03550 Alicante, Spain;
     vbertog@gmail.com; jomoreno@gmail.com
[3] Cardiology Department, General University Hospital Consortium of Valencia, 46014 Valencia, Spain;
     lfacila@gmail.com
[4] Research Group in Electronic, Biomedical and Telecommunication Engineering, University of Castilla-La
     Mancha, 16071 Cuenca, Spain; raul.alcaraz@uclm.es
*   Correspondence: jjrieta@upv.es

Abstract: Since the discovery of pulmonary veins (PVs) as foci of atrial fibrillation (AF), the commonest cardiac arrhythmia, investigation revolves around PVs catheter ablation (CA) results. Notwithstanding, CA process itselfis rather neglected. We aim to decompose crucial CA steps: coronary sinus (CS) catheterization and the impact ofleft and right PVs isolation (LPVI, RPVI), separately. We recruited 40 paroxysmal AF patients undergoing first-time CA and obtained five-minute lead II and bipolar CS recordings during sinus rhythm (SR) before CA (B), after LPVI (L) and after RPVI (R). Among others, duration, amplitude and atrial-rate variability (ARV) were calculated for P-waves and CS local activation waves (LAWs). LAWs features were compared among CS channels for reliability analysis. P-waves and LAWs features were compared after each ablation step (B, L, R). CS channels: amplitude and area were different between distal/medial (p ≤ 0.0014) and distal/mid-proximal channels (p ≤ 0.0025). Medial and distal showed the most and least coherent values, respectively. Correlation was higher in proximal (≥ 93%) than distal (≤ 91%) areas. P-waves: duration was significantly shortened after LPVI (after L: p = 0.0012, − 13.30%). LAWs: insignificant variations. ARV modification was more prominent in LAWs (L: > + 73.12%, p ≤ 0.0480, R: < − 33.94%, p ≤ 0.0642). Medial/mid-proximal channels are recommended during SR. CS LAWs are not significantly affected by CA butthey describe more precisely CA-induced ARV modifications. LPVI provokes the highest impact in paroxysmal AF CA, significantly modifying P-wave duration.

Keywords: atrial fibrillation; catheter ablation; coronary sinus; catheter channels; P-waves; local activation waves; left pulmonary veins; heart rate variability

1. Introduction

Atrial fibrillation (AF) is the prevailing cardiac arrhythmia in the western world. Prolonged lifespan and the connection with a plenty of other comorbidities contribute to the ever-growing AF incidence. Health and economic burden caused by AF alert the need for thorough investigation on its pathophysiology [1]. AF springs principally from pulmonary veins (PVs) [2] and propagates through cardiac structures [3]. The main mechanism assisting the AF propagation is structural remodeling and fibrosis is especially contributing to the alteration of the cardiac anatomy, causing conduction heterogeneity, hence favoring the AF perpetuation [1,4]. Although conduction heterogeneity is more prominent during AF, the anatomical substrate can still be present for both atria even

when patients are in sinus rhythm (SR) [5–7]. As PVs are the main AF foci, their electrical isolation, called catheter ablation (CA), is the star AF treatment [1,8]. Despite the high CA success rates for paroxysmal AF patients, persistent AF cases often require the CA of additional cardiac structures that trigger or propagate the AF activity, known as non-PV triggers [1,3,4,9,10,12].

Many techniques exist to localize non-PV triggers, with complex fractionated atrial electrograms (CFAEs) during AF [4,13,14] or low voltage electrograms (EGMs) during SR [4,15,16] being two of the most established ones. A combination of both techniques along with highly proportioned EGM fractionation has recently indicated sites showing fibrosis, with a high correlation between these areas in AF and SR [6]. Nevertheless, the effect of CA on additional non-PV triggers remains quite controversial. Evidence shows that additional ablation of these sites offers little or no improved results with respect to single PVs ablation [17–19]. It remains unclear, however, whether failure of additional CA applications to provide significant improvement in termination of AF stems from the incapacity of CA on sites other than PVs to terminate AF or from a vague and unclear definition of areas in need of ablation due to highly complex EGMs, thus highlighting the need for more reliable algorithms able to properly evaluate the atrial substrate [6,14].

So far, CA outcome on paroxysmal AF patients is primarily assessed from the analysis of the characteristics of P-waves, which represent the activation of the atria or heart-rate (HR) variability (HRV) analysis, which assesses the ventricular response, controlled by the autonomous nervous system (ANS). P-wave duration (PWD) is the most popular P-wave feature, reflecting the overall time that the wavefront needs to be propagated throughout the atria. Existence of prolonged or short PWD is considered an indicator of AF recurrence in paroxysmal or persistent AF patients, caused by conduction heterogeneity and scarring or shortening of the atrial refractory period, respectively [20–25]. PWD shortening is connected with the elimination of the conduction heterogeneity, hence being a favorable CA marker, while it is the second P-wave part, corresponding to left atrial depolarization, that is mainly modified after CA, possibly due to vicinity with PVs, the main object of CA [26–29]. PWD analysis goes beyond CA procedures, with application in studies predicting the AF occurrence or the risk for higher AF burden after pacemaker implantation [25,30,31].

Apart from PWD, P-wave dispersion, amplitude, area or P-wave to R-peak interval are popular features utilized to predict AF recurrence [26,27,32,33]. P-wave analysis has been additionally applied to frequency domain in order to discern among healthy and AF subjects [34]. HRV is a marker of fine tuning of ANS, which consists of sympathetic and parasympathetic systems and controls sinus rhythm. Evidence shows that people with low HRV are susceptible to AF [35–37]. Energy delivered by radiofrequency (RF) CA (RFCA) can disturb the balance between sympathetic and parasympathetic systems, by stimulating the former and leading to temporary withdrawal of the latter, hence causing HRV attenuation, which in turn has been associated with AF recurrence [38–40].

The number of studies and techniques aiming to analyze the CA effect on the atrial substrate is endless. At the same time, critical CA steps and their impact on the atrial substrate alteration is a rather neglected analysis field. Firstly, the aforementioned studies observing P-wave and HRV alterations only employ recordings acquired before and after CA. This postulates the theory of a uniform impact of left (LPVI) and right PVs isolation (RPVI). It should be considered, though, the possibility of each PV side playing a different role in atrial substrate alteration and hence, in AF activity, a conjecture that can be easily verified by employing signals recorded in between the ablation of LPVI and RPVI, which are already available in the recordings of any electrophysiology laboratory during stepwise CA procedures.

Coronary sinus' (CS) strategical position between left (LA) and right atrium (RA) allows the detection of non-PV triggers and PV reconnection gaps throughout the atria during CA procedures via CS catheterization [41–49]. Despite its extensive use as a CA reference, whether CS analysis could provide reliable information with respect to the AF

substrate modification or which channels of CS catheter are the most appropriate for the analysis are two vital issues that remain unexplored. During CS cannulation, the most proximal pair of electrodes (9–10) is placed close to RA and the most distal pair (1–2) close to LA [44,47]. Notwithstanding, CS catheterization may be rather challenging due to variable CS anatomy and shape, aggrravated by myocardial contraction or the existence of CS dilation, factors that can lead to unstable recordings, especially from the distal tip of the catheter [50–53]. Additionally, anatomical alterations of the, adjacent to CS extremes, mitral annulus across the cardiac cycle in SR may affect furthermore the stability of recordings acquired from distal and proximal electrodes of the CS catheter [54,55]. Considering the aforementioned factors, information recorded across the CS catheter electrodes could vary significantly and the choice of the appropriate channel recruited for the analysis should be made with extreme caution.

The present work aims to elucidate the aforeposed issues regarding the CA procedure, in order to arise the understanding on the mechanisms of important CA steps and their interaction with the CA result. In the first place, the ability of CS channels to describe with the highest precision possible the AF dynamics during SR is assessed and the most and least recommended CS channels are defined. Afterwards, the relevance of CS in substrate modification evaluation due to CA is investigated via analysis of features traditionally applied to ECG recordings and cross-referenced by P-waves and HRV analysis of the ECGs. Finally, the evolution of P-waves and CS LAWs after isolation of either sides of PVs is tracked in order to define the PV side that has the highest impact in atrial substrate modification due to CA.

The manuscript is organized as follows. Section 2 briefly describes the database recruited for the analysis, as well as the preprocessing and analysis steps. Section 3 presents the results, which are further interpreted in Section 4. Main findings are stated in Section 5.

2. Materials and Methods

2.1. Database

Initial database consisted of 61 paroxysmal AF patients without any previous CA sessions. Twenty-one patients were discarded due to extremely low amplitude or presence of noise and artifacts in the extreme channels of the CS recordings, probably due to dynamical change of mitral annulus anatomy during SR and vigorous myocardial contraction causing the movement of the CS cathether. The final database consisted of the remaining 40 patients.

Recordings from a standard 12-lead electrocardiogram (ECG) and a decapolar CS catheter with sampling frequency at 1 kHz were acquired by a Labsystem™ PRO EP recording system (Boston Scientific, Marlborough, MA, USA). Five-minute continuous segments before RFCA initiation (step **B**), after LPVI (step **L**) and after RPVI, which coincides with the end of the RFCA procedure (step **R**), were chosen. The evolution of each ablation step is illustrated in Figure 1a. Step **B** corresponds to 0% of the procedure, step **L** corresponds to 100% of LPVI, 0% of RPVI and 50% of the total ablation procedure, while step **R** corresponds to 100% of the overall procedure. The effect of ablation of each PV side is shown in Figure 1b. A statistically significant difference in features between steps **B** and **L** indicates that LPVI is critical in atrial substrate modification, while a difference between steps **L** and **R** or between **B** and **R** but without the difference between steps **B** and **L** being statistically significant, proves a significant effect of RPVI. Surface analysis was limited to lead II, as P-waves are more prominent in this lead [56].

For the study of the reliability of CS channels in preserving the AF dynamics, final database consisted of a total of 58 step **B** or **R** recordings from the 40 patients of the database. CS catheter consisted of the following channels of bipolar signals: distal (D), mid-distal (MD), medial (M), mid-proximal (MP) and proximal (P), with D channel being the closest to LA and P channel to the RA. Firstly, a multichannel comparison allowed us to define the channels that can record the AF dynamics to the most reliable degree. Selection of the analysis channel for the CS study was then performed among the most

robust channels, with unique favorable criteria the high signal amplitude and low baseline fluctuation. Specific attention was paid so that the same channel would be employed for all CA steps for the same patient.
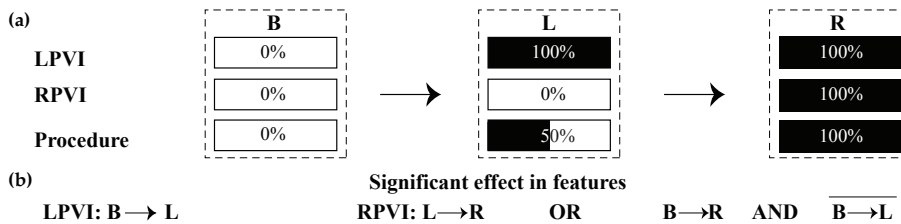
Figure 1. (**a**) Steps of CA procedure for which recordings were extracted and analyzed. In step **B**, no ablation has been performed yet (0%). In step **L**, LPVI has been completed (100%) and hence, we are in the middle of the procedure (50%). Step **R** corresponds to RPVI and to the end of the procedure. Therefore, each step is completed (100%). (**b**) Conditions in order for LPVI or RPVI to have a significant effect on the features under analysis. LPVI: left pulmonary vein isolation; RPVI: right pulmonary vein isolation.

Regarding the CA procedure, all patients underwent circumferential RFCA of PVs, guided by 3-D electroanatomical mapping during SR. RFCA was initiated by performing a crown surrounding left PVs (step **L**), followed by a crown surround right PVs (step **R**). Non-inducibility of AF was confirmed by pacing in all patients and was the endpoint of the procedure.

2.2. Preprocessing

For ECG recordings, powerline interference and high frequency muscle noise were removed by a wavelet-based denoising method [57] followed by a bidirectional low-pass filter with cut-off requency at 70 Hz [58]. Baseline wander was also removed [58].

EGM denoising and mean removal were the first preprocessing steps for CS recordings analysis [59]. Although presence of ventricular activity is not dominant in atrial bipolar signals, far-field activity in line with the R-peak of the ECG recordings has been observed in some cases. Removal of ventricular activity was performed with an adaptive cancellation method [60].

Next, ectopic beats correction was performed. Ectopic beats are premature atrial or ventricular contractions that affect the HRV. In our analysis, ectopic beats in ECGs, if present, did not exceed 4% of total beats. Their correction included the detection and cancellation of the premature complexes and their replacement by a new beat via linear interpolation [61]. Among various ectopic replacement methods, linear interpolation was chosen due to its better performance for time-domain HRV features [62].

Finally, detection and delineation of atrial activations was carried out. P-waves were firstly detected by an adaptive search window prior to the R-peak [63] and then delineated [64]. Local activation waves (LAWs) of CS were detected with an algorithm based on an alternative Botteron's technique [65]. Delineation was performed by firstly smoothing the LAW with a five-point moving average filter [66]. Delineation of both ECG and intracardiac recordings was visually inspected and corrected, if needed, by an expert.

2.3. Main Analysis

Once preprocessed, the duration, amplitude, root mean square (RMS) value, area, number of deflections and inflections (NODI) and slope rate were calculated for P-waves and LAWs, as shown in Figure 2. Final values of these features were calculated by signal-averaging. A brief description of these characteristics is provided as follows. Further details are described elsewhere [66].
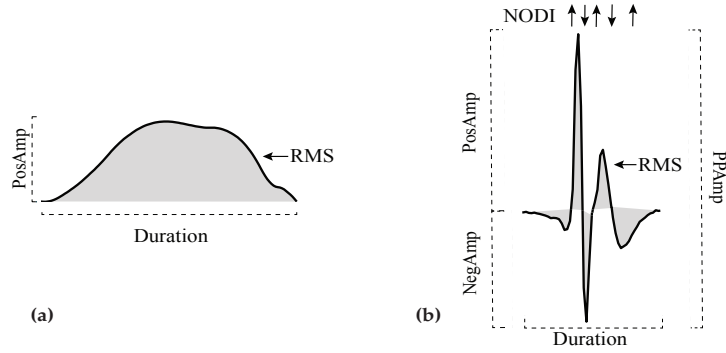
Figure 2. (a): Duration, amplitude, RMS and area (shaded) for a P-wave. **(b)**: Duration, amplitude, RMS, area (shaded) and NODI for a LAW. Upward arrows represent an inflection, while downward arrows a deflection. In the figure, LAW has 3 major inflections and 2 major deflections. RMS: root mean square; NODI: number of deflections and inflections; LAWs: local activation waves.

1. *Duration:* Distance between the onset and offset of each activation.
2. *Amplitude:* Amplitude of positive and negative maximum of each activation were considered as positive (*PosAmp*) and negative amplitude (*NegAmp*), respectively. Peak-to-peak amplitude (*PPAmp*) was the distance between positive and negative maximum points. As P-waves are positive in lead II, only maximum amplitude was calculated for ECG analysis.
3. *RMS:* Let X_n be a time-series, so that $X_n = \{x_1, x_2, \ldots, x_n\}$. *RMS* value is the quadratic mean of the function that defines the time-series. In our case, this function is defined by either the P-wave or LAW waveform.
4. *Area:* Area is calculated as the integration of the signal over the time interval. Trapezoidal method allows this integration, by splitting each signal into smaller and easier to calculate trapezoids. Final area is defined by the cumulative sum of these trapezoids. As LAWs contain both positive (*PosAr*) and negative (*NegAr*) parts, this method was separately applied to each one of them.
5. *NODI:* Deflections and inflections were calculated from the points that cross two auxiliary baselines, at $\pm 25\%$ of the signal amplitude. This metric was only calculated for LAWs, as P-waves do not show multiple major deflections and inflections.
6. *Slope rate:* The rhythm of increasing or decreasing slope was calculated at sample points equal to $i\%$ of the activation duration, with $i = 5, 10, 20$. Slope rate at the maximum point was also computed. The equation calculating these slope rates was the following:

$$S_i = \frac{Amp(t_i) - Amp(t_{onset})}{t_i - t_{onset}}, \tag{1}$$

where $Amp(t_i)$ is the amplitude at the $i\%$ of the activation duration, $Amp(t_{onset})$ is the amplitude at the onset of the activation, t_i is the sample point at the $i\%$ of the activation duration and t_{onset} is the sample point corresponding to the onset of the activation.

Afterwards, features calculated across each recording were analyzed: morphology variability (MV), dispersion and time-domain HRV features.

1. *MV:* A reference signal was firstly created by the 20 most similar activations of the channel under analysis and then correlated with each and every activation, using an adaptive signed correlation index (ASCI) with 12% tolerance [67]. MV was then defined as the percentage of signals that correlated <95% with the reference signal.
2. *Dispersion:* Traditionally, for the calculation of dispersion, more than one ECG lead is employed and the difference between maximum and minimum activation duration across channels is computed. Alternatively, in our case, lead II was just extracted

and P-wave dispersion analysis was performed in this channel because atrial activity presents the highest amplitude. Dispersion was then defined as the difference between the 25th and 75th percentiles of the atrial activations duration of each recording. This way, the effect of signal delineation accuracy is minimized and an extremely long or short activation caused by various factors will not affect significantly the results [68]. Dispersion of EGM recordings was calculated in the same way.

3. *Time-domain HRV features:* HRV analysis is normally performed on R-R intervals, thus describing ventricular response. As in the present work we are focused on atrial analysis, we modified the techniques by substituting R-R peaks by P-wave to P-wave for ECG and LAW to LAW for EGM recordings. As these features describe the atrial response, thus neglecting the effect of the atrioventricular node and other cardiac structures, they will be referred in the remainder of this document as atrial rate variability (ARV) features. Standard deviation of normal-to-normal beat interval (*SDNN*), variance of normal to normal beat interval (*VARNN*) and RMS of successive interbeat differences (*RMSSD*) were calculated for each recording.

2.3.1. Heart Rate Adjustment

Time-domain features of P-wave analysis are affected by variable HR [69]. More specifically, as HR increases, intervals between fiducial points of ECGs shorten. Therefore, HR adjustment is proposed in order to moderate this effect. For this purpose, additionally to the original analysis, a simple HR-adjustment factor is performed. As sampling frequency is 1 kHz, a 60 beat-per-minute recording would show one activation every 1000 sample points. However, as HR is diverse and often deviant from these values, the adjustment factor for the ith activation was set as

$$adj(i) = \frac{1000}{IBI_i},\tag{2}$$

where IBI_i is the interbeat interval between the ith and the $(i-1)^{th}$ activations. Duration and area were normalized by this factor, while slope rates were inversely scaled by it. HR-adjusted values will be shown as $\mathbf{HRA}(y)$, where $y = duration$, *area* or S_i.

2.4. Statistical Analysis

Normality and homoscedasticity were tested with Saphiro-Wilk and Levene tests, respectively [70,71]. According to the results, non-parametric tests were employed for the comparison between populations.

Reliability analysis of the CS channels with respect to AF dynamics was performed on *Duration*, *Amplitude*, *RMS*, *Area* and *NODI*. In the first place, a multichannel comparison via a Kruskal-Wallis (KW) test was employed [72]. Comparison in pairs of two channels was performed with a Mann-Whitney U-test (MWU) [73] with Bonferroni correction. Median values were also calculated at each channel and any significant differences between each one and the remaining channels was explored by as well using a MWU with Bonferroni correction. Afterwards, a reference signal for each channel was calculated as described from MV analysis in Section 2.3. Then, the correlation between the morphology of each channel's reference signal in pairs of two was calculated for each recording, using an ASCI with 12% tolerance.

For P-waves, LAWs and ARV analysis, comparison between ablation steps is performed with KW and post-hoc tests to define which step is crucial are performed with MWU with Bonferroni correction and median and interquartile range calculations. Analysis is performed for P-waves and CS LAWs separately. Percentage of variation (POV) of features was specified for each recording and between two ablation steps as

$$POV(r_i) = (\frac{V_2}{V_1} - 1) \times 100 \ [\%],\tag{3}$$

where r_i is the recording of the ith patient, V_2 is the value of each feature at the posterior step and V_1 is the value of the same feature at the prior step. How POV was modified between ablation steps **B-L** and **L-R** for both P-waves and LAWs was tested with MWU. Finally, HR was measured at each ablation step and compared among all steps with KW.

3. Results

3.1. Analysis of CS Features between Channels

Table 1 shows the results of the multichannel comparison as well as the comparison in pairs of channels, for the selected features. *Amplitude* and *Area* show different values among the CS catheter channels. Paired analysis showed that differences are mostly located between D and M or D and MP channels. A trend has also been observed between values of MD and M channels. Due to Bonferroni correction, α is 0.005, as 10 paired comparisons have been performed. Comparison between D-MD, MD-P and M-MP channels are not illustrated, as they did not show any statistically significant differences ($p > 0.03, 0.38$ and 0.35, respectively).

Table 1. Multichannel comparison (KW) and paired comparison (MWU) for the features defined in CS channels. Statistically significant results are shown with an asterisk (*). In MWU analysis, $\alpha = 0.005$. D: distal; MD: mid-distal; M: medial; MP: mid-proximal; P: proximal.

	KW			MWU				
		D-M	D-MP	D-P	MD-M	MD-MP	M-P	MP-P
Duration	0.2136	0.0188	0.0893	0.4355	0.3502	0.8927	0.2232	0.7001
PosAmp	$< 0.0001 *$	$< 0.0001 *$	$< 0.0001 *$	0.0140	0.0053	0.0038 *	0.0355	0.0502
NegAmp	0.0005 *	0.0002 *	0.0016 *	0.4162	0.0087	0.0587	0.0080	0.0428
PPAmp	0.0001 *	$< 0.0001 *$	0.0002 *	0.1476	0.0087	0.0182	0.0112	0.0491
RMS	0.0003 *	0.0001 *	0.0007 *	0.1644	0.0053	0.0409	0.0182	0.0950
PosAr	0.0008 *	0.0003 *	0.0020 *	0.1826	0.0080	0.0491	0.0182	0.0950
NegAr	0.0024 *	0.0014 *	0.0025 *	0.3384	0.0119	0.0347	0.0207	0.0758
Deflections	0.7925	0.6217	0.2458	0.3258	0.9749	0.5681	0.6126	0.7430
Inflections	0.8045	0.6324	0.7477	0.3711	0.9840	0.4349	0.7831	0.2354

Figure 3 shows the median values obtained for each analyzed feature from the CS. As can be seen, the distal channel showed the longest LAWs *Duration* and lowest LAWs *Amplitude* and *Area* values for most of the features. Medial channel contained the shortest LAWs *Duration* and highest LAWs *Amplitude* values. *Area* was higher in mid-proximal channel, followed by medial channel. Mid-proximal channel showed overall similar behavior as medial channel, with rather high *Amplitude* and short LAWs *Duration* values.
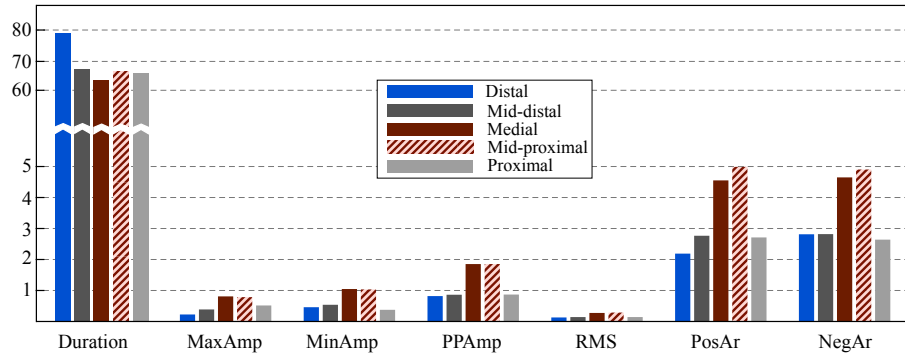
Figure 3. Bar graph for the median values of the analyzed features at each one of the CS channels. Note the break in the vertical scale for the feature *Duration*.

The analysis of channels that varied significantly with respect to the others at each feature is shown in Table 2. Statistical comparison allows the detection of the channels that show the most and least deviant values and can corroborate the results shown in Figure 3.

Table 2. One-vs.-all analysis of defined features for each one of CS channels. Asterisks (*) indicate statistically significant values. Due to multiple comparison, α has been modified to 0.01.

Features	Distal	Mid-Distal	Medial	Mid-Proximal	Proximal
Duration	0.0472	0.8617	0.0837	0.6755	0.7345
PosAmp	< 0.0001 *	0.1688	0.0021 *	0.0061 *	0.8176
NegAmp	0.0038 *	0.4720	0.0019 *	0.0446	0.1317
PPAmp	0.0008 *	0.2669	0.0017 *	0.0204	0.3261
RMS	0.0014 *	0.2762	0.0018 *	0.0394	0.3717
PosAr	0.0022 *	0.3799	0.0027 *	0.0610	0.3555
NegAr	0.0103	0.2427	0.0049 *	0.0526	0.3113
Deflections	0.3181	0.8899	0.8099	0.3745	0.6235
Inflections	0.6108	0.7069	0.7779	0.3422	0.4243

None of the channels showed a statistically different LAWs *Duration* comparing to the remaining ones. Nevertheless, a trend was observed for distal and medial channels. Distal and medial channels showed additionally statistically different values with respect to the remaining channels regarding LAWs *Amplitude* and *Area* features. Mid-proximal channel also showed statistically significant difference than the other channels for positive *Amplitude* and a trend for the remaining *Amplitude* and *Area* features. Combining the aforementioned observations with the median values of the LAWs features for each CS channel presented in Figure 3, we can conclude that *Ampitude* and *Area* are statistically smaller in distal channel and higher in medial channel of the catheter, while duration tends to be longer in distal and shorter in medial channels. Mid-proximal channel shows a trend for high *Amplitude* and *Area* values as well.

Finally, how LAWs morphology of each channel correlated with the morphology of LAWs at each of the remaining channels can be appreciated from Figure 4. Channels of proximal area (MP, P) show higher correlations between their LAWs morphology compared to correlations from distal area (D, MD). Additionally, medial channel showed stronger correlation with proximal (93–95%) than distal area (86–91%). Although all adjacent channels showed relatively strong correlations, the highest values were observed in proximal area.
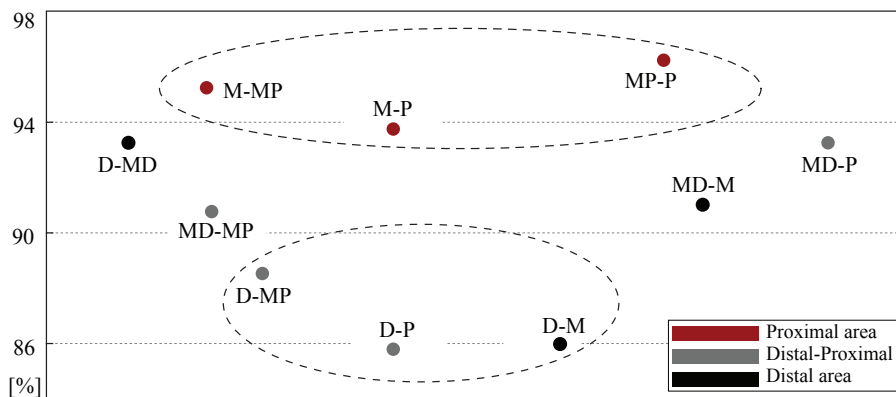
Figure 4. Correlations, as percentage, between the LAWs morphology in various CS catheter channels. The upper ellipse area contains the strongest and the bottom ellipse area the weakest correlations. Stronger correlations are found in proximal area, while moderate or weaker correlations are observed in distal area or between channels that are spatially far away (distal-proximal area).

3.2. Analysis of Features from P-waves and LAWs

The HR measurements did not reveal any statistical difference between HR at different ablation steps. However, a decrease in HR was observed in step **L**, as shown in Table 3.

Table 3. Heart-rate at each ablation step and comparison between three steps (KW). As result indicated a non-significant comparison, no MWU has been performed. KW: Kruskal-Wallis; MWU: Mann-Whitney U-test; B: before CA; L: after LPVI; R: after RPVI.

	B	L	R
Median (iqr)	57.2 (17.0)	55.0 (12.0)	58.6 (13.4)
KW		0.7713	

Table 4. Median (interquartile) values for each feature and results for KW and MWU tests for P-waves. Statistically significant results are shown in (∗). Due to Bonferroni correction, threshold for MWU (last three columns) is $\alpha = 0.0167$.

	Median			**KW**	**MWU**		
Features	**B**	**L**	**R**		**B-L**	**B-R**	**L-R**
Duration [*ms*]	120.0 (12.00)	104.0 (13.00)	106.5 (21.00)	0.003∗	0.001∗	0.009∗	0.558
PosAmp [*mV*]	0.428 (0.303)	0.354 (0.290)	0.374 (0.232)	0.084	0.055	0.097	0.319
PPAmp [*mV*]	0.431 (0.303)	0.356 (0.290)	0.374 (0.232)	0.084	0.056	0.097	0.319
RMS [*mV*]	0.263 (0.179)	0.214 (0.179)	0.230 (0.232)	0.144	0.103	0.150	0.275
PosAr [*mV* × *ms*]	24.63 (12.94)	16.57 (14.62)	20.39 (9.98)	0.141	0.103	0.103	0.438
S_5 [*mV/ms*]	0.005 (0.002)	0.007 (0.004)	0.006 (0.002)	0.162	0.110	0.235	0.211
S_{10} [*mV/ms*]	0.007 (0.002)	0.008 (0.004)	0.007 (0.003)	0.178	0.117	0.420	0.150
S_{20} [*mV/ms*]	0.010 (0.005)	0.011 (0.003)	0.009 (0.005)	0.336	0.384	0.693	0.133
S_{max}[*mV/ms*]	0.010 (0.004)	0.009 (0.004)	0.008 (0.004)	0.823	0.987	0.602	0.602
HRA(*Duration*)	119.5 (57.39)	106.9 (26.04)	101.0 (36.91)	0.159	0.141	0.079	0.740
HRA(*PosAr*)	26.10 (16.94)	19.40 (14.16)	22.12 (14.01)	0.144	0.085	0.110	0.716
HRA(S_5)	0.004 (0.004)	0.006 (0.006)	0.006 (0.003)	0.367	0.261	0.235	0.537
HRA(S_{10})	0.006 (0.003)	0.007 (0.007)	0.007 (0.004)	0.441	0.248	0.402	0.558
HRA(S_{20})	0.010 (0.005)	0.010 (0.008)	0.009 (0.006)	0.801	0.693	0.837	0.517
HRA(S_{max})	0.009 (0.007)	0.008 (0.006)	0.008 (0.006)	0.994	0.962	1.000	0.912
MV	0.605 (0.329)	0.753 (0.335)	0.675 (0.467)	0.476	0.189	0.624	0.646
Dispersion [*ms*]	12.00 (4.000)	11.00 (7.000)	10.00 (4.000)	0.310	0.208	0.176	0.949
SDNN	94.25 (55.32)	99.91 (71.96)	84.28 (62.10)	0.136	0.133	0.862	0.060
VARNN	8.8×10^3 (1.07×10^4)	9.9×10^3 (1.77×10^4)	7.1×10^3 (1.21×10^4)	0.136	0.133	0.862	0.060
RMSSD	95.44 (59.68)	126.79 (95.29)	92.51 (61.73)	0.136	0.052	0.962	0.069

In the same context, amplitude showed a downward trend after step **L**. Despite the key role of step **L** in the modification of *Duration*, when HR adjustment was performed, this step did not show any effect in **HRA**(*Duration*) and neither did step **R**. However, modification of **HRA**(*Duration*) showed a trend when values in the beginning and the end of the procedure were measured (**B-R** comparison), possibly due to a cumulative effect of CA in AF substrate which can be better appreciated quantitatively when isolation is totally performed. Although *Area* modification was not originally found to be statistically significant at each of the ablation steps, HR adjustment revealed for it a trend in **B-L** comparison, falling from 26.10 mV×ms to 19.40 *mV* × *ms*. Finally, it can also be observed that measurements after step **L** showed, in a non-significant level, lower *Amplitude* and *Area* values and higher ARV, *MV* values and *Slope rate* values than steps **B** and **R**.

Regarding LAWs, comparison of each feature among all channels revealed a significant variation of *RMSSD*. Apart from this observation, none of the features varied statistically at any of the ablation steps. However, some trends have been observed. The respective results are shown in Table 5. LAWs showed a trend for shortening between steps **B-R**, as shown by

both *Duration* and **HRA**(*Duration*) results. *MV* showed a trend for amplification after step **L** (**B-L** comparison) which was almost statistically significant. All ARV features employed in this study showed an increasing trend after step **L** (**B-L** comparison) and a decreasing trend after step **R** (**L-R** comparison). Note that threshold for MWU is $\alpha = 0.0167$ due to Bonferroni correction.

Table 5. Median (interquartile) values for each feature and results for KW and MWU tests for CS LAWs. Statistically significant results are shown in (∗). Due to Bonferroni correction, threshold for MWU (last three columns) is $\alpha = 0.0167$. As highest peak is often found in negative amplitude in LAWs, slope rate in **HRA**(S_{max}) is negative.

Features	Median B	L	R	KW	MWU B-L	B-R	L-R
Duration [*ms*]	100.5 (14.00)	97.50 (18.00)	90.00 (23.00)	0.108	0.241	0.055	0.217
PosAmp [*mV*]	0.492 (0.987)	0.509 (0.893)	0.641 (0.775)	0.835	0.646	0.887	0.602
NegAmp [*mV*]	−0.831 (1.572)	−0.779 (0.772)	−0.915 (0.486)	0.892	0.740	0.912	0.646
PPAmp [*mV*]	1.361 (2.624)	1.382 (1.495)	1.570 (1.462)	0.942	0.740	0.937	0.837
RMS [*mV*]	0.150 (0.345)	0.151 (0.195)	0.181 (0.218)	0.847	0.740	0.912	0.558
PosAr [*mV* × *ms*]	4.407 (5.175)	3.718 (5.160)	3.985 (4.836)	0.896	0.670	0.837	0.788
NegAr [*mV* × *ms*]	4.085 (5.485)	3.818 (4.045)	3.992 (4.655)	0.864	0.624	0.937	0.693
Deflections	3.000 (1.000)	3.000 (1.000)	3.000 (1.000)	0.916	0.682	0.889	0.828
Inflections	3.000 (1.000)	3.000 (1.000)	2.500 (1.000)	0.915	0.878	0.810	0.695
S_5 [*mV/ms*]	3.2×10^{-4} (2.1×10^{-4})	3.9×10^{-4} (3.4×10^{-4})	3.8×10^{-4} (5.0×10^{-4})	0.732	0.624	0.837	0.438
S_{10} [*mV/ms*]	4.3×10^{-4} (6.0×10^{-4})	4.4×10^{-4} (5.2×10^{-4})	4.9×10^{-4} $(4.8 \times 10^{-4}$	0.767	0.764	0.558	0.558
S_{20} [*mV/ms*]	3.8×10^{-4} (0.003)	4.7×10^{-4} (0.001)	5.3×10^{-4} (0.001)	0.932	0.887	0.962	0.669
S_{max}[*mV/ms*]	−0.018 (0.058)	−0.019 (0.027)	−0.021 (0.044)	0.996	0.937	0.987	0.987
HRA(*Duration*)	104.8 (32.83)	102.1 (23.50)	91.25 (33.19)	0.159	0.669	0.060	0.200
HRA(*PosAr*)	4.446 (6.861)	3.503 (4.345)	3.832 (4.737)	0.882	0.669	0.693	0.937
HRA(S_5)	3.6×10^{-4} (1.9×10^{-4})	4.1×10^{-4} (3.9×10^{-4})	3.4×10^{-4} (4.1×10^{-4})	0.753	0.558	0.837	0.517
HRA(S_{10})	4.4×10^{-4} (0.001)	4.2×10^{-4} (3.6×10^{-4})	4.7×10^{-4} (0.001)	0.771	0.912	0.558	0.537
HRA(S_{20})	4.1×10^{-4} (0.003)	3.9×10^{-4} (0.001)	5.1×10^{-4} (0.001)	0.836	0.710	0.812	0.580
HRA(S_{max})	−0.015 (0.049)	−0.016 (0.030)	−0.019 (0.047)	0.967	0.887	0.788	0.912
MV	0.028 (0.048)	0.100 (0.103)	0.067 (0.351)	0.056	0.018	0.113	0.692
Dispersion [*ms*]	2.500 (3.000)	2.000 (4.000)	2.000 (6.000)	0.676	0.461	0.923	0.451
SDNN	74.18 (57.56)	96.51 (94.74)	61.75 (73.48)	0.056	0.048	0.912	0.041
VARNN	5.5×10^3 (7.9×10^3)	9.4×10^3 (2.0×10^4)	3.4×10^3 (1.1×10^4)	0.056	0.048	0.912	0.041
RMSSD	98.87 (86.99)	127.4 (119.8)	90.40 (74.41)	0.049∗	0.026	0.764	0.064

POV of all features between each two ablation steps are illustrated in Table 6 for both P-waves and LAWs. Comparison of POV that corresponds to successive step transitions **B-L** and **L-R** can also be seen in the last two columns. In general, POV in P-waves seem to be more prominent than respective POV values in LAWs, especially in the **B-L** comparison. *Duration* in P-waves got reduced by −13.30% after step **L**, while in LAWs by −5.49%. Step **R** did not additionally modify at average the P-waves at all (0.00% POV in **L-R** comparison). For LAWs, step R did reduce LAW *Duration* by an additional −1.93%. Comparison between **B-L** and **L-R** alterations in P-wave *Duration* presented a significant difference ($p < 0.0001$), which was not observed in LAWs, indicating a different effect of LPVI and RPVI in P-wave but not in CS LAWs *Duration* alteration. HR-adjustment did not have a different effect in **B-L** comparison of P-waves with respect to the same comparison for non-normalized *Duration* variation (−13.73% vs. −13.30%, respectively). However, HR-adjustment revealed a slightly higher, albeit not statistically significant, effect of step **R** in **HRA**(*Duration*),

Section C.3. The Dissimilar Impact in Atrial Substrate Modification of Left and 161
Right Pulmonary Veins Isolation after Catheter Ablation of Paroxysmal Atrial
Fibrillation

Table 6. POV for between every two ablation steps for P-waves and LAWs and comparison between POV of successive step transitions **B-L** and **L-R**. Statistically significant results are shown in (∗). POV: percentage of variation.

	B-L [%]		L-R [%]		B-R [%]		MWU (BL-LR)	
Features	P-waves	LAWs	P-waves	LAWs	P-waves	LAWs	P-waves	LAWs
Duration	−13.30	−5.49	0.00	−1.93	−11.01	−7.46	< 0.0001	0.6576
PosAmp	−16.65	−3.58	3.86	0.52	−11.25	−6.51	0.0556	0.6464
PPAmp	−16.04	−7.79	3.80	−2.15	−11.52	−5.09	0.0556	0.7397
RMS	−18.51	0.82	7.51	19.91	−12.39	20.89	0.1032	0.7397
PosAr	−25.68	−5.23	6.50	−1.74	−20.72	−4.06	0.1032	0.6693
S_5	30.95	22.47	−13.75	−1.82	12.95	20.24	0.1101	0.6239
S_{10}	15.75	1.34	−11.23	11.74	−0.73	13.24	0.1173	0.7637
S_{20}	12.84	25.89	−18.35	12.20	−7.87	41.24	0.3843	0.8868
S_{max}	−5.40	4.37	−6.96	7.75	−11.99	12.46	0.9874	0.9370
HRA(*Duration*)	−13.73	−3.89	1.60	−4.46	−14.49	−9.84	0.1412	0.6693
HRA(*PosAr*)	−24.54	−2.90	6.60	−3.86	−19.65	−19.94	0.0847	0.6693
HRA(S_5)	58.69	14.18	−9.34	−16.49	43.87	−4.65	0.2614	0.5583
HRA(S_{10})	13.41	−4.10	−4.38	11.80	8.45	7.21	0.2482	0.9118
HRA(S_{20})	3.35	−5.64	−6.44	32.58	−3.30	25.10	0.6925	0.7160
HRA(S_{max})	−6.60	4.11	−1.21	17.70	−7.74	22.53	0.9621	0.8868
MV	15.00	144.9	−6.11	−5.93	−0.42	172.1	0.1892	0.0176∗
Dispersion	−22.42	0.00	22.22	80.00	−9.55	0.00	0.2084	0.4613
SDNN	28.39	79.80	−24.27	−33.94	0.28	0.92	0.1249	0.0480∗
VARNN	64.86	225.9	−42.64	−55.91	0.57	1.93	0.1249	0.0480∗
RMSSD	45.15	73.12	−28.30	−36.30	0.26	5.43	0.0445∗	0.0257∗

showing an incrementation of +1.60%. For LAWs, **HRA**(*Duration*) slightly mitigated the effect of step **L** (−3.89% for HR-adjustment) and potentiated the effect of step **R** (−4.46%). These results were not statistically significant either. *Amplitude* and **HRA**(*PosAr*) values showed the same kind of variations for P-waves and LAWs, with comparison between **B-L** and **L-R** transitions showing a trend for P-waves and low statistical power for LAWs.

For the remaining features, *MV* showed a rather strong magnification after step **L** by +144.90% in LAWs, whereas the corresponding step in P-waves showed only a +15.00% of *MV* magnification. After step **R**, *MV* dropped by −5.93% in LAWs and by −6.11% in P-waves. Due to very intense variations in *MV* of LAWs, POV evolution between transitions from **B-L** and **L-R** varied significantly ($p = 0.0176$). As already observed in Tables 4 and 5, ARV features showed a notable incrementation after step **L** in both P-waves and LAWs. This is even more prominent in POV analysis, where ARV got increased by up to +225.90% in LAWs and up to +64.86% in P-waves (in *VARNN* in both cases). However, ARV after the end of the procedure (step **R**) got decreased by up to −55.91% in LAWs and −42.64% in P-waves (in *VARNN* in both cases). These very high variations in LAWs analysis led the **B-L** and **L-R** comparison to be statistically significant for all ARV features. As P-waves POV analysis also showed considerable variations but to a lesser extent, only POV in *RMSSD* varied statistically between **B-L** and **L-R**. Figure 5 then shows the POV box and whisker plots for the features that showed any kind of significant alteration or a trend, so that alterations in POV can be better illustrated. From $y-$axis can be additionally observed that POV in LAWs shows more scattered values that span along a wider range than P-waves analysis. This is noticeable at most of the boxplot pairs of Figure 5, but can be especially seen in the subplot of *MV*, where POV in P-waves is in the range of 0 to 1200% while in LAWs in the range of 0 to 12,000%.
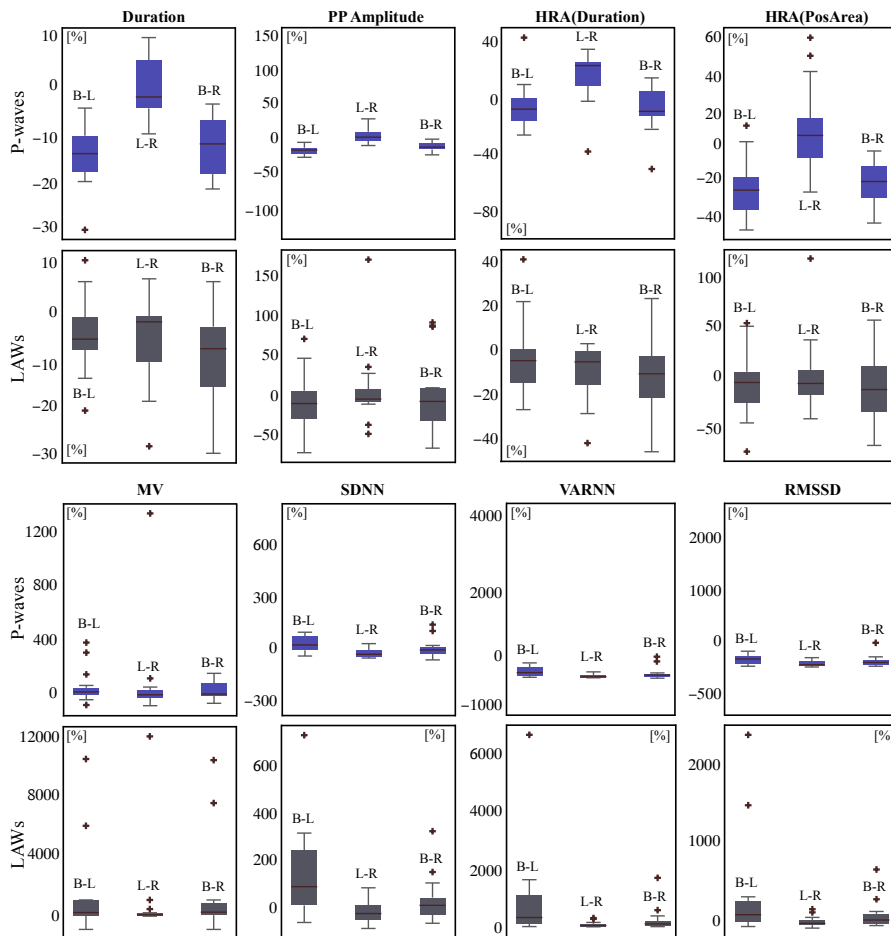
Figure 5. Representation of significant alterations illustrated as boxplots of POV for P-waves features (each top, blue) and LAWs features (each bottom, gray) between the defined ablation steps for selected features. Beware of the different vertical scale in each case for the same feature.

4. Discussion

This multi-approach study had three main objectives. First of all, to define the CS channels that can record with the highest precision and robustness the AF dynamics during SR. The analysis revealed the existence of variability among CS channels especially in *Duration* and *Amplitude* features. Differences were mostly found betweeen distal and medial and between distal and mid-proximal, with a trend between mid-distal and medial channels. A combined interpretation of the analysis of medians and the one-vs-all analysis indicates that distal channel showed the longest *Duration*, whilst the shortest *Duration* has been recorded by the medial channel. Regarding *Amplitude* and *Area* values, these were smaller in distal channel and larger in medial and mid-proximal channels. Proximal area showed the strongest morphological correlations between its channels. On the contrary, correlations in distal area or between distal and proximal channels were weaker. Hence, being the least susceptible channels to exogenous factors during SR, medial and mid-proximal channels are recommended while distal and mid-distal channels are not suggested.

Various studies corroborate these conclusions. CS EGM fractionation analysis was related with AF recurrence during SR in proximal and medial but not in distal channel in a recent study [47]. Fractionation of proximal CS EGMs indicated AF patients in another study employing recordings during AF [74]. Another work found that AF cycle length

analysis in distal channel failed to predict AF termination after CA. In the same study, only mid-proximal channel predicted freedom from AF recurrence [75].

The second objective of the present study was to investigate if CS recordings can describe adequately the substrate modification due to CA, as observed by P-wave analysis. Parallel P-waves and LAWs analysis has been conducted for this purpose. The former represent the entire atria while the latter provide very specific yet crucial information on CS function. Variations were observed to a higher degree in most of the features in P-waves than LAWs. *MV* and ARV features were modified to an exceptionally higher extent in LAWs than P-waves. As CS recordings are closer to the tissue under ablation than surface ECG recordings, variability caused by RF energy deliverance may be illustrated with higher precision by LAWs [38,39]. Variation was more consistent in P-waves than LAWs, while the latter showed higher *Dispersion* in values across all features.

The last but not least purpose of this work was the evaluation of additional recordings acquired during CA in order to understand the role that the ablation of each PV side plays to the modification of the studied features and, as a consequence, to the atrial substrate alteration. A significant P-wave shortening was observed after CA of both PV sides, in line with a plethora of previous studies mainly attributed to fibrotic areas causing conduction delays [20–23]. Interestingly enough, this reduction was observed right after LPVI, with RPVI not showing any additional effect to this feature. *Duration* before CA was 120 ms, dropping down to 104 ms after LPVI and showing a minor increase after RPVI, to 106.5 ms. P-wave *Amplitude* also tended to show a lower value after LPVI which was slightly increased after RPVI, but remained overall smaller than the pre-ablative measurements.

HRV attenuation after CA is considered an indicator of CA success [38–40]. In line with previous studies, ARV in the present study showed a non-significant reduction after the end of the procedure. Nevertheless, recordings obtained after LPVI showed a trend for amplification of ARV values by up to +64.86%. Previous works studying the effect of RF energy in rabbits and students in lying position found that RF exposure can cause HRV incrementation and HR attenuation [76,77]. These findings explain the aforementioned results of the present study. Additionally, HR was indeed found to decrease after LPVI in the present work. Finally, HR-adjustment preserved the variation that was observed in *Duration* after LPVI, although losing statistical power. It also incremented the different effect that RPVI had on *Duration*, showing a slight non-statistical increase of +1.60% after RPVI. The reason for this slight incrementation is the HR acceleration after the end of CA procedure with respect to recordings after LPVI, where RF energy deliverance was still going on. Higher HR leads to generally narrower P-waves, the size of which is retrieved after HR-adjustment. An additional factor that may have a minor effect on this incrementation is a possible deviation of 1–2 ms in P-wave delineation precision, which due to its size (<+2.00% of duration values range) is considered acceptable.

Amplitude in P-waves showed a trend for reduction after LPVI. Although final *Amplitude* was non-statistically reduced with respect to the beginning of the procedure, as in previous studies [27], RPVI slightly but non-significantly increased *Amplitude* values. Contrastly, *Slope rate* was non-significantly increased after LPVI but decreased after RPVI in most of the studied time instances. It is highly possible that RF exposure also has had an effect on *Amplitude* and *Slope rate* features, explaining these variations.

Regarding LAWs, variations of most features show weaker statistical power and lower POV at each ablation step with respect to P-waves analysis. As mentioned afore, *MV* and ARV varied more prominently in LAWs than P-waves. *MV* showed a high incrementation in the order of +144.9% after LPVI and a decrease of −5.93% after RPVI. The reasons for these dramatic changes are not clear. Exposure to RF energy, not only affecting ARV but also *MV* may be an explanation. Recently a study found *MV* in lead V1 P-waves of paroxysmal AF undergoing CA of PVs to decrease after the procedure, as a sign of a successful ablation [78]. Apart from the fact that these results come from P-waves analysis, which in our case show a slight attenuation overall, *MV* in the present analysis was extracted by a template of the 20 most similar activations and not by considering all activations of one recording.

ARV was also increased after LPVI in LAWs and to a higher extent than P-waves (up to +225.9%), possibly due to proximity to the tissue under ablation as explained previously.

To our knowledge, this is the first complete comparative study to perform simultaneous P-waves and LAWs analysis on recordings obtained not only before and after but also during CA of PVs. Recently, a relevant study calculated the organization of ECG recordings before, during and after CA of PVs and did not find any step to affect significantly the organization indices under calculation [79]. As many differences exist with respect to our study, a comparison would not be straightforward. In the first place, individuals studied were persistent AF patients while the present study employed exclusively paroxysmal AF patients. As persistent AF shows more complicated atrial substrate and often presents AF drivers outside of PVs, efficiency of CA of PVs is notably lower with respect to success rates in paroxysmal AF patients [19,80]. Secondly, the procedure consisted of CA of PVs, CA of CFAEs and linear CA of LA. Recordings during the procedure were the recordings after CA of PVs and before CA of CFAEs and linear CA of LA. Hence, the intermediate stage of their analyis would be the final stage of ours and no information is provided about the contribution of left or right PVs. Finally, features employed are different from the features employed in the present study.

The key aspects of CA of PVs for paroxysmal AF patients investigated in the present study improve significantly the understanding of the AF mechanisms during SR and contribute to the knowledge on how these mechanisms respond to each step of CA. Moreover, the CA procedure itself is reconsidered and the most reliable means to analyze CS EGMs are explored. Overall, a more detailed perspective of the CA procedure and the effect of RF exposure to atrial tissue is obtained.

5. Conclusions

LPVI is the critical part of CA of PVs for paroxysmal AF patients, altering significantly the P-wave duration. RF exposure tends to cause temporary ARV incrementation, which is reversed right after the end of the CA procedure. The effect of CA of PVs on CS is less straightforward and takes place to a lesser extent. Thus, other atrial structures may be more indicative of the ablation outcome and should be assessed as alternative references. It should be noted, however, that ARV modifications regarding RF energy are more prominently observed in CS LAWs, possibly due to the vicinity with the tissue under RF exposure. Hence, the employment of CS recordings may be beneficial for the study of ARV alterations during and after CA of PVs. Finally, studies interested in employing CS analysis are encouraged to extract and investigate medial or mid-proximal channels, as they were found to be the most robust, showing the highest coherence between LAWs morphologies. Distal and mid-distal channels, on the other hand, should be avoided as they were prone to variable morphology and less clear activations.

Institutional Review Board Statement: The study was conducted according to the guidelines of the Declaration of Helsinki, complied with Law 14/2007, 3rd of July, on Biomedical Research and other Spanish regulations and was approved by the Ethical Review Board of Saint John's University Hospital (San Juan de Alicante, Alicante, Spain) with protocol code 21/046.

Conflicts of Interest: The authors have no association with commercial entities that could be viewed as having an interest in the general area of the submitted manuscript.

References

1. Hindricks, G.; Potpara, T.; Dagres, N.; Arbelo, E.; Bax, J.J.; Blomstro, C.; Boriani, G.; Castella, M.; Dan, G.A.; Dilaveris, P.E.; et al. 2020 ESC Guidelines for the diagnosis and management of atrial fibrillation developed in collaboration with the European Association of Cardio-Thoracic Surgery (EACTS). *Eur. Heart J.* **2020**, *42*, 374–498. https://doi.org/10.1093/eurheartj/ehaa612s.
2. Haissaguerre, M.; Jaïs, P.; Shah, D.C.; Takahashi, A.; Hocini, M.; Quiniou, G.; Garrigue, S.; Le Mouroux, A.; Le Métayer, P.; Clémenty, J. Spontaneous initiation of atrial fibrillation by ectopic beats originating in the pulmonary veins. *N. Engl. J. Med.* **1998**, *339*, 659–666. https://doi.org/10.1056/NEJM199809033391003.
3. Ioannidis, P.; Zografos, T.; Christoforatou, E.; Kouvelas, K.; Tsoumeleas, A.; Vassilopoulos, C. The Electrophysiology of Atrial Fibrillation: From Basic Mechanisms to Catheter Ablation. *Cardiol. Res. Pract.* **2021**, *2021*, 4109269. https://doi.org/10.1155/2021/4109269.
4. Lau, D.H.; Linz, D.; Schotten, U.; Mahajan, R.; Sanders, P.; Kalman, J.M. Pathophysiology of Paroxysmal and Persistent Atrial Fibrillation: Rotors, Foci and Fibrosis. *Heart Lung Circ.* **2017**, *26*, 887–893. https://doi.org/10.1016/j.hlc.2017.05.119.
5. Mouws, E.M.J.P.; Lanters, E.A.H.; Teuwen, C.P.; van der Does, L.J.M.E.; Kik, C.; Knops, P.; Bekkers, J.A.; Bogers, A.J.J.C.; de Groot, N.M.S. Epicardial Breakthrough Waves During Sinus Rhythm: Depiction of the Arrhythmogenic Substrate? *Circ. Arrhythmia Electrophysiol.* **2017**, *10*, e005145. https://doi.org/10.1161/CIRCEP.117.005145.
6. Jadidi, A.; Nothstein, M.; Chen, J.; Lehrmann, H.; Dössel, O.; Allgeier, J.; Trenk, D.; Neumann, F.J.; Loewe, A.; Müller-Edenborn, B.; et al. Specific Electrogram Characteristics Identify the Extra-Pulmonary Vein Arrhythmogenic Sources of Persistent Atrial Fibrillation—Characterization of the Arrhythmogenic Electrogram Patterns During Atrial Fibrillation and Sinus Rhythm. *Sci. Rep.* **2020**, *10*, 9147. https://doi.org/10.1038/s41598-020-65564-2.
7. Kharbanda, R.K.; Knops, P.; van der Does, L.; Kik, C.; Taverne, Y.; Roos-Serote, M.C.; Heida, A.; Oei, F.; Bogers, A.; de Groot, N. Simultaneous Endo-Epicardial Mapping of the Human Right Atrium: Unraveling Atrial Excitation. *J. Am. Heart Assoc.* **2020**, *9*, e017069. https://doi.org/10.1161/jaha.120.017069.
8. Shah, D.; Haïssaguerre, M.; Jaïs, P. Catheter Ablation of Pulmonary Vein Foci for Atrial Fibrillation. *Thorac. Cardiovasc. Surg.* **1999**, *47*, 352–356. https://doi.org/10.1055/s-2007-1013198.
9. Oral, H.; Knight, B.P.; Tada, H. Pulmonary vein isolation for paroxysmal and persistent atrial fibrillation. *Circulation* **2002**, *11*, 83. https://doi.org/10.1016/s1062-1458(02)00739-0.
10. Della Rocca, D.G.; Tarantino, N.; Trivedi, C.; Mohanty, S.; Anannab, A.; Salwan, A.S.; Gianni, C.; Bassiouny, M.; Al-Ahmad, A.; Romero, J.; et al. Non-pulmonary vein triggers in nonparoxysmal atrial fibrillation: Implications of pathophysiology for catheter ablation. *J. Cardiovasc. Electrophysiol.* **2020**, *31*, 2154–2167. https://doi.org/10.1111/jce.14638.
11. Lin, W.S.; Tai, C.T.; Hsieh, M.H. Catheter ablation of paroxysmal atrial fibrillation initiated by non-pulmonary vein ectopy. *Circulation* **2003**, *12*, 53. https://doi.org/10.1016/j.accreview.2003.09.033.
12. Sánchez-Quintana, D.; López-Mínguez, J.R.; Pizarro, G.; Murillo, M.; Cabrera, J.A. Triggers and anatomical substrates in the genesis and perpetuation of atrial fibrillation. *Curr. Cardiol. Rev.* **2012**, *8*, 310–326. https://doi.org/10.2174/157340312803760721.
13. Nademanee, K.; McKenzie, J.; Kosar, E.; Schwab, M.; Sunsaneewitayakul, B.; Vasavakul, T.; Khunnawat, C.; Ngarmukos, T. A new approach for catheter ablation of atrial fibrillation: Mapping of the electrophysiologic substrate. *J. Am. Coll. Cardiol.* **2004**, *43*, 2044–2053. https://doi.org/10.1016/j.jacc.2003.12.054.
14. Vraka, A.; Hornero, F.; Bertomeu-González, V.; Osca, J.; Alcaraz, R.; Rieta, J.J. Short-Time Estimation of Fractionation in Atrial Fibrillation with Coarse-Grained Correlation Dimension for Mapping the Atrial Substrate. *Entropy* **2020**, *22*, 232. https://doi.org/10.3390/e22020232.
15. Chang, S.L.; Tai, C.T.; Lin, Y.J.; Wongcharoen, W.; Lo, L.W.; Tuan, T.C.; Udyavar, A.R.; Chang, S.H.; Tsao, H.M.; Hsieh, M.H.; et al. Biatrial substrate properties in patients with atrial fibrillation. *J. Cardiovasc. Electrophysiol.* **2007**, *18*, 1134–1139. https://doi.org/10.1111/j.1540-8167.2007.00941.x.
16. Garg, L.; Pothineni, N.V.K.; Daw, J.M.; Hyman, M.C.; Arkles, J.; Tschabrunn, C.M.; Santangeli, P.; Marchlinski, F.E. Impact of Left Atrial Bipolar Electrogram Voltage on First Pass Pulmonary Vein Isolation During Radiofrequency Catheter Ablation. *Front. Physiol.* **2020**, *11*, 594654. https://doi.org/10.3389/fphys.2020.594654.
17. Verma, A.; Jiang, C.y.; Betts, T.R.; Chen, J.; Deisenhofer, I.; Mantovan, R.; Macle, L.; Morillo, C.A.; Haverkamp, W.; Weerasooriya, R.; et al. Approaches to catheter ablation for persistent atrial fibrillation. *N. Engl. J. Med.* **2015**, *372*, 1812–1822. https://doi.org/10.1056/NEJMoa1408288.
18. Cheng, W.H.; Lo, L.W.; Lin, Y.J.; Chang, S.L.; Hu, Y.F.; Hung, Y.; Chung, F.P.; Liao, J.N.; Tuan, T.C.; Chao, T.F.; et al. Ten-year ablation outcomes of patients with paroxysmal atrial fibrillation undergoing pulmonary vein isolation. *Heart Rhythm* **2019**, *16*, 1327–1333. https://doi.org/10.1016/j.hrthm.2019.03.028.
19. Inamura, Y.; Nitta, J.; Inaba, O.; Sato, A.; Takamiya, T.; Murata, K.; Ikenouchi, T.; Kono, T.; Matsumura, Y.; Takahashi, Y.; et al. Presence of non-pulmonary vein foci in patients with atrial fibrillation undergoing standard ablation of pulmonary vein isolation: Clinical characteristics and long-term ablation outcome. *Int. J. Cardiol. Heart Vasc.* **2021**, *32*, 100717. https://doi.org/10.1016/j.ijcha.2021.100717.
20. Simpson, R.J.; Foster, J.R.; Gettes, L.S. Atrial excitability and conduction in patients with interatrial conduction defects. *Am. J. Cardiol.* **1982**, *50*, 1331–1337. https://doi.org/10.1016/0002-9149(82)90471-4.
21. Blanche, C.; Tran, N.; Rigamonti, F.; Burri, H.; Zimmermann, M. Value of P-wave signal averaging to predict atrial fibrillation recurrences after pulmonary vein isolation. *EP Eur.* **2013**, *15*, 198–204. https://doi.org/10.1093/europace/eus251.

22. Chen, Q.; Mohanty, S.; Trivedi, C.; Gianni, C.; Della Rocca, D.G.; Canpolat, U.; Burkhardt, J.D.; Sanchez, J.E.; Hranitzky, P.; Gallinghouse, G.J.; et al. Association between prolonged P wave duration and left atrial scarring in patients with paroxysmal atrial fibrillation. *J. Cardiovasc. Electrophysiol.* **2019**, *30*, 1811–1818. https://doi.org/10.1111/jce.14070.

23. Pranata, R.; Yonas, E.; Vania, R. Prolonged P-wave duration in sinus rhythm pre-ablation is associated with atrial fibrillation recurrence after pulmonary vein isolation—A systematic review and meta-analysis. *Ann. Noninvasive Electrocardiol.* **2019**, *24*, e12653. https://doi.org/10.1111/anec.12653.

24. Auricchio, A.; Özkartal, T.; Salghetti, F.; Neumann, L.; Pezzuto, S.; Gharaviri, A.; Demarchi, A.; Caputo, M.L.; Regoli, F.; De Asmundis, C.; et al. Short P-Wave Duration is a Marker of Higher Rate of Atrial Fibrillation Recurrences after Pulmonary Vein Isolation: New Insights into the Pathophysiological Mechanisms Through Computer Simulations. *J. Am. Heart Assoc.* **2021**, *10*, e018572. https://doi.org/10.1161/JAHA.120.018572.

25. Miao, Y.; Xu, M.; Yang, L.; Zhang, C.; Liu, H.; Shao, X. Investigating the association between P wave duration and atrial fibrillation recurrence after radiofrequency ablation in early persistent atrial fibrillation patients. *Int. J. Cardiol.* **2021**, *351*, 48–54. https://doi.org/10.1016/j.ijcard.2021.12.036.

26. Van Beeumen, K.; Houben, R.; Tavernier, R.; Ketels, S.; Duytschaever, M. Changes in P-wave area and P-wave duration after circumferential pulmonary vein isolation. *EP Eur.* **2010**, *12*, 798–804. https://doi.org/10.1093/europace/eup410.

27. Maan, A.; Mansour, M.; Ruskin, J.N.; Heist, E.K. Impact of catheter ablation on P-wave parameters on 12-lead electrocardiogram in patients with atrial fibrillation. *J. Electrocardiol.* **2014**, *47*, 725–733. https://doi.org/10.1016/j.jelectrocard.2014.04.010.

28. Hu, X.; Jiang, J.; Ma, Y.; Tang, A. Novel P Wave Indices to Predict Atrial Fibrillation Recurrence After Radiofrequency Ablation for Paroxysmal Atrial Fibrillation. *Med. Sci. Monit.* **2016**, *22*, 2616–2623. https://doi.org/10.12659/msm.896675.

29. Vraka, A.; Bertomeu-González, V.; Hornero, F.; Quesada, A.; Alcaraz, R.; Rieta, J.J. Splitting the P-Wave: Improved Evaluation of Left Atrial Substrate Modification after Pulmonary Vein Isolation of Paroxysmal Atrial Fibrillation. *Sensors* **2022**, *22*, 290. https://doi.org/10.3390/s22010290.

30. Alcaraz, R.; Martínez, A.; Rieta, J.J. The P Wave Time-Frequency Variability Reflects Atrial Conduction Defects before Paroxysmal Atrial Fibrillation. *Ann. Noninvasive Electrocardiol.* **2015**, *20*, 433–445. https://doi.org/10.1111/anec.12240s.

31. Murase, Y.; Imai, H.; Ogawa, Y.; Kano, N.; Mamiya, K.; Ikeda, T.; Okabe, K.; Arai, K.; Yamazoe, S.; Torii, J.; et al. Usefulness of P-wave duration in patients with sick sinus syndrome as a predictor of atrial fibrillation. *J. Arrhythmia* **2021**, *37*, 1220–1226. https://doi.org/10.1002/joa3.12604.

32. Wu, J.T.; Dong, J.Z.; Sang, C.H.; Tang, R.B.; Ma, C.S. Prolonged PR interval and risk of recurrence of atrial fibrillation after catheter ablation. *Int. Heart J.* **2014**, *55*, 126–130. https://doi.org/10.1536/ihj.13-231.

33. Salah, A.; Zhou, S.; Liu, Q.; Yan, H. P wave indices to predict atrial fibrillation recurrences post pulmonary vein isolation. *Arq. Bras. Cardiol.* **2013**, *101*, 519–527. https://doi.org/10.5935/abc.20130214.

34. Alcaraz, R.; Martínez, A.; Rieta, J.J. Role of the P-wave high frequency energy and duration as noninvasive cardiovascular predictors of paroxysmal atrial fibrillation. *Computer Methods* and *Programs Biomedicine* **2015**, *119*, 110–119. https://doi.org/10.1016/j.cmpb.2015.01.006.

35. Task Force of the European Society of Cardiology the North American Society of Pacing Electrophysiologys. Heart rate variability. Standards of measurement, physiological interpretation, and clinical use. *Eur. Heart J.* **1996**, *17*, 354–381. https://doi.org/10.1161/01.cir.93.5.1043.

36. Perkiömäki, J.; Ukkola, O.; Kiviniemi, A.; Tulppo, M.; Ylitalo, A.; Kesäniemi, Y.A.; Huikuri, H. Heart rate variability findings as a predictor of atrial fibrillation in middle-aged population. *J. Cardiovasc. Electrophysiol.* **2014**, *25*, 719–724. https://doi.org/10.1111/jce.12402.

37. Habibi, M.; Chahal, H.; Greenland, P.; Guallar, E.; Lima, J.A.C.; Soliman, E.Z.; Alonso, A.; Heckbert, S.R.; Nazarian, S. Resting Heart Rate, Short-Term Heart Rate Variability and Incident Atrial Fibrillation (from the Multi-Ethnic Study of Atherosclerosis (MESA)). *Am. J. Cardiol.* **2019**, *124*, 1684–1689. https://doi.org/10.1016/j.amjcard.2019.08.025.

38. Hsieh, M.H.; Chiou, C.W.; Wen, Z.C.; Wu, C.H.; Tai, C.T.; Tsai, C.F.; Ding, Y.A.; Chang, M.S.; Chen, S.A. Alterations of heart rate variability after radiofrequency catheter ablation of focal atrial fibrillation originating from pulmonary veins. *Circulation* **1999**, *100*, 2237–2243. https://doi.org/10.1161/01.cir.100.22.2237.

39. Chen, P.S.; Chen, L.S.; Fishbein, M.C.; Lin, S.F.; Nattel, S. Role of the autonomic nervous system in atrial fibrillation: pathophysiology and therapy. *Circ. Res.* **2014**, *114*, 1500–1515. https://doi.org/10.1161/CIRCRESAHA.114.303772.

40. Zhu, Z.; Wang, W.; Cheng, Y.; Wang, X.; Sun, J. The predictive value of heart rate variability indices tested in early period after radiofrequency catheter ablation for the recurrence of atrial fibrillation. *J. Cardiovasc. Electrophysiol.* **2020**, *31*, 1350–1355. https://doi.org/10.1111/jce.14448.

41. Maille, B.; Das, M.; Hussein, A.; Shaw, M.; Chaturvedi, V.; Williams, E.; Morgan, M.; Ronayne, C.; Snowdon, R.L.; Gupta, D. Reverse electrical and structural remodeling of the left atrium occurs early after pulmonary vein isolation for persistent atrial fibrillation. *J. Interv. Card. Electrophysiol.* **2020**, *58*, 9–19. https://doi.org/10.1007/s10840-019-00576-1.

42. Daoud, E.G.; Niebauer, M.; Bakr, O.; Jentzer, J.; Man, K.C.; Williamson, B.D.; Hummel, J.D.; Strickberger, S.A.; Morady, F. Placement of electrode catheters into the coronary sinus during electrophysiology procedures using a femoral vein approach. *Am. J. Cardiol.* **1994**, *74*, 194–195. https://doi.org/10.1016/0002-9149(94)90102-3.

43. Antz, M.; Otomo, K.; Arruda, M.; Scherlag, B.J.; Pitha, J.; Tondo, C.; Lazzara, R.; Jackman, W.M. Electrical conduction between the right atrium and the left atrium via the musculature of the coronary sinus. *Circulation* **1998**, *98*, 1790–1795. https://doi.org/10.1161/01.cir.98.17.1790.

44. Santangeli, P.; Marchlinski, F.E. Techniques for the provocation, localization, and ablation of non–pulmonary vein triggers for atrial fibrillation. *Heart Rhythm* **2017**, *14*, 1087–1096. https://doi.org/10.1016/j.hrthm.2017.02.030.

45. Ahmed, N.; Perveen, S.; Mehmood, A.; Rani, G.F.; Molon, G. Coronary Sinus Ablation Is a Key Player Substrate in Recurrence of Persistent Atrial Fibrillation. *Cardiology* **2019**, *143*, 107–113. https://doi.org/10.1159/000501819.

46. Razeghian-Jahromi, I.; Natale, A.; Nikoo, M.H. Coronary sinus diverticulum: Importance, function, and treatment. *Pacing Clin. Electrophysiol. PACE* **2020**, *43*, 1582–1587. https://doi.org/10.1111/pace.14026.

47. Boles, U.; Gul, E.E.; Enriquez, A.; Starr, N.; Haseeb, S.; Abdollah, H.; Simpson, C.; Baranchuk, A.; Redfearn, D.; Michael, K.; et al. Coronary sinus electrograms may predict new-onset atrial fibrillation after typical atrial flutter radiofrequency ablation. *J. Atr. Fibrillation* **2018**, *11*, 1809. https://doi.org/10.4022/jafib.1809.

48. Morita, H.; Zipes, D.P.; Morita, S.T.; Wu, J. The role of coronary sinus musculature in the induction of atrial fibrillation. *Heart Rhythm* **2012**, *9*, 581–589. https://doi.org/10.1016/j.hrthm.2011.11.041.

49. Tahara, M.; Kato, R.; Ikeda, Y.; Goto, K.; Asano, S.; Mori, H.; Iwanaga, S.; Muramatsu, T.; Matsumoto, K. Differential Atrial Pacing to Detect Reconnection Gaps After Pulmonary Vein Isolation in Atrial Fibrillation. *Int. Heart J.* **2020**, *61*, 503–509. https://doi.org/10.1536/ihj.19-584.

50. Mahmud, E.; Raisinghani, A.; Keramati, S.; Auger, W.; Blanchard, D.G.; DeMaria, A.N. Dilation of the coronary sinus on echocardiogram: Prevalence and significance in patients with chronic pulmonary hypertension. *JASE* **2001**, *14*, 44–49. https://doi.org/10.1067/mje.2001.108538.

51. Langenberg, C.J.M.; Pietersen, H.G.; Geskes, G.; Wagenmakers, A.J.M.; Soeters, P.B.; Durieux, M. Coronary Sinus Catheter Placement. *Clin. Investig. Cardiol.* **2003**, *124*, 1259–1265. https://doi.org/10.1378/chest.124.4.1259.

52. Saremi, F.; Thonar, B.; Sarlaty, T.; Shmayevich, I.; Malik, S.; Smith, C.W.; Krishnan, S.; Sánchez-Quintana, D.; Narula, N. Posterior interatrial muscular connection between the coronary sinus and left atrium: Anatomic and functional study of the coronary sinus with multidetector CT. *Radiology* **2011**, *260*, 671–679. https://doi.org/10.1148/radiol.11102278.

53. Vogt, J.; Heintze, J.; Hansky, B.; Güldner, H.; Buschler, H.; Horstkotte, D. Implantation: Tips and tricks–the cardiologist's view. *Eur. Heart J. Suppl.* **2004**, *6*, D47–D52. https://doi.org/https://doi.org/10.1016/j.ehjsup.2004.05.024.

54. Pai, R.G.; Varadarajan, P.; Tanimoto, M. Effect of atrial fibrillation on the dynamics of mitral annular area. *J. Heart Valve Dis.* **2003**, *12*, 31–37.

55. El-Maasarany, S.; Ferrett, C.G.; Firth, A.; Sheppard, M.; Henein, M.Y. The coronary sinus conduit function: Anatomical study (relationship to adjacent structures). *EP Eur.* **2005**, *7*, 475–481. https://doi.org/10.1016/j.eupc.2005.05.013.

56. Meek, S.; Morris, F. ABC of clinical electrocardiography: Introduction. II—basic terminology. *BMJ* **2002**, *324*, 470–473. https://doi.org/10.1136/bmj.324.7335.470.

57. García, M.; Martínez-Iniesta, M.; Ródenas, J.; Rieta, J.J.; Alcaraz, R. A novel wavelet-based filtering strategy to remove powerline interference from electrocardiograms with atrial fibrillation. *Physiol. Meas.* **2018**, *39*, 115006. https://doi.org/10.1088/1361-6579/aae8b1.

58. Sörnmo, L.; Laguna, P., Electrocardiogram (ECG) Signal Processing. In *Wiley Encyclopedia of Biomedical Engineering*; John Wiley and Sons: Hoboken, NJ, USA, 2006; Volume 2, pp. 1298–1313. https://doi.org/10.1002/9780471740360.ebs1482.

59. Martínez-Iniesta, M.; Ródenas, J.; Rieta, J.J.; Alcaraz, R. The stationary wavelet transform as an efficient reductor of powerline interference for atrial bipolar electrograms in cardiac electrophysiology. *Physiol. Meas.* **2019**, *40*, 075003. https://doi.org/10.1088/1361-6579/ab2cb8.

60. Alcaraz, R.; Rieta, J.J. Adaptive singular value cancelation of ventricular activity in single-lead atrial fibrillation electrocardiograms. *Physiol. Meas.* **2008**, *29*, 1351–1369. https://doi.org/10.1088/0967-3334/29/12/001.

61. Martínez, A.; Alcaraz, R.; Rieta, J.J. Detection and removal of ventricular ectopic beats in atrial fibrillation recordings via principal component analysis. In Proceedings of the Annual International Conference of the IEEE Engineering in Medicine and Biology Society, Boston, MA, USA, 30 August–3 September 2011; pp. 4693–4696. https://doi.org/10.1109/IEMBS.2011.6091162.

62. Choi, A.; Shin, H. Quantitative Analysis of the Effect of an Ectopic Beat on the Heart Rate Variability in the Resting Condition. *Front. Physiol.* **2018**, *9*, 922. https://doi.org/10.3389/fphys.2018.00922.

63. Martinez, A.; Alcaraz, R.; Rieta, J.J. A new method for automatic delineation of ECG fiducial points based on the Phasor Transform. In Proceedings of the Annual International Conference of the IEEE Engineering in Medicine and Biology Society, Buenos Aires, Argentina, 31 August–4 September 2010; pp. 4586–4589. https://doi.org/10.1109/IEMBS.2010.5626498.

64. González, F.; Alcaraz, R.; Rieta, J.J. Electrocardiographic P-wave delineation based on adaptive slope Gaussian detection. In Proceedings of the 2017 Computing in Cardiology (CinC), Rennes, France, 24–27 September 2017; pp. 1–4. https://doi.org/10.22489/CinC.2017.236-033.

65. Osorio, D.; Alcaraz, R.; Rieta, J.J. A fractionation-based local activation wave detector for atrial electrograms of atrial fibrillation. In Proceedings of the 2017 Computing in Cardiology (CinC), Rennes, France, 24–27 September 2017; pp. 1–4. https://doi.org/10.22489/CinC.2017.202-031.

66. Vraka, A.; Bertomeu-González, V.; Osca, J.; Ravelli, F.; Alcaraz, R.; Rieta, J.J. Study on How Catheter Ablation Affects Atrial Structures in Patients with Paroxysmal Atrial Fibrillation: The Case of the Coronary Sinus. In Proceedings of the 2020 International Conference on e-Health and Bioengineering (EHB), Iasi, Romania, 29–30 October 2020; pp. 1–4. https://doi.org/10.1109/EHB50910.2020.9280243.

67. Alcaraz, R.; Hornero, F.; Martínez, A.; Rieta, J.J. Short-time regularity assessment of fibrillatory waves from the surface ECG in atrial fibrillation. *Physiol. Meas.* **2012**, *33*, 969–984. https://doi.org/10.1088/0967-3334/33/6/969.

68. Zawadzki, J.; Zawadzki, G.; Radziejewska, J.; Wolff, P.S.; Sławuta, A.; Gajek, J. The P wave dispersion—One pixel, one millisecond. *Rev. Cardiovasc. Med.* **2021**, *22*, 1633. https://doi.org/10.31083/j.rcm2204170.

69. Toman, O.; Hnatkova, K.; Smetana, P.; Huster, K.M.; Šišáková, M.; Barthel, P.; Novotný, T.; Schmidt, G.; Malik, M. Physiologic heart rate dependency of the PQ interval and its sex differences. *Sci. Rep.* **2020**, *10*, 2551. https://doi.org/10.1038/s41598-020-59480-8.

70. Mandelbrot, B.B. Contributions to Probability and Statistics: Essays in Honor of Harold Hotelling. *Siam Rev.* **1961**, *3*, 80–80.

71. Shapiro, S.S.; Wilk, M.B., An Analysis of Variance Test for Normality (Complete Samples). *Biometrika* **1965**, *52*, 591–611.

72. Kruskal, W.H.; Wallis, W.A. Use of ranks in one-criterion variance analysis. *J. Am. Stat. Assoc.* **1952**, *47*, 583–621. https://doi.org/10.2307/2280779.

73. Mann, H.B.; Whitney, D.R. On a Test of Whether one of Two Random Variables is Stochastically Larger than the Other. *Ann. Math. Stat.* **1947**, *18*, 50–60. https://doi.org/10.1214/aoms/1177730491.

74. Oral, H.; Ozaydin, M.; Chugh, A.; Scharf, C.; Tada, H.; Hall, B.; Cheung, P.; Pelosi, F.; Knight, B.P.; Morady, F. Role of the coronary sinus in maintenance of atrial fibrillation. *J. Cardiovasc. Electrophysiol.* **2003**, *14*, 1329–1336. https://doi.org/10.1046/j.1540-8167.2003.03222.x.

75. Di Marco, L.Y.; Raine, D.; Bourke, J.P.; Langley, P. Characteristics of atrial fibrillation cycle length predict restoration of sinus rhythm by catheter ablation. *Heart Rhythm* **2013**, *10*, 1303–1310. https://doi.org/10.1016/j.hrthm.2013.06.007.

76. Misek, J.; Belyaev, I.; Jakusova, V.; Tonhajzerova, I.; Barabas, J.; Jakus, J. Heart rate variability affected by radiofrequency electromagnetic field in adolescent students. *Bioelectromagnetics* **2018**, *39*, 277–288. https://doi.org/10.1002/bem.22115.

77. Misek, J.; Veternik, M.; Tonhajzerova, I.; Jakusova, V.; Janousek, L.; Jakus, J. Radiofrequency Electromagnetic Field Affects Heart Rate Variability in Rabbits. *Physiol. Res.* **2020**, *69*, 633–643. https://doi.org/10.33549/physiolres.934425.

78. Ortigosa, N.; Ayala, G.; Cano, Ó. Variation of P-wave indices in paroxysmal atrial fibrillation patients before and after catheter ablation. *Biomed. Signal Process. Control* **2021**, *66*, 102500. https://doi.org/10.1016/j.bspc.2021.102500.

79. McCann, A.; Vesin, J.M.; Pruvot, E.; Roten, L.; Sticherling, C.; Luca, A. ECG-Based Indices to Characterize Persistent Atrial Fibrillation Before and During Stepwise Catheter Ablation. *Front. Physiol.* **2021**, *12*, 654053. https://doi.org/10.3389/fphys.2021.654053.

80. Knecht, S.; Pradella, M.; Reichlin, T.; Mühl, A.; Bossard, M.; Stieltjes, B.; Conen, D.; Bremerich, J.; Osswald, S.; Kühne, M.; et al. Left atrial anatomy, atrial fibrillation burden, and P-wave duration—Relationships and predictors for single-procedure success after pulmonary vein isolation. *EP Eur.* **2018**, *20*, 271–278. https://doi.org/10.1093/europace/euw376.

Article

The Relevance of Heart Rate Fluctuation when Evaluating Atrial Substrate Electrical Features in Catheter Ablation of Paroxysmal Atrial Fibrillation

Aikaterini Vraka[1] , **José Moreno-Arribas**[2] , **Juan M. Gracia-Baena**[3] , **Fernando Hornero**[3]
Raúl Alcaraz [4] **and José J. Rieta** [1,*]

[1]   BioMIT.org, Electronic Engineering Department, Universitat Politecnica de Valencia, 46022 Valencia, Spain;
      aivra@upv.es; jjrieta@upv.es
[2]   Cardiology Department, Saint John's University Hospital, 03550 Alicante, Spain; jomoreno@gmail.com
[3]   Cardiovascular Surgery Department, Hospital Clínico Universitario de Valencia, 46010 Valencia, Spain;
      gracia_juabae@gva.es ; hornero_fer@gva.es
[4]   Research Group in Electronic, Biomedical and Telecommunication Engineering, University of Castilla-La
      Mancha, 16071 Cuenca, Spain; raul.alcaraz@uclm.es
[*]   Correspondence: jjrieta@upv.es

Abstract: Coronary sinus (CS) catheterization is critical during catheter ablation (CA) of atrial fibrillation (AF). However, the association of CS electrical activity with atrial substrate modification has been barely investigated and mostly limited to analyses during AF. In sinus rhythm (SR), atrial substrate modification is principally assessed at a global level through P-wave analysis. Cross-correlating CS electrograms (EGMs) and P-waves' features could potentiate the understanding of AF mechanisms. Five-minute surface lead II and bipolar CS recordings before, during, and after CA were acquired from 40 paroxysmal AF patients. Features related to duration, amplitude, and heart-rate variability of atrial activations were evaluated. Heart-rate adjustment (HRA) was applied. Correlations between each P-wave and CS local activation wave (LAW) feature were computed with cross-quadratic sample entropy (CQSE), Pearson correlation (PC), and linear regression (LR) with 10-fold cross-validation. The effect of CA between different ablation steps was compared with PC. Linear correlations: poor to mediocre before HRA for analysis at each P-wave/LAW (PC: max. + 18.36%, p = 0.0017, LR: max. + 5.33%, p = 0.0002) and comparison between two ablation steps (max. + 54.07%, p = 0.0205). HRA significantly enhanced these relationships, especially in duration (P-wave/LAW: + 43.82% to + 69.91%, p < 0.0001 for PC and + 18.97% to + 47.25%, p < 0.0001 for LR, CA effect: + 53.90% to + 85.72%, p < 0.0210). CQSE reported negligent correlations (0.6 –1.2). Direct analysis of CS features is unreliable to evaluate atrial substrate modification due to CA. HRA substantially solves this problem, potentiating correlation with P-wave features. Hence, its application is highly recommended.

Keywords: atrial fibrillation; catheter ablation; coronary sinus; P-waves; correlation; atrial substrate; invasive recordings; heart-rate adjustment

1. Introduction

With a prevalence higher than 37 million people worldwide, significant mortality rates, and economic burden, atrial fibrillation (AF) is not only just the most common cardiac arrhythmia, but also a multifactorial threat [1,2]. AF can be classified as a function of its spontaneous termination into two different types: paroxysmal and non-paroxysmal. The former includes AF episodes spontaneously terminating in less than 7 days, while the latter includes AF episodes unable to terminate within 7 days without intervention [2]. Pulmonary veins (PVs) are the principal AF foci, and their catheter ablation (CA) is the cornerstone of AF treatment, especially successful in paroxysmal AF cases [2–5]. Despite the high success rates of the CA of PVs, AF recurrence is not an unusual phenomenon,

especially in persistent AF patients. While early recurrence is mostly associated with PV reconnection, late recurrence may be an indicator of the existence of non-PV triggers [6].

One of the keys to understanding the AF mechanisms and deciding the therapy and personalized follow-up treatment is the detailed analysis of the atrial substrate, which is defined as any changes in structural, electrical, or functional level that sustain the AF activity, also known as atrial remodeling [2]. Although it is not necessary for all of the aforementioned alterations to be present, there is a substantial association between them [7–9]. A successful CA outcome involves a sufficient atrial substrate modification, which implies the interception of the mechanisms favoring the AF perpetuation due to the isolation of the PVs. As in the case of atrial remodeling, substrate modification can happen at three levels: structural, electrical, or functional. Since structural changes are connected with the anatomical alteration of the atria, a blanking period of 3 months is typically used in order to safely assess the structural substrate modification [7,10]. Although electrical and functional—related to freedom from AF—modification have been observed as early as one day after CA, electrical substrate modification can in fact be observed even earlier, immediately after the CA procedure [11–13].

During CA, one or more atrial structures are chosen as a reference, and recordings from a stationary catheter are acquired throughout the procedure [14,15]. The coronary sinus (CS) is the most common reference, as it forms an interatrial electrical bridge and can initiate or propagate the AF activity [16–20]. CS catheterization allows the mapping of the entire atria. CS pacing can induce AF, and depending on the CS channels where pacing has been performed, triggers in the left (LA) or right atrium (RA), as well as in the CS musculature can be detected [21–23]. Nevertheless, variable CS anatomy and vivid cardiac contraction can complicate the CS cannulation procedure, and the selection of the proper CS channel for analysis should be performed with caution and may differ for recordings in AF or in sinus rhythm (SR). Recently, a study alerted the risk of high noise prevalence in recordings from the distal tip of the CS catheter during SR [13].

The pivotal role of CS not only in AF initiation or perpetuation, but also in AF mapping has led to the further investigation into the clinical information that can be acquired from the CS electrograms (EGMs). During AF, the analysis of the dominant frequency (DF) or complexity of CS EGMs from PV and non-PV CA has been quite fruitful in predicting the AF recurrence [24–26]. Additionally, DF in CS EGMs has been recruited in order to define the endpoint for the CA of PVs and complex EGMs [27]. The existence of complex EGMs in CS has also been associated with AF prevalence [28]. Despite the high interest in CS EGMs during AF, little or no attention has been paid to CS function during SR and its modification after CA procedures. Prolonged conduction time measured between EGMs from RA and CS in recordings acquired before CA of PVs and complex EGMs has shown high predictive power for atrial tachyarrhythmia occurrence [29]. Moreover, in CA of atrial flutter, fractionation in the EGMs of CS can predict the incidence of AF [30].

Although they present interesting findings, studies focused on the CS analysis during SR are few and mainly involve additional CA applications. Nevertheless, the CS function during CA of PVs only, as well as the alterations that may be provoked by the CA are yet to be discovered. Given the high significance of CS for the CA procedure and the fact that CS EGMs provide information at a local level, an analysis focusing on the CS during the CA of PVs and how the CA procedure modifies its function could potentiate the perception on the AF mechanisms during SR. Any important findings could be recruited along with already established methods in order to provide a new perspective into the AF analysis. The wide availability of CS recordings from CA sessions makes the investigation of this assumption quite feasible. However, the lack of major analyses that could serve as a reference for the observation of the CS function alteration raise the need for alternative studies that are vastly applied to investigate the atrial substrate modification.

During the CA procedure, electrocardiogram (ECG) recordings from the skin surface are simultaneously acquired along with the recordings from the intracardiac catheters and are vastly used to observe the atrial substrate modification. In CA sessions performed under SR, analysis is mainly focused on either of two parameters: P-waves or heart-rate

variability (HRV). The P-wave is the ECG part that represents the atrial depolarization [31]. Hence, P-wave variations after CA reflect changes in the atrial contractility. Many studies have revealed the capability of P-wave parameters such as P-wave duration, amplitude, as well as the frequency domain analysis of assessing the CA outcome [32–39]. P-wave duration is probably the most relevant feature, as it measures the duration of the atrial depolarization [40]. The rationale behind P-wave duration analysis is that the P-wave duration values come as a function of the anatomical abnormalities assisting the AF propagation and that the P-wave shortening, especially occurring in the left atrial P-wave part, is indicative in the freedom from AF after the CA procedure [36,38,41–43].

Being a measure of calibration between the sympathetic and parasympathetic nervous systems [44], HRV is the other popular evaluator of CA outcome [45,46]. It can be assessed by the variation between successive R-R intervals, high- and low-frequency analysis or Lyapunov exponents and Kolmogorov entropy, among other methods [44,47]. The reduction of HRV after radiofrequency (RF) CA is a natural, albeit temporary, side effect of the CA procedure that is gradually restored over time [48] and can predict AF recurrence [49]. The main mechanisms causing HRV reduction are the RF energy emitted in the PV tissue, stimulating the sympathetic nerve fibers and causing temporal parasympathetic nervous system withdrawal [48]. Recently, it was demonstrated that high parasympathetic tone after cryoballoon CA is also connected with AF recurrence [50].

Despite the high significance of P-waves and HRV analysis for atrial substrate modification evaluation after the CA of PVs, these parameters provide information on the global atrial substrate modification or the ventricular response, in the case of HRV. However, how critical structures are affected by the CA procedure is yet to be discovered. Constant pacing of CS for AF mapping may alter its functionality. Whether and to what extent this is reflected in the conventional substrate modification assessment techniques remain unknown. The aim of the current study is to investigate this presumption. For this purpose, any possible linear or nonlinear correlations between ECG and CS recordings are explored in order to provide new insights into the pathophysiological AF mechanisms during SR and their interaction with the most popular AF treatment, CA.

The remainder is organized as follows. The database and analysis methods are presented in Section 2, where also the statistical analysis is explained. Results are shown in Section 3, and they are further analyzed in Section 4, where relevant work is also described. The manuscript is completed with the conclusions presented in Section 5.

2. Methods

Recordings of 40 paroxysmal AF patients undergoing the RFCA of PVs for the first time were employed. Isolation was performed by creating lesions surrounding each PV side (left or right), guided by 3D electroanatomical mapping. The procedure started with the RFCA of the left PVs, followed by the RFCA of the right PVs. Whenever tricuspid isthmus (TCI) block was observed, TCI isolation was performed following RFCA. The endpoint of the procedure was bi-directional electrical isolation of all pulmonary veins after adenosine administration. Recordings from a standard 12-lead electrocardiogram (ECG) and a decapolar CS catheter with a sampling frequency of 1 kHz were acquired by a Labsystem™ PRO EP recording system (Boston Scientific, Marlborough, MA, USA) for five minutes before, during, and after the CA procedure. Recordings during the CA procedure were acquired after the isolation of left pulmonary veins (LPVI). P-wave analysis was performed using recordings from lead II, while the channel of bipolar CS recordings with the least fluctuations and the highest amplitude was selected for the CS analysis. This channel varied among patients, but was always the same for one patient at all three time points from which the recordings were obtained. In case all channels showed a high amplitude and clear signals, medial or mid-proximal channels were selected [13].

2.1. Preprocessing

ECG preprocessing contained the removal of power-line interference, high-frequency muscle noise, and baseline wander [51,52]. Ectopic beats were present in some of the

recordings, with a maximum prevalence of 4% of total beats. Ectopic beat removal contained the ectopic detection, cancellation, and replacement by linear interpolation [53,54]. After ectopics removal, P-waves were detected and delineated [55,56].

CS recordings' preprocessing started with denoising, mean removal, and cancellation of ventricular activity, if present, by an adaptive cancellation method [57,58]. Afterwards, local activation waves (LAWs) were detected and delineated [59,60]. Delineation was then inspected and corrected by two experts for both invasive and surface recordings.

2.2. Data Analysis

After P-wave and LAW detection, the following features were calculated at each activation for both P-waves and LAWs and then averaged over each recording:

- *Duration:* Once delineated, the interval between the onset and offset of each activation was considered as its duration.
- *Amplitude:* Maximum (Amp_{max}) and peak-to-peak (PP) amplitudes. For ECGs, P-wave Amp_{max} and PP concur, since P-waves in lead II are positive. The root mean square (RMS) is the quadratic mean of the function that defines each activation.
- *Area:* Area of the positive parts of the signal ($PosAr$), calculated by the integration over the time interval of the amplitude of each activation with the trapezoidal method.
- *Slope rate:* Increasing or decreasing rhythm at 5%, 10%, 20% of total duration of each P-wave/LAW, as well as at its maximum point, calculated as:

$$S_i = \frac{Amp(i) - Amp(onset)}{t_i - t_{onset}}, \tag{1}$$

where $Amp(i)$ is the amplitude at $i = 5$, 10, 20% or the peak of the activation, $Amp(onset)$ is the amplitude at the onset, and t_i and t_{onset} are the sample points at $i = 5$, 10, 20% or the peak and the onset, respectively. *Slope rate* is always positive for P-waves, as their peaks always present a positive amplitude. For LAWs, *slope rate* can be negative as well.

Since the analysis of the present study is focused on atrial activations, HRV analysis was calculated by measuring successive P-wave or LAW intervals. Hence, it will be referred to in the remainder of the manuscript as atrial rate variability (ARV). ARV was calculated across each surface and invasive recording analyzing the standard deviation of the normal-to-normal P-wave or LAW interval ($SDNN$), the variance of normal-to-normal P-wave or LAW interval ($VARNN$), and the RMS of successive differences ($RMSSD$) between two P-waves or LAWs [44].

In order to compensate for the effect of fluctuations in heart rate (HR) on several features [61], an HR adjustment (HRA) was performed by scaling them by the following factor:

$$sf_i = \frac{1000}{IBI_i}, \tag{2}$$

where IBI_i is the inter-beat interval between the ith and the $(i-1)^{th}$ activations. HRA was used to scale *Duration* (**HRA**($Duration$)) and *Area* (**HRA**($PosAr$)) and scale inversely *Slope rate* (**HRA**(S_i)).

2.3. Statistical Analysis

Any possible linear or nonlinear relationships between P-waves and CS LAWs were investigated. Linear correlations between each P-wave and CS LAW of every recording were assessed with Pearson's correlation and linear regression with 10-fold cross-validation, and nonlinear relationships were assessed with cross-quadratic sample entropy (CQSE). An example of how linear correlations between each P-wave and CS LAW were calculated can be seen in Figure 1a. As ARV features are calculated across each recording and do not correspond to activation-based analysis, they were excluded from this step.
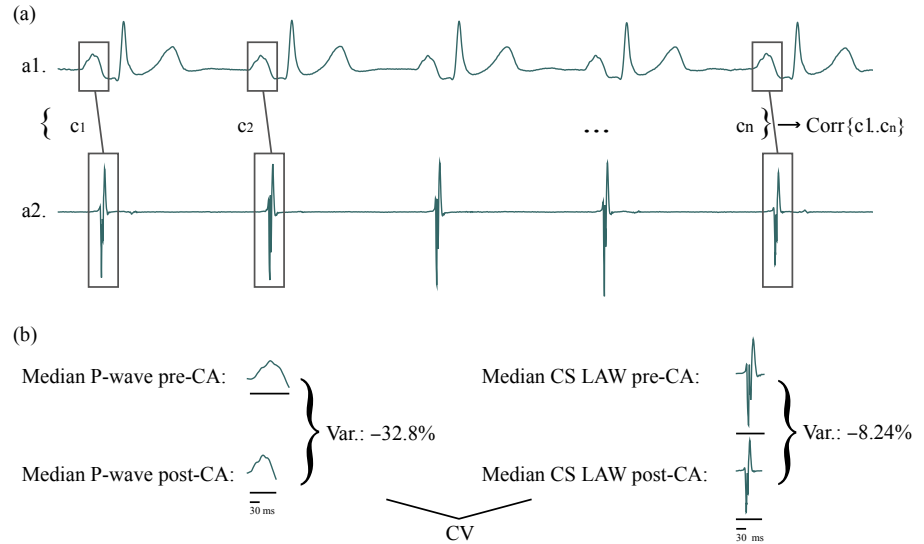
Figure 1. (**a**) Representation of how correlations between features of each P-wave (a1) and CS LAW (a2) of one patient are computed. (**b**) CV of the same patient, example shown for *Duration*, for recordings before and after CA. Variation due to CA in *Duration* is calculated for surface (left) and invasive (right) recordings. Correlation between the surface and invasive variations is then calculated across the entire patient cohort. CS: coronary sinus; LAW: local activation wave; CV: correlation of variation; CA: catheter ablation.

Correlation of CA-induced variation (CV) between P-wave and CS LAW features including ARV was investigated by Pearson's correlation, which performs a bidirectional comparison. This step allows the comparison between the effect that CA had on CS function and the effect that CA had on the entire atria. For each patient and each feature, the CA-induced variation was the percentage of alteration, calculated as the median value after CA with respect to the median value before CA:

$$\text{CV} = \left(\frac{value\_after}{value\_before} - 1\right) \times 100 \ (\%).\tag{3}$$

Figure 1b shows an example of how CV is calculated. The normality of the results was tested with the Shapiro–Wilk test, and final correlations are expressed as medians, as the values did not follow a normal distribution [62].

Linear regression can only assess the one-way relationship between a dependent variable a and one or more independent variables $b_1, b_2, \cdots, b_n$, where n is the number of independent variables or predictors. Linear regression with only one independent variable b is called simple linear regression, and the equation describing it is the following [63]:

$$a = \beta_0 + \beta_1 \times b + \epsilon,\tag{4}$$

where β_0 is the intercept, β_1 is the gradient or regression coefficient, and ϵ is the random error, normally distributed for simple linear regression models. In that case, the null hypothesis for β_1 comes from the t-test and is therefore the same whether a is the dependent or the independent variable. Regression analysis can provide various coefficients that can be further processed or used directly in order to evaluate the accuracy of the model. As the aim of this analysis is the calculation of the correlation between surface and invasive recordings, the coefficient of determination (R^2-*adjusted*) was recruited.

The conventional coefficient of determination (R^2) describes how well the data fit the regression model and is expressed as a percentage, where 0% indicates that the dependent variable is not related at all to the built model, while 100% shows an absolute concordance between the dependent variable and the model. R^2-*adjusted* additionally adjusts for the number of terms that are added to the model in a way that only the predictors that really affect the dependent variable are considered, thus resulting in a more unbiased result. R^2-*adjusted* is always equal to or less than R^2.

In general, cross-entropies allow the comparison between two time-series of different origins [64,65]. They are used to evaluate dynamic changes between two series and observe any similarities they may have. For this analysis, CQSE was chosen as an enhanced version of cross-sample entropy, allowing the tolerance r to vary in order to achieve better conditional probability estimates [66].

Any bias due to discrepancies in the values of the time-series should be removed before performing the CQSE [65]. This is achieved by normalizing each time-series as follows:

$$x'(i) = \frac{x(i) - \bar{x}}{std(x)},$$

(5)

where $x'(i)$ is the $i - th$ sample of N-length time-series $X = \{X(1), X(2), \dots, X(N)\}$, $\bar{x}$ is the mean value, and std is the standard deviation.

Details about the computation of CQSE can be found elsewhere [65,66]. In brief, given two time-series $X = \{X(1), X(2), \cdots, X(N)\}$ and $Y = \{Y(1), Y(2), \cdots, Y(M)\}$ of length N and M, respectively, the probability that X_i^m patterns of length m are similar to Y_j^m patterns with a tolerance r is

$$A^m(r) = \frac{1}{N-m} \times \sum_{i=1}^{N-m} \left[\frac{1}{M-m} \sum_{j=1}^{M-m} \times \Theta(r - d_{ij}^m) \right],$$

(6)

where Θ is the Heaviside function and d_{ij}^m the distance between X_i^m and Y_j^m.

Respectively, for a template of length $m + 1$, the probability that two patterns X_i^{m+1} and Y_j^{m+1} are similar is the following:

$$A^{m+1}(r) = \frac{1}{N-m-1} \times \sum_{i=1}^{N-m-1} \left[\frac{1}{M-m-1} \sum_{j=1}^{M-m-1} \times \Theta(r - d_{ij}^{m+1}) \right].$$

(7)

Then, CQSE is calculated as

$$CQSE(m, r, N, M) = -ln\frac{A^{m+1}(r)}{A^m(r)} + ln(2r).$$

(8)

After multiple iterations, this analysis was performed with $m = 1$ and $r = 0.35$, as these parameters provided the best results.

3. Results

The effect of scaling for HRA on *Duration* can be observed in Figure 2. While *Duration* values between each P-wave and CS LAW do not seem to correlate, when HRA is applied, they seem to follow a more similar pattern (Figure 2a). For the same recording, linear regression notably improves after HRA, and the values seem more coherent (Figure 2b).
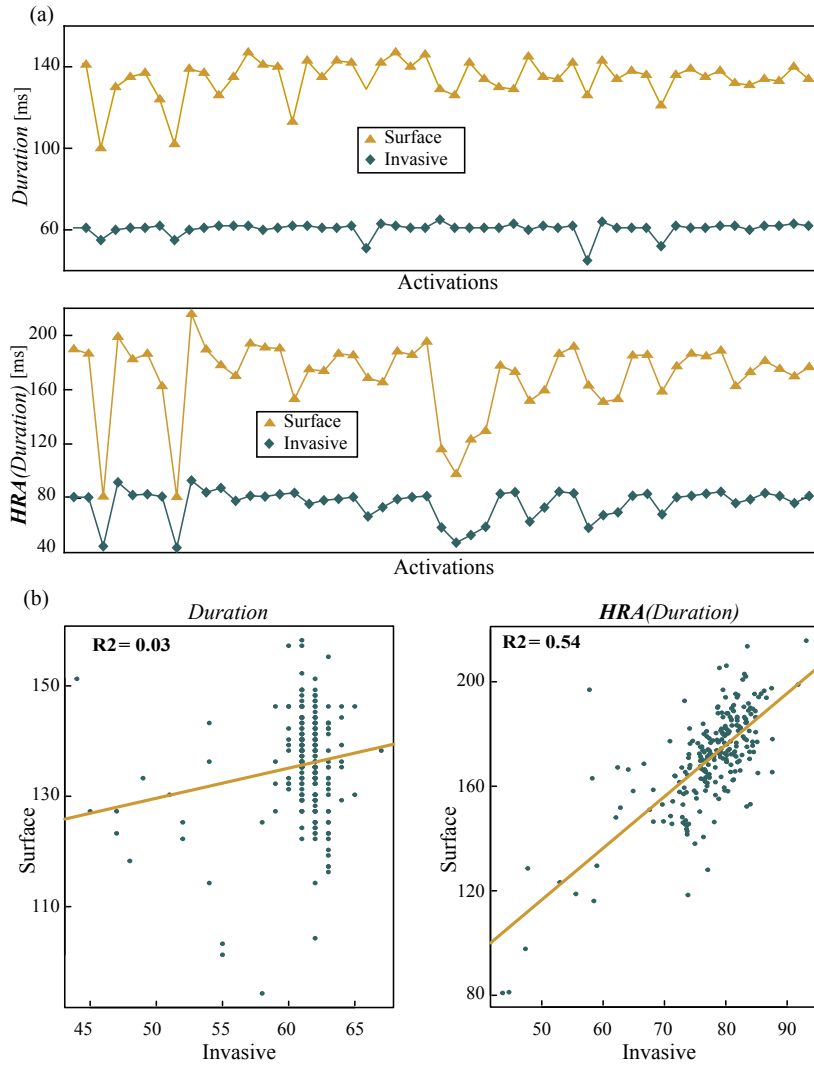
Figure 2. Example of how HRA affects the correlation of the computed features. (**a**) Time instance of 50 activations for the correlation of *Duration*, unprocessed (top) and after HRA (bottom). (**b**) Linear regression of the same recording before (left) and after (right) HRA. Linear correlation increased from $R^2 = 0.03$ to $R^2 = 0.54$. HRA: heart-rate adjustment.

3.1. Linear Analysis

The results of Pearson correlation when each P-wave were compared with the corresponding LAW (P-wave/LAW analysis) by Pearson's correlation, as illustrated in Figure 3 and shown further in detail in Table 1. *Amplitude* and *Area* features showed low positive and negative statistically significant correlations (-3.92% to $+18.36\%$, $p < 0.0142$) regardless of the observation point (recordings before, during, or after CA). S_{max} also showed a negligent positive correlation in recordings before and during CA. No statistically significant correlations were found for the remaining features.
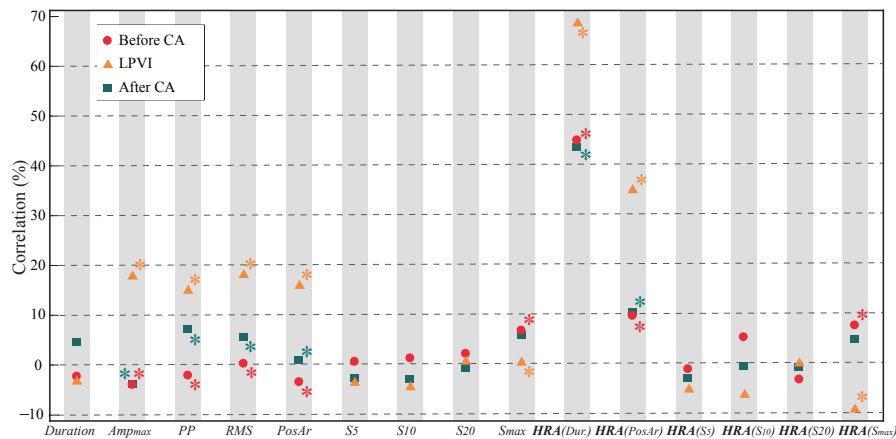
Figure 3. Pearson correlation between surface and invasive features of each activation, measured before CA (red), after LPVI or during CA (green), and after the end of the CA procedure (blue). Statistically significant results are marked with an asterisk ($*$).

Table 1. Correlations (%) and p values for Pearson analysis between surface and invasive features for each and every activation. Statistically significant results are shown in **bold**. LPVI: left pulmonary vein isolation; PP: peak-to-peak amplitude; RMS: root mean square; S_i: *Slope rate* at i% of *Duration*.

| Feature | $\mathbf{Corr_{pre}}$ | | $\mathbf{Corr_{LPVI}}$ | | $\mathbf{Corr_{post}}$ | |
	ρ [%]	p value	ρ [%]	p value	ρ [%]	p value
Duration	-2.19	0.1291	-3.08	0.1040	4.53	0.2221
Amp_{max}	$\mathbf{-3.87}$	**0.0001**	**18.05**	**0.0001**	$\mathbf{-3.92}$	**0.0001**
PP	$\mathbf{-1.98}$	**0.0090**	**15.19**	**0.0033**	**7.26**	**0.0016**
RMS	**0.38**	**0.0019**	**18.36**	**0.0017**	**5.46**	**0.0142**
PosAr	$\mathbf{-3.30}$	**0.0032**	**16.18**	**0.0015**	**0.99**	**0.0142**
S_5	0.76	0.4283	-3.93	0.1863	-2.59	0.2170
S_{10}	1.47	0.2359	-4.15	0.3062	-2.82	0.2923
S_{20}	2.38	0.0839	0.97	0.3927	-0.64	0.1426
S_{max}	**7.05**	**0.0066**	**0.71**	**0.0114**	5.96	0.1300
HRA(*Duration*)	**45.25**	**< 0.0001**	**69.91**	**< 0.0001**	**43.82**	**< 0.0001**
HRA(*PosAr*)	**10.00**	**0.0142**	**35.40**	**< 0.0001**	**10.66**	**0.0425**
HRA(S_5)	-0.70	0.2707	-4.84	0.0703	-2.55	0.2249
HRA(S_{10})	5.71	0.2337	-5.68	0.1593	-0.13	0.1738
HRA(S_{20})	-2.78	0.1431	0.60	0.0843	-0.44	0.1187
HRA(S_{max})	**8.09**	**< 0.0001**	$\mathbf{-8.65}$	**0.0091**	5.21	0.1623

After HRA, **HRA**(*Duration*) showed a notably higher correlation ($+43.82$% to $+69.91$%, $p < 0.0001$). The correlation between **HRA**(*Area*) of each P-wave and LAW also increased, still showing low values ($+10.00$% to $+35.40$%, $p \leq 0.0425$). The effect of scaling on S_{max} was minor, with correlations either remaining almost the same or becoming negative ($+0.71$%, $p = 0.0114$ for non-HRA versus -8.65%, $p = 0.0091$ for HRA in recordings during CA).

When LR analysis was performed, statistical power remained the same for each feature as in Pearson correlation analysis. Nonetheless, correlations became weaker due to cross-validation. The effect of HRA was also present, converting *Duration* from low and statistically insignificant ($+0.22$% to $+0.69$%, $p < 0.2221$) to low or moderate and statistically significant ($+18.97$% to $+47.25$%, $p < 0.0001$) for **HRA**(*Duration*), as can be observed in Table 2. In both Pearson's correlation and LR, features reached higher concordance during CA (after LPVI), especially after HRA.

Table 2. Linear regression analysis results between surface and invasive features for each and every activation. Statistically significant results are shown in **bold**.

Feature	Pre-CA R^2-adj[%]	Pre-CA p value	LPVI R^2-adj[%]	LPVI p value	Post-CA R^2-adj[%]	Post-CA p value
Duration	0.56	0.1291	0.69	0.1040	0.22	0.2221
Amp_{max}	**2.68**	**0.0100**	**4.27**	**0.0001**	**2.12**	**0.0094**
PP	**2.12**	**0.0090**	**2.34**	**0.0033**	**3.49**	**0.0016**
RMS	**5.33**	**0.0019**	**3.60**	**0.0017**	**4.12**	**0.0142**
PosAr	**2.94**	**0.0032**	**3.24**	**0.0015**	**1.40**	**0.0148**
S_5	0.12	0.4283	0.32	0.1863	0.20	0.2170
S_{10}	0.17	0.2359	0.02	0.3062	0.05	0.2923
S_{20}	0.61	0.0840	0.09	0.3927	0.38	0.1426
S_{max}	**2.07**	**0.0066**	**1.98**	**0.0114**	0.52	0.1300
HRA(*Duration*)	**20.32**	**< 0.0001**	**47.25**	**< 0.0001**	**18.97**	**< 0.0001**
HRA(*PosAr*)	**1.90**	**0.0142**	**12.22**	**< 0.0001**	**1.03**	**0.0425**
HRA(S_5)	0.72	0.2707	0.86	0.0703	0.18	0.2249
HRA(S_{10})	0.14	0.2337	0.43	0.1593	0.24	0.1739
HRA(S_{20})	0.47	0.1431	0.78	0.0843	0.47	0.1187
HRA(S_{max})	**7.65**	**< 0.0001**	**2.11**	**0.0091**	0.38	0.1623

CV between P-waves and LAWs can be seen in Figure 4 and Table 3. Before HRA, only *RMS* (+54.07%, $p = 0.0205$) at the third transition, measuring the difference in features between the end of LPVI and the end of CA and S_{10} (+26.29%, $p = 0.0009$) at the first transition, measuring the difference in features between the beginning of CA and the end of LPVI, showed small to moderate correlations. In this case as well, HRA enhanced this effect for **HRA**(S_{10}) (+73.23%, $p = 0.0055$) and additionally revealed a moderate to high CV for **HRA**(*Duration*) (+53.90% to +85.72%, $p < 0.0210$). The effect of CA in ARV was quite similar for P-waves and LAWs, as can be observed from the moderate to high CV that they showed (+48.33% to +94.20%, $p < 0.0422$). While the effect of LPVI seemed to affect in a more similar way the activation-based features and especially **HRA**(*Duration*) of P-waves and LAWs, CV for ARV features was notably lower after LPVI, lacking statistical significance in most of the cases.
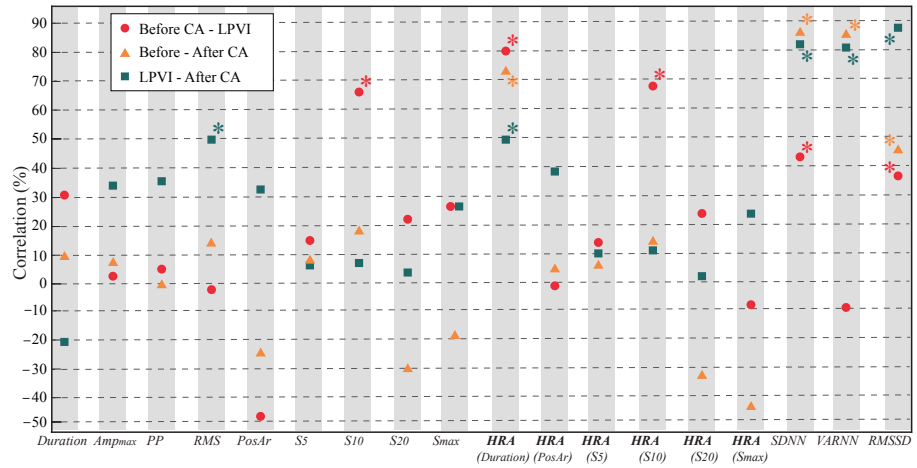
Figure 4. Pearson correlation between surface and invasive features for the variation measured between the recordings before CA and after LPVI (red), before the beginning and after the end of the CA procedure (orange), and after LPVI and after the end of the CA procedure (green). Statistically significant results are marked with asterisk (∗).

Table 3. Pearson's correlations (%) and p values between LAWs and P-waves for CV measured every two ablation steps. Statistically significant results are shown in **bold**. CV: correlation of variation.

Feature	$\mathbf{CV_{pre\ CA-LPVI}}$		$\mathbf{CV_{pre-post\ CA}}$		$\mathbf{CV_{LPVI-post}}$	
	ρ [%]	p value	ρ [%]	p value	ρ [%]	p value
Duration	34.82	0.1567	13.31	0.5984	-17.58	0.4854
Amp_{max}	6.16	0.8081	11.40	0.6253	38.24	0.1173
PP	8.67	0.7326	3.56	0.8885	39.20	0.1077
RMS	1.41	0.9556	18.28	0.4679	**54.07**	**0.0205**
PosAr	-43.37	0.0722	-20.56	0.4131	36.60	0.1352
S_5	18.78	0.4555	11.53	0.6486	10.31	0.6840
S_{10}	**26.29**	**0.0009**	22.54	0.3684	10.44	0.6803
S_{20}	26.29	0.2919	-26.10	0.2955	7.77	0.7593
S_{max}	-14.36	0.5690	-14.37	0.5695	31.11	0.2089
HRA(*Duration*)	85.72	< 0.0001	78.89	< 0.0001	53.90	0.0210
HRA(*PosAr*)	2.76	0.9135	9.01	0.7220	42.64	0.0776
HRA(S_5)	17.84	0.4788	10.33	0.6835	13.94	0.5811
HRA(S_{10})	73.23	0.0055	18.91	0.4523	15.06	0.5508
HRA(S_{20})	28.33	0.2546	-28.46	0.2523	5.88	0.8167
HRA(S_{max})	-3.91	0.8776	-39.45	0.1052	28.70	0.2482
SDNN	48.33	0.0422	92.75	< 0.0001	89.15	< 0.0001
VARNN	17.44	0.4883	92.23	< 0.0001	86.63	< 0.0001
RMSSD	42.12	0.0817	51.23	0.0297	94.20	< 0.0001

3.2. Nonlinear Analysis

The scatterplot of Figure 5 shows median CQSE values for all features of each recording. From the box and whiskers plot of the same figure, it can be seen that the median values are found in the range from about 0.6 to 1.2, a fact that does not suggest strong nonlinear relationships between surface and invasive features. Unlike linear analysis, scaling for HR compensation did not improve the nonlinear relationships.
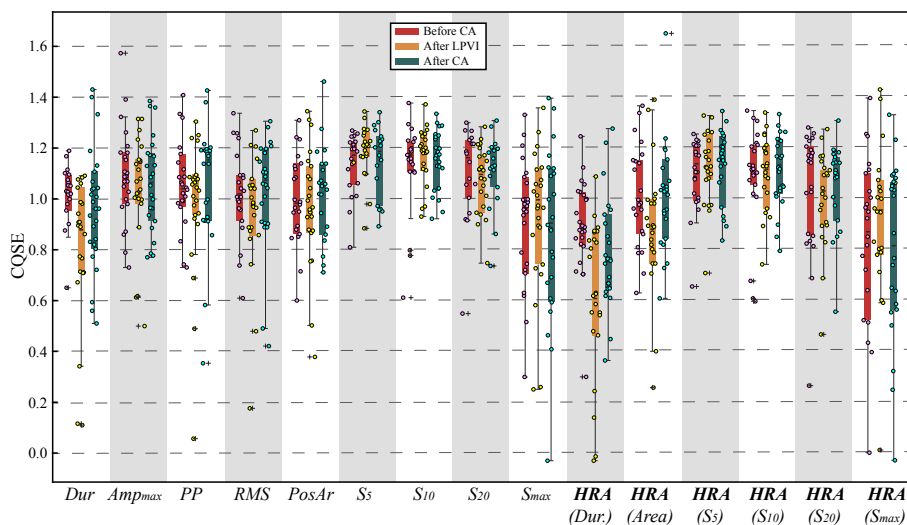
Figure 5. Combined box and whiskers plot with scatterplot for CQSE between surface and invasive features before (left), after LPVI (centre), and after full CA (right). *Dur*: Duration.

4. Discussion

Invasive EGM analysis is at the frontline of atrial substrate evaluation, assisting the detection of areas with structural remodeling [7,10]. During AF, these areas are specified as areas with a high dominant frequency and low-voltage EGMs or areas with highly complex EGMs, and various techniques have been developed to facilitate their detection as possible

non-PV ablation targets [7,67,68]. During SR, the detection of areas sustaining the AF activity is achieved with the help of specific atrial sites that are used for pacing [10,14]. CS is the principal atrial site used for this purpose, allowing the detection of non-PV triggers spanning throughout the atria, while it has also been the object of non-PV CA, as it can trigger or sustain AF [14,16,22,23].

Considering the pivotal role of CS in AF perpetuation, as well as in AF mapping during CA procedures, more concrete knowledge on CS function and how it is affected by CA allows a different perspective on the atrial substrate modification due to the CA of AF. At the same time, given the popularity and effectiveness of P-waves and HRV in the atrial substrate modification analysis, correlating CS LAWs with P-waves acquired from ECGs allows a direct comparison with one of the most established methods in assessing the substrate modification. This was the original objective of the present study. For this purpose, recordings before, during, and after CA were acquired.

Before HRA, correlations found either between each P-wave and CS LAW or between lead II and CS recordings, when the correlation of CA-induced variations was assessed, were mainly loose and observed when *Amplitude*, *Area*, or *Slope rate* features were analyzed. Therefore, in SR, any attempt to observe the P-waves' evolution through CS recordings or vice versa would lead to the loss of information. The effect of each CA step on P-waves and CS LAWs was not similar either. Nonlinear analysis also failed to detect any strong relationships between P-waves and CS LAWs. Despite the important role of CS in CA, the aforementioned findings suggest that it functions in a way that is different than that observed from the P-waves, which refer to the entire atria.

Although no significant correlations between P-wave and CS LAW features were detected, the present study led to an interesting revelation. Recordings after LPVI were acquired while RF energy was being emitted to PVs, possibly affecting the functionality of the atria. At the same time, RF energy was proven to affect the autonomous nervous system both during and after RFCA, in a different way [48,69,70]. During RF energy application, HR is decreased and HRV is increased. HRV incrementation implies a possible masking of the correlation in *Duration* between surface and invasive recordings, which should be unmasked after HRA. Indeed, although in all cases, HRA had a significant effect in the correlation of *Duration*, comparison after LPVI especially benefited from the application of HRA to the analyzed features. As CS is closer to the tissue under ablation, it is quite possible that HRV is more intense in CS recordings, being responsible for the low and negative correlations observed before HRA.

When assessing the correlation of the effect of each CA step between P-wave and CS LAW features, LPVI was once more the critical step that affected the variation of *Duration* in a more similar way. In our case, ARV was measured from time-domain HRV analysis on the atrial instead of ventricular activations of lead II and CS recordings in order to focus on the atrial rate and its fluctuations along the procedure. Unlike activation-based features, higher discrepancies between the ARV of surface and invasive recordings were observed after LPVI with respect to the remaining CA steps. This observation corroborates the theory of the different and probably more prominent effect of RF energy on CS function, manifested by the difference in ARV between the surface and invasive recordings during RF exposure and explains the significant role of HRA in potentiating the correlation of *Duration*. It should also be noted that although not highly correlated, the effect of CA on the *Duration* of P-wave and LAWs after HRA is similar. After the end of the procedure, ARV correlation between surface and invasive recordings notably increased. Previous studies reported temporary autonomous nervous system impairment as a consequence of RFCA manifested by decreased HRV [48,49]. This effect may also explain the high correlation of ARV features after the CA procedure in the present study.

As already mentioned, scaling in order to compensate for the HR variations had a major effect on linear analysis results regarding *Area* and *Duration* features. Moderate or moderate to high correlations were revealed for the latter, reaching up to 85.72% of concordance regarding the effect of LPVI on P-wave and CS LAW **HRA**(*Duration*). These correlations were hidden by the variable HR observed across the recordings due to the

effect of RF applications [61,71]. Although correlation levels between P-wave and CS LAW *Duration* even after scaling do not imply an absolute tuning, it would be impossible to appreciate the similarity degree without this adjustment. As P-wave *Duration* is probably one of the most highlighted atrial electrical characteristics recruited to assess atrial substrate modification [33,36,41,42,72], the unbiased processing of this feature is of high importance. Therefore, studies combining the analysis of surface and invasive recordings acquired during SR are highly suggested to apply scaling techniques in order to achieve more robust results.

In AF research, the correlation between surface and invasive recordings has been primarily performed in order to verify the reliability of noninvasive methods in describing or mapping the atrial substrate [73]. Nonetheless, some of them report interesting findings regarding the association between parameters from ECG recordings and invasive EGMs. During SR, correlations have been found between the *Duration* of lead II P-waves and right atrium (RA) LAWs on AF and sick sinus syndrome patients [74]. Nonlinear correlations between RA recordings and recordings from lead II or V1 have also been observed during AF [75]. Finally, the analysis of post-operative recordings of V1 channel and unipolar RA EGMs during AF showed high correlations on f-wave organization and amplitude [76].

Compared to the present study, an essential difference exists in the aforementioned works. The invasive part of the these studies employed recordings from various RA sites, where fibrosis can also be found, versus recordings acquired only from CS in the present study [77]. Given the position of CS between the left atrium (LA), where PVs are found, and the RA, which also contributes to the AF perpetuation, and additionally taking into account the previous works, we would accordingly expect a more direct and robust relationship between CS LAWs and P-waves, which in any case was weak, but not negligent.

A limitation of the present study, which could affect the weak CS LAWs' and P-waves' correlations, is the not very large dataset analyzed. A significantly wider database could reaffirm or, by contrast, vary the findings of the current study. In any case, electrical substrate modification involves multiple atrial sites, expressing atrial alteration in a cumulative way. Therefore, one possible explanation, other than the small dataset, is that substrate alteration is a collective process, and the correlation between P-waves and various atrial sites, one by one, would fail to show significant relationships. Another possible explanation is that specific atrial sites correlate to a higher degree with P-wave behavior, and CS is not one of them. In that case, correlation with more atrial sites should be investigated. Nevertheless, this is a complex procedure, as the catheter placed in the atria is constantly moving and continuous recordings from one site cannot be easily acquired.

5. Conclusions

The lack of very high linear or nonlinear correlations between surface P-waves and invasive CS LAWs may discourage the employment of CS analysis to assess CA-induced changes of atrial function, as well as the possibility to predict the effect of CA from CS LAWs' analysis. However, a scaling technique to mitigate the effect of variable HR has notably potentiated the surface-invasive correlations, and its implementation is suggested in analyses comparing between the characteristics of surface and invasive recordings. For a more detailed and in-depth analysis, the processing of simultaneous recordings both from surface ECG leads and CS EGMs is also encouraged.

Author Contributions: Conceptualisation, A.V., R.A., and J.J.R.; methodology, A.V., R.A., and J.J.R.; software, A.V.; validation, A.V., J.M.-A., J.M.G.-B., F.H., R.A., and J.J.R.; resources, J.M.-A., J.M.G.-B., F.H., and J.J.R.; data curation, A.V., J.M.-A., J.M.G.-B., and F.H.; writing—original draft preparation, A.V.; writing—review and editing, A.V., J.M.-A., J.M.G.-B., F.H., R.A., and J.J.R.; All authors have read and agreed to the published version of the manuscript.

References

1. Virani, S.S.; Alonso, A.; B enjamin, E.J.; Bittencourt, M.S.; C allaway, C.W.; Carson, A.P.; Chamberlain, A.M.; Chang, A.R.; Cheng S; et al. on Epidemiology. Heart Disease and Stroke Statistics 2020 Update: A report from the American Heart Association. **2020**, *141*, e139–e596. doi:10.1161/CIR.0000000000000757.

2. Hindricks, G.; Potpara, T.; Dagres, N.; Arbelo, E.; Bax, J.J.; Blomstro, C.; Boriani, G.; Castella, M.; Dan, G.A.; Dilaveris, P.E.; et al. 2020 ESC Guidelines for the diagnosis and management of atrial fibrillation developed in collaboration with the European Association of Cardio-Thoracic Surgery (EACTS). *Eur. Heart J.* **2020**, *42*, 374–498. doi:10.1093/eurheartj/ehaa612s.

3. Haissaguerre, M.; Jaïs, P.; Shah, D.C.; Takahashi, A.; Hocini, M.; Quiniou, G.; Garrigue, S.; Le Mouroux, A.; Le Métayer, P.; Clémenty, J. Spontaneous initiation of atrial fibrillation by ectopic beats originating in the pulmonary veins. *New Engl. J. Med.* **1998**, *339*, 659–666. doi:10.1056/NEJM199809033391003.

4. Shah, D.; Haïssaguerre, M.; Jaïs, P. Catheter Ablation of Pulmonary Vein Foci for Atrial Fibrillation. *Thorac. Cardiovasc. Surg.* **1999**, *47*, 352–356. doi:10.1055/s-2007-1013198.

5. Oral, H.; Knight, B.; Tada, H. Pulmonary vein isolation for paroxysmal and persistent atrial fibrillation. *ACC Curr. J. Rev. 11*, 2002, 11, 83 https://doi.org/10.1016/S1062-1458(02)00739-0.

6. Cheng, W.H.; Lo, L.W.; Lin, Y.J.; Chang, S.L.; Hu, Y.F.; Hung, Y.; Chung, F.P.; Liao, J.N.; Tuan, T.C.; Chao, T.F.; et al. Ten-year ablation outcomes of patients with paroxysmal atrial fibrillation undergoing pulmonary vein isolation. *Heart Rhythm* **2019**, *16*, 1327–1333. doi:10.1016/j.hrthm.2019.03.028.

7. Lau, D.H.; Linz, D.; Schotten, U.; Mahajan, R.; Sanders, P.; Kalman, J.M. Pathophysiology of Paroxysmal and Persistent Atrial Fibrillation: Rotors, Foci and Fibrosis. *Heart Lung Circ.* **2017**, *26*, 887–893. doi:10.1016/j.hlc.2017.05.119.

8. Thomas, L.; Abhayaratna, W.P. Left Atrial Reverse Remodeling: Mechanisms, Evaluation, and Clinical Significance. *JACC Cardiovasc. Imaging* **2017**, *10*, 65–77. doi:10.1016/j.jcmg.2016.11.003.

9. Knecht, S.; Pradella, M.; Reichlin, T.; Mühl, A.; Bossard, M.; Stieltjes, B.; Conen, D.; Bremerich, J.; Osswald, S.; Kühne, M.; et al. Left atrial anatomy, atrial fibrillation burden, and P-wave duration-relationships and predictors for single-procedure success after pulmonary vein isolation. *EP Eur.* **2018**, *20*, 271–278. doi:10.1093/europace/euw376.

10. Maille, B.; Das, M.; Hussein, A.; Shaw, M.; Chaturvedi, V.; Williams, E.; Morgan, M.; Ronayne, C.; Snowdon, R.L.; Gupta, D. Reverse electrical and structural remodelling of the left atrium occurs early after pulmonary vein isolation for persistent atrial fibrillation. *J. Interv. Card. Electrophysiol.* **2020**, *58*, 9–19. doi:10.1007/s10840-019-00576-1.

11. Wen, S.; Indrabhinduwat, M.; Brady, P.A.; Pislaru, C.; Miller, F.A.; Ammash, N.M.; Nkomo, V.T.; Padang, R.; Pislaru, S.V.; Lin, G. Post Procedural Peak Left Atrial Contraction Strain Predicts Recurrence of Arrhythmia after Catheter Ablation of Atrial Fibrillation. *Cardiovasc. Ultrasound* **2021**, *19*, 22. doi:10.1186/s12947-021-00250-5.

12. Liu, H.T.; Lee., H.L.; Wo, H.T.; Chang, P.C.; Wen, M. S.; Lin, F. C.; Yeh, S., J.; Chou, C. C. P wave duration ≥50 ms P edicts Poor Left A rial Fu ction And Ablation Out omes in Non-paroxysmal Atrial F brillation. J. Electrocardiol. **2021** *69*, 124 131. doi:10.1016/jelectrocard.2021.10.003.

13. Vraka, A.; Bertomeu-González, V.; Fácila, L.; Moreno-Arribas, J.; Alcaraz, R.; Rieta, J.J. The Dissimilar Impact in Atrial Substrate Modificationof Left and Right Pulmonary Veins Isolation after Catheter Ablation of Paroxysmal Atrial Fibrillation. *J. Pers. Med.* **2022**, *12*, 462. doi:10.3390/jpm12030462.

14. Santangeli, P.; Marchlinski, F.E. Techniques for the provocation, localization, and ablation of non–pulmonary vein triggers for atrial fibrillation. *Heart Rhythm* **2017**, *14*, 1087–1096. doi:10.1016/j.hrthm.2017.02.030s.

15. Young, M.L.; Niu, J. Using coronary sinus ostium as the reference for the slow pathway ablation of atrioventricular nodal reentrant tachyarrhythmia in children. *J. Arrhythmia* **2020**, *36*, 712–719. doi:10.1002/joa3.12379.

16. Antz, M.; Otomo, K.; Arruda, M.; Scherlag, B.J.; Pitha, J.; Tondo, C.; Lazzara, R.; Jackman, W.M. Electrical conduction between the right atrium and the left atrium via the musculature of the coronary sinus. *Circulation* **1998**, *98*, 1790–1795. doi:10.1161/01.cir.98.17.1790.

17. Tritto, M.; Zardini, M.; De Ponti, R.; Salerno-Uriarte, J.A. Iterative atrial tachycardia originating from the coronary sinus musculature. *J. Cardiovasc. Electrophysiol.* **2001**, *12*, 1187–1189. doi:10.1046/j.1540-8167.2001.01187.x.

18. Giudici, M.; Winston, S.; Kappler, J.; Shinn, T.; Singer, I.; Scheiner, A.; Berrier, H.; Herner, M.; Sample, R. Mapping the coronary sinus and great cardiac vein. *PACE* **2002**, *25*, 414–419. doi:10.1046/j.1460-9592.2002.00414.x.

19. Ahmed, N.; Perveen, S.; Mehmood, A.; Rani, G.F.; Molon, G. Coronary Sinus Ablation Is a Key Player Substrate in Recurrence of Persistent Atrial Fibrillation. *Cardiology* **2019**, *143*, 107–113. doi:10.1159/000501819.

20. Razeghian-Jahromi, I.; Natale, A.; Nikoo, M.H. Coronary sinus diverticulum: Importance, function, and treatment. *PACE* **2020**, *43*, 1582–1587. doi:10.1111/pace.14026.

21. Morita, H.; Zipes, D.P.; Morita, S.T.; Wu, J. The role of coronary sinus musculature in the induction of atrial fibrillation. *Heart Rhythm* **2012**, *9*, 581–589. doi:10.1016/j.hrthm.2011.11.041.

22. Oral, H.; Ozaydin, M.; Chugh, A.; Scharf, C.; Tada, H.; Hall, B.; Cheung, P.; Pelosi, F.; Knight, B.P.; Morady, F. Role of the coronary sinus in maintenance of atrial fibrillation. *J. Cardiovasc. Electrophysiol.* **2003**, *14*, 1329–1336. doi:10.1046/j.1540-8167.2003.03222.x.

23. Haïssaguerre, M.; Hocini, M.; Takahashi, Y.; O'Neill, M.D.; Pernat, A.; Sanders, P.; Jonsson, A.; Rotter, M.; Sacher, F.; Rostock, T.; et al. Impact of catheter ablation of the coronary sinus on paroxysmal or persistent atrial fibrillation. *J. Cardiovasc. Electrophysiol.* **2007**, *18*, 378–386. doi:10.1111/j.1540-8167.2007.00764.x.

24. Yoshida, K.; Ulfarsson, M.; Tada, H.; Chugh, A.; Good, E.; Kuhne, M.; Crawford, T.; Sarrazin, J.F.; Chalfoun, N.; Wells, D.; et al. Complex electrograms within the coronary sinus: Time- and frequency-domain characteristics, effects of antral pulmonary vein isolation, and relationship to clinical outcome in patients with paroxysmal and persistent atrial fibrillation. *J. Cardiovasc. Electrophysiol.* **2008**, *19*, 1017–1023. doi:10.1111/j.1540-8167.2008.01175.x.

25. Marco, L.Y.D.; Raine, D.; Bourke, J.P.; Langley, P. Characteristics of atrial fibrillation cycle length predict restoration of sinus rhythm by catheter ablation. *Heart Rhythm* **2013**. *10*, 1303–1310. doi:10.1016/j.hrthm.2013.06.007.

26. Yin, X.; Zhao, Z.; Gao, L.; Chang, D.; Xiao, X.; Zhang, R.; Chen, Q.; Cheng, J.; Yang, Y.; Xi, Y.; et al. Frequency Gradient Within Coronary Sinus Predicts the Long-Term Outcome of Persistent Atrial Fibrillation Catheter Ablation. *J. Am. Heart Assoc.* **2017**, *6*, e004869. doi:10.1161/JAHA.116.004869.

27. Yoshida, K.; Chugh, A.; Good, E.; Crawford, T.; Myles, J.; Veerareddy, S.; Billakanty, S.; Wong, W.S.; Ebinger, M.; Pelosi, F.; et al. A critical decrease in dominant frequency and clinical outcome after catheter ablation of persistent atrial fibrillation. *Heart Rhythm* **2010**, *7*, 295–302. doi:10.1016/j.hrthm.2009.11.024.

28. Teh, A.W.; Kalman, J.M.; Kistler, P.M.; Lee, G.; Sutherland, F.; Morton, J.B.; Vohra, J.K.; Sparks, P.B. Prevalence of fractionated electrograms in the coronary sinus: comparison between patients with persistent or paroxysmal atrial fibrillation and a control population. *Heart Rhythm* **2010**, *7*, 1200–1204. doi:10.1016/j.hrthm.2010.05.011.

29. Kanemaru, Y.; Arima, Y.; Kaikita, K.; Kiyama, T.; Kaneko, S.; Ito, M.; Yamabe, H.; Motozato, K.; Yamanaga, K.; Fujisue, K.; et al. Elongation of the high right atrium to coronary sinus conduction time predicts the recurrence of atrial fibrillation after radiofrequency catheter ablation. *Int. J. Cardiol.* **2020**, *300*, 147–153. doi:10.1016/j.ijcard.2019.10.044.

30. Boles, U.; Gul, E.E.; Enriquez, A.; Starr, N.; Haseeb, S.; Abdollah, H.; Simpson, C.; Baranchuk, A.; Redfearn, D.; Michael, K.; et al. Coronary Sinus Electrograms May Predict New-onset Atrial Fibrillation After Typical Atrial Flutter Radiofrequency Ablation (CSE-AF). *J. Atr. Fibrillation* **2018**, *11*, 1809. doi:10.4022/jafib.1809.

31. McGuinness, S.; McKee, A.; Sidebotham, D. Chapter 8-Monitoring. In *Cardiothoracic Critical Care*; Butterworth-Heinemann: Oxford, UK, 2007; pp. 120–137. https://doi.org/10.1016/B978-075067572-7.50011-4.

32. Stafford, P.J.; Vincent, R. Spectrotemporal and spectral turbulence analysis of the signal-averaged P wave in paroxysmal atrial fibrillation. *J. Electrocardiol.* **1997**, *30*, 79–86. doi:10.1016/s0022-0736(97)80013-1.

33. Van Beeumen, K.; Houben, R.; Tavernier, R.; Ketels, S.; Duytschaever, M. Changes in P-wave area and P-wave duration after circumferential pulmonary vein isolation. *EP Eur.* **2010**, *12*, 798–804. doi:10.1093/europace/eup410.

34. Vassilikos, V.; Dakos, G.; Chatzizisis, Y.S.; Chouvarda, I.; Karvounis, C.; Maynard, C.; Maglaveras, N.; Paraskevaidis, S.; Stavropoulos, G.; Styliadis, C.I.; et al. Novel non-invasive P wave analysis for the prediction of paroxysmal atrial fibrillation recurrences in patients without structural heart disease: a prospective pilot study. *Int. J. Cardiol.* **2011**, *153*, 165–172. doi:10.1016/j.ijcard.2010.08.029.

35. Salah, A.; Zhou, S.; Liu, Q.; Yan, H. P wave indices to predict atrial fibrillation recurrences post pulmonary vein isolation. *Arq. Bras. Cardiol.* **2013**, *101*, 519–527. doi:10.5935/abc.20130214.

36. Maan, A.; Mansour, M.; Ruskin, J.N.; Heist, E.K. Impact of catheter ablation on P-wave parameters on 12-lead electrocardiogram in patients with atrial fibrillation. *J. Electrocardiol.* **2014**, *47*, 725–733. doi:10.1016/j.jelectrocard.2014.04.010.

37. Alcaraz, R.; Martínez, A.; Rieta, J.J. The P Wave Time-Frequency Variability Reflects Atrial Conduction Defects before Paroxysmal Atrial Fibrillation. *Ann. Noninvasive Electrocardiol.* **2015**, *20*, 433–445. doi:10.1111/anec.12240.

38. Kizilirmak, F.; Demir, G.G.; Gokdeniz, T.; Gunes, H.M.; Cakal, B.; Guler, E.; Karaca, I.O.; Omaygenç, M.O.; Yılmaz, F.; Olgun, F.E.; et al. Changes in Electrocardiographic P Wave Parameters after Cryoballoon Ablation and Their Association with Atrial Fibrillation Recurrence. *Ann. Noninvasive Electrocardiol.* **2016**, *21*, 580–587. doi:10.1111/anec.12364.

39. Ortigosa, N.; Ayala, G.; Cano, Ó. Variation of P-wave indices in paroxysmal atrial fibrillation patients before and after catheter ablation. *Biomed. Signal Process. Control* **2021**, *66*, 102500. doi:10.1016/j.bspc.2021.102500.

40. Simpson, R.J.; Foster, J.R.; Gettes, L.S. Atrial excitability and conduction in patients with interatrial conduction defects. *Am. J. Cardiol.* **1982**, *50*, 1331–1337. doi:10.1016/0002-9149(82)90471-4.

41. Chen, Q.; Mohanty, S.; Trivedi, C.; Gianni, C.; Della Rocca, D.G.; Canpolat, U.; Burkhardt, J.D.; Sanchez, J.E.; Hranitzky, P.; Gallinghouse, G.J.; et al. Association between prolonged P wave duration and left atrial scarring in patients with paroxysmal atrial fibrillation. *J. Cardiovasc. Electrophysiol.* **2019**, *30*, 1811–1818. doi:10.1111/jce.14070.

42. Pranata, R.; Yonas, E.; Vania, R. Prolonged P-wave duration in sinus rhythm pre-ablation is associated with atrial fibrillation recurrence after pulmonary vein isolation-A systematic review and meta-analysis. *Ann. Noninvasive Electrocardiol.* **2019**, *24*, e12653. doi:10.1111/anec.12653.

43. Vraka, A.; Bertomeu-González, V.; Hornero, F.; Quesada, A.; Alcaraz, R.; Rieta, J.J. Splitting the P-Wave: Improved Evaluation of Left Atrial Substrate Modification after Pulmonary Vein Isolation of Paroxysmal Atrial Fibrillation. *Sensors* **2022**, *22*, 290. doi:10.3390/s22010290.

44. Task Force of the European Society of Cardiology the North American Society of Pacing Electrophysiology. Heart rate variability. Standards of measurement, physiological interpretation, and clinical use. *Eur. Heart J.* **1996**, *17*, 354–381. doi:10.1161/01.cir.93.5.1043.

45. Perkiömäki, J.; Ukkola, O.; Kiviniemi, A.; Tulppo, M.; Ylitalo, A.; Kesäniemi, Y.A.; Huikuri, H. Heart rate variability findings as a predictor of atrial fibrillation in middle-aged population. *J. Cardiovasc. Electrophysiol.* **2014**, *25*, 719–724. doi:10.1111/jce.12402.

46. Habibi, M.; Chahal, H.; Greenland, P.; Guallar, E.; Lima, J.A.C.; Soliman, E.Z.; Alonso, A.; Heckbert, S.R.; Nazarian, S. Resting Heart Rate, Short-Term Heart Rate Variability and Incident Atrial Fibrillation (from the Multi-Ethnic Study of Atherosclerosis (MESA)). *Am. J. Cardiol.* **2019**, *124*, 1684–1689. doi:10.1016/j.amjcard.2019.08.025.

47. Huikuri, H.V.; Mäkikallio, T.H.; Perkiömäki, J. Measurement of heart rate variability by methods based on nonlinear dynamics. *J. Electrocardiol.* **2003**, *36 Suppl*, 95–99. doi:10.1016/j.jelectrocard.2003.09.021.

48. Hsieh, M.H.; Chiou, C.W.; Wen, Z.C.; Wu, C.H.; Tai, C.T.; Tsai, C.F.; Ding, Y.A.; Chang, M.S.; Chen, S.A. Alterations of heart rate variability after radiofrequency catheter ablation of focal atrial fibrillation originating from pulmonary veins. *Circulation* **1999**, *100*, 2237–2243. doi:10.1161/01.cir.100.22.2237.

49. Zhu, Z.; Wang, W.; Cheng, Y.; Wang, X.; Sun, J. The predictive value of heart rate variability indices tested in early period after radiofrequency catheter ablation for the recurrence of atrial fibrillation. *J. Cardiovasc. Electrophysiol.* **2020**, *31*, 1350–1355. doi:10.1111/jce.14448.

50. Călburean, P.A.; Osorio, T.G.; Sorgente, A.; Almorad, A.; Pannone, L.; Monaco, C.; Miraglia, V.; Al Housari, M.; Mojica, J.; Bala, G.; et al. High vagal tone predicts pulmonary vein reconnection after cryoballoon ablation for paroxysmal atrial fibrillation. *PACE* **2021**, *44*, 2075–2083. doi:10.1111/pace.14408.

51. Sörnmo, L.; Laguna, P. Electrocardiogram (ECG) Signal Processing. In *Wiley Encyclopedia of Biomedical Engineering*; John Wiley and Sons: Hoboken, NJ, USA, 2006; Volume 2, pp. 1298–1313. doi:10.1002/9780471740360.ebs1482.

52. García, M.; Martínez-Iniesta, M.; Ródenas, J.; Rieta, J.J.; Alcaraz, R. A novel wavelet-based filtering strategy to remove powerline interference from electrocardiograms with atrial fibrillation. *Physiol. Meas.* **2018**, *39*, 115006. doi:10.1088/1361-6579/aae8b1.

53. Martínez, A.; Alcaraz, R.; Rieta, J.J. Detection and removal of ventricular ectopic beats in atrial fibrillation recordings via principal component analysis. In Proceedings of the 2011 Annual International Conference of the IEEE Engineering in Medicine and Biology Society, Boston, MA, USA, 30 August–3 September 2011; pp. 4693–4696. doi:10.1109/IEMBS.2011.6091162.

54. Choi, A.; Shin, H. Quantitative Analysis of the Effect of an Ectopic Beat on the Heart Rate Variability in the Resting Condition. *Front. Physiol.* **2018**, *9*, 922. doi:10.3389/fphys.2018.00922.

55. Martinez, A.; Alcaraz, R.; Rieta, J.J. A new method for automatic delineation of ECG fiducial points based on the Phasor Transform. In Proceedings of the 2010 Annual International Conference of the IEEE Engineering in Medicine and Biology, Buenos Aires, Argentina, 31 August–4 September 2010; pp. 4586–4589. doi:10.1109/IEMBS.2010.5626498.

56. González, F.; Alcaraz, R.; Rieta, J.J. Electrocardiographic P-wave delineation based on adaptive slope Gaussian detection. In Proceedings of the 2017 Computing in Cardiology (CinC), Rennes, France, 24–27 September 2017; pp. 1–4. doi:10.22489/CinC.2017.236-033.

57. Alcaraz, R.; Rieta, J.J. Adaptive singular value cancelation of ventricular activity in single-lead atrial fibrillation electrocardiograms. *Physiol. Meas.* **2008**, *29*, 1351–1369. doi:10.1088/0967-3334/29/12/001.

58. Martínez-Iniesta, M.; Ródenas, J.; Rieta, J.J.; Alcaraz, R. The stationary wavelet transform as an efficient reductor of powerline interference for atrial bipolar electrograms in cardiac electrophysiology. *Physiol. Meas.* **2019**, *40*, 075003. doi:10.1088/1361-6579/ab2cb8.

59. Osorio, D.; Alcaraz, R.; Rieta, J.J. A fractionation-based local activation wave detector for atrial electrograms of atrial fibrillation. In Proceedings of the 2017 Computing in Cardiology (CinC), Rennes, France, 24–27 September 2017; pp. 1–4. doi:10.22489/CinC.2017.202-031.

60. Vraka, A.; Bertomeu-González, V.; Osca, J.; Ravelli, F.; Alcaraz, R.; Rieta, J.J. Study on How Catheter Ablation Affects Atrial Structures in Patients with Paroxysmal Atrial Fibrillation: The Case of the Coronary Sinus. In Proceedings of the 2020 International Conference on e-Health and Bioengineering (EHB), Iasi, Romania, 29–30 October 2020; pp. 1–4. https://doi.org/10.1109/EHB50910.2020.9280243.

61. Toman, O.; Hnatkova, K.; Smetana, P.; Huster, K.M.; Šišáková, M.; Barthel, P.; Novotný, T.; Schmidt, G.; Malik, M. Physiologic heart rate dependency of the PQ interval and its sex differences. *Sci. Rep.* **2020**, *10*, 2551. doi:10.1038/s41598-020-59480-8.

62. Shapiro, S.S.; Wilk, M.B. *An Analysis of Variance Test for Normality (Complete Samples)*; Oxford University Press: Oxford, UK, 1965; Volume 52, pp. 591–611.

63. Yan, X.; Su, X.G., Simple Linear Regression. In *Linear Regression Analysis: Theory and Computing*; World Scientific: Singapore, 2009; pp. 9–39. doi:10.1142/9789812834119_0002.

64. Pincus, S.M. Irregularity and asynchrony in biologic network signals. In *Numerical Computer Methods, Part C*; Academic Press: Cambridge, MA, USA, 2000; Volume 321, pp. 149–182. https://doi.org/10.1016/S0076-6879(00)21192-0.

65. Alcaraz, R.; Rieta, J.J. Nonlinear synchronization assessment between atrial and ventricular activations series from the surface ECG in atrial fibrillation. *Biomed. Signal Process. Control* **2013**, *8*, 1000–1007. doi:https://doi.org/10.1016/j.bspc.2013.01.009.

66. Lake, D.E.; Moorman, J.R. Accurate estimation of entropy in very short physiological time series: The problem of atrial fibrillation detection in implanted ventricular devices. *Am. J. Physiol.* **2011**, *300*, H319–H325. 10.1152/ajpheart.00561.2010.

67. Vraka, A.; Hornero, F.; Bertomeu-González, V.; Osca, J.; Alcaraz, R.; Rieta, J.J. Short-Time Estimation of Fractionation in Atrial Fibrillation with Coarse-Grained Correlation Dimension for Mapping the Atrial Substrate. *Entropy* **2020**, *22*, 232. doi:10.3390/e22020232.

68. de Groot, N.; Shah, D.; Boyle, P.M.; Anter, E.; Clifford, G.D.; Deisenhofer, I.; Deneke, T.; van Dessel, P.; Doessel, O.; Dilaveris, P.; et al. Critical appraisal of technologies to assess electrical activity during atrial fibrillation: A position paper from the European Heart Rhythm Association and European Society of Cardiology Working Group on eCardiology in collaboration with the Heart Rhythm Society, Asia Pacific Heart Rhythm Society, Latin American Heart Rhythm Society and Computing in Cardiology. *EP Eur.* **2021**, *24*, 313–330. https://doi.org/10.1093/europace/euab254.

69. Misek, J.; Belyaev, I.; Jakusova, V.; Tonhajzerova, I.; Barabas, J.; Jakus, J. Heart rate variability affected by radiofrequency electromagnetic field in adolescent students. *Bioelectromagnetics* **2018**, *39*, 277–288. doi:10.1002/bem.22115.

70. Misek, J.; Veternik, M.; Tonhajzerova, I.; Jakusova, V.; Janousek, L.; Jakus, J. Radiofrequency Electromagnetic Field Affects Heart Rate Variability in Rabbits. *Physiol. Res.* **2020**, *69*, 633–643. doi:10.33549/physiolres.934425.

71. Chen, P.S.; Chen, L.S.; Fishbein, M.C.; Lin, S.F.; Nattel, S. Role of the autonomic nervous system in atrial fibrillation: pathophysiology and therapy. *Circ. Res.* **2014**, *114*, 1500–1515. doi:10.1161/CIRCRESAHA.114.303772.

72. Martínez, A.; Alcaraz, R.; Rieta, J.J. Study on the P-wave feature time course as early predictors of paroxysmal atrial fibrillation. *Physiol. Meas.* **2012**, *33*, 1959–1974. doi:10.1088/0967-3334/33/12/1959.

73. Rodrigo, M.; Climent, A.M.; Hernández-Romero, I.; Liberos, A.; Baykaner, T.; Rogers, A.J.; Alhusseini, M.; Wang, P.J.; Fernández-Avilés, F.; Guillem, M.S.; et al. Noninvasive Assessment of Complexity of Atrial Fibrillation: Correlation With Contact Mapping and Impact of Ablation. *Circ. Arrhythmia Electrophysiol.* **2020**, *13*, e007700. doi:10.1161/CIRCEP.119.007700.

74. Liu, Z.; Hayano, M.; Hirata, T.; Tsukahara, K.; Quin, Y.; Nakao, K.; Nonaka, M.; Ishimatsu, T.; Ueyama, C.; Yano, K. Abnormalities of electrocardiographic P wave morphology and their relation to electrophysiological parameters of the atrium in patients with sick sinus syndrome. *PACE* **1998**, *21*, 79–86. doi:10.1111/j.1540-8159.1998.tb01064.x.

75. Yahyazadeh, S.; Firoozabadi, S.; Haghjoo, M.; Parvaneh, S. Quantitative relation between chaotic features of surface electrocardiogram and Intracardiac Electrogram. In Proceedings of the 2010 Computing in Cardiology, Belfast, UK, 26–29 September 2010; pp. 593–596.

76. Alcaraz, R.; Hornero, F.; Rieta, J.J. Validation of surface atrial fibrillation organization indicators through invasive recordings. In Proceedings of the 2011 Annual International Conference of the IEEE Engineering in Medicine and Biology Society, Boston, MA, USA, 30 August–3 September 2011; pp. 5519–5522. doi:10.1109/IEMBS.2011.6091408.

77. Kharbanda, R.; Knops, P.; van der Does, L.; Kik, C.; Taverne, Y.; Roos-Serote, M.; Heida, A.; Oei, F.; Bogers, A.; de Groot, N. Simultaneous Endo-Epicardial Mapping of the Human Right Atrium: Unraveling Atrial Excitation. *J. Am. Heart Assoc.* **2020**, *9*, e017069. doi:10.1161/JAHA.120.017069.

Bibliography

[1] D. Evan Bedford. The ancient art of feeling the pulse. *British heart journal*, 13(4):423–437, 1951.

[2] William Dock. The lure of medical history: Young and helmholtz: The master minds of medicine. *California and western medicine*, 29(3):182–184, 1928.

[3] Sumeet S Chugh, Joseph L Blackshear, Win-Kuang Shen, Stephen C Hammill, and Bernard J Gersh. Epidemiology and natural history of atrial fibrillation: clinical implications. *Journal of the American College of Cardiology*, 37(2):371–378, 2001.

[4] M. Haïssaguerre, P. Jaïs, D. C. Shah, A. Takahashi, M. Hocini, G. Quiniou, S. Garrigue, A. Le Mouroux, P. Le Métayer, and J. Clémenty. Spontaneous initiation of atrial fibrillation by ectopic beats originating in the pulmonary veins. *The New England journal of medicine*, 339:659–666, 1998.

[5] Aikaterini Vraka, Fernando Hornero, Vicente Bertomeu-González, Joaquín Osca, Raúl Alcaraz, and José J. Rieta. Short-time estimation of fractionation in atrial fibrillation with coarse-grained correlation dimension for mapping the atrial substrate. *Entropy*, 22, 2020.

[6] Aikaterini Vraka, Vicente Bertomeu-González, Fernando Hornero, Aurelio Quesada, Raúl Alcaraz, and José J. Rieta. Splitting the p-wave: Improved evaluation of left atrial substrate modification after pulmonary vein isolation of paroxysmal atrial fibrillation. *Sensors*, 22(1), 2022.

[7] Aikaterini Vraka, Vicente Bertomeu-González, Lorenzo Fácila, José Moreno-Arribas, Raúl Alcaraz, and José J. Rieta. The dissimilar impact in atrial substrate modificationof left and right pulmonary veins isolation after catheter ablation of paroxysmal atrial fibrillation. *Journal of Personalized Medicine*, 12(3):462, 2022.

[8] Aikaterini Vraka, José Moreno-Arribas, Juan M. Gracia-Baena, Fernando Hornero, Raúl Alcaraz, and José J. Rieta. The relevance of heart rate fluctuation when evaluating atrial substrate electrical features in catheter ablation of paroxysmal atrial fibrillation. *Journal of Cardiovascular Development and Disease*, 9:176, 2022.

[9] Giuseppe Lippi, Fabian Sanchis-Gomar, and Gianfranco Cervellin. Global epidemiology of atrial fibrillation: An increasing epidemic and public health challenge. *International journal of stroke : official journal of the International Stroke Society*, 16:217–221, 2021.

[10] Gerhard Hindricks, Tatjana Potpara, Nikolaos Dagres, Elena Arbelo, Jeroen J. Bax, Carina Blomström-Lundqvist, Giuseppe Boriani, et al. 2020 esc guidelines for the diagnosis and management of atrial fibrillation developed in collaboration with the european association for cardio-thoracic surgery (eacts): The task force for the diagnosis and management of atrial fibrillation of the european society of cardiology (esc) developed with the special contribution of the european heart rhythm association (ehra) of the esc. *European heart journal*, 42:373–498, 2021.

[11] Marcus F Stoddard, Phillip R Dawkins, Charles R Prince, and Naser M Ammash. Left atrial appendage thrombus is not uncommon in patients with acute atrial fibrillation and a recent embolic event: A transesophageal echocardiographics tudy. *Journal of the American College of Cardiology*, 25(2):452–459, 1995.

[12] T Jared Bunch, Brian G Crandall, J Peter Weiss, Heidi T May, Tami L Bair, Jeffrey S Osborn, Jeffrey L Anderson, Joseph B Muhlestein, Benjamin D Horne, Donald L Lappe, et al. Patients treated with catheter ablation for atrial fibrillation have long-term rates of death, stroke, and dementia similar to patients without atrial fibrillation. *Journal of cardiovascular electrophysiology*, 22(8):839–845, 2011.

[13] Alan S Go, Kristi Reynolds, Jingrong Yang, Nigel Gupta, Judith Lenane, Sue Hee Sung, Teresa N Harrison, Taylor I Liu, and Matthew D Solomon. Association of burden of atrial fibrillation with risk of ischemic stroke in adults with paroxysmal atrial fibrillation: the kp-rhythm study. *JAMA cardiology*, 3(7):601–608, 2018.

[14] Marco Zuin, Loris Roncon, Angelina Passaro, Cristina Bosi, Carlo Cervellati, and Giovanni Zuliani. Risk of dementia in patients with atrial fibrillation: Short versus long follow-up. a systematic review and meta-analysis. *International journal of geriatric psychiatry*, 36:1488–1500, 2021.

[15] Giovanni Luca Botto, Giovanni Tortora, Maria Carla Casale, Fabio Lorenzo Canevese, and Francesco Angelo Maria Brasca. Impact of the pattern of atrial fibrillation on stroke risk and mortality. *Arrhythmia & electrophysiology review*, 10:68–76, 2021.

[16] Liza Thomas and Walter P. Abhayaratna. Left atrial reverse remodeling: Mechanisms, evaluation, and clinical significance. *JACC. Cardiovascular imaging*, 10:65–77, 2017.

[17] Baptiste Maille, Moloy Das, Ahmed Hussein, Matthew Shaw, Vivek Chaturvedi, Emmanuel Williams, Maureen Morgan, Christina Ronayne, Richard L. Snowdon, and Dhiraj Gupta. Reverse electrical and structural remodeling of the left atrium occurs early after pulmonary vein isolation for persistent atrial fibrillation. *Journal of interventional cardiac electrophysiology : an international journal of arrhythmias and pacing*, 58:9–19, 2020.

[18] Dennis H. Lau, Dominik Linz, Ulrich Schotten, Rajiv Mahajan, Prashan-than Sanders, and Jonathan M. Kalman. Pathophysiology of paroxysmal and persistent atrial fibrillation: Rotors, foci and fibrosis. *Heart, lung & circulation*, 26:887–893, 2017.

[19] Anand N. Ganesan, Derek P. Chew, Trent Hartshorne, Joseph B. Sel-vanayagam, Philip E. Aylward, Prashanthan Sanders, and Andrew D. Mc-Gavigan. The impact of atrial fibrillation type on the risk of thromboem-bolism, mortality, and bleeding: a systematic review and meta-analysis. *European heart journal*, 37:1591–1602, 2016.

[20] Sven Knecht, Maurice Pradella, Tobias Reichlin, Aline Mühl, Matthias Bossard, Bram Stieltjes, David Conen, Jens Bremerich, Stefan Osswald, Michael Kühne, and Christian Sticherling. Left atrial anatomy, atrial fibril-lation burden, and p-wave duration-relationships and predictors for single-procedure success after pulmonary vein isolation. *Europace*, 20:271–278, 2018.

[21] Stanley Nattel, Brett Burstein, and Dobromir Dobrev. Atrial remodeling and atrial fibrillation: mechanisms and implications. *Circulation. Arrhyth-mia and electrophysiology*, 1, 2008.

[22] Andreas Bollmann, Daniela Husser, Luca Mainardi, Federico Lombardi, Philip Langley, Alan Murray, José Joaquín Rieta, José Millet, S. Bertil Ols-son, Martin Stridh, and Leif Sörnmo. Analysis of surface electrocardio-grams in atrial fibrillation: techniques, research, and clinical applications. *Europace*, 8:911–926, 2006.

[23] Laurent Uldry, Jérôme Van Zaen, Yann Prudat, Lukas Kappenberger, and Jean-Marc Vesin. Measures of spatiotemporal organization differentiate persistent from long-standing atrial fibrillation. *Europace*, 14:1125–1131, 2012.

[24] Raúl Alcaraz, Fernando Hornero, Arturo Martínez, and José J. Rieta. Short-time regularity assessment of fibrillatory waves from the surface ecg in atrial fibrillation. *Physiological measurement*, 33:969–984, 2012.

[25] Leif Sörnmo, Raúl Alcaraz, Pablo Laguna, and José Joaquín Rieta. *Charac-terization of f Waves*, chapter 6, pages 221–279. Atrial Fibrillation from an Engineering Perspective. Springer, Cham., 2018.

[26] Junbeom Park, Chungkeun Lee, Eran Leshem, Ira Blau, Sungsoo Kim, Jung Myung Lee, Jung-A. Hwang, Byung-Il Choi, Moon-Hyoung Lee, and Hye Jin Hwang. Early differentiation of long-standing persistent atrial fib-rillation using the characteristics of fibrillatory waves in surface ecg multi-leads. *Scientific reports*, 9:2746, 2019.

[27] Juan Ródenas, Pilar Escribano, Miguel Martinez-Iniesta, Manuel García, Fernando Hornero, José J Rieta, and Raúl Alcaraz. Time variability of fibrillatory waves energy predicts long-term outcome of atrial fibrillation

concomitant surgical ablation. In *2020 Computing in Cardiology*, pages 1–4. IEEE, 2020.

[28] Eva María Cirugeda Roldan, Sofía Calero, Víctor Manuel Hidalgo, José Enero, José Joaquín Rieta, and Raúl Alcaraz. Multi-scale entropy evaluates the proarrhythmic condition of persistent atrial fibrillation patients predicting early failure of electrical cardioversion. *Entropy*, 22:748.

[29] Katarina Van Beeumen, Richard Houben, Rene Tavernier, Stefan Ketels, and Mattias Duytschaever. Changes in p-wave area and p-wave duration after circumferential pulmonary vein isolation. *Europace*, 12:798–804, 2010.

[30] Coralie Blanche, Nam Tran, Fabio Rigamonti, Haran Burri, and Marc Zimmermann. Value of p-wave signal averaging to predict atrial fibrillation recurrences after pulmonary vein isolation. *Europace*, 15:198–204, 2013.

[31] Abhishek Maan, Moussa Mansour, Jeremy N. Ruskin, and E. Kevin Heist. Impact of catheter ablation on p-wave parameters on 12-lead electrocardiogram in patients with atrial fibrillation. *Journal of electrocardiology*, 47:725–733, 2014.

[32] Filiz Kizilirmak, Gultekin Gunhan Demir, Tayyar Gokdeniz, Haci Murat Gunes, Beytullah Cakal, Ekrem Guler, Ibrahim Oguz Karaca, Mehmet Onur Omaygenç, Fatih Yılmaz, Fatih Erkam Olgun, and Fethi Kilicaslan. Changes in electrocardiographic p wave parameters after cryoballoon ablation and their association with atrial fibrillation recurrence. *Annals of noninvasive electrocardiology*, 21:580–587, 2016.

[33] Raymond Pranata, Emir Yonas, and Rachel Vania. Prolonged p-wave duration in sinus rhythm pre-ablation is associated with atrial fibrillation recurrence after pulmonary vein isolation-a systematic review and meta-analysis. *Annals of noninvasive electrocardiology*, 24:e12653, 2019.

[34] Satoshi Yanagisawa, Yasuya Inden, Hiroya Okamoto, Aya Fujii, Yusuke Sakamoto, Keita Mamiya, Toshiro Tomomatsu, Rei Shibata, and Toyoaki Murohara. Electrocardiogram characteristics of p wave associated with successful pulmonary vein isolation in patients with paroxysmal atrial fibrillation: Significance of changes in p-wave duration and notched p wave. *Annals of noninvasive electrocardiology*, 25:e12712, 2020.

[35] Angelo Auricchio, Tardu Özkartal, Francesca Salghetti, Laura Neumann, Simone Pezzuto, Ali Gharaviri, Andrea Demarchi, Maria Luce Caputo, François Regoli, Carlo De Asmundis, Gian-Battista Chierchia, Pedro Brugada, Catherine Klersy, Tiziano Moccetti, Ulrich Schotten, and Giulio Conte. Short p-wave duration is a marker of higher rate of atrial fibrillation recurrences after pulmonary vein isolation: New insights into the pathophysiological mechanisms through computer simulations. *Journal of the American Heart Association*, 10:e018572, 2021.

[36] Fabienne Kreimer, Assem Aweimer, Andreas Pflaumbaum, Andreas Mügge, and Michael Gotzmann. Impact of p-wave indices in prediction of atrial fibrillation-insight from loop recorder analysis. *Annals of noninvasive electrocardiology*, 26:e12854, 2021.

[37] Yuxia Miao, Min Xu, Ling Yang, Chunxu Zhang, Huannian Liu, and Xiaoliang Shao. Investigating the association between p wave duration and atrial fibrillation recurrence after radiofrequency ablation in early persistent atrial fibrillation patients. *International journal of cardiology*, 351:48 – 54, 2021.

[38] Hao-Tien Liu, Hui-Ling Lee, Hung-Ta Wo, Po-Cheng Chang, Ming-Shien Wen, Fen-Chiung Lin, San-Jou Yeh, and Chung-Chuan Chou. P wave duration ≥150 ms predicts poor left atrial function and ablation outcomes in non-paroxysmal atrial fibrillation. *Journal of electrocardiology*, 69:124–131, 2021.

[39] Yosuke Murase, Hajime Imai, Yasuhiro Ogawa, Naoaki Kano, Keita Mamiya, Tomoyo Ikeda, Kei Okabe, Kenji Arai, Shinji Yamazoe, Jun Torii, and Katsuhiro Kawaguchi. Usefulness of p-wave duration in patients with sick sinus syndrome as a predictor of atrial fibrillation. *Journal of arrhythmia*, 37:1220–1226, 2021.

[40] Natasja de Groot, Dipen Shah, Patrick M Boyle, Elad Anter, Gari D Clifford, Isabel Deisenhofer, Thomas Deneke, Pascal van Dessel, Olaf Doessel, Polychronis Dilaveris, et al. Critical appraisal of technologies to assess electrical activity during atrial fibrillation: a position paper from the european heart rhythm association and european society of cardiology working group on ecardiology in collaboration with the heart rhythm society, asia pacific heart rhythm society, latin american heart rhythm society and computing in cardiology. *EP Europace*, 24(2):313–330, 2021.

[41] Szilvia Herczeg, John J. Keaney, Edward Keelan, Claire Howard, Katie Walsh, Laszlo Geller, Gabor Szeplaki, and Joseph Galvin. Classification of left atrial diseased tissue burden determined by automated voltage analysis predicts outcomes after ablation for atrial fibrillation. *Disease markers*, 2021:5511267, 2021.

[42] Usama Boles, Enes Elvin Gul, Andres Enriquez, Neasa Starr, Sohaib Haseeb, Hoshiar Abdollah, Christopher Simpson, Adrian Baranchuk, Damian Redfearn, Kevin Michael, Wilma Hopman, and Benedict Glover. Coronary sinus electrograms may predict new-onset atrial fibrillation after typical atrial flutter radiofrequency ablation (cse-af). *Journal of atrial fibrillation*, 11:1809, 2018.

[43] Atul Verma, Chen-yang Jiang, Timothy R. Betts, Jian Chen, Isabel Deisenhofer, Roberto Mantovan, Laurent Macle, Carlos A. Morillo, Wilhelm Haverkamp, Rukshen Weerasooriya, Jean-Paul Albenque, Stefano Nardi,

Endrj Menardi, Paul Novak, Prashanthan Sanders, and S.T.A.R. A.F. I. I. Investigators. Approaches to catheter ablation for persistent atrial fibrillation. *The New England journal of medicine*, 372:1812–1822, 2015.

[44] Saurabh Kumar and Gregory F. Michaud. Catheter ablation for paroxysmal atrial fibrillation: Time to focus more on trigger ablation? *Circulation. Arrhythmia and electrophysiology*, 9, 2016.

[45] Panagiotis Ioannidis, Theodoros Zografos, Evangelia Christoforatou, Konstantinos Kouvelas, Andreas Tsoumeleas, and Charalambos Vassilopoulos. The electrophysiology of atrial fibrillation: From basic mechanisms to catheter ablation. *Cardiology research and practice*, 2021:4109269, 2021.

[46] Rohit Kharbanda, Paul Knops, Lisette van der Does, Charles Kik, Yannick Taverne, Maarten Roos-Serote, Annejet Heida, Frans Oei, Ad Bogers, and Natasja de Groot. Simultaneous endo-epicardial mapping of the human right atrium: Unraveling atrial excitation. *Journal of the American Heart Association*, 9:e017069, 2020.

[47] Raúl Alcaraz and José J. Rieta. Sample entropy of the main atrial wave predicts spontaneous termination of paroxysmal atrial fibrillation. *Medical engineering & physics*, 31:917–922, 2009.

[48] Koonlawee Nademanee, John McKenzie, Erol Kosar, Mark Schwab, Buncha Sunsaneewitayakul, Thaveekiat Vasavakul, Chotikorn Khunnawat, and Tachapong Ngarmukos. A new approach for catheter ablation of atrial fibrillation: mapping of the electrophysiologic substrate. *Journal of the American College of Cardiology*, 43:2044–2053, 2004.

[49] Yenn-Jiang Lin, Ching-Tai Tai, Shih-Lin Chang, Li-Wei Lo, Ta-Chuan Tuan, Wanwarang Wongcharoen, Ameya R. Udyavar, Yu-Feng Hu, Chien-Jung Chang, Wen-Chin Tsai, Tsair Kao, Satoshi Higa, and Shih-Ann Chen. Efficacy of additional ablation of complex fractionated atrial electrograms for catheter ablation of nonparoxysmal atrial fibrillation. *Journal of cardiovascular electrophysiology*, 20:607–615, 2009.

[50] Dennis H. Lau, Bart Maesen, Stef Zeemering, Pawel Kuklik, Arne van Hunnik, Theodorus A. R. Lankveld, Elham Bidar, Sander Verheule, Jan Nijs, Jos Maessen, Harry Crijns, Prashanthan Sanders, and Ulrich Schotten. Indices of bipolar complex fractionated atrial electrograms correlate poorly with each other and atrial fibrillation substrate complexity. *Heart rhythm*, 12:1415–1423, 2015.

[51] Claire A. Martin, James P. Curtain, Parag R. Gajendragadkar, David A. Begley, Simon P. Fynn, Andrew A. Grace, Patrick M. Heck, Munmohan S. Virdee, and Sharad Agarwal. Ablation of complex fractionated electrograms improves outcome in persistent atrial fibrillation of over 2 year's duration. *Journal of atrial fibrillation*, 10:1607, 2018.

[52] Sotirios Nedios, Frank Lindemann, Jordi Heijman, Harry J. G. M. Crijns, Andreas Bollmann, and Gerhard Hindricks. Atrial remodeling and atrial fibrillation recurrence after catheter ablation : Past, present, and future developments. *Herz*, 46:312–317, 2021.

[53] Amir S. Jadidi, Heiko Lehrmann, Cornelius Keyl, Jérémie Sorrel, Viktor Markstein, Jan Minners, Chan-Il Park, Arnaud Denis, Pierre Jaïs, Mélèze Hocini, Clemens Potocnik, Juergen Allgeier, Willibald Hochholzer, Claudia Herrera-Siklody, Steve Kim, Youssef El Omri, Franz-Josef Neumann, Reinhold Weber, Michel Haïssaguerre, and Thomas Arentz. Ablation of persistent atrial fibrillation targeting low-voltage areas with selective activation characteristics. *Circulation. Arrhythmia and electrophysiology*, 9, 2016.

[54] Fiyyaz Ahmed-Jushuf, Francis Murgatroyd, Para Dhillon, and Paul A. Scott. The impact of the presence of left atrial low voltage areas on outcomes from pulmonary vein isolation. *Journal of arrhythmia*, 35:205–214, 2019.

[55] Xiaomeng Yin, Ziming Zhao, Lianjun Gao, Dong Chang, Xianjie Xiao, Rongfeng Zhang, Qi Chen, Jie Cheng, Yanzong Yang, Yutao Xi, and Yunlong Xia. Frequency gradient within coronary sinus predicts the long-term outcome of persistent atrial fibrillation catheter ablation. *Journal of the American Heart Association*, 6:e004869, 2017.

[56] Yoga Waranugraha, Ardian Rizal, Dion Setiawan, and Indra Jabbar Aziz. Additional complex fractionated atrial electrogram ablation does not improve the outcomes of non-paroxysmal atrial fibrillation: A systematic review and meta-analysis of randomized controlled trials. *Indian heart journal*, 73:63–73, 2021.

[57] Susan Cheng, Michelle J Keyes, Martin G Larson, et al. Long-term outcomes in individuals with prolonged PR interval or first-degree atrioventricular block. *Jama*, 301(24):2571–2577, 2009.

[58] Vishy Mahadevan. Anatomy of the heart. *Surgery (Oxford)*, 36(2):43–47, 2018.

[59] Robert H Whitaker. Anatomy of the heart. *Medicine*, 38(7):333–335, 2010.

[60] Anthony J. Weinhaus. *Handbook of Cardiac Anatomy, Physiology and Devices, Third Edition*, chapter Anatomy of the Human Heart, pages 61–88. Springer International Publishing, 2015.

[61] Syed Shah, Gopinath Gnanasegaran, Jeanette Sundberg-Cohon, and John R. Buscombe. *The Heart: Anatomy, Physiology and Exercise Physiology*, pages 3–22. Springer Berlin Heidelberg, Berlin, Heidelberg, 2009.

[62] Lionel Opie. *Heart physiology : from cell to circulation*. Lippincott Williams & Wilkins : Philadelphia, 2004.

[63] Arnold M. Katz. *Physiology of the heart*. Lippincott Williams and Wilkin, 2010.

[64] Alan Kennedy, Dewar D. Finlay, Daniel Guldenring, Raymond Bond, Kieran Moran, and James McLaughlin. The cardiac conduction system: Generation and conduction of the cardiac impulse. *Critical care nursing clinics of North America*, 28:269–279, 2016.

[65] Mark W Barnett and Philip M Larkman. The action potential. *Practical Neurology*, 7(3):192–197, 2007.

[66] Ary L. Goldberger, Zachary D. Goldberger, and Alexei Shvilkin. Chapter 3 - how to make basic ecg measurements. In Ary L. Goldberger, Zachary D. Goldberger, and Alexei Shvilkin, editors, *Goldberger's Clinical Electrocardiography (Ninth Edition)*, pages 11–20. Elsevier, ninth edition edition, 2018.

[67] Steve Meek and Francis Morris. Abc of clinical electrocardiography.introduction. i-leads, rate, rhythm, and cardiac axis. *BMJ (Clinical research ed.)*, 324:415–418, 2002.

[68] Ary L. Goldberger, Zachary D. Goldberger, and Alexei Shvilkin. Chapter 4 - ecg leads. In Ary L. Goldberger, Zachary D. Goldberger, and Alexei Shvilkin, editors, *Goldberger's Clinical Electrocardiography (Ninth Edition)*, pages 21–31. Elsevier, ninth edition edition, 2018.

[69] Ary L. Goldberger, Zachary D. Goldberger, and Alexei Shvilkin. Chapter 2 - ecg basics: Waves, intervals, and segments. In Ary L. Goldberger, Zachary D. Goldberger, and Alexei Shvilkin, editors, *Goldberger's Clinical Electrocardiography (Ninth Edition)*, pages 6–10. Elsevier, ninth edition edition, 2018.

[70] Ary L. Goldberger, Zachary D. Goldberger, and Alexei Shvilkin. Chapter 6 - electrical axis and axis deviation. In Ary L. Goldberger, Zachary D. Goldberger, and Alexei Shvilkin, editors, *Goldberger's Clinical Electrocardiography (Ninth Edition)*, pages 41–49. Elsevier, ninth edition edition, 2018.

[71] Johnny Chee and Swee-Chong Seow. *The Electrocardiogram*, pages 1–53. Springer Berlin Heidelberg, Berlin, Heidelberg, 2007.

[72] Ary L. Goldberger, Zachary D. Goldberger, and Alexei Shvilkin. Chapter 15 - supraventricular arrhythmias, part ii: Atrial flutter and atrial fibrillation. In Ary L. Goldberger, Zachary D. Goldberger, and Alexei Shvilkin, editors, *Goldberger's Clinical Electrocardiography (Ninth Edition)*, pages 144–155. Elsevier, ninth edition edition, 2018.

[73] Daniel A. Hyman, Vincent Siebert, Xiaoming Jia, Mahboob Alam, Glenn N. Levine, Salim S. Virani, and Yochai Birnbaum. Risk assessment of stroke in patients with atrial fibrillation: Current shortcomings and future directions. *Cardiovascular drugs and therapy*, 33:105–117, 2019.

[74] Maurits Allessie, Jannie Ausma, and Ulrich Schotten. Electrical, contractile and structural remodeling during atrial fibrillation. *Cardiovascular research*, 54:230–246, 2002.

[75] Takahito Takagi, Keijiro Nakamura, Masako Asami, Yasutake Toyoda, Yoshinari Enomoto, Masao Moroi, Mahito Noro, Kaoru Sugi, and Masato Nakamura. Impact of right atrial structural remodeling on recurrence after ablation for atrial fibrillation. *Journal of arrhythmia*, 37:597–606, 2021.

[76] Li-Wei Lo and Shih-Ann Chen. Cardiac remodeling after atrial fibrillation ablation. *Journal of atrial fibrillation*, 6:877, 2013.

[77] Gordon K Moe, Werner C Rheinboldt, and J.A Abildskov. A computer model of atrial fibrillation. *American Heart Journal*, 67(2):200–220, 1964.

[78] Maurits Allessie and F. Bonke. Experimental evaluation of moe's multiple wavelet hypothesis of atrial fibrillation. *Cardiac electrophysiology and arrhythmias*, pages 265–275, 1985.

[79] Natasja de Groot, Lisette van der Does, Ameeta Yaksh, Eva Lanters, Christophe Teuwen, Paul Knops, Pieter van de Woestijne, Jos Bekkers, Charles Kik, Ad Bogers, and Maurits Allessie. Direct proof of endo-epicardial asynchrony of the atrial wall during atrial fibrillation in humans. *Circulation. Arrhythmia and electrophysiology*, 9:e003648, 2016.

[80] Christopher Kowalewski. Mapping atrial fibrillation : An overview of potential mechanisms underlying atrial fibrillation. *Herz*, 46:305–311, 2021.

[81] Xin Xie, Gang Yang, Xiaorong Li, Jinbo Yu, Fengxiang Zhang, Weizhu Ju, Hongwu Chen, Mingfang Li, Kai Gu, Dian Cheng, Xuecheng Wang, Yizhang Wu, Jian Zhou, Xiaoqian Zhou, Baowei Zhang, Pipin Kojodjojo, Kejiang Cao, Bing Yang, and Minglong Chen. Prevalence and predictors of additional ablation beyond pulmonary vein isolation in patients with paroxysmal atrial fibrillation. *Frontiers in cardiovascular medicine*, 8:690297, 2021.

[82] Emmanouil Charitakis, Silvia Metelli, Lars O. Karlsson, Antonios P. Antoniadis, Ioan Liuba, Henrik Almroth, Anders Hassel Jönsson, Jonas Schwieler, Skevos Sideris, Dimitrios Tsartsalis, Elena Dragioti, Nikolaos Fragakis, and Anna Chaimani. Comparing efficacy and safety in catheter ablation strategies for paroxysmal atrial fibrillation: A network meta-analysis of randomized controlled trials. *Diagnostics*, 12:433, 2022.

[83] Ghassen Cheniti, Stephane Puyo, Claire A. Martin, Antonio Frontera, Konstantinos Vlachos, Masateru Takigawa, Felix Bourier, Takeshi Kitamura, Anna Lam, Carole Dumas-Pommier, Xavier Pillois, Thomas Pambrun, Josselin Duchateau, Nicolas Klotz, Arnaud Denis, Nicolas Derval, Hubert Cochet, Frederic Sacher, Remi Dubois, Pierre Jais, Meleze Hocini, and Michel Haissaguerre. Noninvasive mapping and electrocardiographic imaging in atrial and ventricular arrhythmias. *Cardiac electrophysiology clinics*, 11:459–471, 2019.

[84] R. C. Barr, M. Ramsey, and M. S. Spach. Relating epicardial to body surface potential distributions by means of transfer coefficients based on geometry measurements. *IEEE transactions on bio-medical engineering*, 24:1–11, 1977.

[85] Maria S. Guillem, Andreu M. Climent, Francisco Castells, Daniela Husser, Jose Millet, Arash Arya, Christopher Piorkowski, and Andreas Bollmann. Noninvasive mapping of human atrial fibrillation. *Journal of cardiovascular electrophysiology*, 20:507–513, 2009.

[86] Marianna Meo, Thomas Pambrun, Nicolas Derval, Carole Dumas-Pomier, Stéphane Puyo, Josselin Duchâteau, Pierre Jaïs, Mélèze Hocini, Michel Haïssaguerre, and Rémi Dubois. Noninvasive assessment of atrial fibrillation complexity in relation to ablation characteristics and outcome. *Frontiers in physiology*, 9:929, 2018.

[87] R. J. Simpson, J. R. Foster, and L. S. Gettes. Atrial excitability and conduction in patients with interatrial conduction defects. *The American journal of cardiology*, 50:1331–1337, 1982.

[88] M. H. Hsieh, C. W. Chiou, Z. C. Wen, C. H. Wu, C. T. Tai, C. F. Tsai, Y. A. Ding, M. S. Chang, and S. A. Chen. Alterations of heart rate variability after radiofrequency catheter ablation of focal atrial fibrillation originating from pulmonary veins. *Circulation*, 100:2237–2243, 1999.

[89] Zhenyan Zhu, Weiming Wang, Yamin Cheng, Xiaoqing Wang, and Jianhui Sun. The predictive value of heart rate variability indices tested in early period after radiofrequency catheter ablation for the recurrence of atrial fibrillation. *Journal of cardiovascular electrophysiology*, 31:1350–1355, 2020.

[90] Mohammadali Habibi, Harjit Chahal, Philip Greenland, Eliseo Guallar, João A. C. Lima, Elsayed Z. Soliman, Alvaro Alonso, Susan R. Heckbert, and Saman Nazarian. Resting heart rate, short-term heart rate variability and incident atrial fibrillation (from the multi-ethnic study of atherosclerosis (mesa)). *The American journal of cardiology*, 124:1684–1689, 2019.

[91] Miguel Martínez-Iniesta, Juan Ródenas, José J. Rieta, and Raúl Alcaraz. The stationary wavelet transform as an efficient reductor of powerline interference for atrial bipolar electrograms in cardiac electrophysiology. *Physiological measurement*, 40:075003, 2019.

[92] Sanjiv M. Narayan, David E. Krummen, Kalyanam Shivkumar, Paul Clopton, Wouter-Jan Rappel, and John M. Miller. Treatment of atrial fibrillation by the ablation of localized sources: Confirm (conventional ablation for atrial fibrillation with or without focal impulse and rotor modulation) trial. *Journal of the American College of Cardiology*, 60:628–636, 2012.

[93] Luigi Yuri Di Marco, Daniel Raine, John P. Bourke, and Philip Langley. Characteristics of atrial fibrillation cycle length predict restoration of sinus rhythm by catheter ablation. *Heart rhythm*, 10:1303–1310, 2013.

[94] Pedro Adragão, Pedro Carmo, Diogo Cavaco, João Carmo, António Ferreira, Francisco Moscoso Costa, Maria Salomé Carvalho, João Mesquita, Rita Quaresma, Francisco Belo Morgado, and Miguel Mendes. Relationship between rotors and complex fractionated electrograms in atrial fibrillation using a novel computational analysis. *Revista portuguesa de cardiologia*, 36:233–238, 2017.

[95] Amir Jadidi, Mark Nothstein, Juan Chen, Heiko Lehrmann, Olaf Dössel, Jürgen Allgeier, Dietmar Trenk, Franz-Josef Neumann, Axel Loewe, Björn Müller-Edenborn, and Thomas Arentz. Specific electrogram characteristics identify the extra-pulmonary vein arrhythmogenic sources of persistent atrial fibrillation - characterization of the arrhythmogenic electrogram patterns during atrial fibrillation and sinus rhythm. *Scientific reports*, 10:9147, 2020.

[96] Jongmin Hwang, Hyoung-Seob Park, Seongwook Han, Cheol Hyun Lee, In-Cheol Kim, Yun-Kyeong Cho, Hyuck-Jun Yoon, Jin Wook Chung, Hyungseop Kim, Chang-Wook Nam, Seung-Ho Hur, Jin Young Kim, Yun Seok Kim, and Woo Sung Jang. Ablation of persistent atrial fibrillation based on high density voltage mapping and complex fractionated atrial electrograms: A randomized controlled trial. *Medicine*, 100:e26702, 2021.

[97] Eva Cirugeda-Roldán, Daniel Novak, Vaclav Kremen, David Cuesta-Frau, Matthias Keller, Armin Luik, and Martina Srutova. Characterization of complex fractionated atrial electrograms by sample entropy: An international multi-center study. *Entropy*, 17(11):7493–7509, 2015.

[98] Alex Baher, Benjamin Buck, Manuel Fanarjian, J. Paul Mounsey, Anil Gehi, Eugene Chung, Fadi G. Akar, Charles L. Webber, Joseph G. Akar, and James P. Hummel. Recurrence quantification analysis of complex-fractionated electrograms differentiates active and passive sites during atrial fibrillation. *Journal of cardiovascular electrophysiology*, 30:2229–2238, 2019.

[99] Koji Kumagai, Kentaro Minami, Yoshinao Sugai, and Shigeru Oshima. Evaluation of the atrial substrate based on low-voltage areas and dominant frequencies after pulmonary vein isolation in nonparoxysmal atrial fibrillation. *Journal of arrhythmia*, 34:230–238, 2018.

[100] Pasquale Santangeli and Francis E. Marchlinski. Techniques for the provocation, localization, and ablation of non-pulmonary vein triggers for atrial fibrillation. *Heart rhythm*, 14:1087–1096, 2017.

[101] Yusuke Kanemaru, Yuichiro Arima, Koichi Kaikita, Takuya Kiyama, Shozo Kaneko, Miwa Ito, Hiroshige Yamabe, Kota Motozato, Kenshi Yamanaga, Koichiro Fujisue, Daisuke Sueta, Seiji Takashio, Satoshi Araki, Hiroki Usuku, Taishi Nakamura, Takashi Fukunaga, Satoru Suzuki, Yasuhiro Izumiya, Kenji Sakamoto, Hirofumi Soejima, Eiichiro Yamamoto, Hiroaki

Kawano, Hisanori Kanazawa, and Kenichi Tsujita. Elongation of the high right atrium to coronary sinus conduction time predicts the recurrence of atrial fibrillation after radiofrequency catheter ablation. *International journal of cardiology*, 300:147–153, 2020.

[102] Mathijs S. van Schie, Annejet Heida, Yannick J. H. J. Taverne, Ad J. J. C. Bogers, and Natasja M. S. de Groot. Identification of local atrial conduction heterogeneities using high-density conduction velocity estimation. *Europace*, 23:1815–1825, 2021.

[103] S. Honarbakhsh, R. J. Schilling, M. Orini, R. Providencia, M. Finlay, E. Keating, P. D. Lambiase, A. Chow, M. J. Earley, S. Sporton, and R. J. Hunter. Left atrial scarring and conduction velocity dynamics: Rate dependent conduction slowing predicts sites of localized reentrant atrial tachycardias. *International journal of cardiology*, 278:114–119, 2019.

[104] Kentaro Yoshida, Magnus Ulfarsson, Hiroshi Tada, Aman Chugh, Eric Good, Michael Kuhne, Thomas Crawford, Jean F. Sarrazin, Nagib Chalfoun, Darryl Wells, Krit Jongnarangsin, Frank Pelosi, Frank Bogun, Fred Morady, and Hakan Oral. Complex electrograms within the coronary sinus: Time- and frequency-domain characteristics, effects of antral pulmonary vein isolation, and relationship to clinical outcome in patients with paroxysmal and persistent atrial fibrillation. *Journal of Cardiovascular Electrophysiology*, 19(10):1017–1023, 2008.

[105] Geoffrey Lee, Kurt Roberts-Thomson, Andrew Madry, Steven Spence, Andrew Teh, Patrick M. Heck, Saurabh Kumar, Peter M. Kistler, Joseph B. Morton, Prashanthan Sanders, and Jonathan M. Kalman. Relationship among complex signals, short cycle length activity, and dominant frequency in patients with long-lasting persistent AF: A high-density epicardial mapping study in humans. *Heart Rhythm*, 8(11):1714–1719, 2011.

[106] Wen Chin Tsai, Yenn Jiang Lin, Hsuan Ming Tsao, Shih Lin Chang, Li Wei Lo, Yu Feng Hu, Chien Jung Chang, Wei Hua Tang, Ta Chun Tuan, Ameya R. Udyavar, Ji Hung Wang, and Shih Ann Chen. The optimal automatic algorithm for the mapping of complex fractionated atrial electrograms in patients with atrial fibrillation. *Journal of Cardiovascular Electrophysiology*, 21(1):21–26, 2010.

[107] Yenn Jiang Lin, Men Tzung Lo, Shih Lin Chang, Li Wei Lo, Yu Feng Hu, Tze Fan Chao, Fa Po Chung, Jo Nan Liao, Chin Yu Lin, Huan Yu Kuo, Yi Chung Chang, Chen Lin, Ta Chuan Tuan, Hsu Wen Vincent Young, Kazuyoshi Suenari, Van Buu Dan Do, Suunu Budhi Raharjo, Norden E. Huang, and Shih Ann Chen. Benefits of Atrial Substrate Modification Guided by Electrogram Similarity and Phase Mapping Techniques to Eliminate Rotors and Focal Sources Versus Conventional Defragmentation in Persistent Atrial Fibrillation. *JACC: Clinical Electrophysiology*, 2(6):667–678, 2016.

[108] Sonia Ammar-Busch, Tilko Reents, Sebastien Knecht, Thomas Rostock, Thomas Arentz, Mattias Duytschaever, Thomas Neumann, Bruno Cauchemez, Jean Paul Albenque, Gabriele Hessling, and Isabel Deisenhofer. Correlation between atrial fibrillation driver locations and complex fractionated atrial electrograms in patients with persistent atrial fibrillation. *PACE - Pacing and Clinical Electrophysiology*, 41(10):1279–1285, 2018.

[109] Andrew W. Teh, Peter M. Kistler, Geoffrey Lee, Caroline Medi, Patrick M. Heck, Steven J. Spence, Paul B. Sparks, Joseph B. Morton, Prashanthan Sanders, and Jonathan M. Kalman. The relationship between complex fractionated electrograms and atrial low-voltage zones during atrial fibrillation and paced rhythm. *Europace*, 13(12):1709–1716, 2011.

[110] Karen T.S. Konings, Charles J.H.J. Kirchhof, Joep R.L.M. Smeets, Hein J.J. Wellens, Olaf C. Penn, and Maurits A. Allessie. High-density mapping of electrically induced atrial fibrillation in humans. *Circulation*, 89(4):1665–1680, 1994.

[111] Tiago P. Almeida, Gavin S. Chu, João L. Salinet, Frederique J. Vanheusden, Xin Li, Jiun H. Tuan, Peter J. Stafford, G. André Ng, and Fernando S. Schlindwein. Minimizing discordances in automated classification of fractionated electrograms in human persistent atrial fibrillation. *Medical and Biological Engineering and Computing*, 54(11):1695–1706, 2016.

[112] J. M T De Bakker and F. H M Wittkampf. The pathophysiologic basis of fractionated and complex electrograms and the impact of recording techniques on their detection and interpretation. *Circulation: Arrhythmia and Electrophysiology*, 3(2):204–213, 2010.

[113] Adrian Luca and Jean-Marc Vesin. Correlation dimension as a measure of the atrial fibrillation capture during atrial septal pacing. In *Computing in Cardiology 2014*, pages 545–548, 2014.

[114] Adrian Luca, Andrea Buttu, Etienne Pruvot, Patrizio Pascale, Laurence Bisch, and Jean Marc Vesin. Nonlinear analysis of right atrial electrograms predicts termination of persistent atrial fibrillation within the left atrium by catheter ablation. *Physiological Measurement*, 37(2):347–359, 2016.

[115] James L. Wells, Robert B. Karp, Nicholas T. Kouchoukos, William A.H. Maclean, Thomas N. James, and Albert L. Waldo. Characterization of Atrial Fibrillation in Man: Studies Following Open Heart Surgery. *Pacing and Clinical Electrophysiology*, 60(3):426–438, 1978.

[116] F. Censi, V. Barbaro, P. Bartolini, G. Calcagnini, A. Michelucci, and S. Cerutti. Non-linear coupling of atrial activation processes during atrial fibrillation in humans. *Biological Cybernetics*, 85(10):195–201, 2001.

[117] Bart P.T. Hoekstra, Cees G.H. Diks, Maurits A. Allessie, and Jacob De Goedb. Nonlinear Analysis of Epicardial Atrial Electrograms of Electrically Induced Atrial Fibrillation in Man. *Journal of Cardiovascular Electrophysiology*, 6(6):419–440, 1995.

[118] Thomas Schreiber and Andreas Schmitz. Surrogate time series, 2000.

[119] Peter Grassberger and Itamar Procaccia. Measuring the strangeness of strange attractors. *Physica D: Nonlinear Phenomena*, 9(1-2):189–208, 1983.

[120] A. Corana, A. Casaleggio, C. Rolando, and S. Ridella. Efficient computation of the correlation dimension from a time series on a LIW computer. *Parallel Computing*, 17(6-7):809–820, 1991.

[121] Andrew M. Fraser and Harry L. Swinney. Independent coordinates for strange attractors from mutual information. *Physical Review A*, 33(2):1134–1140, 1986.

[122] James Theiler. Statistical precision of dimension estimators. *Physical Review A*, 41(6):3038–3051, 1990.

[123] Benoit. Mandelbrot. Contributions to probability and statistics: Essays in honor of harold hotelling (ingram olkin, sudhist g. ghurye, wassily hoeffding, william g. madow, and henry b. mann, eds.). *SIAM Review*, 3(1):80–80, 1961.

[124] S. S. Shapiro and M. B. Wilk. An analysis of variance test for normality (complete samples). *Biometrika*, 52(3-4):591–611, 1965.

[125] William H. Kruskal and W. Allen Wallis. Use of ranks in one-criterion variance analysis. *Journal of the American Statistical Association*, 47(260):583–621, 1952.

[126] H. B. Mann and D. R. Whitney. On a test of whether one of two random variables is stochastically larger than the other. *Ann. Math. Statist.*, 18(1):50–60, 1947.

[127] James W. Havstad and Cindy L. Ehlers. Attractor dimension of nonstationary dynamical systems from small data sets. *Physical Review A*, 39(2):845–853, 1989.

[128] Ray G. Huffaker. Phase Space Reconstruction from Time Series Data: Where History Meets Theory. 2010 International European Forum, February 8-12, 2010, Innsbruck-Igls, Austria 100455, International European Forum on System Dynamics and Innovation in Food Networks, 2010.

[129] V. Barbaro, P. Bartolini, G. Calcagnini, F. Martelli, and S. Morelli. A comparison of methods for the classification of atrial fibrillation from intra-atrial electrograms. In *Proceedings of the 20th Annual International Conference of the IEEE Engineering in Medicine and Biology Society*, volume 20, pages 94–97, 1998.

[130] Giandomenico Nollo, Mattia Marconcini, Luca Faes, Francesca Bovolo, Flavia Ravelli, and Lorenzo Bruzzone. An automatic system for the analysis and classification of human atrial fibrillation patterns from intracardiac electrograms. *IEEE Transactions on Biomedical Engineering*, 55(9):2275–2285, 2008.

[131] M. Kirchner, L. Faes, E. Olivetti, R. Riccardi, M. Scaglione, F. Gaita, and R. Antolini. Local electrical characterisation of human atrial fibrillation. In *Computers in Cardiology*, pages 499–502, 2000.

[132] V. Křemen, L. Lhotská, M. MacAš, R. Čihák, V. Vančura, J. Kautzner, and D. Wichterle. A new approach to automated assessment of fractionation of endocardial electrograms during atrial fibrillation. *Physiological Measurement*, 29(12):1371–1381, 2008.

[133] Charlotte L. Haley, Lorne J. Gula, Rodrigo Miranda, Kevin A. Michael, Adrian M. Baranchuk, Christopher S. Simpson, Hoshiar Abdollah, Adam J. West, Selim G. Akl, and Damian P. Redfearn. Validation of a novel algorithm for quantification of the percentage of signal fractionation in atrial fibrillation. *Europace*, 15(3):447–452, 2013.

[134] Valentina D A Corino, Massimo W Rivolta, Roberto Sassi, Federico Lombardi, and Luca T Mainardi. Ventricular activity cancellation in electrograms during atrial fibrillation with constraints on residuals' power. *Med Eng Phys*, 35(12):1770–7, 2013.

[135] Jose J Rieta, Fernando Hornero, Raul Alcaraz, and David Moratal. Ventricular artifacts cancellation from atrial epicardial recordings in atrial tachyarrhythmias. *Conf Proc IEEE Eng Med Biol Soc*, 2007:6504–7, 2007.

[136] Ahmed Salah, Shenghua Zhou, Qiming Liu, and Hui Yan. P wave indices to predict atrial fibrillation recurrences post pulmonary vein isolation. *Arquivos brasileiros de cardiologia*, 101:519–527, 2013.

[137] Xiaoliang Hu, Jingzhou Jiang, Yuedong Ma, and Anli Tang. Novel p wave indices to predict atrial fibrillation recurrence after radiofrequency ablation for paroxysmal atrial fibrillation. *Medical science monitor : international medical journal of experimental and clinical research*, 22:2616–2623, 2016.

[138] Qiong Chen, Sanghamitra Mohanty, Chintan Trivedi, et al. Association between prolonged P-wave duration and left atrial scarring in patients with paroxysmal atrial fibrillation. *Journal of cardiovascular electrophysiology*, 30:1811–1818, 2019.

[139] Raúl Alcaraz, Arturo Martínez, and José J Rieta. The p wave time-frequency variability reflects atrial conduction defects before paroxysmal atrial fibrillation. *Annals of Noninvasive Electrocardiology*, 20(5):433–445, 2015.

[140] Junbeom Park, Tae-Hoon Kim, Jihei Sara Lee, et al. Prolonged PR interval predicts clinical recurrence of atrial fibrillation after catheter ablation. *Journal of the American Heart Association*, 3:e001277, 2014.

[141] Jin-Tao Wu, Jian-Zeng Dong, Cai-Hua Sang, Ri-Bo Tang, and Chang-Sheng Ma. Prolonged pr interval and risk of recurrence of atrial fibrillation after catheter ablation. *International heart journal*, 55:126–130, 2014.

[142] Justin W. Smith, Wesley T. O'Neal, M. Benjamin Shoemaker, et al. PR-interval components and atrial fibrillation risk (from the atherosclerosis risk in communities study). *The American journal of cardiology*, 119:466–472, 2017.

[143] Adrian Baranchuk and Antoni Bayés de Luna. The P-wave morphology: what does it tell us? *Herzschrittmachertherapie+ Elektrophysiologie*, 26(3):192–199, 2015.

[144] G. Van Steenkiste, L. Vera, A. Decloedt, S. Schauvliege, T. Boussy, and G. van Loon. Endocardial electro-anatomic mapping in healthy horses: Normal sinus impulse propagation in the left and right atrium and the ventricles. *Veterinary journal (London, England : 1997)*, 258:105452, 2020.

[145] Chang Yi Li, Jing Rui Zhang, Wan Ning Hu, and Song Nan Li. Atrial fibrosis underlying atrial fibrillation. *International Journal of Molecular Medicine*, 47(3):1–1, 2021.

[146] Dirk De Bacquer, Julie Willekens, and Guy De Backer. Long-term prognostic value of P-wave characteristics for the development of atrial fibrillation in subjects aged 55 to 74 years at baseline. *The American journal of cardiology*, 100(5):850–854, 2007.

[147] Leif Sörnmo and P. Laguna. *Electrocardiogram (ECG) Signal Processing*, volume 2, pages 1298–1313. John Wiley and Sons, United States, 2006.

[148] Manuel García, Miguel Martínez-Iniesta, Juan Ródenas, José J. Rieta, and Raúl Alcaraz. A novel wavelet-based filtering strategy to remove powerline interference from electrocardiograms with atrial fibrillation. *Physiological measurement*, 39:115006, 2018.

[149] Arturo Martínez, Raúl Alcaraz, and José J Rieta. Ventricular activity morphological characterization: ectopic beats removal in long term atrial fibrillation recordings. *Comput Methods Programs Biomed*, 109(3):283–92, 2013.

[150] Ahyoung Choi and Hangsik Shin. Quantitative analysis of the effect of an ectopic beat on the heart rate variability in the resting condition. *Frontiers in physiology*, 9:922, 2018.

[151] Arturo Martínez, Raúl Alcaraz, and José Joaquín Rieta. Application of the phasor transform for automatic delineation of single-lead ECG fiducial points. *Physiological Measurement*, 31(11):1467–85, 2010.

[152] Francisco González, Raúl Alcaraz, and José Joaquín Rieta. Electrocardiographic P-wave delineation based on adaptive slope gaussian detection. In *Computing in Cardiology, CinC 2007, Rennes, France, September 24-27, 2017*. www.cinc.org, 2017.

[153] Ondřej Toman, Katerina Hnatkova, Peter Smetana, et al. Physiologic heart rate dependency of the PQ interval and its sex differences. *Scientific reports*, 10:2551, 2020.

[154] Jakub Misek, Igor Belyaev, Viera Jakusova, Ingrid Tonhajzerova, Jan Barabas, and Jan Jakus. Heart rate variability affected by radiofrequency electromagnetic field in adolescent students. *Bioelectromagnetics*, 39(4):277–288, 2018.

[155] Peng-Sheng Chen, Lan S. Chen, Michael C. Fishbein, Shien-Fong Lin, and Stanley Nattel. Role of the autonomic nervous system in atrial fibrillation: pathophysiology and therapy. *Circulation research*, 114:1500–1515, 2014.

[156] Jakub Misek, Marcel Veternik, Ingrid Tonhajzerova, Viera Jakusova, Ladislav Janousek, and Jan Jakus. Radiofrequency electromagnetic field affects heart rate variability in rabbits. *Physiological Research*, 69(4), 2020.

[157] M. Antz, K. Otomo, M. Arruda, B. J. Scherlag, J. Pitha, C. Tondo, R. Lazzara, and W. M. Jackman. Electrical conduction between the right atrium and the left atrium via the musculature of the coronary sinus. *Circulation*, 98:1790–1795, 1998.

[158] M. Tritto, M. Zardini, R. De Ponti, and J. A. Salerno-Uriarte. Iterative atrial tachycardia originating from the coronary sinus musculature. *Journal of cardiovascular electrophysiology*, 12:1187–1189, 2001.

[159] Michael Giudici, Stuart Winston, James Kappler, Timothy Shinn, Igor Singer, Avram Scheiner, Helen Berrier, Mark Herner, and Ross Sample. Mapping the coronary sinus and great cardiac vein. *PACE*, 25:414–419, 2002.

[160] Iman Razeghian-Jahromi, Andrea Natale, and Mohammad Hossein Nikoo. Coronary sinus diverticulum: Importance, function, and treatment. *PACE*, 43:1582–1587, 2020.

[161] Hiroshi Morita, Douglas P. Zipes, Shiho T. Morita, and Jiashin Wu. The role of coronary sinus musculature in the induction of atrial fibrillation. *Heart rhythm*, 9:581–589, 2012.

[162] Hakan Oral, Mehmet Ozaydin, Aman Chugh, Christoph Scharf, Hiroshi Tada, Burr Hall, Peter Cheung, Frank Pelosi, Bradley P. Knight, and Fred Morady. Role of the coronary sinus in maintenance of atrial fibrillation. *Journal of cardiovascular electrophysiology*, 14:1329–1336, 2003.

[163] Michel Haïssaguerre, Mélèze Hocini, Yoshihide Takahashi, Mark D. O'Neill, Andrej Pernat, Prashanthan Sanders, Anders Jonsson, Martin Rotter, Frederic Sacher, Thomas Rostock, Seiichiro Matsuo, Leonardo Arantés, Kang Teng Lim, Sébastien Knecht, Pierre Bordachar, Julien Laborderie, Pierre Jaïs, George Klein, and Jacques Clémenty. Impact of catheter ablation of the coronary sinus on paroxysmal or persistent atrial fibrillation. *Journal of cardiovascular electrophysiology*, 18:378–386, 2007.

[164] E. Mahmud, A. Raisinghani, S. Keramati, W. Auger, D. G. Blanchard, and A. N. DeMaria. Dilation of the coronary sinus on echocardiogram: prevalence and significance in patients with chronic pulmonary hypertension. *JASE*, 14:44–49, 2001.

[165] Chris J. M. Langenberg, Henk G. Pietersen, Gijs Geskes, Anton J. M. Wagenmakers, Peter B. Soeters, and Marcel Durieux. Coronary sinus catheter placement. *Clinical Investigations Cardiology*, 124:1259–1265, 2003.

[166] Farhood Saremi, Benjamin Thonar, Taraneh Sarlaty, Irene Shmayevich, Shaista Malik, Clyde W. Smith, Subramaniam Krishnan, Damián Sánchez-Quintana, and Navneet Narula. Posterior interatrial muscular connection between the coronary sinus and left atrium: anatomic and functional study of the coronary sinus with multidetector ct. *Radiology*, 260:671–679, 2011.

[167] Jürgen Vogt, Johannes Heintze, Bert Hansky, Holger Güldner, Helga Buschler, and Dieter Horstkotte. Implantation: tips and tricks–the cardiologist's view. *European Heart Journal Supplements*, 6(suppl_D):D47–D52, 2004.

[168] Ramdas G. Pai, Padmini Varadarajan, and Masato Tanimoto. Effect of atrial fibrillation on the dynamics of mitral annular area. *The Journal of heart valve disease*, 12:31–37, 2003.

[169] Shirley El-Maasarany, Colin G. Ferrett, Anthony Firth, Mary Sheppard, and Michael Y. Henein. The coronary sinus conduit function: anatomical study (relationship to adjacent structures). *EP Europace*, 7:475–481, 2005.

[170] Raúl Alcaraz and José Joaquín Rieta. Adaptive singular value cancelation of ventricular activity in single-lead atrial fibrillation electrocardiograms. 29:1351–1369, 2008.

[171] Diego Osorio, Raúl Alcaraz, and José J Rieta. A fractionation-based local activation wave detector for atrial electrograms of atrial fibrillation. In *2017 Computing in Cardiology (CinC)*, pages 1–4, 2017.

[172] Xin Yan and Xiao Gang Su. *Simple Linear Regression*, pages 9–39. World Scientific, Singapore, 2009.

[173] Douglas E. Lake and J. Randall Moorman. Accurate estimation of entropy in very short physiological time series: the problem of atrial fibrillation detection in implanted ventricular devices. *American journal of physiology*, 300:H319–H325, 2011.

[174] Raúl Alcaraz and José J Rieta. Nonlinear synchronization assessment between atrial and ventricular activations series from the surface ecg in atrial fibrillation. *Biomedical Signal Processing and Control*, 8(6):1000–1007, 2013.

[175] Miguel Rodrigo, Andreu M. Climent, Ismael Hernández-Romero, Alejandro Liberos, Tina Baykaner, Albert J. Rogers, Mahmood Alhusseini, Paul J.

Wang, Francisco Fernández-Avilés, Maria S. Guillem, Sanjiv M. Narayan, and Felipe Atienza. Noninvasive assessment of complexity of atrial fibrillation: Correlation with contact mapping and impact of ablation. *Circulation. Arrhythmia and electrophysiology*, 13:e007700, 2020.

[176] Z. Liu, M. Hayano, T. Hirata, K. Tsukahara, Y. Quin, K. Nakao, M. Nonaka, T. Ishimatsu, C. Ueyama, and K. Yano. Abnormalities of electrocardiographic p wave morphology and their relation to electrophysiological parameters of the atrium in patients with sick sinus syndrome. *PACE*, 21:79–86, 1998.

[177] S. Yahyazadeh, S. Firoozabadi, M. Haghjoo, and S. Parvaneh. Quantitative relation between chaotic features of surface electrocardiogram and intracardiac electrogram. In *2010 Computing in Cardiology*, pages 593–596, 2010.

[178] R. Alcaraz, F. Hornero, and J. J. Rieta. Validation of surface atrial fibrillation organization indicators through invasive recordings. In *2011 Annual International Conference of the IEEE Engineering in Medicine and Biology Society*, pages 5519–5522, 2011.

[179] Emanuela Finotti, Aurelio Quesada, Edward J. Ciaccio, Hasan Garan, Fernando Hornero, Raúl Alcaraz, and José J. Rieta. Practical considerations for the application of nonlinear indices characterizing the atrial substrate in atrial fibrillation. *Entropy (Basel, Switzerland)*, 24, 2022.

[180] Raúl Alcaraz, Fernando Hornero, and José J. Rieta. Electrocardiographic spectral features for long-term outcome prognosis of atrial fibrillation catheter ablation. *Annals of biomedical engineering*, 44:3307–3318, 2016.

[181] Aikaterini Vraka, Fernando Hornero, Vicente Bertomeu-González, Joaquín Osca, Raúl Alcaraz, and José J. Rieta. Short-time estimation of fractionation in atrial fibrillation with coarse-grained correlation dimension for mapping the atrial substrate. *Entropy*, 22, 2020.

[182] Simona Petrutiu, Alan V. Sahakian, and Steven Swiryn. Abrupt changes in fibrillatory wave characteristics at the termination of paroxysmal atrial fibrillation in humans. *Europace*, 9:466–470, 2007.

[183] Theo Lankveld, Stef Zeemering, Daniel Scherr, Pawel Kuklik, Boris A. Hoffmann, Stephan Willems, Burkert Pieske, Michel Haïssaguerre, Pierre Jaïs, Harry J. Crijns, and Ulrich Schotten. Atrial fibrillation complexity parameters derived from surface ecgs predict procedural outcome and long-term follow-up of stepwise catheter ablation for atrial fibrillation. *Circulation. Arrhythmia and electrophysiology*, 9:e003354, 2016.

[184] Pilar Escribano, Juan Rodenas, Miguel A. Arias, Philip Langley, Jose J. Rieta, and Raul Alcaraz. Novel time-frequency features of the fibrillatory waves improve catheter ablation outcome prediction of persistent atrial fibrillation. In *2020 International Conference on e-Health and Bioengineering (EHB)*, pages 1–4, 2020.

[185] Leif Sörnmo, Andrius Petrėnas, and Vaidotas Marozas. *Databases and Simulation*, pages 49–71. Springer International Publishing, Cham, 2018.

[186] Joshua S. Richman and J. Randall Moorman. Physiological time-series analysis using approximate entropy and sample entropy. 278:H2039–H2049, 2000.

List of Figures

List of Tables

Lisf of Acronyms

AF	Atrial fibrillation
AFCL	Atrial fibrillation cycle length
ANS	Autonomous nervous system
APD	Action potention duration
AR	Atrial remodeling
ARV	Atrial rate variability
ASCI	Adaptive signed correlation index
AV	Atrioventricular
BPSM	Body potential surface mapping
CA	Catheter ablation
CF	Correction factor
CFAEs	Complex fractionated atrial electrograms
CGCD	Coarse-grained correlation dimension
CL	Cycle length
CorDim	Correlation dimension
CQSE	Cross-quadratic sample entropy
CS	Coronary sinus
CT	Computed tomography
D	Distal
DAD	Delayed after-depolarization
DF	Dominant frequency
EAD	Early after-depolarization
ECG	Electrocardiogram
ECGI	Electrocardiogram imaging
EGM	Electrogram
FIRM	Focal impulse and rotor mapping
HR	Heart rate
FWA	f-wave amplitude
HRV	Heart rate variability
IBI	Interbeat interval
KW	Kruskal-Wallis
LA	Left atrium
LAT	Local activation timing
LAWs	Local activation waves
LPVI	Left pulmonary vein isolation

LR	Linear regression
LV	Low voltage
M	Medial
MAW	Main atrial wave
MD	Mid-distal
MP	Mid-proximal
MV	Morphology variability
MWU	Mann-Whitney U-test
NODI	Number of deflections and inflections
P	Proximal
PCC	Pearson's correlation coefficient
PDGF	Platelet derived growth factor
PLI	Poweline interference
PosAr	Positive area
POV	Percentage of variation
PSD	Power spectral density
PV	Pulmonary vein
PVI	Pulmonary vein isolation
PWD	P-wave duration
RA	Right atrium
RF	Radiofrequency
RMS	Root-mean square
RMSSD	Root-meaan square of successive interbeat differences
ROC	Receiver-operating characteristic
RPVI	Right pulmonary vein isolation
SA	Sinoatrial
SDNN	Standard deviation of normal-to-normal intervals
SE	Sample entropy
SFM	Spectral flatness measure
SR	Sinus rhythm
SVM	Support vector machine
TGF-β_1	Transforming growth factor-β_1
VARNN	Variance of normal-to-normal interval
WCT	Wilson's central teminal